

Geomagnetic Diurnal Variation Studies Using Global Models & Observatory Data at Quiet & Moderately Disturbed Times

Thesis submitted in accordance with the requirements of the
University of Liverpool for the degree of Doctor in Philosophy

by

Elvis Vwede Onovughe

March 2015



UNIVERSITY OF
LIVERPOOL

Abstract

In this thesis we investigate and analyse the nature and behaviour of the external field variations of the geomagnetic field for quiet and moderately disturbed days using geomagnetic observatory measurements and field models. We use spherical harmonic modelling, led by available geomagnetic observatory measurements and past models (particularly the Comprehensive Model of Sabaka et al. 2004).

As an initial step, we extended the lifespan of the Comprehensive Model (CM4) beyond its 2002.5 lifespan to allow for use of current data. We produced profile plots of the diurnal field and generated global maps of the field and compare these with the CM4 model, to see how well the CM4 model could reasonably predict ground variation of the diurnal field outside its lifespan and for days away from quiet time. The comparison shows that away from quiet time period, the CM4 model is producing more reasonable predictions than expected, despite the lack of active data in the original model dataset. The CM4 model fits the regional type features of the geomagnetic components, but not doing well predicting the short term features during period of rapid variations (seen as 'wiggles' in the profile plots) , especially for the X- component. Also, comparing the modelled diurnal maps of the CM4 and observatory data shows that increasing the spherical harmonic degree produces a better match between the CM4 model and the data. Our result reveals that the external field description included in the CM4 model could not sufficiently explain the field variation for days away from quiet time.

The CM4 model predicts the Y- and Z- components variations better than the X; this may be due to the fact that the X component is more affected by external field sources. As a result we introduced the use of an additional geomagnetic activity index (the RC index), to enable us to establish the nature of the rapid variation seen in the data for days away from quiet time. We looked for this using eigenanalysis (covariance matrices, eigenvectors and eigenvalues), detrending the data sequences with spline fits, and comparing the observatory data residuals with the RC index values. We also looked at the coherence and correlation between small scale features showing up in the rapid variation, to try to establish the global scale of the variations. We analysed this by simple running average method, correlation and cross-correlation coefficients between the residuals of the observatory data components and the RC index.

Our results show that our data for days away from quiet time, particularly the X component, include a strong component in the rapid variations related to large-scale external field variation arising from the magnetospheric ring current. For example we are able to reproduce features in our plots that show a very strong coherence and correlation existing between the X component of our observatory data residuals and the RC index. This is also seen in the same components of the observatories at different locations within the same geographical region, and at some different geographical regions. This allows us to characterise the RC index as being a good representation for rapid variations globally. Also, it makes us optimistic that it may be useful to look at rapid variation observatory results for combined observatory stations as a good technique for remote referencing in aeromagnetic surveying.

Acknowledgements

First and foremost, my eternal gratitude goes to God Almighty for the gift of life, the strength and opportunity to achieve my dream of a PhD degree. It is to You I dedicate this thesis.

I would like to thank the Federal University of Petroleum Resources Effurun (FUPRE) and the Tertiary Education Trust Fund (TETFUND) Nigeria who funded this study through their Academic Staff Training and Development Grant.

I owe a huge thank you and gratitude to my supervisor, Professor Richard Holme, for his guidance over the past four years. Richard taught me things I thought I would never understand, reassured me with encouraging words when overwhelmed by what looked like an impossible task and taught me how to question thoughts and express ideas on my own. Richard's patience with me and support helped me overcome many situations and finish this thesis. I hope one day I will become as good a supervisor/advisor to my students as Richard has been to me.

I am also grateful to all those I met at various conferences, workshops, and seminars, who I have useful conversations with. I am particularly grateful to Nils Olsen for his useful suggestions that helped enormously.

Thanks for the lovely friends I made at Liverpool, past and present, who helped me on this journey to PhD – Victoria Ridley Taylor and Gemma Kelly for helping me initially with my computing (skills and codes). Mohammed Bukar, for hosting me in my early days in Liverpool, helping me settle down, and all his advice, support and encouragement. Oshaine Blake for all the football games and trashy talks that took my mind off difficult moments and kept me sane. To the entire postgraduate research students in the department, unfortunately too many to mention, who provided the brilliant academic and social environment in the department.

Thanks to my Nigerian friends and members of Redeem Christian Church of God (RCCG) Love Assembly Liverpool: to Pastor Fola Olaoye for the spiritual and social upliftment; to Thomas, Celestine, Ohio, Ezikpe, Ayo, Ayobamile, Phillip, and many more.

Special thanks to Christy Nwokomah for being by my side over the past one year. I honestly don't know how I would have done this without you.

To Sally Edeamrere. For all your prayers, for inspiring me, consoling me, updating me and keeping me abreast with local and intimate gossips from home which makes my longing for home bearable.

Finally, thanks to my family in Nigeria: my brothers and sisters, and to my mum for all your prayers.

I am hugely grateful.

Contents

| | |
|--|------------|
| Abstract | i |
| Acknowledgements | ii |
| List of Figures | vii |
| List of Tables | x |
| 1 Introduction, Background and Motivation | 1 |
| 1.1 Geomagnetic Time Variations | 3 |
| 1.1.1 Long term variations | 3 |
| 1.2 Short Term Variations | 3 |
| 1.2.1 Irregular variations | 4 |
| 1.2.2 Regular variations | 4 |
| 1.3 Historical Background of Diurnal Variation | 5 |
| 1.4 Motivation | 7 |
| 1.5 Thesis Outline | 8 |
| 2 The Earth's Magnetic Field | 9 |
| 2.1 Sources Contributing to the Earth's Magnetic Field | 10 |
| 2.1.1 The core field | 11 |
| 2.1.2 The crustal field | 13 |
| 2.2 The External Fields | 14 |
| 2.2.1 Magnetosphere | 15 |
| 2.2.2 Ionosphere | 16 |
| 2.2.3 Induced fields | 18 |
| 2.2.4 The ring current | 18 |
| 2.3 Magnetic Activity Indices | 19 |
| 2.3.1 Kp index | 21 |
| 2.3.2 Dst index | 22 |

| | |
|---|-----------|
| 2.3.3 RC index | 23 |
| 2.4 Measuring the Geomagnetic Field | 25 |
| 2.4.1 Observatories | 25 |
| 2.4.2 Satellites | 27 |
| 2.5 Mathematical Description of the Geomagnetic Field and Modelling Techniques | 30 |
| 2.5.1 Spherical harmonic analysis | 31 |
| 2.5.2 Existing models and modelling techniques | 33 |
| 2.5.3 The comprehensive models | 34 |
| 2.6 Earth's Magnetic Field Summary | 37 |
| 3 Modelling the Magnetic Diurnal Variation | 38 |
| 3.1 Modelling Background/Theory | 38 |
| 3.1.1 Inverse theory/modelling | 38 |
| 3.1.2 Data selection in modelling | 39 |
| 3.2 Data Used in this Thesis | 40 |
| 3.3 Testing the CM4 Model | 40 |
| 3.3.1 Geographical plots of quiet time datasets | 41 |
| 3.3.2 Geographical plots of datasets away from quiet time | 46 |
| 3.3.3 Misfit between the CM4 model and observatory data | 50 |
| 3.3.4 Trends in failure times of model | 51 |
| 3.4 Global Maps of the Diurnal Field | 52 |
| 3.4.1 Approach: How CM4 models the field | 53 |
| 3.4.2 Regularised minimum-norm approach | 53 |
| 3.4.3 Damping Parameter | 55 |
| 3.4.4 Model/data comparison | 56 |
| 3.4.5 Spatial power spectrum | 64 |
| 3.4.6 Spatial differences | 65 |
| 3.5 Modelling Summary | 67 |

| | | |
|----------|--|-----------|
| 4 | Correlated Errors, Residuals and Covariant Modelling | 68 |
| 4.1 | RC versus Dst | 68 |
| 4.2 | Uncertainty Estimates of Geomagnetic Field Models | 70 |
| 4.3 | Geomagnetic Field Model Residuals | 72 |
| 4.4 | Data Covariant Matrices and EigenAnalysis | 72 |
| 4.4.1 | Methodology: Penalised least-squares spline | 72 |
| 4.4.2 | Results of covariance/eigenanalysis | 74 |
| 4.4.3 | Discussion/analysis | 78 |
| 4.4.4 | Combined observatory locations | 82 |
| 4.4.5 | Comparing with RC | 84 |
| 4.4.6 | Combined observatories | 91 |
| 4.5 | Removing Error Source | 94 |
| 4.6 | Covariant Modelling Summary | 94 |
| | | |
| 5 | Modelling Small Scale Features | 97 |
| 5.1 | Running Average Approach | 97 |
| 5.2 | Coherence between Small Scale Features Analysis | 99 |
| 5.2.1 | Results for data corrected for CM4 (ionospheric and magnetospheric fields).. | 99 |
| 5.2.2 | Results for raw data, data corrected for ionosphere only, and data corrected for magnetosphere only | 102 |
| 5.3 | Comparison with Observatory Showing Equatorial Electrojet Influences | 110 |
| 5.4 | Cross-Correlation Function | 111 |
| 5.4.1 | Correlation between observatory data residuals and the RC index | 112 |
| 5.4.2 | Correlation between observatory locations | 117 |
| 5.5 | Small Scale Features Summary | 121 |

| | | |
|----------|---|------------|
| 6 | Synthesis, Additional Analysis and Future Work | 122 |
| | 6.1 Synthesis and Discussion | 122 |
| | 6.2 Implications for Magnetic Surveys | 125 |
| | 6.2.1 Applications | 126 |
| | 6.3 Effects of Equatorial Electrojets | 128 |
| | 6.4 Suggestion for Future Work | 128 |
| | Appendix | 129 |
| | Additional Information | 129 |
| | Bibliography | 133 |

List of Figures

| | | |
|------|---|----|
| 1.1 | Magnetogram showing a typical Sq daily variation profile on a quiet day (Kp=10)..... | 2 |
| 1.2 | Magnetogram showing a geomagnetic storm (Kp=9-) | 4 |
| 1.3 | Representation of the Sq current system | 6 |
| 2.1 | Earth's magnetic field dipole representation | 9 |
| 2.2 | Total field intensity (F) at the Earth's surface in 2010 as predicted by IGRF-11 model. | 10 |
| 2.3 | Current sources contributing to the near-Earth magnetic field | 11 |
| 2.4 | Spatial power spectrum of the geomagnetic field at the Earth's surface | 12 |
| 2.5 | Vertical component of the lithospheric magnetic field at satellite altitude of 400km above the mean Earth radius | 14 |
| 2.6 | Currents and plasma populations within the magnetosphere | 15 |
| 2.7 | Profile of the different strata in the ionosphere | 17 |
| 2.8 | Dominant current systems associated with the ionosphere | 17 |
| 2.9 | Equivalent external ionospheric current system that sustains quiet-time variation... | 18 |
| 2.10 | Locations of observatories used in calculating Kp, Dst, PC and AE indices | 20 |
| 2.11 | Musical diagram key illustrating magnetic Kp index | 21 |
| 2.12 | Locations of observatories used in calculating RC index | 24 |
| 2.13 | World-wide distribution of magnetic observatories | 26 |
| 2.14 | Distribution of ground magnetic observatory data | 27 |
| 2.15 | Distribution of high-precision satellite mission in time | 28 |
| 2.16 | Components of the geomagnetic field measurement | 30 |
| 2.17 | Residual progression after magnetic fields from the three main source regions is removed with the comprehensive model | 36 |
| 3.1 | Quiet time diurnal variation comparison of X, Y, Z components for CM4 model predictions to observatory data for African stations | 42 |
| 3.2 | Quiet time diurnal variation comparison of X, Y, Z components for CM4 model predictions to observatory data for Asian stations | 42 |
| 3.3 | Quiet time diurnal variation comparison of X, Y, Z components for CM4 model predictions to observatory data for European stations | 43 |
| 3.4 | Quiet time diurnal variation comparison of X, Y, Z components for CM4 model predictions to observatory data for North American stations | 43 |
| 3.5 | Quiet time diurnal variation comparison of X, Y, Z components for CM4 model predictions to observatory data for South American stations | 44 |
| 3.6 | Quiet time diurnal variation comparison of X, Y, Z components for CM4 model predictions to observatory data for Oceania stations | 44 |
| 3.7 | Moderately disturbed day comparison of X, Y, Z components for CM4 model predictions to observatory data for African stations | 47 |
| 3.8 | Moderately disturbed day comparison of X, Y, Z components for CM4 model predictions to observatory data for Asians stations | 47 |
| 3.9 | Moderately disturbed day comparison of X, Y, Z components for CM4 model predictions to observatory data for European stations | 48 |
| 3.10 | Moderately disturbed day comparison of X, Y, Z components for CM4 model predictions to observatory data for North American stations | 48 |

| | | |
|------|--|----|
| 3.11 | Moderately disturbed day comparison of X, Y, Z components for CM4 model predictions to observatory data for South American stations | 49 |
| 3.12 | Moderately disturbed day comparison of X, Y, Z components for CM4 model predictions to observatory data for Oceania stations | 49 |
| 3.13 | Diurnal variation field of Z component modelled at surface for comparison between the CM4 model and the observatory station data for spherical harmonic degree 1 | 58 |
| 3.14 | Diurnal variation field of Z component modelled at surface for comparison between the CM4 model and the observatory station data for spherical harmonic degree 3 | 59 |
| 3.15 | Diurnal variation field of Z component modelled at surface for comparison between the CM4 model and the observatory station data for spherical harmonic degree 5 | 60 |
| 3.16 | Diurnal variation field of Z component modelled at surface for comparison between the CM4 model and the observatory station data for spherical harmonic degree 7 | 61 |
| 3.17 | Diurnal variation field of Z component modelled at surface for comparison between the CM4 model and the observatory station data for spherical harmonic degree 8 | 62 |
| 3.18 | Roughness against fit for different spherical harmonic truncation | 64 |
| 3.19 | Differences between CM4 model predictions and observatory data at spherical harmonic degree 5 at 0, 6, 12 and 18 hours | 66 |
| 3.20 | Differences between CM4 model predictions and observatory data at spherical harmonic degree 7 at 0, 6, 12 and 18 hours | 66 |
| 4.1 | Comparison between RC and Dst | 68 |
| 4.2 | Plot of residuals of X, Y, Z components used for calculating eigenvalues and eigenvectors for data corrected for CM4 (ionosphere and magnetosphere) | 79 |
| 4.3 | Plot of residuals of X, Y, Z components corrected for ionosphere only, used for calculating eigenvalues and eigenvectors | 80 |
| 4.4 | Plot of residuals of X, Y, Z components uncorrected for CM4 (raw data) used for calculating eigenvalues and eigenvectors | 81 |
| 4.5 | Plot of residuals of X, Y, Z components corrected for magnetosphere only used for calculating eigenvalues and eigenvectors | 81 |
| 4.6 | Residual plots of X, Y, Z components of combined European observatories used for calculating eigenvalues and eigenvectors | 84 |
| 4.7 | Residual plots of X, Y, Z components of combined observatories (one European and one non-European) used for calculating eigenvalues and eigenvectors | 84 |
| 4.8 | Comparison between the X residuals and RC for raw data (uncorrected) at different global observatory sites | 86 |
| 4.9 | Comparison between the X residuals of observatory data corrected for CM4 and RC at different global observatory sites | 87 |
| 4.10 | Comparison between the X residuals corrected for ionosphere and RC at different global observatory sites | 88 |
| 4.11 | Comparison between the X residuals corrected for magnetosphere and RC at different global observatory sites | 89 |
| 4.12 | Comparison between RC and combined Niemegek (NGK) and L'Aquila (AQU) observatory X component data residuals in Europe | 92 |
| 4.13 | Comparison between RC and combined Niemegek (NGK) and Mbour (MBO) observatory X component data residuals | 93 |
| 4.14 | Comparison between RC and combined Budkov (BDV) and Bangui (BNG) | |

| | | |
|------|--|-----|
| | observatory X component data residuals. Non-RC observatories | 93 |
| 4.15 | Observatory residual plots showing amplitude of field components before and after the attempted error removal application | 96 |
| 5.1 | Detrended data sequences (with one-hour running average) for, RC index residuals, X component residuals at AAE, Y component residuals at AQU, and Z component residuals at BMT | 98 |
| 5.2 | Comparison between observatory components (X, Y, Z) residuals corrected for CM4 model (ionospheric and magnetospheric) and RC index | 100 |
| 5.3 | Comparison between observatory components (X, Y, Z) residuals uncorrected with CM4 model (raw data) and RC index | 104 |
| 5.4 | Comparison between observatory components (X, Y, Z) residuals corrected for ionosphere and RC index | 106 |
| 5.5 | Comparison between observatory components(X, Y, Z) residuals corrected for magnetosphere and RC index | 108 |
| 5.6 | Comparison between X, Y and Z residuals and RC index residual for Huancayo (HUA) electrojet observatory | 111 |
| 5.7 | Cross-correlation between X, Y and Z residuals and RC index residual for raw data in selected observatory locations in different geographical region of the Earth | 113 |
| 5.8 | Cross-correlation between X, Y and Z residuals and RC index residual for data corrected with CM4 (for both ionosphere and magnetosphere) in selected observatory locations in different geographical region of the Earth | 114 |
| 5.9 | Correlation and cross-correlation profiles between observatories in same geographical regions | 119 |
| 5.10 | Correlation and cross-correlation profiles between observatories in different geographical regions | 120 |

List of Tables

| | | |
|-----|--|-----|
| 2.1 | K_p , PC, AE, and D_{st} geomagnetic activity indices | 20 |
| 2.2 | The K_p network observatories | 22 |
| 2.3 | Location of D_{st} network observatories | 22 |
| 2.4 | Location of RC network observatories | 24 |
| 2.5 | Satellite missions of relevance for geomagnetic field modelling | 30 |
| 3.1 | Relative misfit between CM4 model and observatory data for quiet and moderately disturbed periods | 51 |
| 3.2 | List of models of the time-varying magnetic field which have used the regularised approach | 56 |
| 3.3 | Residuals of the CM4 model and Observatory station data for different Universal times and spherical harmonic degrees | 63 |
| 4.1 | Eigenvalues and eigenvectors measurements for selected single observatories | 77 |
| 4.2 | Eigenvalues and eigenvectors measurements for two combined European observatories | 82 |
| 4.3 | Eigenvalues and eigenvectors measurements for combined observatories (European and non-European) | 83 |
| 5.1 | Cross-correlation coefficients of X, Y and Z components of the geomagnetic diurnal field with the RC index for selected observatory locations in the different geographical regions of the Earth | 116 |
| 5.2 | Cross-correlation coefficients of X component between observatory sites located within the same geographical locations | 118 |
| 5.3 | Cross-correlation coefficients of X component between observatory sites located at different geographical locations | 118 |

Chapter 1

Introduction, Background and Motivation

Introduction

The Earth's magnetic quiet-time daily variation is one of the most consistent components of the time-varying part of the Earth's magnetic field (Kane, 1976; Lilley et al.1999). This daily geomagnetic variation at any location shows myriads of irregular changes in the field representing the superposition of many spectral components whose amplitudes generally increase with increasing period (Campbell, 1989). These changes and variations are easiest to observe during periods of low solar activity when irregular disturbances are less frequent.

As a result they are referred to as Solar Quiet, Sq.

The Sq magnetic field variation has been referred to as the manifestation of an ionospheric current system, since it originates primarily from the ionosphere. More recently, components of Sq have been identified as originating from the Earth's magnetosphere (Maus and Luhr, 2005). Some evidence of oceanic tides on the magnetic daily variation has also been obtained (Larsen and Cox, 1966). Daily variations are further influenced by the effects of induction in the solid earth and oceans (Kuvshinov, 2008). Particularly strong signals are seen in equatorial regions, associated with a current running along the dip equator particularly near noon, local time, the equatorial electrojet.

Over the last couple of decades, the overall characterisation of the geomagnetic field has been vastly improved by the modelling of data from three low-orbiting satellites: Ørsted, CHAMP and Sac-C; results from these and other gravity-focussed missions led to the designation of the so-called "International Decade of Geopotential Research" (Friis-Christensen et al., 2009). These satellite research missions plus others, starting as far back as the 1960s have thrown more light on the magnetosphere/ionosphere interactions, resulting in a complete re-evaluation of the ionospheric dynamo theory. Richmond et al. (1976) and Richmond (1979) however, showed that winds in the 80 – 200km region arising from solar heating were still the most likely cause of Sq, and those magnetospheric sources are only secondary importance at middle and low latitudes.

A typical Sq signature pattern, as illustrated in figure 1.1, shows a classical rise in intensity at about sunrise (typified by the X component), peaks at about noon local time and falls towards the sunset period. Quiet-day or Sq field variations about a daily mean level change slightly in amplitude and phase through the months of the year. Solar activities, with sunspot number, control the percentage of magnetically quiet days (Sq-producing days). According to Campbell (1997), the quietest geomagnetic days usually occur on, or a year after, the minimum sunspot number. The study and analysis of quiet day and active day field variations now finds utility in improvement of satellite field modelling.

Current geomagnetic field models use geomagnetic 'quiet' data i.e. geomagnetic data for times and period when magnetic activity is low. The geomagnetic index (Kp) is commonly used as a criterion for choosing these intervals (Joselyn, 1989). These geomagnetic field models are necessary and required for various applications. These include understanding the dynamics of the Earth's interior, tectonic and lithospheric structure, studying the core flow, circulation of plasma and energy in the upper atmosphere and length of day studies. At peaks of geomagnetic activity there are many

systems on Earth which can be affected. These include electrical grids/installations, communication equipment (both audio & visual), electronic radar, etc. (Kivelson and Russell, 1995).

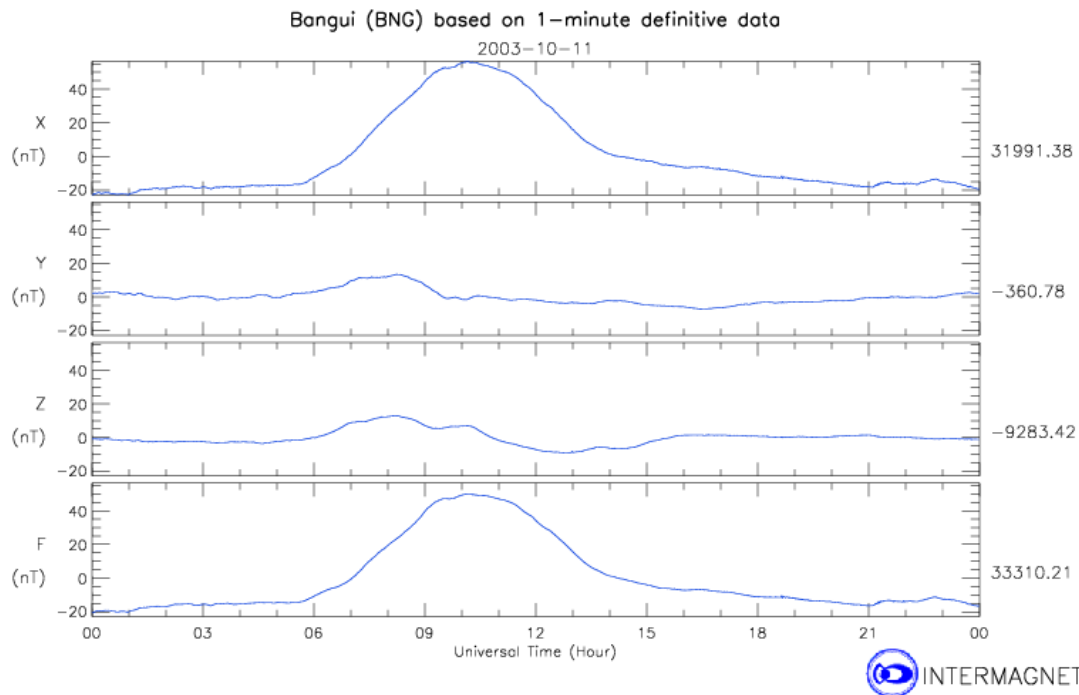


Figure 1.1: Magnetogram from Bangui observatory showing a typical Sq daily variation signature profile on a day of low magnetic activity (solar quiet day), Kp = 1o. (INTERMAGNET)

With the current high availability of satellite and observatory data, global modelling of the magnetic field is improving, providing more useful options when dealing with removal/separation of various field sources. When considering the external fields (where Sq originates from), there exists models such as the Comprehensive Model (CM4) of Sabaka (Sabaka et al. 2004). As a result an improved geomagnetic Sq model which provides a good understanding of the geomagnetic Sq field will go a long way in improving our understanding of the geomagnetic field and the effects produced as a result of its activities.

Over the years, much has been learned about many components of the geomagnetic field, particularly the geomagnetic quiet-time daily variation (Sq), but the daily variation for days away from quiet time have not received as much attention as its quiet-time counterpart. In this thesis we use publicly available measurements from ground geomagnetic observatory stations to model the geomagnetic Sq field and other aspects of diurnal variation. It is of particular interest to consider the behaviour of Sq for days away from quiet time. How does the field vary and behave during these times?

To build a premise for the following discussion, we devote this opening chapter to developing a common examination of the general scientific background, theory and motivation that form the basis for the research. We begin in section 1.1 with a review of our understanding of geomagnetic time variations, with a brief discussion of its long term variations. Section 1.2 followed with a discussion of the short term variations, its irregular and regular variations. In section 1.3, we present a brief overview of the development of magnetic diurnal variation, and does not purport to be comprehensive. We conclude in section 1.4 by outlining the justification and motivation for studying

magnetic diurnal variation Sq field and other aspects of diurnal variation, followed in section 1.5 by an outline of the work conducted and presented in this thesis.

1.1 Geomagnetic Time Variations

The geomagnetic field changes significantly with time, varying over a huge range of timescales. The variations in time can be from milliseconds up to millions of years, and can be periodic or completely random. The geomagnetic time variations can be classified into two main classes:

- Long term variations
- Short term variations

Apart from the duration, what differentiates them is that long term variations find their origin from dynamics of the Earth's interior, while short term variations derive their origin from sources external to the Earth. Long term variations are called secular variation and are on scale of few years to centuries and beyond (Langel, 1987; Lanza and Meloni, 2006), and appeared as main field variations. The short term variations often cause intense variations in the field and can be on a scale of milliseconds to a few days, hardly exceeding a year in duration. They are produced by currents in the magnetosphere (see section 2.2.1) and ionosphere (see section 2.2.2), and also by currents induced in the Earth's crust by oceans (see section 2.2.3). Their rapidity and intensity make them very apparent in geomagnetic observatory data/magnetogram.

1.1.1 Long Term Variations

Secular variation was discovered in 1634 by Henry Gellibrand (Pumfrey, 1989), through geomagnetic measurements which showed that the declination of the Earth's field was not only a function of position, but also of time. Both secular variation and main field are believed to originate in the Earth's core. Changes produced by secular variation (declination, inclination and intensity of the main field) are small but still recognisable when looking at geomagnetic data ranging over several years. Secular variation gives important information about the dynamics of flow at the core mantle boundary (CMB), and the origin of the geomagnetic field (Bloxham et al.1989; Hulot et al.2002; Olsen and Manda, 2008).

Secular variation find applications in research on constructing and improving new theoretical models which replicates the current systems that generates the field, and in paleomagnetism, where the most significant contribution is the discovery of the so called geomagnetic field reversal – exchange of position between the north and south poles.

1.2 Short Term Variations

Short term variations in the geomagnetic field are related to the variations in the external field. This results from the dominance of the Sun. Here, I have discussed short term variations under two classes – the regular variations, which are caused by the orbital motion and/or rotation of celestial bodies, and the irregular variations, which are what catches one's eye, because they are often of large intensities due to their rapid time changes in the field. They are most apparent when looking at magnetogram. I will start by discussing the irregular variations first.

1.2.1 Irregular Variations

The interaction between the magnetic field of the solar wind and the magnetosphere causes the irregular variations in the geomagnetic field. This interaction leads to time varying currents in the magnetosphere and ionosphere, involving plasma and energy, and results in induced currents in the mantle and oceans (at their most extreme). Geomagnetic storms results from these sudden and repeated (not regular) changes in the magnetosphere, affecting all elements of the geomagnetic field, with variations of several hundred nTs. The duration can range from a few hours to several days (Love, 2008).

Figure 1.2 is an example of a magnetic storm measured at Barrow observatory on 20th November, 2003. All the components (X, Y, Z) are given in nT. According to the magnetogram, there was a storm that day causing disturbances in all three components (more severe on X and Y).

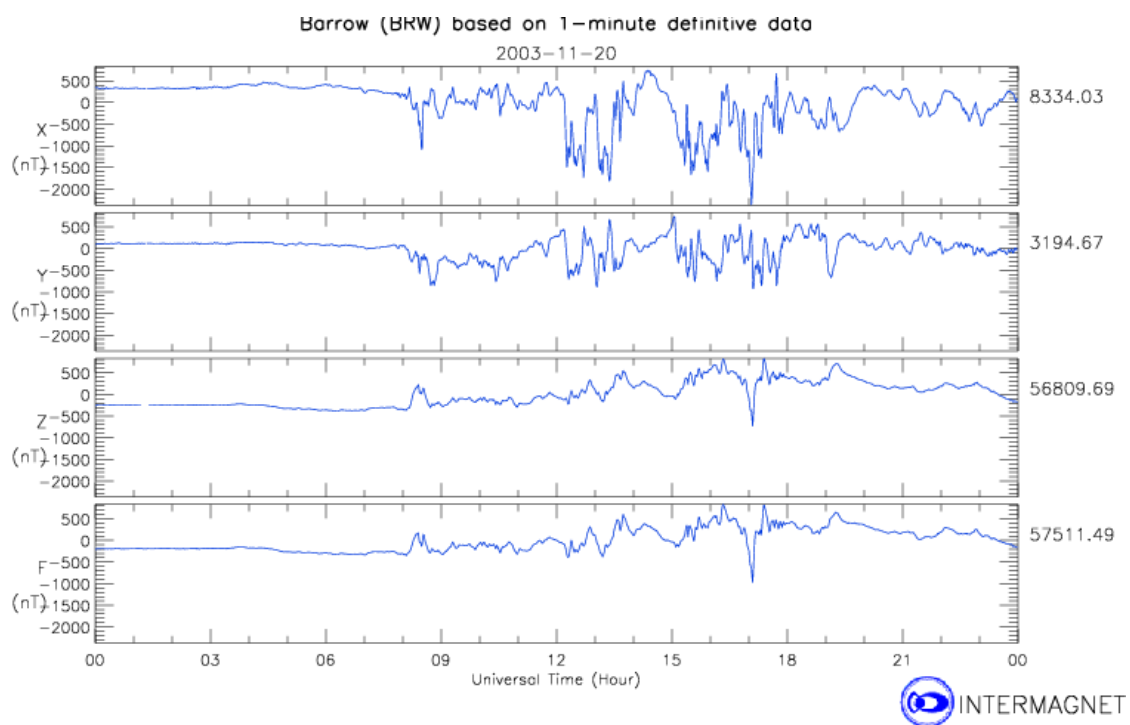


Figure 1.2: Magnetogram from Barrow (BRW) observatory showing a geomagnetic storm on 20/11/2003. The X, Y, and Z components are given in nT. The severity of the storm can be seen more on the X and Y components. With a Kp = 9- (INTERMAGNET)

1.2.2 Regular Variations

Due to the Earth's rotation and its orbital movement around the Sun and Moon's orbit around Earth, regular variation results in the geomagnetic field. The most prominent of the regular variations is the diurnal variation (solar daily variation). Diurnal variation is caused by the current system in the ionosphere, which drives winds from the day-night temperature difference and electrically conducting tidal winds caused by gravitational forces of the Sun and Moon. The currents in the ionosphere are negligible on the night side compared to daylight hours. This is because the solar radiation ionises the upper atmosphere during the day, increasing the density of ions that make up the currents in the ionosphere. The daily variation is only visible in magnetograms on days of low magnetic activity (solar quiet days) due to its relatively small intensities. Corresponding days of high magnetic activity are called solar disturbed days. The amplitude of the daily variation are of the

order of 10-100nT, and depends on time of year, solar activity and geomagnetic latitude. Figure 1.1 shows the characteristic behaviour of the diurnal (S_q) variation field.

Other regular variations showing magnetic effects include 27 days period corresponding to the rotation of the Sun's most active latitude zones, and Lunar variation due to gravitation of the Moon causing tides. The external field variations depend on the Sun and reach a maximum in intensity every 11 years – called the 11-year-solar-cycle.

1.3 Historical Background of Diurnal Variation

The S_q , diurnal variation or daily variation, depending on the authors and their interest, of the geomagnetic field was discovered by English Researchers, Graham and Watchmaker, through the observation of a compass needle motions in 1722 (Walker, 1866, Klausner et al, 2013). Graham also introduced the distinction between quiet and disturbed days.

Canton, in 1759, found in London that the mean range of daily oscillation of the needle on quiet days was larger in summer than in winter (over 13' in summer and less than 7' in winter). This was the first mention of annual period (Courtilot and Le Mouel, 1988).

In 1782, Dominique Cassini showed that the daily variation could not be due to daily variation in temperature.

Constant and detailed observations of the field became regular in the early part of the nineteenth century with far reaching and everlasting contributions to the study of geomagnetism by scientists, including Carl Friedrich Gauss. Gauss paid great attention to the quality of observations, making it possible to detect changes of a few arcseconds over a few minutes of time. In 1838, in his *Allgemeine Theorie des Erdmagnetismus*, Gauss introduced method of measuring absolute magnetic intensity, which allows one to follow variations in the full vector field. Gauss and Wilhelm Weber went on to discover the daily and longer variations of all remaining geomagnetic elements, other than D and I. He (Gauss) also derived the mathematical technique for separating the external and internal contributions to the surface field. He achieved this with his novel global analysis of the Earth's main field – Spherical Harmonic Analysis (SHA).

In 1866, Walker published the first modern textbook on geomagnetism in which he noticed a geomagnetic ordering of the S_q behaviour and proposed the existence of a unique magnetic equator (Walker, 1866).

Stewart (1882) put forward the theory that these variations are due to currents induced by dynamo action in some conducting layer of ionised gas (unknown then) on the sunlight side of the upper atmosphere, by a regular system of winds carrying the conducting gas across the lines of force of the main geomagnetic field. His discovery was the first scientific indication of the existence of an ionosphere. But before Stewart (1882) put forward his idea of an atmospheric dynamo theory to account for daily variations, there were several ideas. Among them were the 'drift current theory' and the 'diamagnetic layer theory'. These theories were discussed by Chapman and Bartels (1940) who concluded that none of them gave effects sufficiently large to account for the observations. With a limited set of observatory data, Schuster (1889, 1902) use the spherical harmonic analysis developed by Gauss to actually proved that the S_q source is external to the Earth; he further showed that external currents were a result of dynamo action (Schuster, 1908). Stewart (1882) deduced the ionospheric region 43 years before the discovery was formally credited to the later radiowave

studies in the 1920s. He reasoned that, “conductive currents established by the Sun’s heating influence in the upper regions of the atmosphere are to be regarded as conductors moving across lines of magnetic force and are, thus, the vehicle of electric currents which act upon the magnetometer.” He went on to conclude, using laboratory studies of ionized rarefied gases, that in this upper region the “conductivity may be much greater than has hitherto been supposed.” And went on to predict a day/night change in conductivity and surface field contributions from the secondary (induced) currents in the Earth.

Schuster (1908) also computed the upper atmospheric conductivity necessary to support the Sq dynamo current system (as shown in figure 1.3) a full 17 years before the radiowave discovery of the ionosphere. He ascribed this to the ionization of the atmosphere by solar ultraviolet radiation, and concluded that the sunspot variation of Sq resulted from the increase in that ionization at high sunspot times.

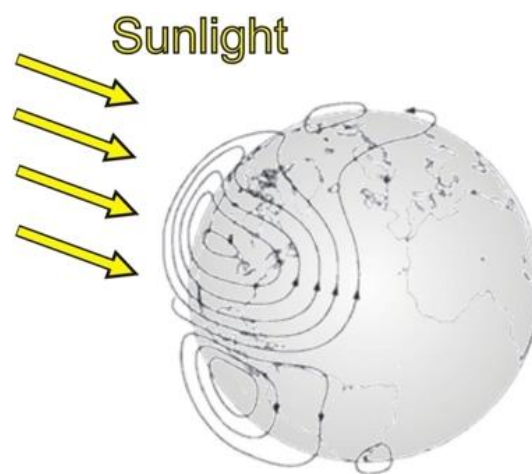


Figure 1.3: Schematic representation of the Sq current system. The diurnal nature of Sq originates from the concentration of these hemispherical vortices on the dayside of the Earth. The Equatorial Electrojet (EEJ) occupies the region between the two vortices. (Torta et al. 1997)

The explosive growth of the intense research and study on the ionosphere during the early/mid-20th century expanded our knowledge of the ionosphere and its surrounding. This also led to more research and studies on the theory of Sq.

Numerous studies were initiated to explain the behaviour of the ionospheric source of Sq field changes. Maeda (1955) and Kato (1956) calculated the ionospheric wind distribution responsible for Sq. Some studies and phenomena were brought to the world’s attention like the day-to-day variability of Sq studied by Hasegawa (1936a, b, c), the intense equatorial electrojet current (Bartels and Johnson, 1940a,b; Egedal, 1947, 1948), the theoretical explanations of the large increase in Sq(H) variation near the dip equator locations (Chapman,1951) and the major refinements of the dynamo theory of Sq (Maeda, 1952, 1955; Kato, 1956).

The expansion of the global observatory programme and the resulting establishment of World Data Centres as depositories of geomagnetic records during the International Geophysical Year (1957-1959), increased the spate of research and painted a new picture of the behaviour of Sq (Malin, 1973; Malin and Gupta, 1977; Campbell and Schiffmacher, 1985, 1988). Lots of the eye opening studies on the Sq behaviour came from this period with more light thrown on the magnetosphere/ionosphere interactions, helped by the advent of satellite research, which forced a complete review of the ionospheric dynamo theory (Price,1969; Pudovkin, 1974); but Richmond et

al. (1976) and Richmond (1979) showed that winds in the ionospheric region (80 – 200km) arising from solar heating were still the most likely cause of Sq currents; magnetospheric sources are only of secondary importance, especially at middle and low latitudes.

Progress in the studies of equatorial electrojet currents of Sq in the 1960s threw more light on understanding of an aspect of Sq current systems. In their studies, Chapman and Rao (1965) summarized this equatorial electrojet Sq current using analysis of the field variations from nine equatorial observatories, and described the location of the jet with respect to the geographic equator, range of increased of Sq with sunspot numbers and the loss of equatorial field enhancement with depletion of local E-region ionization. Other studies show that winds driving the dynamo in the ionospheric dynamo in the equatorial region were sensitive functions of location as well as local and universal time (Schieldreg et al., 1973)

The satellite research period which started in the 1960s not only resulted in more understanding of the magnetospheric/ionospheric interactions, but also showed the direction of the solar wind field at the magnetospheric boundary was important to the response of particles and fields measured at high latitudes.

Besides the daily magnetic field variation generally denoted by S , there is also a systematic though smaller periodic variation discovered by Kreil (1839) called the lunar daily magnetic variation denoted by L . It is a lunisolar variation associated with the period of rotation of the Earth relative to the moon. The source is believed to be similar to the atmospheric dynamo similar to that which gives rise to S .

1.4 Motivation

Magnetic mapping exercises involve measuring the amplitude or total field component of the geomagnetic field. Removing the time-varying part of this total field is a task of data magnetic reduction, and the most common time variation is the quiet daily variation, Sq. Even though much has been learned about many components of the geomagnetic field, Sq has not been intensively studied, especially the behaviour of Sq away from quiet time.

It is the aim of this study to use publicly available measurements from geomagnetic observatories around the world to investigate and analyse the geomagnetic diurnal variation, and hope that the understanding may in future lead to new improved models of the Sq and other aspects of diurnal variation. The study will aim to particularly consider the behaviour of Sq away from quiet time or higher levels of magnetic activity. To do this we will rely on spherical harmonic modelling of available geomagnetic data; well-characterised internal and magnetospheric components will be subtracted from the data, and global maps of the residual field generated at different local times.

Improving the global model of Sq and trying to establish the nature of variations for days away from quiet time to see how well we can understand them is very important, as it will directly inform the understanding of diurnal variation and its application in magnetic methods, especially geophysical exploration (aeromagnetic survey). Usually, magnetic surveys focus on the crustal field, which varies with long time-scale in other words, it is effectively constant. Significant effort is expended in removing the effects of external origin, with short-time scales (Sq and its induced components), from magnetic survey data. So the understanding and prediction of diurnal variation and its induced components has considerable economic application, as the diurnal variation (particularly its non-

diurnal variation) is the primary source of noise in aeromagnetic survey. Better understanding of Sq (and its induced component) and the nature of the variations away from quiet time, may lead to better procedures for correction of survey data.

1.5 Thesis Outline

Having established the background to, theories and basis for studying geomagnetic Sq diurnal variation, Chapter 2 explores the Earth's magnetic field. We consider the sources contributing to the Earth's magnetic field, information on magnetic activity indices, measuring the geomagnetic field, as well as various models in existence and the main model used in this thesis.

Chapter 3 focusses on modelling the magnetic diurnal field, both during quiet time and away from quiet time. An integral part is using the CM4 model to create models of the geomagnetic diurnal field at the Earth's surface, after the removal of well characterised internal and magnetospheric components from the data, prior to generating global maps of the diurnal field at different local times and spherical harmonic degrees.

Chapter 4 is dedicated to correlated errors, residuals and covariant modelling. After comparing the CM4 model and the observatory data, we need to explain the part of the observed field unmatched and not explained by the CM4 model. We look at the eigenvalues and eigenvectors from the residuals of the observatory and CM4 model data. The rest of the chapter is dedicated to matching the observatory data residuals against the RC index, to see if these variations seen are well fitted with the RC index.

In Chapter 5 we look at small scale features not resolved from the previous chapter. Here we assess the coherence and agreement between the residuals of the observatory data and RC index, comparing the results between them to establish the global spread of the variation, for correlation and cross-correlation coefficients.

Finally, the thesis concludes in Chapter 6 with some additional analysis, reviewing the main conclusions of the work, including attempt to look at the implications for magnetic surveys, and look forward to future work still to be done.

Chapter 2

The Earth's Magnetic Field

The following section will provide a brief overview of some important features, our understanding and observation of the geomagnetic field. We focus on the aspects most important for this study.

The idea that the Earth behaves like a great magnet was first proposed and published by Gilbert in 1600 in his *De Magnete* (Gilbert, 1600). Gilbert's work was extraordinary, not only for geomagnetism, but also for the fact that up till then it was only the second time that a unifying global property had been identified, after the much earlier discovery that the Earth was a sphere. Gilbert's work included seventeen years of his own research and brought together all the previous knowledge of geomagnetism. A major element of his work was the investigation of how a sphere of lodestone, which is a naturally magnetised piece of mineral magnetite, affected small magnetised needles placed on it.

The Earth's magnetic field affects our lives in many ways. The magnetic field shields us from cosmic radiation, it gives rise to the breath-taking natural phenomena of aurora, and it has been used for navigation through centuries. The need for reliable navigation increased as trading over large distances became more and more common as civilization evolved. Thus there was a strong incentive to monitor and study the magnetic field, and systematic observations began centuries ago.

To first approximation the Earth's magnetic field is that of a dipole at the Earth's centre, with the dipole axis tilted at approximately 12° with respect to the rotational axis, seen in figure 2.1. The magnetic south pole of the Earth's field points towards the geographic North Pole and vice versa. The magnetic field is predominantly generated in the liquid outer core, where convection of highly conducting material drives a self-sustaining dynamo. At the Earth's surface, currently the field strength is about 60,000 nT at the poles and 30,000 nT at the equator.

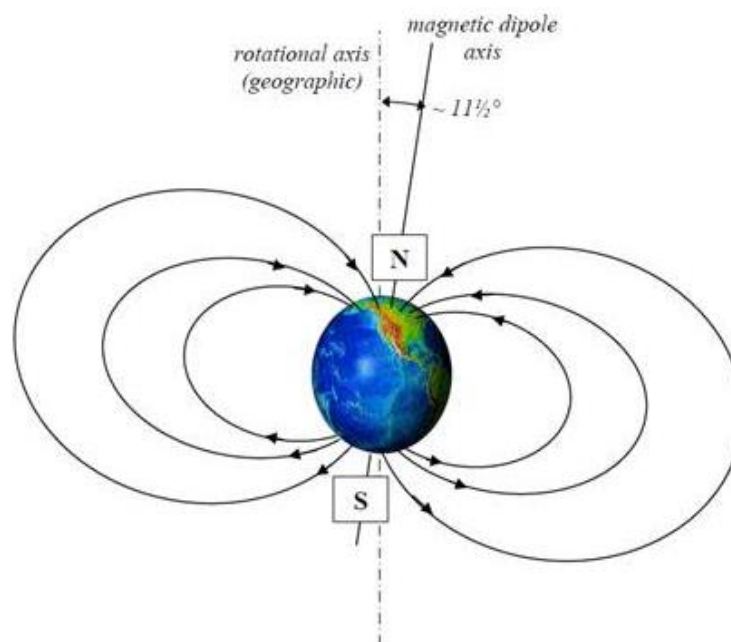


Figure 2.1: To a first approximation, the Earth's magnetic field is like the field of a magnetic dipole. (Lanza and Meloni, 2006)

Figure 2.2 shows the total intensity of the magnetic field at the surface. The centre of the dipole (only a representation) is displaced a few hundred kilometres from the Earth's centre, which gives rise to the South-Atlantic anomaly, also seen in figure 2.2. In this area the field is weaker and the protection against cosmic radiation is lower. This can be directly observed by the failure of satellites flying over the South-Atlantic anomaly. Due to the safety of airline staff and passengers, aircrafts are routed around the anomaly.

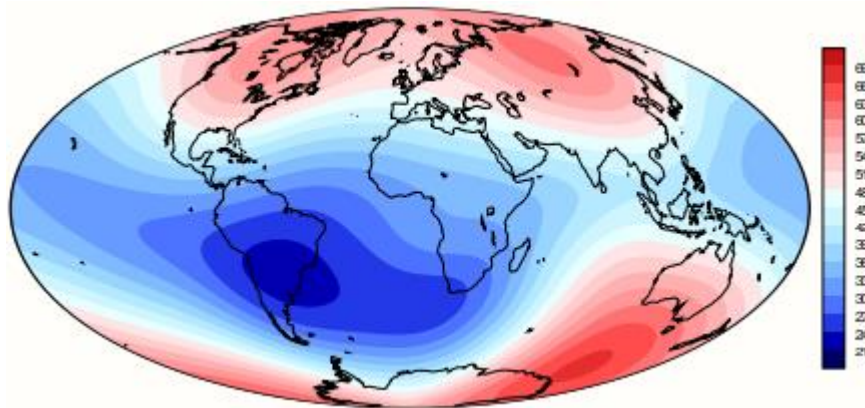


Figure 2.2: Total field intensity (F) at the Earth's surface in 2010 as predicted by the IGRF-11 model. Units in microTesla. The reduced intensity over the South Atlantic Anomaly (SAA) is the most remarkable non-dipolar feature. (Finlay et al. 2009)

The chapter begins with an overview of the sources contributing to the geomagnetic field in section 2.1. Next in section 2.2, the external field (magnetosphere and ionosphere), and the induced fields is discussed. In section 2.3, we present a review of the different magnetic activity indices. Section 2.4 is dedicated to discussion on measuring the geomagnetic field, while section 2.5 presents the mathematical description of the geomagnetic field, spherical harmonic analysis, existing models and modelling techniques. Finally in section 2.6, the chapter concludes with a summary of the various presentations in the chapter.

2.1 Sources Contributing to the Earth's field

The magnetic field measured at the Earth's surface or on board satellites is the sum of contributions from many different sources, internal, found below (in form of electrical currents and magnetised material) and external, above (in form of electrical currents only) the Earth's surface, which can be divided into two groups as shown in figure 2.3. The largest contributor is from the core field originating in the fluid outer core, which reaches intensities of around 55, 000 nT at satellite altitude (in this case 400 km). The lithospheric field typically ranges ± 20 nT when measured at satellite altitudes, but can be much higher at the surface where it is closer to its source region. In the atmosphere currents generated in the ionosphere and magnetosphere also produce their own magnetic fields, which can vary widely in intensity, both spatially and temporally, due to the solar inputs. Each of these sources produces contributions with specific spatial and temporal properties, which makes their identification and investigation of the contribution possible. These sources are examined and discussed further below.

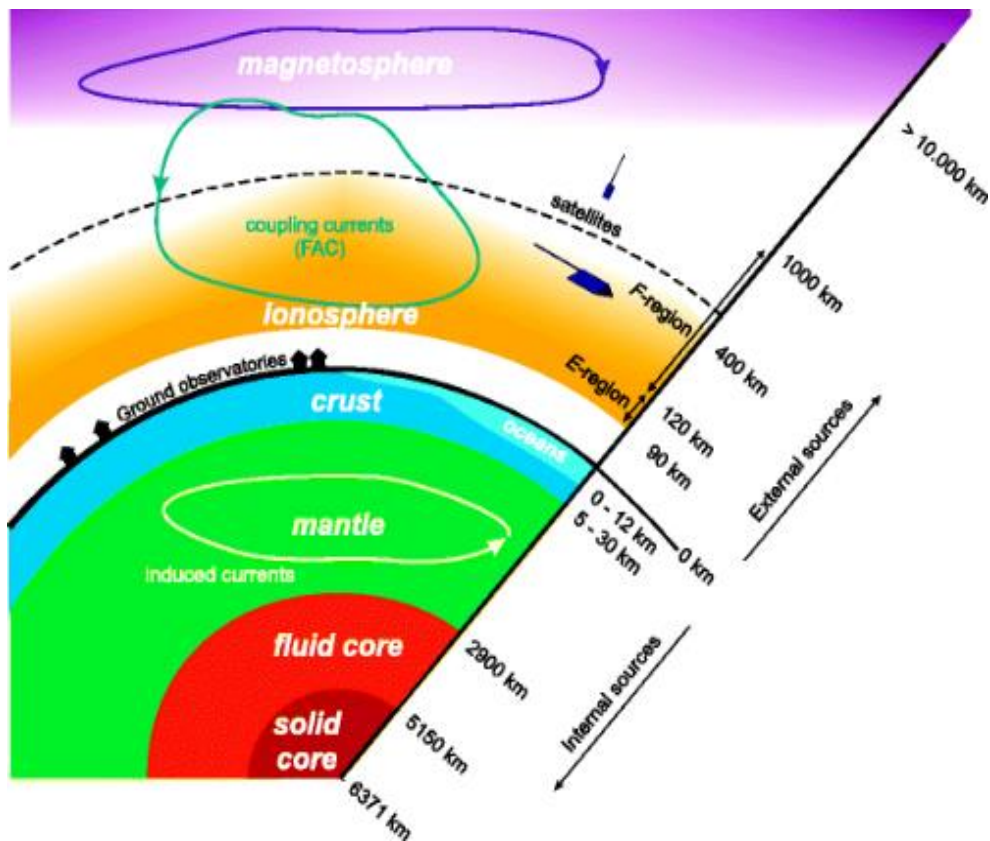


Figure 2.3: Sketch of the various sources contributing to the near-Earth magnetic field (from Olsen et al., 2010)

2.1.1 The Core Field

The Earth's magnetic field has been known for many thousands of years (Merrill et al. 1998), but was not until the nineteenth century that the core field was proven to be internal to the Earth. The core field, consisting of Iron-Nickel alloy, often referred to as the 'main' field, produces the largest contribution to the geomagnetic field. This is about 97% of the field observed at the Earth's surface. It is generated by electrical currents and driven by a dynamo process inside the Earth's molten outer core (Dormy and Le Mouel, 2008; Jonkers, 2007). The conducting iron convects from the inner core up to the Core Mantle Boundary (CMB) and it's deviated due to Earth's rotation by Coriolis forces. As a fundamental process, the convective motion of the conducting fluid within the field induces electromotive forces which maintain electrical currents, and therefore the magnetic field, against ohmic dissipation (Olsen et al., 2010c)

The main field features a dominant dipolar structure tilted by about 11° from the Earth's rotation axis as shown in Figure 2.1. Hence, the horizontal component points mainly in north-south direction and allows compasses to orient. At the poles, the field intensity amounts presently to 60,000 nT at the poles and decreases to its half, 30,000 nT, near the equator (Sabaka et al., 2002). The core field is not static, instead exhibiting significant spatial and temporal variation when viewed on long timescales. Furthermore, the strength of the dipole is currently (since 1840, and probably earlier [Suttie et al.2011]) decaying at a rate of about 15 nT/yr (Gubbins et al., 2006). While at the same time there is a general westward drift of the entire field, as well as smaller range regional change. Edmund Halley's famous voyages between 1698 and 1700 in the North and South Atlantic oceans led him to discover this phenomenon, which in itself led to the first declination chart of the Earth published in 1702 (Merrill et al., 1998).

Much of this change, which is long term, and originating in the core is known as secular variation (SV) as a first time derivative. Even though details of the cause of this secular variation (the SV itself is understood) are not yet fully understood, SV are clearly evident in the time-series of magnetic vector field data from geomagnetic observatories.

During the last years, much attention has been drawn to abrupt changes detectable in the SV. Especially the last century's time series of the second derivative of the East component shows jumps. Those geomagnetic jerks as they are usually called (Courtillot and Le Mouel, 1984) happen to appear globally. Since Alexandrescu et al. (1995) detected jerks by wavelet analysis, several of these events are broadly accepted. Prominent examples are the jerks in 1969 and 1978 (Courtillot and Le Mouel, 1988).

These jerks which are believed to be of internal origin (Malin and Hodder, 1982; Dormy and Manda, 2005; Manda et al. 2010) have important implications for some core related studies such as variations in changes in the angular momentum in the core, variations in the length of day (Holme and de Viron, 2005; 2013), lower mantle conductivity (Nagao et al., 2003), etc.

The magnetic field has a complex nature which allows it to be used to probe many diverse regions of the Earth (Whaler, 2007). In situ measurements of the core are beyond technological reach, and so all our knowledge about the state of the core is based on measurements at or above the Earth's surface, theoretical studies and small scale simulation experiments. The core field and its secular variation are among the few means available for studying the properties of the outer core (Olsen et al., 2002). This has been used to study the core-mantle interactions and to constrain flow in the core and the dynamo process thought to be responsible for producing the field (Holme and Olsen, 2006). Only a part of the core field reaches the Earth's surface and is observable. This is because its small-scale contributions, spatially, are masked by the crustal field and therefore only its largest scales can be recovered, corresponding to spherical harmonic degree 14 and below (this is illustrated in spatial power spectrum plot shown in fig 2.4) (Olsen et al., 2010c). This, in addition to the fact that the high frequency part of the core field is screened by the finite conductivity of the mantle, puts severe limitations on the possibility of recovering the spatiotemporal structure of the core field, no matter the quality of magnetic field observations (Alexandrescu et al. 1999).

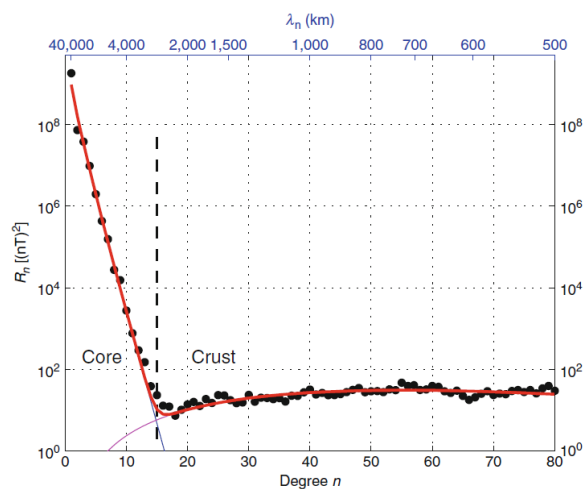


Figure 2.4 Spatial power spectrum of geomagnetic field at the Earth's surface. Black dot represent spectrum of recent field model, blue represents theoretical spectra for the core, magenta for crustal part of the field, while red shows their superposition. The sharp 'knee' at about degree $n = 14$, representing the black vertical dash line, shows the separation between the core and crustal fields. Core field dominate at large scales ($n < 14$), while crustal field dominate at smaller scales ($n > 14$) (from Olsen et al., 2010c).

2.1.2. The Crustal Field

While not nearly having the same level of intensity as the core, the Earth's lithosphere has an associated magnetic field, commonly referred to as the crustal or lithospheric field, which arises from the remanent magnetism in the magnetic rocks of the crust and upper mantle (generally assumed to be induced). It is responsible for the second largest contribution to the magnetic field of the solid earth as measured at the surface of the Earth (Mandea and Purucker, 2005). The crustal magnetic field on the earth is small scale, reflecting the process (internal and external) that shaped the earth. At space craft altitude, it reaches amplitude of about 20nT (Langlais et al., 2009). The main characteristic of the crustal field is that it is weak (Maus et al., 2002) and overlapped by other field sources in the magnetic field measurements. Hence, its complete description requires a large amount of spatially dense measurements covering the earth's surface and various altitudes. The amount of magnetisation depends on various parameters, such as the strength and direction of the ambient magnetic field, the mineralogy of the rock sample, its magnetic phase and domain, whether single or multi-domain and how easily the domain walls move under the influence of the ambient field, its grain size and shape, the amount of chemical alteration, and the temperature. This makes the subject of rock magnetism of considerable complexity but the mechanisms are well known in principle (Thebault et al., 2010; Dunlop and Özdemir 2007).

The rocks found in the Earth's crust are capable of carrying both remanent and induced magnetisations. As crustal rocks cool through their Curie temperature, they acquire a remanent magnetic field proportional to the ambient field at the time; sedimentary rocks can also acquire a permanent field component dependent on the ambient field around the time of their compaction (Whaler and Langel, 1996). This crustal field source is spatially limited to a relatively thin layer of about 20-50km thick. Depending on the local heat flow, it may exceed 60km or be less than 20km in local areas (Maule et al., 2009), since below it the internal temperature of the Earth rises to a level above the Curie temperature which can mitigate the formation and maintenance of remanent magnetic fields (as rocks heated above their Curie temperature becomes practically non-magnetic) or induced fields i.e. ferromagnetic mechanism doesn't work.

Since it is essentially static over time, at least on time scales comparable to the core and external field sources, a mapping of crustal field on its own is referred to as an anomaly map. There is high variability of the magnitude of the field at Earth's surface with amplitude reaching thousands of nT and highly dependent upon the characteristic geology of the region. This can be gleaned from features such as the Bangui Anomaly in Central African Republic and the Kursk Anomaly in Russia (Mozzoni, 2008). Magnetic anomaly maps of crustal magnetisation have been produced through ship and airborne surveys; however, such near surface surveys cannot reliably determined magnetic anomalies with wavelengths of more than 500km (Maus et al., 2002). A key issue in producing global magnetic anomaly maps is the control of the longest wavelengths (Ravat et al., 2002). Only short wavelengths are resolvable (less than 2500km or above spherical harmonic degree, $n=13$), as longer wavelengths are masked by the much larger core field (as shown in figure 2.4).

Satellites can provide global perspective of magnetic anomalies with wavelengths of more than a few hundred kilometres (Sabaka et al., 2004; Olsen et al., 2006; Maus et al., 2007). High quality measurements from satellite missions (Ørsted, CHAMP, Sac-C and Swarm) are opening a new era in mapping of the crustal magnetic anomalies and have greatly improved the spatial resolution of lithospheric magnetic field models. This is inevitably opening new possibilities and opportunities for

geophysical and geological interpretation. Figure 2.5 is an example of the Comprehensive Model (CM4) lithospheric field model for spherical harmonic degrees 15-45. The map clearly identifies major magnetic anomalies in West Africa, Gulf of Mexico, South Australia, etc.

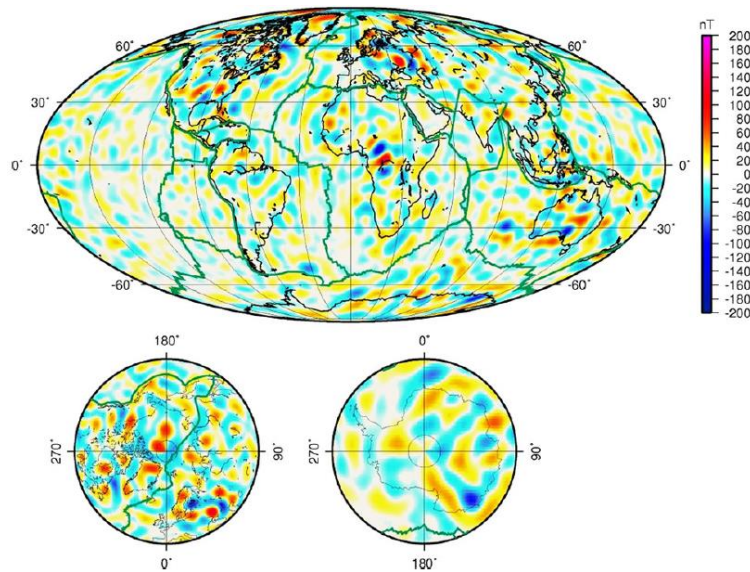


Figure 2.5: Vertical component of the CM4 lithospheric magnetic field model at satellite altitude at the Earth reference radius, with plate boundaries indicated in thick dark green lines (from Sabaka et al., 2004).

The crustal field shows a tendency to scale with the strength of the main field which makes it particularly weak in the South Atlantic and strong at the poles. Magnetic Anomaly maps have many uses, ranging from geologic prospecting to paleomagnetic studies.

2.2 The External Fields

The source of the remaining contribution of the Earth's magnetic field variation, not from within the Earth, comes from complex system of currents in the ionosphere and magnetosphere and are termed external field variations. The external magnetic field as observed at or near the Earth's surface is the combined effect of the resultant magnetic fields from these various current systems at any single time. Much of the external field variation on Earth is powered by driving forces arising directly or indirectly from the Sun. The Earth resides in a magnetic environment imposed by the presence of the solar wind plasma which streams from the Sun. Interaction between the Earth's magnetic field and the solar wind defines the Earth's magnetic field environment (Mandea et al., 2005).

The external magnetic field sources can be roughly divided into three classes (Maus and Luhr, 2005). These are the magnetospheric currents above satellites, ionospheric currents below satellites and field-aligned currents (FAC) connecting the two regions. The solar wind from the Sun modifies the current systems in the magnetosphere and ionosphere, thereby producing magnetic variations on varying timescales from seconds to solar cycle. This solar wind, which is a plasma of ionized atoms and electrons, radiates outwards from the Sun, with an average velocity of about 450km/s (Siscoe and Odstrcil, 2008; Potgieter, 2005). The nature of the plasma is highly conductive and this enables it to carry with it the Sun's magnetic field, called Interplanetary Magnetic Field (IMF). Due to its infinite conductivity, the solar wind confines the Earth's magnetic field to a cavity called magnetosphere whose inner boundary is the ionosphere. Currents in both the magnetosphere and ionosphere cause magnetic fields which have been measured throughout the magnetosphere (Langel et al., 1996).

2.2.1 Magnetosphere

The magnetosphere is the region formed out of the solar wind flow of plasma by the interaction with the Earth's magnetic field. It is an elongated structure interfacing with the Sun's solar wind at approximately $10R_E$ (Earth radii) on the sunward side (dayside), under quiet conditions (Pulkkinen, 2007), while in the anti-sunward direction, the field lines stretch into the magnetotail which extends to at least $60R_E$ (Langel et al., 1996). The magnetosphere contains various large-scale regions, which vary in terms of the composition, energies, and densities of the plasma that occupy them.

There is great variability in the morphology of the magnetosphere, but the basic morphology of the magnetosphere is fixed to the Sun (Langel et al., 1996). The magnetosphere is a very highly dynamic structure as shown in figure 2.6, and it responds quite dramatically to changes in dynamic pressure of the solar wind. It has strong dependence on the orientation of the interplanetary magnetic field (IMF) and solar wind properties (Menvielle and Marchaudon, 2007). The ultimate source of energy is the interaction with the solar wind. Some of the energy extracted from the interaction goes directly into driving various magnetospheric processes, while some is stored in the magnetotail to be released later in substorms. The principal means by which energy is transferred from the solar wind to the magnetosphere is a process known as reconnection which occurs when the IMF is oriented antiparallel to the orientation of the Earth's field lines (Dungey, 1961; Lester et al., 2006). This orientation allows IMF lines to merge, resulting in the transfer of energy, mass and momentum from the solar wind to the magnetosphere. The complicated system of currents which exists within the magnetosphere helps to dissipate the energy, which is then transferred to the magnetosphere from the solar wind.

The outer boundary of the magnetosphere is the magnetopause. Generally, the strongest currents in the magnetosphere are located in the boundary layers. The magnetopause currents cancel the Earth's magnetic field outside and cause to swell by pressuring the field within the cavity (Olsen et al., 2010b). This produces an elongated tail, within which is a current sheet called neutral-sheet currents, a region of high plasma density which flow between the northern and southern lobes of the tail where the magnetic field lines are in opposing directions (Langel et al., 1996).

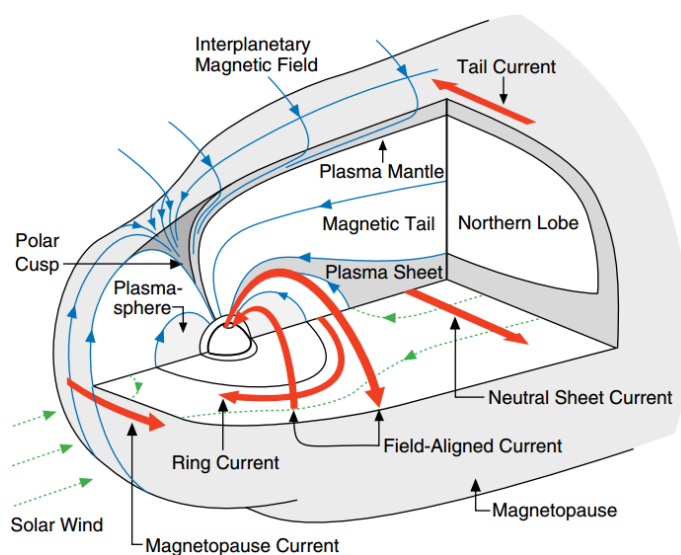


Figure 2.6: Cutaway illustration of the magnetosphere showing its plasma regions and current system (from Russell, 2000).

As a result of the interaction between the solar wind and magnetosphere plasma, the magnetopause (or Chapman-Ferraro) current flows at the magnetopause boundary (Menvielle and Marchaudon, 2007). A Field-aligned current (Birkeland currents) which flows along magnetic field lines also linked the magnetosphere and ionosphere. The interaction of these currents with the radiation belts near the Earth produces a ring current in the dipole equatorial plane which encircles the Earth partially (Olsen et al., 2010b). When the entire magnetosphere is disturbed and this condition persists for several hours, the term magnetic storm is used to describe the state of the magnetosphere at this point. The primary measure of the intensity of a magnetic storm is the strength of the ring current, which is quantified by the D_{st} index (see section 2.3.2) (Gonzalez et al., 1994; O'Brien and McPherron, 2000). The ring current resides in the inner magnetosphere circling the Earth near the equatorial plane, and is the main source of the magnetospheric field (Lesur et al., 2005).

2.2.2 Ionosphere

The ionosphere represents the partially ionised upper atmosphere and lower boundary of the magnetosphere, extending from approximately 60km-1000km. but more importantly, it represents one of the main sinks of energy transmitted from the solar wind to the magnetosphere (Lester et al., 2006). It is created by solar radiation and particle precipitation that ionise the neutral atmosphere, making it the electrically conducting part of the upper atmosphere where solar radiation, X-ray and ultraviolet (UV) ray maintains partial ionisation (Love, 2008; Kivelson and Russell, 1995). The ionosphere is divided into three main strata (shown in figure 2.7), each layer independently produced via absorption of solar heat and respond differently (Backus et al.'1996; Luhmann, 1995):

- D-region (60-90km): Deepest of the layers and maintained by the most energetic radiation which can penetrate to this low altitude. This region is also of particular importance for radio communication.
- E-region (90-130km): Ionized mainly by soft X-ray (1-10nm) and UV radiation. Disappears at night because the primary source of ionisation is no longer present.
- F-region (130-600km): Densest part of the ionosphere where the highest ionospheric plasma densities reside, and signals penetrating this layer will escape to space. It is further subdivided into F1 and F2 regions, which merges during the night.

Heating of the ionosphere drives tides in the atmosphere. These tidally driven winds present in the ionospheric dynamo region generate currents which peak between 100-150km altitude (Stening, 2003; Langel et al., 1996; Olsen et al., 2010b). Figure 2.8 shows the important currents flowing in the ionosphere. These currents are present owing to the diurnal variation of solar heating, with some effect of differential attraction of the Sun and Moon. During quiet times, when the magnetic field is relatively undisturbed by solar activity, these ionospheric dynamo currents give distinct diurnal variation to observatory magnetograms. These resulting fields are called solar quiet field variations or Sq (Langel et al., 1996; Love, 2008). These currents take the form of two circulating systems (see figure 2.9), with anti-clockwise vortex and a clockwise vortex in the northern and southern hemispheres respectively (Kuvshinov, 2008).

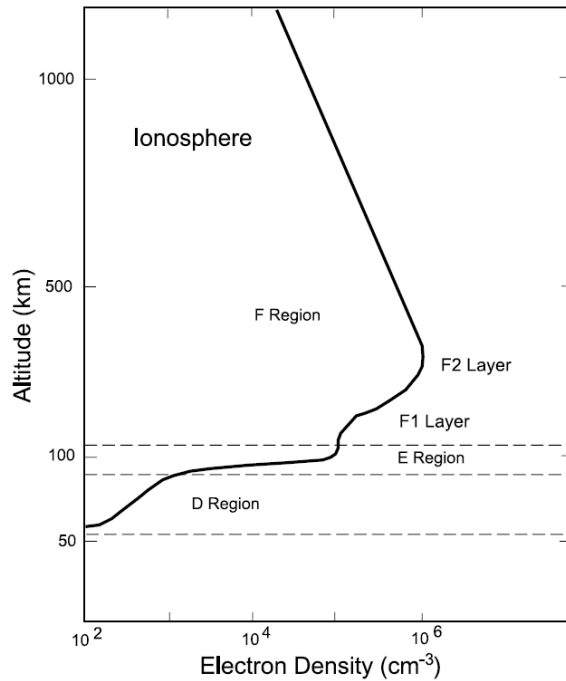


Figure 2.7: Profile of the ionosphere showing the different strata of D, E and F (which splits into F1 and F2 on the dayside) (from Kivelson and Russell, 1995).

At the dip equator, the magnetic field is strictly horizontal, where the magnetic field lines are near parallel to the surface of the Earth. The configuration give rise to an enhanced effective Hall conductivity, called Cowling conductivity. This result in a strong eastward Hall current, called the equatorial electrojet (EEJ), flowing along the dayside dip equator. At equatorial observatories, the quiet day magnetic field variations are enhanced fivefold (Olsen et al., 2010b) or threefold (Kuvshinov, 2008) or by a factor of two (Langel et al., 1996), in the daily variation of the horizontal component of the magnetic field.

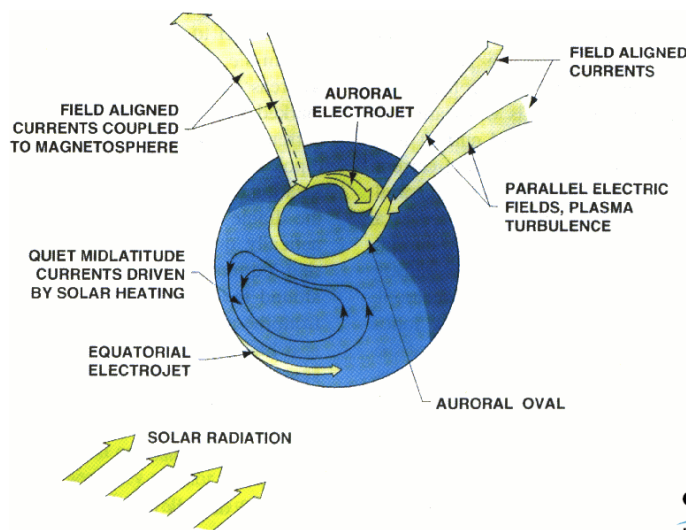


Figure 2.8: The dominant current systems associated with the Earth's ionosphere, after Langel et al. (1996)

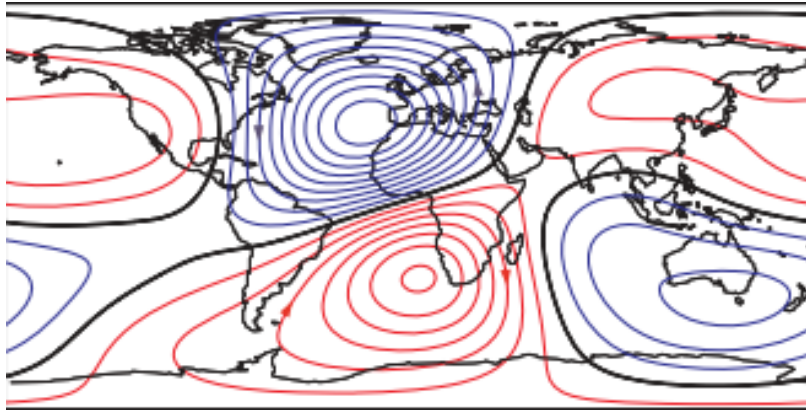


Figure 2.9: Circulating electric current systems in the ionosphere that sustain quiet-time variation. Contour lines indicate 10-kA increments; more densely packed contour lines indicate higher local current density. Red contours indicate clockwise circulating current and blue contours anti-clockwise current. From Love (2008).

Besides Sq daily variations, ground magnetic perturbations are also caused by a secondary component due to gravitational attraction of the moon, termed the L effect (L for Lunar). The resultant field produced from L variations is much smaller than the Sq field (Yamazaki and Kosch, 2014) and difficult to isolate, because of the similarity between the length of the solar and lunar days. Although more complex and dependent on lunar phase as well as season, this signal is not of great concern to magnetic surveys, except possibly at high latitudes where it can, at times, reach 10nT in amplitude (Regan and Rodriguez, 1981).

2.2.3 Induced Fields

These are externally induced fields and highly time varying which produced secondary induced currents in the oceans and the electrically conducting Earth's interior (Olsen et al., 2010b). They are the topic of electromagnetic induction studies (Parkinson and Hutton, 1989; Constable, 2007). Furthermore, secondary currents are produced by motional induced induction through the motion of electrically conducting seawater through the Earth's internal magnetic field (Olsen et al., 2010b; Kuvshinov and Olsen, 2005; Maus 2001b).

The amplitude of induced contributions decreases with period i.e. about one-third of the observed daily Sq variation in the horizontal components is of induced origin (Olsen et al., 2010b; Maus and Weidelt, 2004; Schmucker, 1985). But the size and amplitude of this induced field vary greatly depending on the strength, period, scale of the source (ionospheric and magnetospheric current systems) of the inducing field, and the conductivity structure of the Earth (Olsen et al., 2010b;)

2.2.4 The Ring Current

The ring current is the main source of the magnetospheric field (Lesur et al., 2005), flowing between $4R_E$ and $6R_E$ (Baumjohann and Nakamura, 2001). It resides in the inner magnetosphere circling the Earth near the equatorial plane, flowing along the magnetopause on the sunward side and the magnetotail on the anti-sunward side. It arises from trapped ions drifting longitudinally across the geomagnetic field lines (Stern, 2006). It is the key element of magnetic storms in the near Earth space (Daglis et al., 1999), and it is the primary measure of the intensity of the strength of a magnetic storm, which is quantified by the D_{st} (see section 2.3.2) (Gonzalez et al., 1994; O'Brien and McPherron, 2000). It consist of current due to the eastward (electron) and westward (proton) drift in the radiation belts (Russell, 2001), but is mainly westward (Langel et al., 1996).

The ring current causes a net decrease in the magnetic field on the surface of the Earth (Dessler and Parker, 1959; Sckopke, 1966; Russell, 2001) as opposed to the magnetopause current that causes an increase (Russell, 2001). The ring current strength varies depending on the local time, especially during magnetically active periods, producing the highest intensity near the dipole equatorial plane (Langel et al., 1996). There has been wider interest in magnetic storms owing to severe effects they have on technological systems. Reports have referred to disturbances or even permanent damage of telecommunication and navigation satellites, telecommunication cables, and power grids (Lanzerotti, 1994; Kappenman et al., 1997; Daglis et al., 1999). The ring current achieves closure in and out of the ionosphere through the field-aligned currents (FAC) (Sabaka et al., 2002).

2.3 Magnetic Activity Indices

An attempt to characterise geomagnetic activity was first made as early as 1885, aimed at estimating geomagnetic disturbances on a daily basis (Menvielle, 2001). Geomagnetic disturbances are monitored at ground-based magnetic observatories, and the measurements of the magnetic field (in terms of the three magnetic field components, X Y Z) made at these observatories are used to derive geomagnetic indices. These indices describe irregular variations in the field and give much information about the magnetospheric and ionospheric phenomena, where they originate from (Mayaud, 1980; Love and Remick, 2007; Verbanac et al., 2010).

Geomagnetic indices are important for many reasons, and therefore used in different research domains. There are two main purposes when defining geomagnetic indices:

- To estimate global magnetic field characteristics, which attempts to describe, on a planetary scale, the magnetic activity or some of its components.
- To fully describe field variations associated with isolated physical events/activities; example is the D_{st} index specifically designed for monitoring ring current.

Geomagnetic indices provide data series, often used to identify quiet or disturbed data, and allow for statistical, modelling or direct studies over long time periods to make it possible to characterize physical processes (Menvielle, 1998). There are various geomagnetic indices based on different measurements and related to different ionospheric and magnetospheric processes. K_p and D_{st} indices are typically used for data selection (see section 3.1) when modelling the geomagnetic field, with the D_{st} commonly used in external field parameterization (Olsen et al., 2007). Auroral Electroject (AE) index provides a measure of the overall activity of the electrojects (Menvielle and Marchaudon, 2007), and have been used to study phenomena such as magnetic storms (Nikolaeva et al., 2011), and characteristics of substorms (Kullen et al., 2009), solar wind parameters (Murayama, 1882), total energy dissipation in the Northern hemisphere (Østgaard et al., 2002) and auroral X-ray intensity (Zhao and Tu, 2005); while the Polar Cap (PC) index monitors geomagnetic activity over the polar caps, generated by the solar wind coupling with the magnetosphere (Troshichev et al., 1988).

Table 2.1 gives a list of some commonly used indices, and the derivation scheme of the 'classical' IAGA indices (the observatories used are shown in figure 2.10), including the time intervals used for their calculations. We have described in more detail below some of the indices utilized in this present study (including a newly introduced index, the RC index).

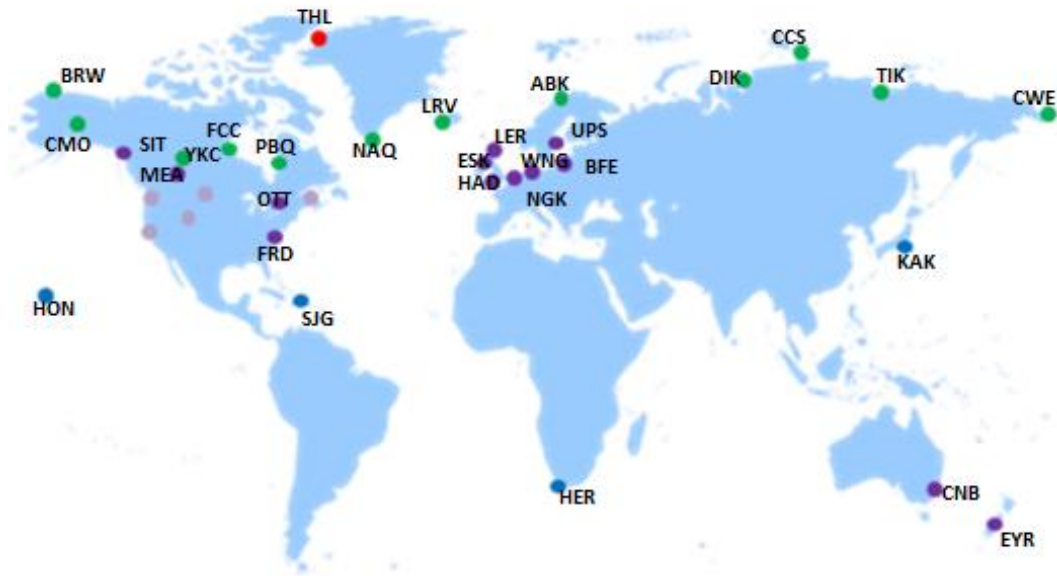


Figure 2.10: Magnetometer station locations used to calculate some geomagnetic indices: Planetary Geomagnetic (K_p) – Purple, Disturbed Storm Time (D_{st}) – Blue, Polar Cap (PC) – Red, Auroral Electrojet (AE) – Green

| Indices (beginning of the data series) | Measured Quantity Baseline | Time interval | Network |
|---|--|--------------------------|--|
| Planetary Indices K_p (since 1932) | K indices | 3 hours | Network of 13 stations: 11 boreal ones and 2 austral ones(see figure 2.10) |
| Polar Cap Index PC (since 1977) | Derivations ΔH & ΔD (nT) In the horizontal components. Baseline: Quiet level | 1 minute | Network of 2 Polar Cap stations. North (PC_N): THL South (PC_S): VOS |
| Auroral indices AE (since July 1957; missing data in 1976-1977) | Derivations ΔH (nT) In the horizontal component H. Baseline: Sq variation | 1 minute (since 1978) | Network of 12 stations in the boreal auroral zone. |
| Equatorial Index D_{st} (since 1957) | Variation ΔH (nT) Of the horizontal component H Baseline: Secular variation | 1 hour | Network of 4 low latitude stations. |

Table 2.1: K_p , PC, AE, and D_{st} geomagnetic activity indices (After Berthelier, 1993)

2.3.1 K_p Index

The principal geomagnetic disturbance index is called the K index obtained from the H component of the magnetic field (or D component if it is more disturbed than H) and divides activity into 10 levels (Campbell, 1997). It was introduced by Bartels et al., (1939), and the first to be proposed at an international level and adopted in 1939 by the International Association of Terrestrial Magnetism and Electricity. Subsequent refinement led finally to the definition of the planetary K index, K_p (Bartels, 1949; Thomsen, 2004).

The K_p index is used in the study of geomagnetism to describe planetary geomagnetic activity. It attempts to provide an approximate global proxy of the overall geomagnetic activity by measuring the magnetic disturbances and effects of solar radiation derived from K-indices at 13 observatories shown in table 2.2. It is a 3-hour magnetic activity index and widely used for measuring the level of magnetospheric activity. Since being introduced by Bartels (1949), other magnetic indices have been developed, but K_p have been one of the most widely used index, due partly to its ready availability and its long existence, for exploring the causes and consequences of geomagnetic activity (Thomsen, 2004). Many magnetospheric properties correlate well with it, from latitudinal extent of the auroral (Feldstein and Starkov, 1967; Thomsen, 2004). In contrast to the K scale which has values 0 to 9, K_p index scale has further divisions, 0o, 0+, 1-, 1o, 1+, 2-, 2o, 2+,, 9-, 9o (see figure 2.11). The values 0-3 are in accord with quiet state of geomagnetic activity, 4 is in accord with disturbed ones, and 5-9 correspond to magnetic storms of different intensity described by D_{st} index.

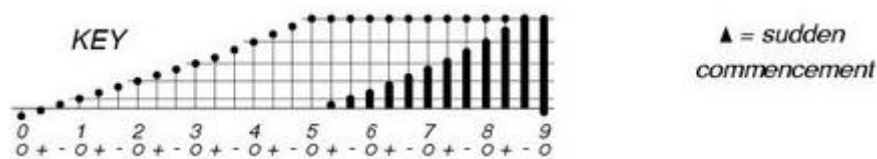


Figure 2.11: Musical diagram key illustrating geomagnetic K_p index (from GFZ POTSDAM).

Two disadvantages of the K_p as a global magnetic index is:

- It has very little input from southern hemisphere Most of the 13 stations used are mostly at subauroral latitudes and the locations favour northern hemisphere and European continent (even though the distribution is highly non-uniform) (see figure 2.10).
- By using a three hour range selection, a frequency dependence is introduced, which makes K_p discriminates against slowly changing, major departures of the field, like the storm recovery phase, and therefore, favours the irregular variations near 3 hours in period (Campbell, 1997).

Despite these problems, K_p is still very useful in preliminary selection of disturbed and quiet day's data and in general geomagnetic studies – such as solar cycle variations in magnetic activity, auroral boundary size (Milan et al., 2010; Carbary, 2005), interplanetary magnetic field parameters (Barkhatov et al., 2008) and solar wind velocity (Snyder and Neugebauer, 1963).

| Observatory | Code | Latitude | Longitude | Active |
|----------------|------|----------|-----------|-----------|
| Abinger | ABN | 51.11° | 359.37° | 1932-1957 |
| Hartland | HAD | 51.00° | 353.50° | 1957-now |
| Agincourt | AGN | 43.47° | 280.44° | 1932-1969 |
| Ottawa | OTT | 45.26° | 284.27° | 1969-now |
| Cheltenham | CLH | 38.42° | 283.12° | 1932-1957 |
| Fredericksburg | FRD | 38.20° | 282.60° | 1957-now |
| Eskdalemuir | ESK | 55.30° | 356.80° | 1932-now |
| Lerwick | LER | 60.10° | 358.80° | 1932-now |
| Lovö | LOV | 59.34° | 17.82° | 1954-2004 |
| Uppsala | UPS | 59.19° | 17.21° | 2004-now |
| Meanook | MEA | 54.62° | 246.65° | 1932-now |
| Rude Skov | RSV | 55.51° | 12.27° | 1932-1984 |
| Brorfelde | BFE | 55.60° | 11.70° | 1984-now |
| Sitka | SIT | 57.06° | 224.67° | 1932-now |
| Wingst | WNG | 53.80° | 9.10° | 1938-now |
| Witteveen | WIT | 52.49° | 6.40° | 1932-1988 |
| Niemegk | NGK | 52.04° | 12.41° | 1988-now |
| Amberley | AML | -43.09° | 172.43° | 1932-1978 |
| Eyrewell | EYR | -43.42° | 172.35° | 1978-now |
| *Toolangi | TOO | -37.32° | 145.28° | 1919-1986 |
| Canberra | CNB | -35.18° | 149.00° | 1978-now |

Table 2.2: K_p Network stations: Northern hemisphere stations are in red and southern hemisphere stations in black. *The Toolangi observatory operated until early 1986. Absolute control of the variometers at Toolangi ceased at the end of June 1979 after which mean magnetic values were no longer reported. Rapid variation phenomena ceased to be reported after 1981 and K-indices ceased to be scaled after September 1984. The vario- meters at Toolangi were finally dismantled in February 1986. Having been established in 1978, the Canberra Magnetic Observatory gradually replaced Toolangi as the principal magnetic observatory in the south-eastern Australian region. The reporting of mean values began in 1979, the reporting of K-indices began in 1981, and the reporting of rapid variation phenomena began in 1982.

2.3.2 D_{st} Index

The Disturbed Storm Time (D_{st}) index is one of the commonly used geomagnetic indices to indicate the severity of global magnetic disturbances. It measures the magnetic field (in nT) created by the ring current caused by trapped particles around the Earth, using hourly values derived from measurements by four observatory stations located near the geomagnetic equator (shown in figure 2.10 and table 2.3).

| # | Observatory | Code | Latitude | Longitude |
|---|-------------|------|----------|-----------|
| 1 | Hermanus | HER | -34.40° | 19.22° |
| 2 | Honolulu | HON | 21.32° | 201.98° |
| 3 | Kakioka | KAK | 36.23° | 140.18° |
| 4 | San Juan | SJG | 18.11° | 293.85° |

Table 2.3: Locations of D_{st} observatories

The discovery of D_{st} started when Moss (1910) observed the existence of a general depression of the horizontal magnetic field, recorded in magnetometer data at near-equatorial observatories. But it was Chapman (1919) who first used the name ' D_{st} ' for the average storm-time signature of the field disturbance, identified after the removal of a baseline and the regular daily variations. The exact formulation of D_{st} was firmly settled in 1964 (Campbell, 1997), and was then officially

adopted by IAGA as a standard activity index in 1969 (Resolution 2. p 123, in IAGA Bulletin 27, Madrid, 1969).

D_{st} , unlike the K_p index which parameterises mid-latitudes activity, is aimed at monitoring the axisymmetric part of the magnetospheric ring current in the horizontal component (Sugiura, 1964; Menvielle and Marchaudon, 2007). At latitudes near the dipole equator, the horizontal component of magnetic disturbance is dominated by the intensity of the magnetospheric ring. The magnetic field is thus affected by geomagnetic storms, which decreases the geomagnetic field at the Earth's surface, and this depression is what D_{st} measures (O'Brien and McPherron, 2000). The D_{st} index is a direct measurement of the hourly average of this disturbance across multiple magnetic observatories, but the computation involves careful removal of quiet time values from the horizontal component traces and an adjustment for location (McPherron, 1995). However, Campbell (1996) had shown that it is not purely a ring current contribution, but additional contributions come from the dayside magnetopause current, field-aligned currents, tail currents and induced currents in the ground (Kamide et al., 1998; Karinen and Mursula, 2005).

The D_{st} index is one of the most widely used indices in studies of the magnetosphere (Love and Remick, 2007), and still a reliable indicator of the size and magnitude of the magnetospheric activity at mid-to-low-latitudes where the ring current dominates (Mendes Jr. et al., 2006). Studies such as solar wind parameters (Murayama, 1982), ring current investigations and field modelling have widely employed the use of D_{st} .

Despite the above, D_{st} index derivation has a major problem of been limited in terms of the distribution of contributing observatory stations (the four locations are unevenly spaced in longitude, with large gap in central Asia and three located in the Northern hemisphere) (Campbell, 1997).

2.3.3. RC Index

D_{st} Index is used traditionally in geomagnetic field modelling as a measure of and describing the time-space structure of the magnetospheric ring current for data selection and for accounting for the magnetic field of the ring current (RC) (Sugiura, 1964; Olsen, 2002; Olsen et al., 2014). However, the baseline of D_{st} is known to change with time (Olsen et al., 2005; Luhr and Maus, 2010; Olsen et al., 2014) and D_{st} only measures the axially symmetric ring current (Olsen, 2002). This hampers its use in geomagnetic field modelling (Olsen et al., 2014).

In an attempt to improve the parameterization and time dependence of the ring current, the 'RC' index was constructed (Olsen, 2002; Thomson and Lesur, 2007). RC index describes the strength of the magnetospheric ring current, even during geomagnetic quiet conditions, at a time when D_{st} baseline shows instabilities and so give less-optimal results (Olsen et al., 2014).

RC is derived from values generated at 21 geomagnetic observatories distributed at world-wide locations at mid and low latitudes. The world-wide locations of RC observatories are shown in figure 2.12 and table 2.4. It is derived using horizontal component only and consists of the sum of the magnetospheric and induced part (similar to D_{st}). Using RC improved the fit to the data considerably (Olsen, 2002) and shows good agreement with the D_{st} index (section 4.1).

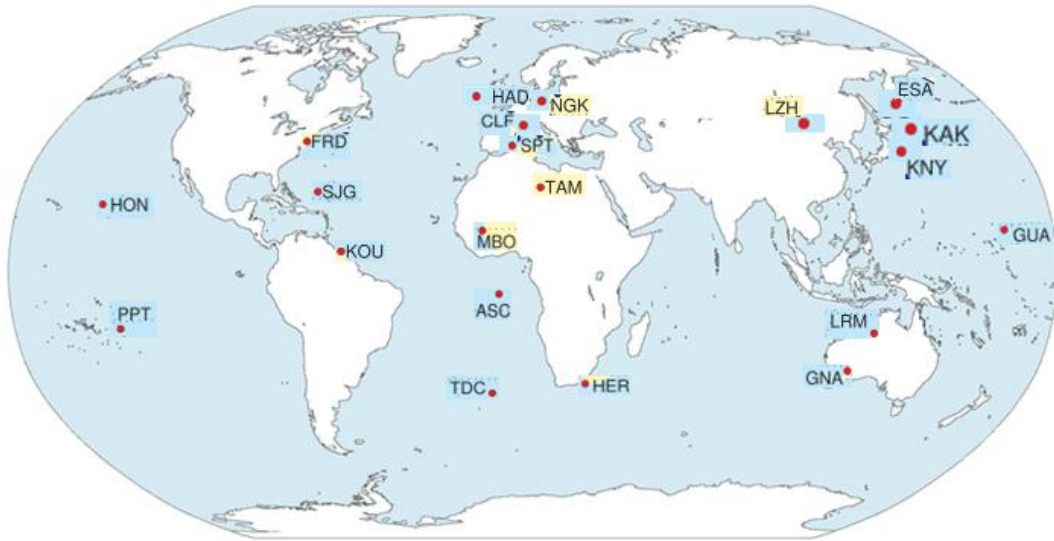


Figure 2.12: World-wide locations of the observatories used for calculating the RC index.

| # | Observatory | Code | Latitude | Longitude |
|----|------------------|------|----------|-----------|
| 1 | Ascension Island | ASC | -7.95° | 345.62° |
| 2 | Chambon la Foret | CLF | 48.02° | 2.27° |
| 3 | Esahi | ESA | 39.24° | 141.36° |
| 4 | Fredericksburg | FRD | 38.20° | 282.60° |
| 5 | Gnangara | GNA | -31.78° | 115.95° |
| 6 | Guam | GUA | 13.59° | 144.87° |
| 7 | Hartland | HAD | 51.00° | 353.50° |
| 8 | Hermanus | HER | -34.40° | 19.22° |
| 9 | Honolulu | HON | 21.32° | 201.98° |
| 10 | Kakioka | KAK | 36.23° | 140.18° |
| 11 | Kanoya | KNY | 31.42° | 130.88° |
| 12 | Kourou | KOU | 5.21° | 307.27° |
| 13 | Learmonth | LRM | -22.22° | 114.10° |
| 14 | Lanzhou | LZH | 36.09° | 103.85° |
| 15 | Mbour | MBO | 14.38° | 343.03° |
| 16 | Niemegk | NGK | 52.04° | 12.41° |
| 17 | Pamatai | PPT | -17.57° | 210.43° |
| 18 | San Juan | SJG | 18.11° | 293.85° |
| 19 | San Pablo-Toledo | SPT | 39.55° | 355.65° |
| 20 | Tamanrasset | TAM | 22.79° | 5.53° |
| 21 | Tristan da Cunha | TDC | -37.07° | 347.69° |

Table 2.4: Locations of the RC observatories

2.4 Measuring the Geomagnetic Field

To fully describe the magnetic field, it is necessary to either measure the intensity and two angles of direction or three orthogonal components. Systematic and direct measurements and mapping of the geomagnetic field have existed for almost two hundred years, with useable measurements made earlier. This measurement of the magnetic field are continuously made around the world at geomagnetic observatories, and obtained at all kinds of exotic locations, ranging from land, oceans, aircraft and more recently satellite surveys. All these activities are providing information about the magnetic field's morphology and time-evolution.

Early records of direct measurements of the geomagnetic field came mainly from ship logs, used for navigation purposes; while ground based measurements date back to 1600 in Paris and London (Kono, 2007). Gauss established the first permanent observatories (Whaler, 2007). Before then, he had invented and developed, in the mid-19th century, a method for measuring the absolute intensities through the calculation of the vector field (Jackson et al., 2000; Whaler, 2007). Since then, a network of observatories have been established all over the world, even though the coverage has been uneven (Southern hemisphere and the oceans are poorly covered, while there is great density of stations in Europe).

The advent of satellite in the latter part of the 20th century for satellite magnetic observations altered the role of observatories significantly, producing more global and homogeneous coverage. Observatory data, when combined with satellite data, where available, can provide good spatial and temporal coverage; with the satellite data providing much accurate information on the magnetospheric field.

2.4.1 Observatories

Magnetic observatories carry out continuous and accurate monitoring of the strength and direction of the geomagnetic field over many years, making measurements at least every minute (Macmillan and Olsen, 2013). Today, there are more than 200 observatories in operation globally (Mandea, 2006). The earliest dedicated magnetic observatory date back to the 1840s. Multiple factors determine the siting and distribution of observatories, including availability of suitable land, local expertise, funds, energy supply, etc. (Macmillan and Olsen, 2013; Macmillan, 2007a). This has resulted in the global spread of magnetic observatories to be highly uneven, with sparse coverage in the Southern hemisphere and the oceans, and dense coverage in Europe (see figure 2.13).

From these magnetic observatories, direct measurement of the Earth's magnetic field are continuously (intermittently in some cases) made around the world. The observatory data produced from these observatory measurements reveal how the magnetic field of the Earth varies on a wide range of scales, from seconds to centuries (Love, 2008; Macmillan and Olsen, 2013); which has led to better understanding of the processes both within and outside the Earth.

In magnetic observatories, absolute vector measurements of the magnetic field are recorded accurately and continuously. The fundamental measurements recorded are one-minute values of the vector components and scalar intensity. From these measurements, hourly, monthly and annual means are computed. The one-minute data are important for studying variations in the geomagnetic field external to the Earth, in particular, the daily variation and magnetic storms (Mandea and Purucker, 2005). In order for magnetic observatories to produce and maintain accurate magnetic

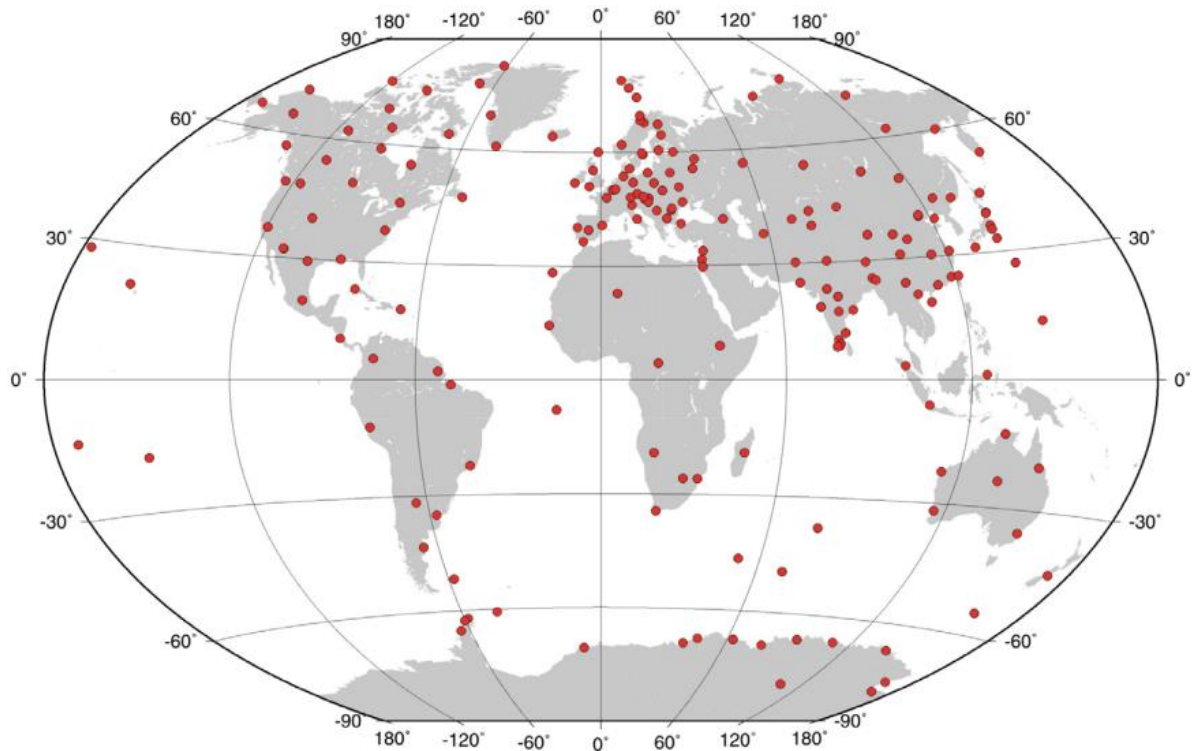


Figure 2.13: World-wide observatory spatial distribution

measurements and recordings, they must operate under carefully controlled conditions devoid of sources of anthropogenic magnetic interference or noise. This has led to siting of observatories in relatively remote locations (Love, 2008), with many having to move due to encroaching expanding settlements, towns and cities.

Modern ground magnetic observatories use similar instrumentation (fluxgate magnetometers) to make measurements of the magnetic field components. These instruments, also known as variometers, because they measure the variation of the field, are subject to instrument drift arising from sources both within and outside the instrument (temperature effects) and also instrument mounting stability (Mandea and Purucker, 2005). The data are processed and final 'definitive' data produced, after a baseline (established using absolute measurements of the field) is used for correction, and application of other required processing like scaling factors, offsets, temperature responses and timing errors.

Traditionally, annual mean values were provided as observatory data, and have been used for deriving magnetic field models, but in the recent past, the number of observatories providing hourly mean values (or one-minute) have increased, allowing for a better characterization of the external field variations (Olsen et al., 2010) (see figure 2.14). International campaigns, like the International Geophysical Year (IGY) in 1957-1958, led to a rapid increase in the number of observatories and stimulated observatory data processing. With improvements in instrument technology, this has enabled increase in production of one-minute data as the standard observatory product (Olsen et al., 2010; Olsen et al., 2007; Love, 2008).

In 1987, International Real-time Magnetic Observatory Network (INTERMAGNET) was established, a scheme piloted by the British Geological Survey (BGS) and the United States Geological Survey (USGS), to exchange geomagnetic data in near real time. "INTERMAGNET objective is to establish a

global network of cooperating digital magnetic observatories adopting modern standard specifications for measuring and recording equipment in order to facilitate data exchange and the production of geomagnetic data products in close to real time.” (Kerridge, 2001).

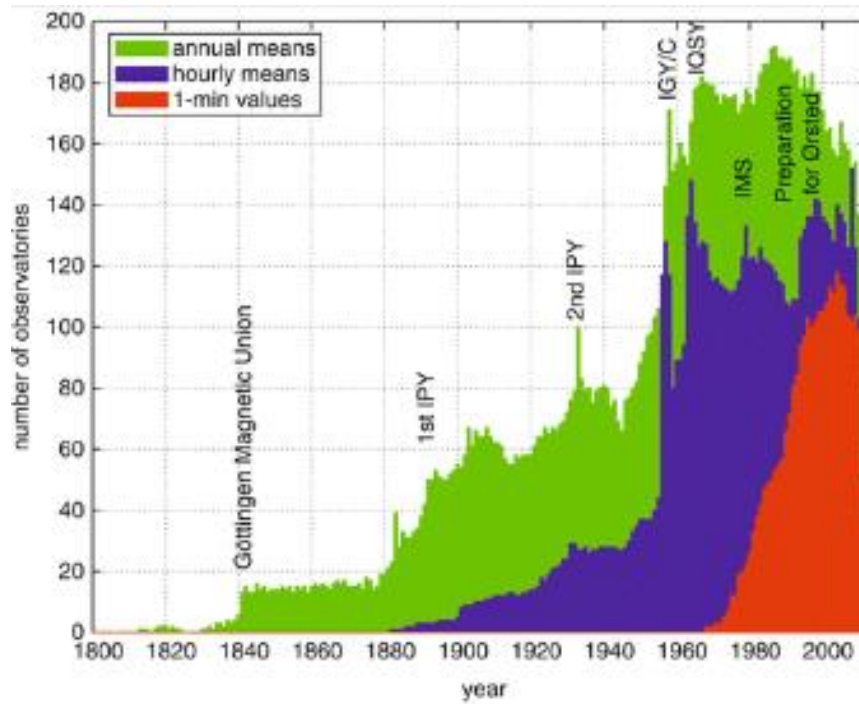


Figure 2.14: Distribution of ground magnetic observatory data. From Olsen et al., 2010

In addition to geomagnetic observatories (which monitor the variation of the geomagnetic field at a given location), magnetic repeat stations are precisely located points on the Earth’s surface, where high quality measurements of the three components of the geomagnetic field are regularly taken to the highest possible accuracy. This is taken for a few hours or even days (Newitt et al., 1996; Turner et al., 2007; Macmillan, 2007a), in order to determine the geomagnetic secular variation. The role is to complement magnetic observatories, by providing data in areas where installation of full observatory would be too costly or impossible due to various factors (Lalanne et al., 2013). Repeat stations offer better spatial resolution than observatory data but do not provide continuous data (Olsen et al., 2010).

2.4.2 Satellites

Observations of the geomagnetic field have been done systematically at ground based observatories for centuries, providing long term data. Since the 1960s, the Earth magnetic field have been observed intermittently by satellites (Mandea, 2006). Satellites provides opportunity to collect data globally at a uniform precision and accuracy; and the possibility to be able to measure the geomagnetic field from space using satellites have completely revolutionized geomagnetic field modelling. Satellites have the advantage that they can observe the magnetic field globally, and this ability to provide global data makes satellites invaluable for studies of the magnetic field.

Recent models of the geomagnetic field have been generated by magnetic observations made possible by low-Earth-orbiting (LEO) satellites at altitude below 1000km (Olsen et al., 2010). These satellites measured the geomagnetic field providing systematic, global, dense and homogeneous data sets for decades. Currently, Swarm mission is continuing in this acquisition of high quality

measurements of the near-Earth magnetic field, which will help generate new improved models of the geomagnetic field. Figure 2.15 shows a timeline of high-precision satellite missions for observing and recording the Earth's magnetic field.

The POGO (Polar Orbiting Geophysical Observatory) satellite missions (1965-1971), provided the early satellite missions that focus on measuring the magnetic field. They recorded only scalar values (Cain and Sweeney, 1973; Regan, 1979; Olsen et al., 2002). Two of the satellites, OGO-4 and OGO-6, measured the field at all local times; the third, OGO-2, only made observations at local times of dawn and dusk due to malfunction.

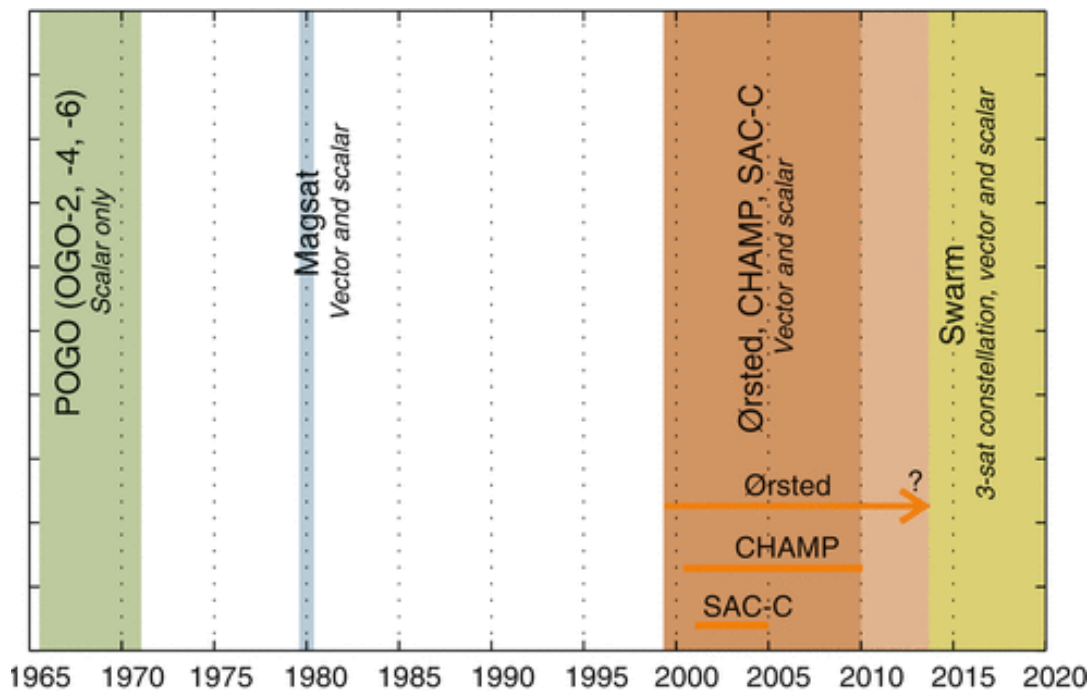


Figure 2.15: Distribution of high-precision satellite missions in time (from Olsen et al., 2010)

In October 1979, about eight years after POGO, MAGSAT (Magnetic Field Satellite) was launched into orbit (Langel and Estes, 1985). MAGSAT was the first spacecraft to collect and supply precise, global absolute vector field measurement data of the near-Earth magnetic field (Rajaram, 1993). MAGSAT was only in operation for 6 months (1979-1980), but it nevertheless completely changed our understanding to the field (even though it didn't contribute to the field itself) with good spatial coverage, providing much needed vector data for geomagnetic modelling and give new and valuable information about the ionosphere (Purucker, 2007).

It took almost 20 years after the MAGSAT mission for the acquisition of measurements of near-Earth magnetic vector field, similar to those of MAGSAT, to be revisited, with the launching of Danish satellite, Ørsted (Neubert et al., 2001) in 1999. This marked the start of the Decade of Geopotential Field Research, an international effort which ushered in a resurgence and promotion of continuous gravity and geomagnetic field modelling in near-Earth environment (Friis-Christensen et al., 2008). Ørsted has an elliptical polar orbit inclined at 98° , with an average altitude of 760km, 650km at perigee and 860km at apogee (Olsen, 2005; Manda, 2006). The satellite orbits the Earth, with the orbit changing by 0.9min/day and sampling all local times. The instrumentation used on Ørsted is a technological improvement on that used on MAGSAT, and has been a model for satellites that followed Ørsted (Olsen et al., 2007). Ørsted is still in operation currently; however, only scalar

measurements of the field are available since 2005. During this period there were also two additional satellite field mapping missions – CHAMP and Ørsted-2 experiment on board the SAC-C satellite (an Argentine product).

The Challenging Minisatellite Payload (CHAMP) was a low-Earth orbiting German satellite (Reigber et al., 2002) launched in 2000 to provide high precision gravity and magnetic field measurements. CHAMP had a nearly circular orbit with an inclination of 87.3° , an initial altitude of 454km, decreasing to about 360km after five years in orbit (Maus et al., 2005b), by May 2010 to 290km and in September 2010 CHAMP re-entered the Earth's atmosphere (Matzka et al., 2010). CHAMP moved much more rapidly through local time, when compared to Ørsted, at 5.45min/day, and allowed homogeneous global data coverage of the Earth (Mandea, 2006).

SAC-C (Satellite Argentino de Observacion de la Tiena) is an Argentine satellite launched in 2000. It is a near circular, sun-synchronised orbit sampling at 720km and 97° inclination. It was fixed in local time, crossing the equator at 10:24 and 22:24 local time. A copy of Ørsted, packaged with different absolute instrument, called Ørsted-2, was also launched aboard SAC-C. Unfortunately, no vector data are available from SAC-C satellite, due to cabling problem that prevented any altitude data measurements (Olsen and Kotsiaros, 2011).

One of the biggest challenges to the accuracy of present geomagnetic field models, is the contributions from external currents, which vary rapidly in both space and time; and because satellites are not at fixed location it is difficult to separate spatial from temporal variations (Olsen et al., 2007). A solution to this is to use multiple satellites to measure the field simultaneously over different regions of the globe (Friis-Christensen et al., 2008). This has led to the current satellite mission, Swarm.

SWARM is a constellation mission comprising three identical satellites to study the dynamics of the Earth's magnetic field and its interactions with the Earth system (Friis-Christensen et al., 2006, 2008; Olsen et al., 2013). SWARM was launched in late 2013 and its mission is to provide the best ever survey of the geomagnetic field and its temporal evolution (Olsen et al., 2007; Friis-Christensen et al., 2008; Olsen et al., 2013). Two of the satellites are flying side-by-side at lower altitude of 450km (initial), measuring the East-West gradient of the magnetic field and the third one is flying at higher altitude of 530km in a different local time to the lower pair (Olsen et al., 2007). SWARM simultaneously obtains a space-time characterisation of both the internal field sources and the ionospheric-magnetospheric current systems (Olsen et al., 2013). The data provided by SWARM create opportunities for improving existing and to maybe create new, geomagnetic models of the geomagnetic field with higher resolution and better source-separation compared to previous missions (Friis-Christensen et al., 2008). Table 2.5 contains a summary of information about the various satellite missions mentioned above.

| Satellite | Launch | Year(s) in Operation | Altitude (Km) | Inclination | Data type | Local Time |
|----------------|--------|----------------------|---------------|-------------|-----------------------------|------------------------------|
| POGO | 1965 | 1965-1971 | 400-1500 | 86° | Scalar | All Local Times |
| MAGSAT | 1979 | 1979-1980 | 352-561 | 96.7° | Scalar Vector | 6:00/18:00 |
| Ørsted | 1999 | Still in Operation | 630-880 | 98° | Scalar Vector | All Local Times |
| CHAMP | 2000 | 2000-2010 | 350-450 | 87.3° | Scalar Vector | All Local Times |
| SAC-C | 2000 | 2000-2013 | 700 | 98.2° | Scalar Vector (Ørsted-2) | 10:20, 09:20 (As of 2005) |
| SWARM A + B | 2013 | Still in Operation | 450 | 87.4° | Scalar Vector | All Local Times |
| SWARM C | 2013 | Still in Operation | 530 | 88° | Scalar Vector | All Local Times |

Table 2.5: Satellite missions of relevance for geomagnetic field modelling.

2.5 Mathematical Description of the Geomagnetic Field and Modelling Techniques

The geomagnetic field is a 3D vector field, B (magnetic flux density), and so can be represented at any point in time and space by vector magnitude and direction. It can also be expressed in several coordinate systems. When dealing with magnetic measurements of surface data for ground based observatories, the observations are decomposed into geographic coordinates – the field is resolved into horizontal component, H and vertical component, Z (with Z positive downwards). The horizontal component H is a vector parallel to the Earth’s surface and directed towards magnetic north. It is resolved in two directions – X , the direction of local meridian (which is positive north) and Y , the direction perpendicular to the meridian (which is positive eastwards). These directions are used to define the inclination (I), the angle between the horizontal plane (H) and the total field (F). The inclination represents the downward vertical dip seen in the compass needle; while the declination (D) represents the angle between magnetic north (H) and the geographic north (X), as shown by figure 2.16.

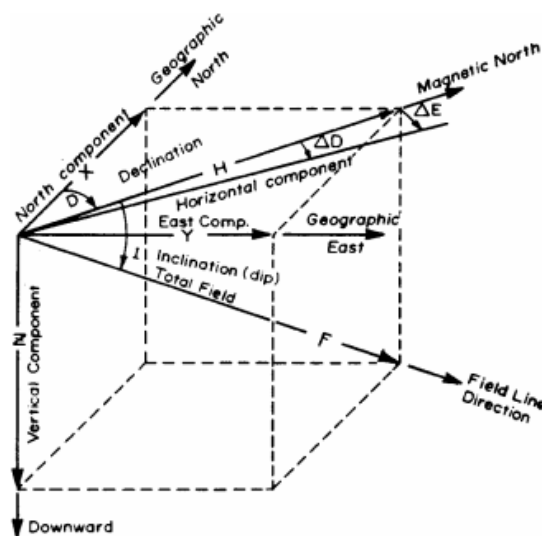


Figure 2.16: Components of the geomagnetic field measurements (from Campbell, 1997).

By simple geometry, we obtain:

$$X = H\cos(D), Y = H\sin(D) \quad 2.1$$

$$\text{Where } H = \sqrt{X^2 + Y^2} \quad 2.2$$

the Declination, D,

$$D = \arctan \frac{Y}{X} \quad 2.3$$

and Inclination, I,

$$I = \arctan \frac{Z}{H} = \arctan \left(\frac{Z}{\sqrt{X^2 + Y^2}} \right) \quad 2.4$$

Total field, F is given by,

$$F = \sqrt{H^2 + Z^2} = \sqrt{X^2 + Y^2 + Z^2} \quad 2.5$$

When dealing with satellite measurements, the geographic coordinate frame is altered, and the components transformed to spherical geocentric coordinates with radial, co-latitudinal and longitudinal components:

$$B = (B_r, B_\theta, B_\phi)$$

Here Z, rather than pointing downwards, points instead to the centre of a spheroid Earth, becoming a geocentric frame. The components transforms directly to spherical geocentric coordinates as:

$$X = -B_\theta \quad 2.6$$

$$Y = B_\phi \quad 2.7$$

$$Z = -B_r \quad 2.8$$

Equations 2.6 – 2.8 is only an approximate, and not a problem for this thesis.

2.5.1 Spherical Harmonic Analysis

Gauss invented and applied the spherical harmonic expansions on magnetic data, a natural way of separating the internal and external sources of the field. Spherical harmonic analysis is the most commonly used technique for representing the geomagnetic field (Olsen et al., 2007; Manda and Purucker, 2005).

Maxwell's equations, following Manda (2007), Manda and Purucker (2005) derivation, are used as the starting point for developing the field components from spherical harmonics (Langel, 1987).

$$\nabla \times B = \mu_0 J, \quad 2.9$$

$$\nabla \cdot B = 0, \quad 2.10$$

A fundamental property of magnetic fields is that they are divergence-free (Maxwell's 2nd equation).

Where B is the magnetic induction/flux density in Tesla (T), μ_0 is permittivity of free space, J is current density.

In a source free region, where curl B = 0, the magnetic field, B, can be expressed in spherical coordinates (r, θ, ϕ) as negative gradient of scalar potential

$$B_{(r, \theta, \phi)} = -\nabla V_{(r, \theta, \phi)} \quad 2.11$$

this satisfies Laplace equation, due to equation 2.10.

$$\nabla \cdot \nabla V = \nabla^2 V = 0 \quad 2.12$$

where V is a scalar potential.

At the surface of the Earth,

$$V = V_i + V_e, \quad 2.13$$

where V_i and V_e represents the internal and external potential respectively.

When equation 2.13 is expanded in spherical harmonics (Mandea and Purucker, 2005) with co-latitude, θ , longitude, ϕ , and radius, the solution is a spherical harmonic expansion:

$$\begin{aligned} V(r, \theta, \phi) = & a \sum_{n=1}^{\infty} \sum_{m=0}^n \left(\frac{a}{r}\right)^{n+1} [g_n^m \cos(m\phi) + h_n^m \sin(m\phi)] P_n^m(\cos\theta) \\ & + a \sum_{n=1}^{\infty} \sum_{m=0}^n \left(\frac{r}{a}\right)^n [q_n^m \cos(m\phi) + s_n^m \sin(m\phi)] P_n^m(\cos\theta) \end{aligned} \quad 2.14$$

where $P_n^m(\cos\theta)$ are the Schmidt-normalised associated Legendre functions, (g_n^m, h_n^m) and (q_n^m, s_n^m) are the Gauss coefficients, conventionally given in nanotesla (nT), describing the internal and external sources for degree n and order m, a is the radius of the Earth and r denotes the radial distance of the observation from the centre of the Earth.

Each order of expansion has its physical interpretation, with n = 1 representing a dipole, n = 2 a quadrupole, n = 3 an octupole, etc. There is no n = 0 term, which would represent a magnetic monopole. Gauss coefficients of the International Geomagnetic Reference Field (IGRF) 10th Generation magnetic field model can be found listed in Macmillan and Maus (2005). The most recent version, the 11th Generation IGRF, has a definitive main field model for epoch 2005.0, a main field model for epoch 2010.0, and a linear predictive secular variation model for 2010.0-2015.0 (Finlay et al., 2010).

The relationship between the magnetic components and the potential are

$$B_r = -\frac{\partial V}{\partial r}$$

$$B_\theta = \frac{-1}{r} \frac{\partial V}{\partial \theta}$$

$$B_{\phi} = \frac{-1}{r \sin \theta} \frac{\partial V}{\partial \phi} \quad 2.15$$

giving the total intensity (scalar) as

$$B = \sqrt{B_r^2 + B_{\theta}^2 + B_{\phi}^2} \quad 2.16$$

In equation 2.14, the first sum represents the field from internal sources, where the amplitude decreases as the distance from the Earth increases. The second sum describes the field from external sources, where its amplitude decreases as distance from Earth decreases.

Therefore, considering only the external sources, the potential is,

$$V_e(r, \theta, \phi) = a \sum_{n=1}^{\infty} \sum_{m=0}^n \left(\frac{r}{a}\right)^n [q_n^m \cos(m\phi) + s_n^m \sin(m\phi)] P_n^m(\cos\theta) \quad 2.17$$

2.5.2 Existing Models and Modelling Techniques

Geomagnetic field models are highly important tools for studying and describing the magnetic field during different epochs and under different conditions. The methods or techniques used vary across different models; however, the problem of extracting high quality data for use in creating these models is the same and highly challenging. Since the field measured contain superposition of field from different sources (main field, lithospheric and external fields from magnetospheric and ionospheric currents), separating is not only not straightforward but a major challenge in geomagnetic field modelling.

When modelling the geomagnetic field with observatory and satellite data, two main approaches are usually considered. One is the ‘Comprehensive Approach’, where the major sources contributing to the field are parameterized and simultaneously solved for (Sabaka et al., 2002, 2004) (see section 2.5.3 for more on the Comprehensive Model). The second approach is to filter or average the data before modelling the field, to minimise the influence of unmodelled external fields (Maus et al., 2007).

There are various geomagnetic field models used for different purposes, but the most widely used model is the International Geomagnetic Reference Field (IGRF) model. It is a relatively simple predictive model, which the international geomagnetic community developed as a general purpose main field and secular variation model (Maus et al., 2005). It is published at 5 year intervals by the International Association of Geomagnetism and Aeronomy (IAGA). It is designed to predict the field of internal origin both for instantaneous epoch and the following 5 year interval. IGRF is used for many purposes, both by scientists and commercial organisations. It is used extensively in studies of the external magnetic field, with many ionospheric and magnetospheric models (i.e. Tsyganenko, 2002a) using the IGRF to describe the internal field. One of its main uses initially was in regional magnetic surveys – subtracting an internationally agreed global model from measurements making it much easier to combine adjacent surveys (Macmillan and Finlay, 2011). Now, calculations of geomagnetic coordinate systems almost exclusively use IGRF, using the centred dipole in particular (Macmillan and Finlay, 2011).

Other existing recent geomagnetic field models of note include:

- The CHAOS series of models (Olsen et al., 2006; Olsen and Mandeia, 2008; Olsen et al., 2009, 2010, 2014).
- The Tsyganenko models (Tsyganenko, 1989, 1995, 1996, 2002a). Have an entirely different focus to the other models. Designed to represent the configuration of the magnetosphere, generally during active magnetic conditions, rather than aiming to describe the quiet time internal field.
- The Main Field (MF) series of models (Maus et al., 2005, 2006b, 2007a, 2008).
- The Potsdam Magnetic Model of the Earth (POMME) series of models (Maus et al., 2005b, 2006c, 2010).
- The GFZ Reference Internal Magnetic Model (GRIMM) models (Lesur et al., 2008, 2010).
- BGS/G/L/0706 model (global internal field model for spherical harmonic degree 60) (Thomson and Lesur, 2007), and
- The Comprehensive Model (CM) series of model, the phase four (CM4) is used in this study and described in more details in the next section below.

2.5.3 The Comprehensive Models

The basic idea behind the comprehensive model (CM) series is to co-estimate the major field sources using many different data sets. It uses the ‘comprehensive approach’ in a joint inversion of ground based and satellite field measurements to co-estimate and describe field contributions from core, lithospheric and external (magnetospheric and ionospheric) fields, along with their associated Earth-induced signals. In most other field models, only some of the sources e.g. the internal and magnetospheric fields, are modelled simultaneously, while fields from other sources e.g. the ionospheric field are modelled separately. Errors may be introduced into the field model using this approach, as the separation of fields due to various sources may be erroneous. This is because the parameters of the field model at each stage are fitted to a field originating partly from a source not parameterized by the field model.

The comprehensive model was created by Sabaka et al. (1993, 2002, 2004), and based on only quiet time data from both satellites and observatories. It is not considered predictive (nevertheless, for external fields we use it as predictive), since the parameterization relies on input of known data such as magnetic indices. Hypothetically, this analysis of ground based and satellite measurements together, used in the comprehensive model allows for the parameterization of all sources, provided the parameter set are treated consistently (Mandeia and Purucker, 2005).

A separation of the various source fields is facilitated when data from different altitudes are included. The main field (core and crustal) and induced fields are internal to both satellites and observatories, and the magnetospheric field external to both satellites and observatories (see figure 2.2). The ionospheric field is internal to satellites, but external to the observatories; hence, the use of satellite data can help with the separation of the internal (core and crustal), induced and ionospheric sources from the magnetospheric sources, while the observatory data can help separate the induced (time-varying) fields and secular variation from the fields due to ionospheric and magnetospheric fields. As a result, it is theoretically possible to separate ionospheric, magnetospheric and induced + internal fields when analysing observatory and satellite data jointly, if the model parameters are co-estimated. The comprehensive model series is now in its fourth phase.

GSFC (12/93) and GSFC (8/95-SqM)

The GSFC (12/93) [Sabaka and Baldwin, 1993] and the GSFC (8/95-SqM) [Langel et al., 1996] models (phase 1 and 2 respectively) were the first and second attempts respectively at comprehensive modelling of the geomagnetic field. Both models were based on observatory and satellite quiet-time data from POGO and MAGSAT. The models included representation of the core and crustal fields and secular variation. Local time variations and the D_{st} index were used in modelling the ionospheric, magnetospheric and induced fields, and the strength of the ring current respectively. Seasonal variations of the ionospheric and magnetospheric fields were included in the GSFC (8/95-SqM) model.

Comprehensive Model 3 (CM3)

CM3 (Sabaka et al., 2002) is the third model in the series, and it is much more extensive than its predecessors. In addition to the new sources included in CM3, the description and parameterization of the sources already included in the previous two comprehensive models were extended and refined. The new sources included field aligned currents and their seasonal variations, and the influence of solar activity on the ionospheric field. One of the extensions made in the CM3 model is the estimation of the crustal field to a smaller scale i.e. higher degree, including the application of a more sophisticated mantle conductivity model for estimating the induced fields.

CM3 was derived from quiet-time POGO and MAGSAT satellites and observatory data spanning a period from 1960 through 1985. It had 16,594 parameters, estimated from 591,432 data points via weighted least squares inversion. CM3 describe the static field up to degree and order 65.

Comprehensive Model 4 (CM4)

CM4 (Sabaka et al., 2004) was derived only a couple of years after CM3. It is the latest comprehensive model and the one used in this study. The parameterization of the field sources in CM3 and CM4 are basically the same. The major difference between both models is the inclusion of data from Ørsted and CHAMP in CM4. This inclusion meant a great improvement of CM4 from CM3. The data set for CM4 was extended with observatory and satellite data (with vector and scalar data from Ørsted and scalar data from CHAMP) up to July 2002; hence, CM4 spans from 1960 through 2002.5. It has 25,243 model parameters, estimated by an iteratively reweighted least squares method from 2,156,832 data points.

In the CM4 model, terms in the first part of equation 2.14 (internal) have been retained only up to a degree truncation level, N_{max} , that is justified by the data, or in the case of satellite, up to the degree at which it is believed that the lithospheric field begins to dominate the series (the Main field) taken to be 13 (Langel and Estes, 1982; Sabaka et al. 2002). Spherical harmonic models of the lithospheric fields derived from data with estimates of the main, magnetospheric and ionospheric fields removed, indicates that noise becomes dominant somewhere between $N_{max} = 60$ and 70 (Ravat et al. 1995). The degree truncation level for the lithospheric field for the CM4 is set at $N_{max} = 65$ (Sabaka et al. 2002, 2004).

For the external field sources, the truncation levels set for the CM4 model varies for the ionosphere and the magnetosphere. For the ionosphere, it is relatively straightforward. The potential (V_{ion}) is expanded to degree (N_{max}) 60 and order (M_{max}) 12 respectively [equation (25)] of Sabaka et al. (2002). For the magnetosphere, the situation is more complicated because of the coordinate

systems used to define the current systems responsible, which do not translate directly to truncation levels on a spherical harmonic expansion. The potential (V_{mag}) of the magnetospheric field is expressed in terms of 800 real coefficients/parameters.

The external field sources, particularly the ionospheric, depend upon solar activity. The influence of solar activity is represented by an amplification factor, assumed to be equal for all harmonics, which is a function of absolute $F_{10.7}$ solar flux values (Olsen 1993). An increase in the Sun's surface activity leads to an increase in ionospheric conductivity, resulting in an increase in ionospheric current (Takeda et al. 1986, 2002a). This can be measured by $F_{10.7}$. In CM4, the quasi-dipole (QD) ionospheric expansion coefficients are redefined with a dependence upon the solar radiation flux index, $F_{10.7}$. The relationship (dependence) is a linear relationship. This means that increasing solar flux inflates the whole ionospheric current system (and induced contributions) without changing its shapes (Sabaka et al. 2002; 2004). The external field of magnetospheric sources is dominated by features that vary with ring current intensity, season and solar wind parameters, and modulated by the D_{st} index. The relevant external harmonic coefficients of the magnetospheric contributions vary with D_{st} linearly (Langel and Estes, 1985a). It is noted that this linear relationship is adopted only for the dipole terms ($n = 1$), and that the temporal variability of $D_{st}(t)$ is modulated by both seasonal and diurnal oscillations to help describe any local time asymmetries (Sabaka et al. 2002).

The K_p and D_{st} activity indices are used to select quiet-time data in CM4. Both scalar and vector data were used for all altitudes and for all local times in satellite data. MAGSAT and Ørsted vector were also weighted to account for attitude error (Holme and Bloxham, 1996). Due to the simultaneous description of most of the known field sources, CM4 has extensive applications e.g. as reference models, which makes it advantageous for studies where isolation of the field from one or several specific sources are desired, like this investigation.

The core code, tables of coefficients and magnetic indices (D_{st} and $F_{10.7}$) are available at <http://core2.gsfc.nasa.gov/cm/>, along with example driver codes for generating certain types of results from the model. The examples are written in FORTRAN, but the core code is available in FORTRAN and several flavours of matlab code. For this study, I have made use of a variation of the example 2 code, which calculates the external and induced fields, and excludes large portion of the field due to the Earth's core. This effectively removes a baseline value so the diurnal variation (the object of this study) can be seen. Figure 2.17 is an example of how the different component fields from the main sources regions add together when treated with the comprehensive model.

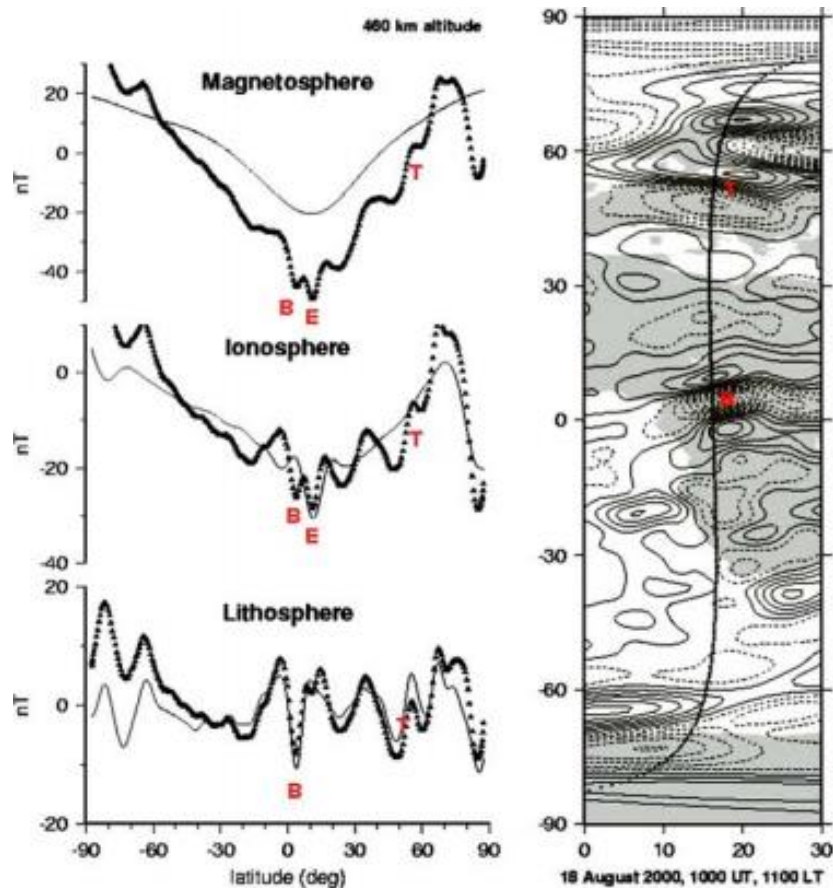


Figure 2.17: Residual progression against latitude for the three main source regions after the magnetic field is corrected with CM4 model (Sabaka et al,2004). The profile shows the scalar field B of a CHAMP ascending (North-going) pass on 18 August 2000 beginning at 1000UT and crossing the equator at 15° W and 1100UT. This is for a magnetically quiet day with $K_p = 0+$ for the previous 3-h period, $Dst = -3nT$ and $|d(Dst)/dt| \leq 4nT.h^{-1}$. The symbols represent residuals with respect to the main field (up to degree 13) plus all the fields label in the panel above. The line is the prediction from the field component labelled in the current panel. Figure on the right shows the location of the subsatellite point and includes a contour map of the scalar field B originating in the lithosphere from the CM4 model. For full description of this diagram see Mandaia and Purucker (2005).

2.6 Earth's Magnetic Field Summary

In this chapter we have provided an overview of the features of the Earth's magnetic field relevant to this study. We have discussed the various sources contributing to the geomagnetic field, how the field is measured and the magnetic activity indices that help in the description of the different field sources and their estimates.

The mathematical techniques used in describing the field, spherical harmonic analysis and the models used for studying and describing the field were also outlined. Most of these presented here in this chapter are not without consequence later in the thesis. The models are the tools used extensively in describing and resolving much of the issues encountered in geomagnetic research. In this study, we have used the CM4 model exclusively.

In the next chapter, our focus now turns to testing the CM4 model predictability, and modelling the geomagnetic diurnal field using the comprehensive model presented here.

Chapter 3

Modelling the Magnetic Diurnal Variation

Having mentioned and discussed the model used in this study and the reason for it, we now turn our attention to data selection in modelling, testing the dataset on the CM4 code to see if the updating of the time span done on the code works, and finally applying the datasets to construct and produce models of the geomagnetic diurnal field at surface.

We begin with a brief discussion of the fundamental concept which governs magnetic field modelling – Inverse Theory/Modelling, generalised data selection criteria in magnetic field modelling. This is followed by outlining the data used in this study and testing the CM4 model code. This is especially important as we extended the lifespan of the CM4 model beyond its original span of 1960 through 2002.5. This was achieved by updating the CM4 code with more recent magnetic indices data, as the external field parts of CM4 are driven by D_{st} and F10.4, plus time and location. In the second part of the chapter we discussed the CM4 modelling approach and creating and generating global maps of the diurnal field at the Earth's surface from CM4 and observatory station data.

3.1 Modelling Background/Theory

3.1.1 Inverse theory/modelling

Advancements in both observation and theory over the centuries have made our knowledge of the Earth and much of its solar system to be particularly developed. The inverse theory/modelling is a general concept that is used to convert observed measurements into information about a physical process that we are interested in. Inverse theory/modelling can be conceptually formulated as:

Data \rightarrow Model Parameters

It is considered as 'inverse' to the forward modelling which relates the model parameters to the data that we observed:

Model Parameters \rightarrow Data

With forward modelling, a property may be calculated at a desired place and time for a specified process, uniquely, only one solution for the classified input. The administered model and predefined physical parameters are defined, such that

$$V' = M(V) \tag{3.1}$$

(In this case, the coefficients are of the external field, i.e. q_n^m and s_n^m)

Where V' is the calculated expected observation/data; V represents the known model parameters and M is an operator (matrix) which denotes the model function and describes the explicit relationship between the observation/data(V') and model parameter(V).

Since in most physical systems, we do not ever have enough information to uniquely constrain our solutions because the operator does not contain unique equations, the reverse situation to the

forward modelling may be prescribed or required. This is where inferences about the physical systems (model parameters) are taken from the observations/data, such that

$$V = M^{-1} (V') \quad 3.2$$

The model parameters that fit the data are solved for by inverting M , the matrix operator, to directly convert the measurements into the model parameters. This is the process referred to as Inverse Theory/Modelling. The objective is to obtain the coefficients (V) that can accurately represent the Earth's magnetic diurnal field by trying to fit the data collected from the magnetic observatory stations around the globe (V').

Inverse modelling problems are typically ill-posed, as opposed to forward modelling problems which are straight-forward and well-posed. Some of these problems associated with inverse modelling are Existence, Construction, Stability and Non-uniqueness (Hadamard, 1923; Tarantola, 2005). Almost all geophysical inverse problems are non-unique. Mathematically, they are expressed as Fredholm integral equations. Backus and Gilbert (1967, 1968), who were the first to formally identify this in a geophysical sense, showed that for a continuous inverse problem, if one solution exists and the data are finite, there are infinite number of solutions which exist. The problem of stability is also often violated, because solutions constructed are numerically unstable. If both non-uniqueness and instability are encountered in an inverse modelling problem, the problem may be described as an ill-posed problem. In most geophysical investigations, the data are finite, but the model is infinite.

3.1.2 Data Selection in Modelling

Internal magnetic field modelling restricts the input data set to include, ideally only quiet magnetic data, taken during local night time periods under quiet magnetic conditions. This is in order to reduce or minimise the influence of more rapid varying external fields and other transient effects. Careful selection of data in geomagnetic field modelling not only minimises the volume of noise and unwanted contributions from unmodelled fields, it also reduces the volume of data used, even though this often times result in over 90% of available data being discarded (Whaler, 2007).

In order to restrict and limit contributions from external and unmodelled field influences, it is standard to use only night-time data. This is because solar activity which is evident during daytime is the main factor influencing the external magnetic field. Therefore, identifying magnetically quiet periods (periods of low magnetic activity) becomes significantly important. In magnetic field modelling, it has become common to choose these magnetically quiet periods by using geomagnetic activity indices (see section 2.3). Since the K_p index is the most widely used index for identifying magnetic quiet period, the data selected are required to have a K_p value ≤ 2.0 (or less) and same value for the preceding three hour interval. The D_{st} index also plays a role in selecting quiet time data, as it indicates the severity of global magnetic disturbances coming from the large scale magnetospheric field and the ring current. A Typical selection criteria for quiet period using D_{st} are $|D_{st}| \leq 20\text{nT}$ and a rate of change of D_{st} , $|d(D_{st})/dt| \leq 2\text{nT/hr}$.

K_p and D_{st} are generally used for selection criteria at low- to mid-latitudes, as it has been shown by Ritter et al. (2004b) that they are not well suited for selecting quiet periods at high latitudes. In addition to the D_{st} index, the Interplanetary Magnetic Field (IMF) is also an important data selection parameter when the external field influences are a factor. This is because the interaction of the IMF with the magnetic field influences disturbances in the external magnetic field.

The above criteria are true and generally accepted and used when modelling the main magnetic field. For the sake of this investigation, both quiet time and moderately disturbed time data have been selected and used. This is because the main objective of this study is that we are trying to establish the nature of variations of the field for days away from quiet time to see how well we can understand them.

3.2. Data Used in This Thesis

For the purpose of this study we use data from about a hundred and twenty (120) ground magnetic observatories scattered around the world. All the observatory data used are daily (within a 24 hour period).

We have chosen data from both the International Quiet Days (classified as the five quietest days in each month based on criteria agreed by the geomagnetism community), all with $K_p < 20$, which we called the 'quiet' datasets, and data from moderately disturbed days, all with $K_p \leq 5$, which we called the 'disturbed' datasets. The disturbed datasets were chosen to see how well the model performed during disturbed times, as we are trying to establish the nature of the variations for days away from quiet time to see how well we can understand them.

The datasets are for the following dates:

'Quiet' Time Dataset;

- 7th September, 2003
- 14th September, 2003
- 28th September, 2003
- 29th September, 2003
- 30th September, 2003

Moderately 'Disturbed' Time Dataset;

- 9th September, 2003
- 25th September, 2003
- 5th May, 2006
- 30th May, 2006
- 4th July, 2006

3.3 Testing the CM4 Model

Just as mentioned in section (2.5.3), the CM4 model is the model used for this study. Although CM4 model is a quiet time model, we chose it for the purpose of this study because it is a model which models all the different sources of the near-Earth magnetic field. It is the best and most effective in the co-estimation and parameterization of all the field contributions, from core, lithosphere, and the external to their associated Earth-induced signals. A variation of the examples 2 code is used. Since the study is dealing with magnetic diurnal variation, and the external and induced variation fields are of interest, this code generates the primary and induced components of the external (magnetospheric and ionospheric) fields, excluding large portion of the field due to the Earth's core. The code produces X, Y, and Z components of the field, so the variation can be studied, and compared at different times with the observatory data prediction.

Since we extended the original lifespan of CM4 (1960 – 2002.5) to recent times (2012) by updating the CM4 with more recent magnetic indices data for the external field parts (D_{st} and F10.7), we needed to test the model to see how well it is performing. This was done first for quiet time days, and then for moderately disturbed days. Data from more than a hundred and twenty INTERMAGNET standard magnetic observatory stations reporting around the globe were used. Due to space constraint we show selected examples from different geographical region of the globe to show how the field is behaving and how the CM4 performed after the updating of the code and extension of the model original lifespan to recent times (post 2002.5).

3.3.1 Geographical Plots of Quiet Time Datasets

Figures 3.1 to 3.6 shows plots for the three magnetic field components, X, Y and Z for quiet daily variation ($K_p \leq 2-$) in September, 2003 of observatory stations from different regions of the globe. Time is for Universal Time (UT) hours. The observatory data for all the field components (X, Y, Z) used in generating the plots were all centred i.e. with zero mean. The observed plots show daily variation and it is particularly evident all the components in most of the plots. The plots clearly show that the model is performing reasonably well in matching the observatory station data, especially in Europe where it is particularly doing very well. As can be seen, the CM4 model tries to model the observatory station data and understand how the field is behaving. The signature pattern obtained and seen in the figures reflects very well the Sq variations as expected for these regions and latitudes. It is well known that the X component of the geomagnetic field, especially at low latitude stations, have a maximum (X_{max}) around local noon and minimum value (X_{min}) between 1800 and 0600 local time. This is evident, especially in the African and South American stations (figures 3.1 and 3.5).

The geomagnetic daily variation, Sq has a spatial dependence primarily on latitude and affected by other factors including time of year and level of solar activity. The Sq field varies smoothly with location and universal time (UT) (Courtilot and Le Mouel, 1988). This is because it is largely a local time field that can be roughly represented by a current system fixed to the Sun. This variation with location is seen in most of the plots presented. Matsushita and Maeda (1965) have also reported its longitudinal dependence. The field variation signatures in our plots show the average pattern at the different geographical locations. The differences observed between all the regions mainly consist of slight phase and magnitude differences, contrasting behaviours are also particularly noticeable in the different components (X, Y, Z).

The X component in the African and Asian regions show very similar behaviour characterized by a positive peak before or around noon (figures 3.1 and 3.2), while in the European and North American region, this peak is negative (before noon in Europe and after noon in North America), accompanied by a positive secondary peak in the morning (figures 3.3 and 3.4). In the South American sector, the X component shows a similar variation as that of the African sector, but with a positive peak showing after noon (figure 3.5). As for the Oceania region, Gwangara (GNA) and the Amsterdam Island (AMS) are characterized by a morning minimum and an afternoon maximum, while Guam (GUA) and Kakadu (KDU) have morning maximum and an afternoon minimum; with the CM4 model producing a better prediction of the X component variation in GUA and KDU than in GNA and AMS (figure 3.6).

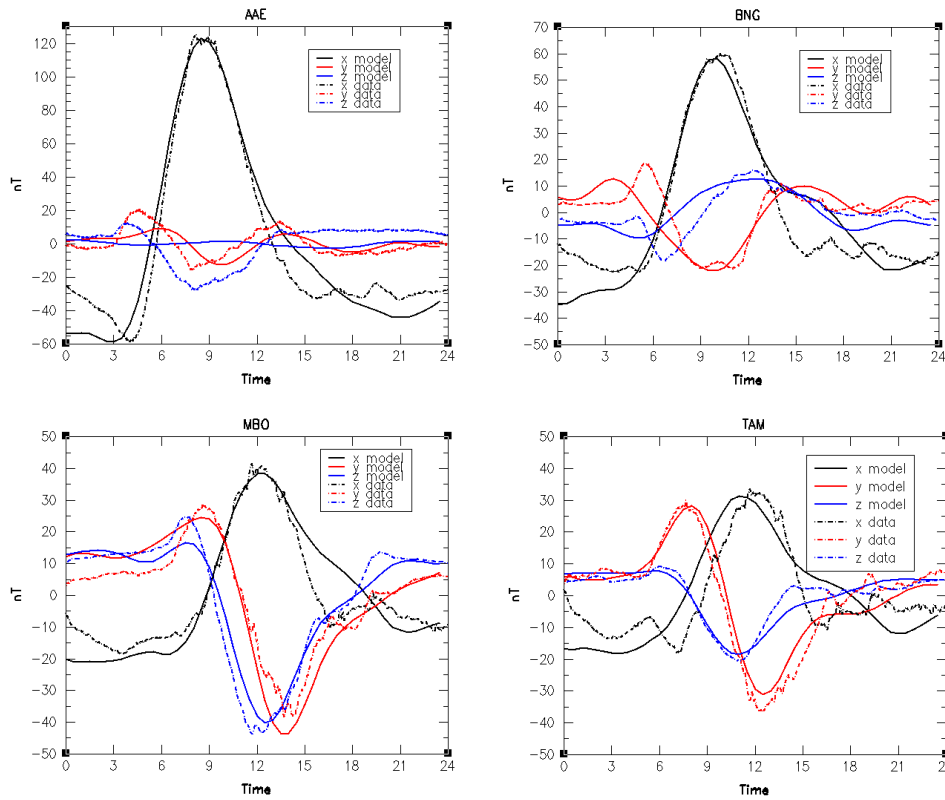


Figure 3.1: Quiet time diurnal variation comparison of X, Y, Z components for CM4 model predictions to the observatory station data for African stations (Addis Ababa, AAE; Bangui, BNG; Mbour, MBO and Tamanrasset, TAM) on 30/09/2003

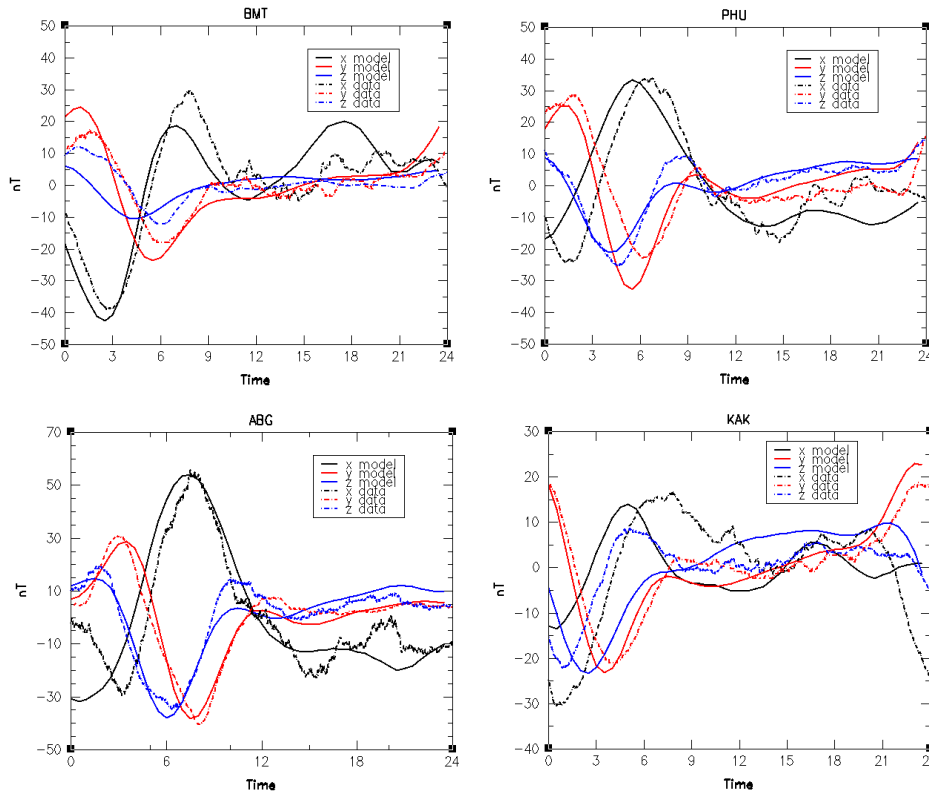


Figure 3.2: Quiet time diurnal variation comparison of X, Y, Z components for CM4 model predictions to the observatory station data for Asian stations (Beijing Ming Tombs, BMT; Phuthuy, PHU; Alibag, ABG and Kakiika, KAK) on 30/09/2003.

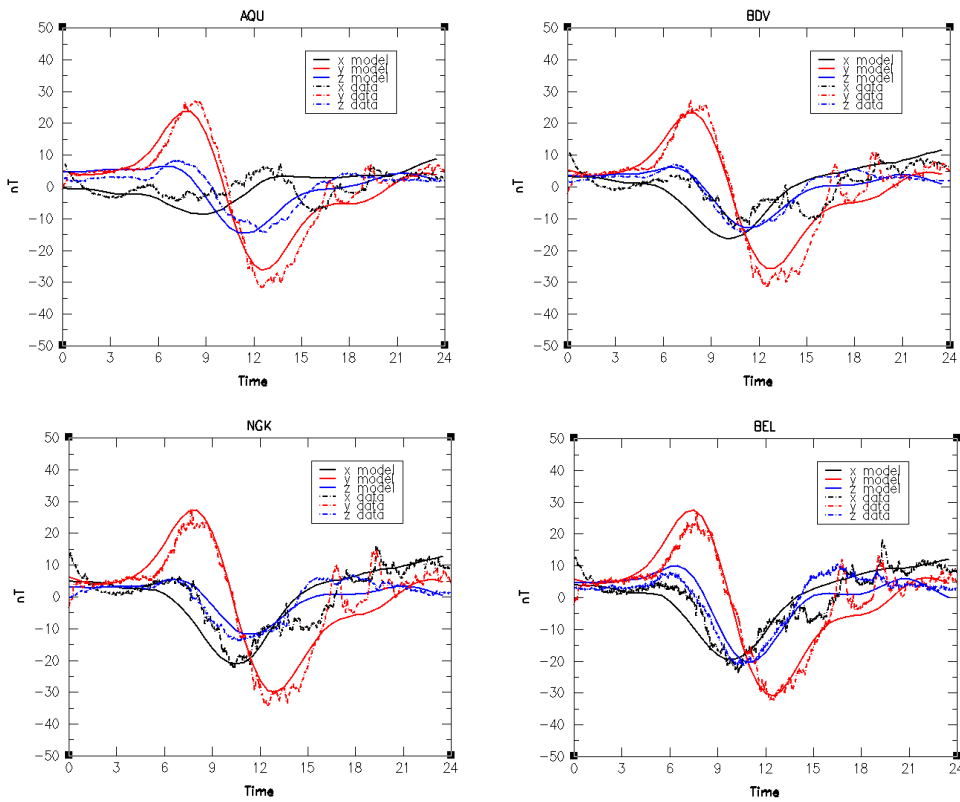


Figure 3.3: Quiet time diurnal variation comparison of X, Y, Z components for CM4 model predictions to the observatory station data for European stations (L'Aquila, AQU; Budkov, BDV; Niemegek, NGK and Belsk, BEL) on 30/09/2003.

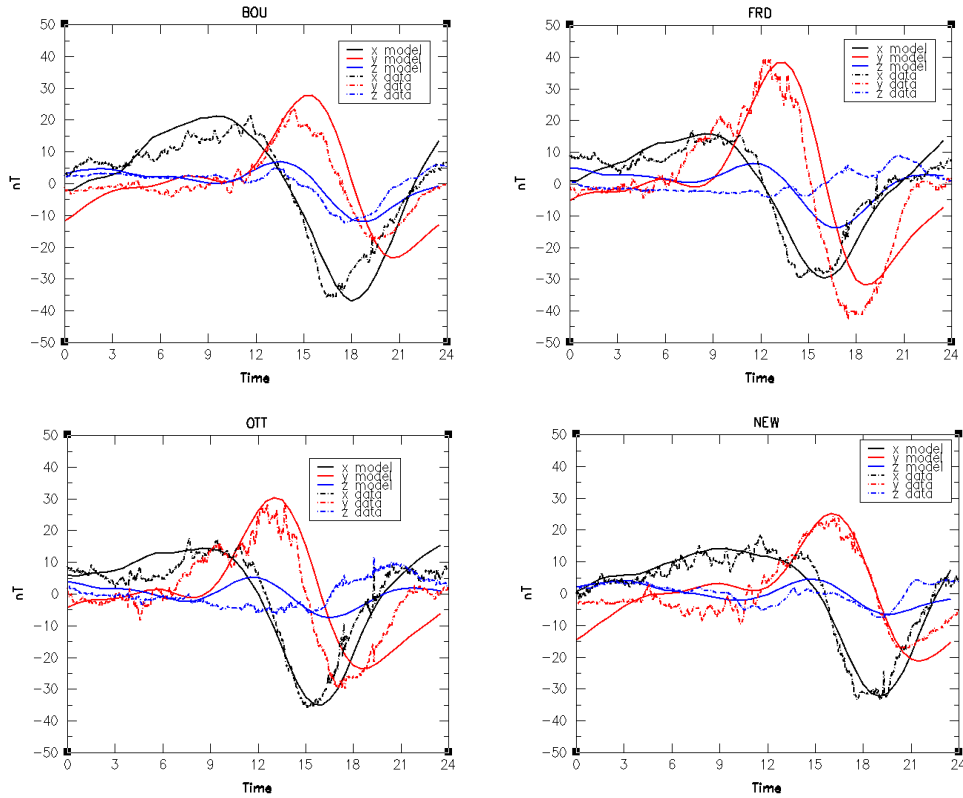


Figure 3.4: Quiet time diurnal variation comparison of X, Y, Z components for CM4 model predictions to the observatory station data for North American stations (Boulder, BOU; Fredericksburg, FRD; Ottawa, OTT and Newport, NEW) on 30/09/2003.

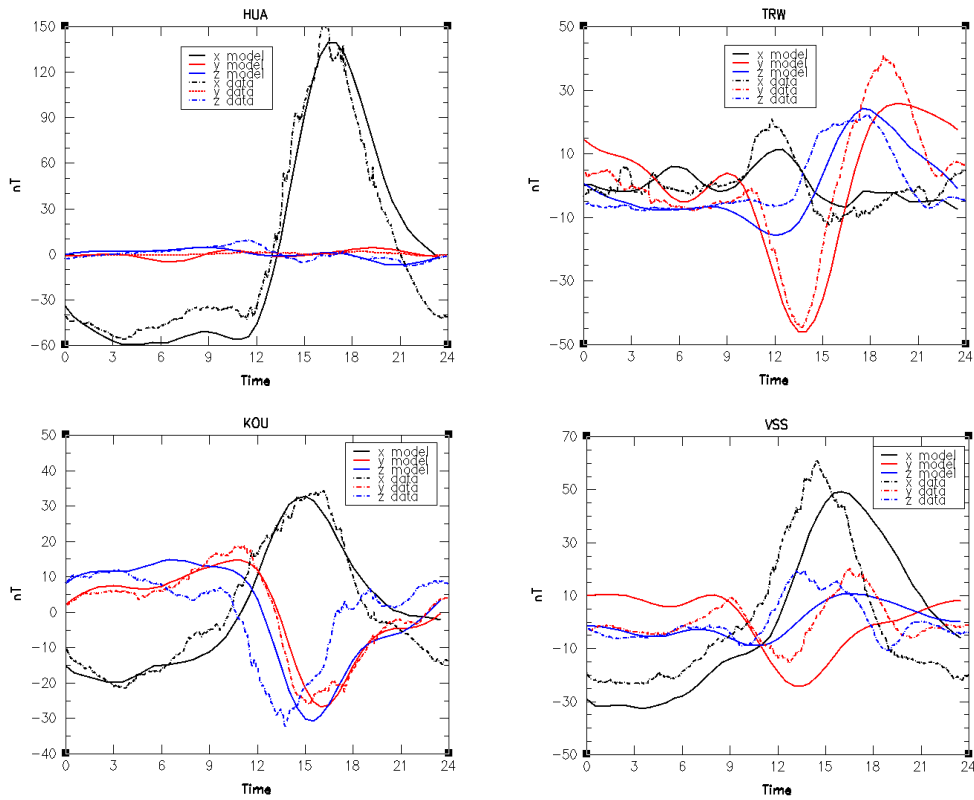


Figure 3.5: Quiet time diurnal variation comparison of X, Y, Z components for CM4 model predictions to the observatory station data for South American stations (Huancayo, HUA; Trelew, TRW; Kourou, KOU and Vassouras, VSS) on 30/09/2003.

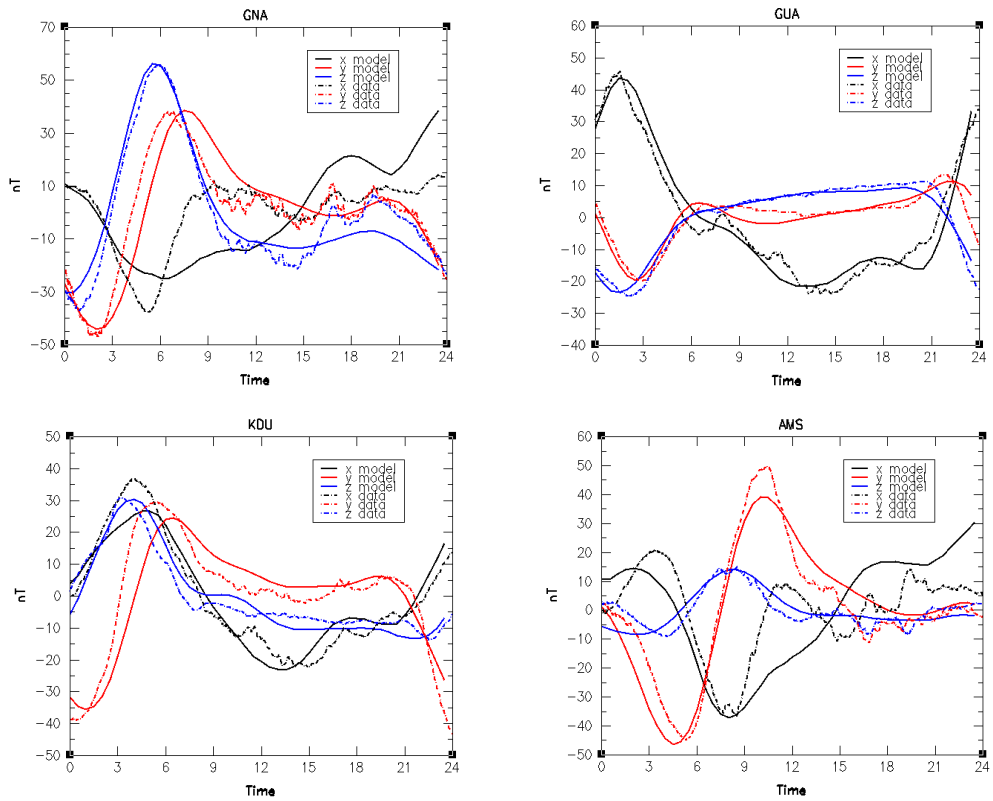


Figure 3.6: Quiet time diurnal variation comparison of X, Y, Z components for CM4 model predictions to the observatory station data for Oceanian stations (Gnangara, GNA; Guam, GUA; Kakadu, KDU and Martin de Vivies, AMS) on 30/09/2003.

The Y component features a negative variation largely confined to the early morning hours in the Asian sector (figure 3.2), contrasting with the largely daytime negative variation in the African and South American sectors, except Huancayo (HUA) (figures 3.1 and 3.5). European observatories feature a pronounced positive variation in the morning hours followed by a negative variation in the afternoon (figure 3.3). The North American observatories, on their part, show this pronounced positive variation in Y as an afternoon maximum followed by an immediate minimum peak in the evening (figure 3.4). The Oceania observatories produce an early morning minimum which peaks within the time range (0200-0300hours UT) in most of the stations for the Y component, except AMS which had its own minimum at about 0500hours UT (figure 3.6). This minimum is followed by a positive variation in the region peaking before noon.

In most of the regions, the Y component shows a reverse of the X component behaviour. In North American and European stations the Sq amplitude for the X component is largely small (approximately 20nT) compared to the amplitude of the Y component (approximately 30nT). The Sq amplitude of the X component at African and South American stations is larger than the other stations. This enhancement of the Sq amplitude may have been caused by a significant enhancement of ionospheric conductivity due to Cowling effect (Hirono, 1952). Very near the dip equator, the amplitude of X variation increases abnormally. This is considered the effect of the narrow equatorial electrojet (EEJ). We observe this abnormal increase in South American (HUA), African (AAE) and Asian stations (ABG), with the increase more in HUA than in AAE and ABG. This is because, as we know, the electrojet strength in American longitudes is higher than that in Asian and African longitudes (Rastogi, 2006). The amplitude of the X component is thus expectedly consistently maximum within the electrojet zone as a result of the EEJ phenomenon. African, Asian and South American stations follow identical pattern in much of the X and Y components. The X and Y components in African and South American stations show similar signatures, except in HUA where we see a somewhat flat signature in the Y component.

With the Z component, it is observed that it does not feature strong geographical dependence. It shows pronounced negative minimum most of the day in African, Asian, European, and North American regions. The behaviour of the signature of the X, Y, and Z components of these selected observatories are a representation of much of the stations studied in the different geographical regions.

The fit between the CM4 model and the observatory station data seems to be roughly associated with latitude (as would be expected), proximity and geographical region. From all the figures, it shows that certain stations behave in similar ways and shows features in common with each other, including short time features which are recorded simultaneously at all the stations. This is evident in all three magnetic components, X, Y and Z – showing there is a geographical relationship to this behaviour. Some of these sharp features also show global occurrence, especially seen in the dusk part of the X component in most of the stations in the different geographic regions; lacking only in North America, South America (except Trelew, TRW, in Argentina) and Guam, GUA, in Oceania. This geographical behaviour and relationship is most obvious in the European observatory stations (Figure 3.3), where these can be easily seen. In the European stations, the CM4 model fit well the X, Y, Z components of the observatory data compared to observatory stations other geographic regions. This may be due to the great density of observatory stations available in Europe, and the fact that they are fairly close to each other, so expected to behave in a similar way. They show features common with each other, including short time features which are recorded simultaneously

at most of the observatory stations. This reinforces the point that certain stations behave in similar ways and there is a geographical relationship to this behaviour. But there is limit to this geographical extent, as some observatory stations may record features opposite to this geographical behaviour (i.e. when statistically disrupted by short periods when something odd happens in a particular station), and measures a peak at one station, but minimum at other stations e.g. AQU compared with BDV, NGK, and BEL for X component just before noon in figure 3.3.

Generally, the features for the different regions are in agreement with the Sq variation for the different geographical zones. What we can see from the examples above is that while the features in the CM4 model are sometimes not the same as the observatory station data in the example plots, they show similar patterns, which is encouraging; showing that the extension we did to the original lifespan of the CM4 model code seem to be working.

3.3.2 Geographical Plots of Datasets away from Quiet Time

As explained previously (see section 2.5.3), the dataset used to calculate the CM4 model is chosen for its lack of geomagnetic activity. The driving inputs for the external field terms (ionosphere and magnetosphere) in the spherical harmonic expansion are D_{st} and F10.7 indices respectively. D_{st} in particular allows the CM4 model to respond to active conditions outside of the original geomagnetic activity remit. Figures 3.7 to 3.12 shows the signature plots obtained for comparison of the CM4 model predictions to the observatory station data for different regions of the globe. The signature plots of the comparison of CM4 model predictions to the observatory station data is for a moderately disturbed day, 30th May, 2006 with a $K_p \leq 5.0$. Just like the quiet time observatory data ($k_p \leq 2$ -), these ones were also centred (i.e. zero mean).

The signatures of the geomagnetic components of the observatory data show Sq variation just as the data for quiet time, but these have variations that are expectedly more rapid due to higher magnetic activity, with fluctuations particularly seen in the X component. The variation also show spatial dependence, and the components of the observatory data behave similarly in different geographical regions, conforming largely to observation seen our quiet time data in section 3.3.1. The observatory stations show features in common with each other, including the short period variations which show global spread. While the patterns in the model prediction of the observatory data components are often not the same, they show many similar features, and the CM4 model is seen to produce better response than expected.

Just as we saw for the quiet time data, the CM4 model is performing better in European observatories than others. This is particularly noticeable in the Y component (figure 3.9). This impressive performance of the CM4 model in matching the Y component of the observatory data also extends to the North African stations (figure 3.10) and to some extent the African and Asian stations (figures 3.7 and 3.8). In South American and Oceania stations, the fit between the CM4 model and the Y component of the observatory station data is noticeable more in the morning up till the early afternoon hours (figures 3.11 and 3.12).

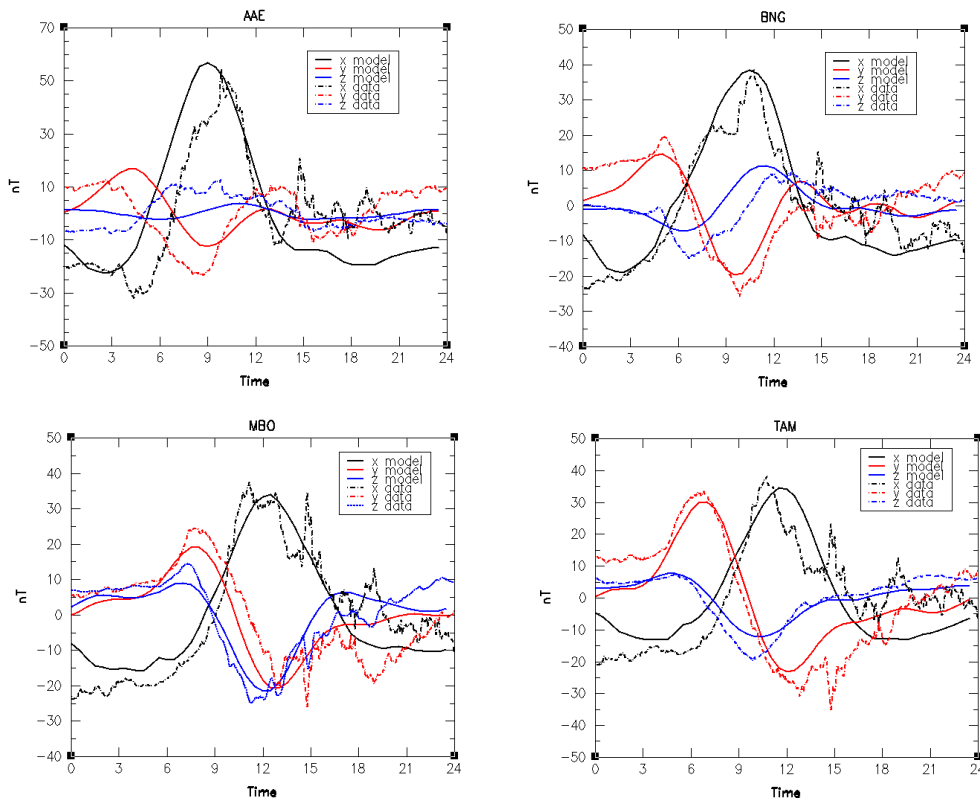


Figure 3.7: Moderately disturbed day comparison of X, Y, Z components for CM4 model predictions to the observatory station data for African stations (Addis Ababa, AAE; Bangui, BNG; Mbour, MBO and Tamanrasset, TAM) on30/05/2006.

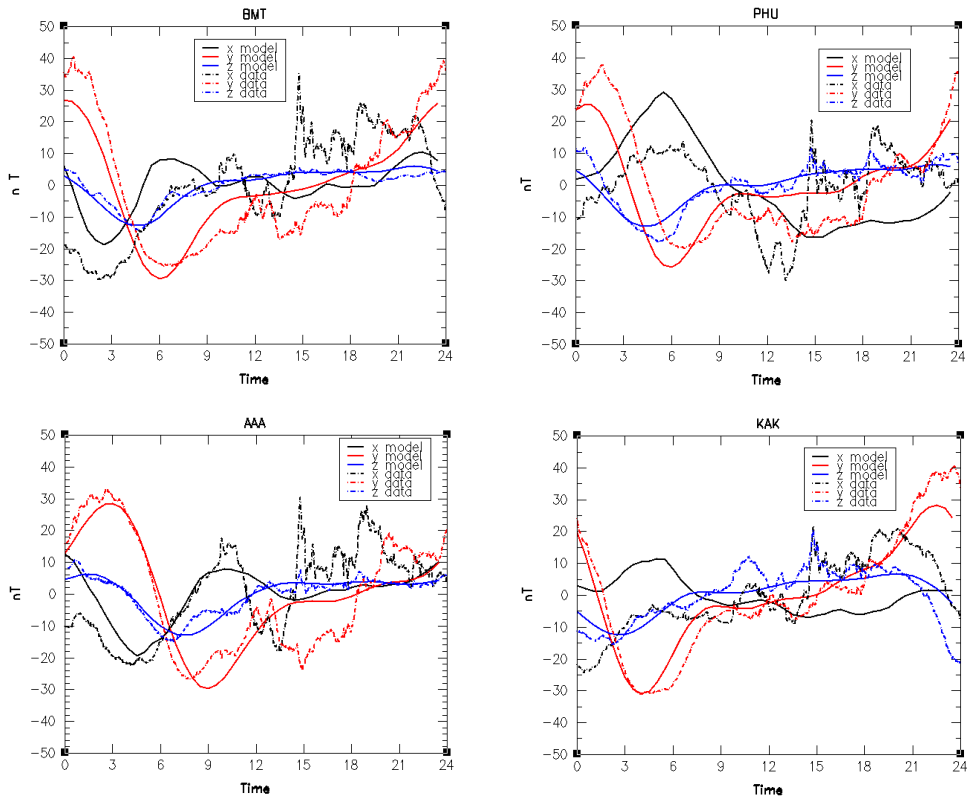


Figure 3.8: Moderately disturbed day comparison of X, Y, Z components for CM4 model predictions to the observatory station data for Asian stations (Beijing Ming Tombs, BMT; Phuthuy, PHU; Alibag, ABG and Kakioka, KAK) on30/05/2006.

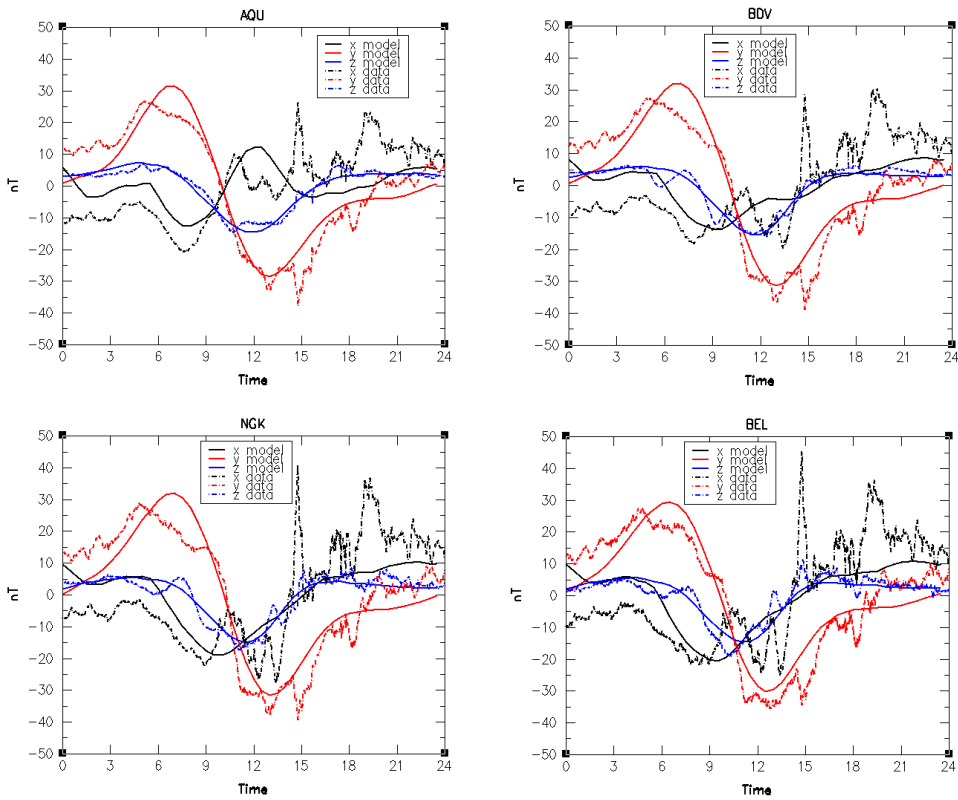


Figure 3.9: Moderately disturbed day comparison of X, Y, Z components for CM4 model predictions to the observatory station data for European stations (Niemegk, NGK; L'Aquila, AQU; Budkov, BDV; and Belsk, BEL) on30/05/2006.

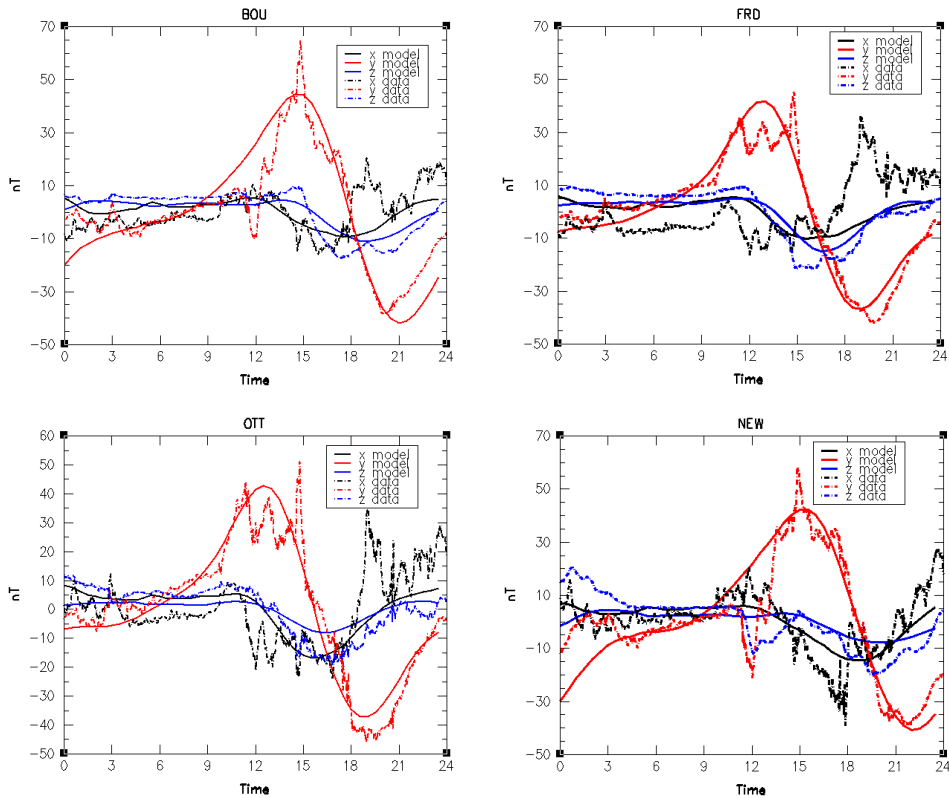


Figure 3.10: Moderately disturbed day comparison of X, Y, Z components for CM4 model predictions to the observatory station data for North American stations (Boulder, BOU; Del Rio, DLR; Fresno, FRN and Ottawa, OTT) on30/05/2006.

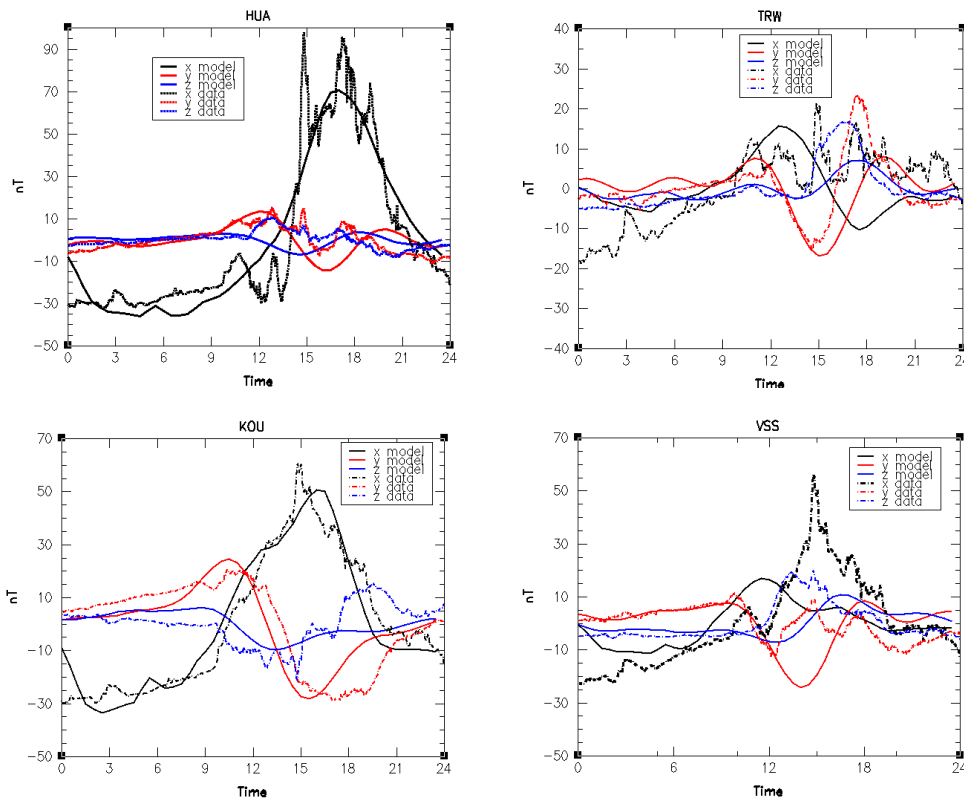


Figure 3.11: Moderately disturbed day comparison of X, Y, Z components for CM4 model predictions to the observatory station data for South American stations (Huancayo, HUA; Vassouras, VSS; Trelew, TRW; and Kourou, KOU) on30/05/2006.

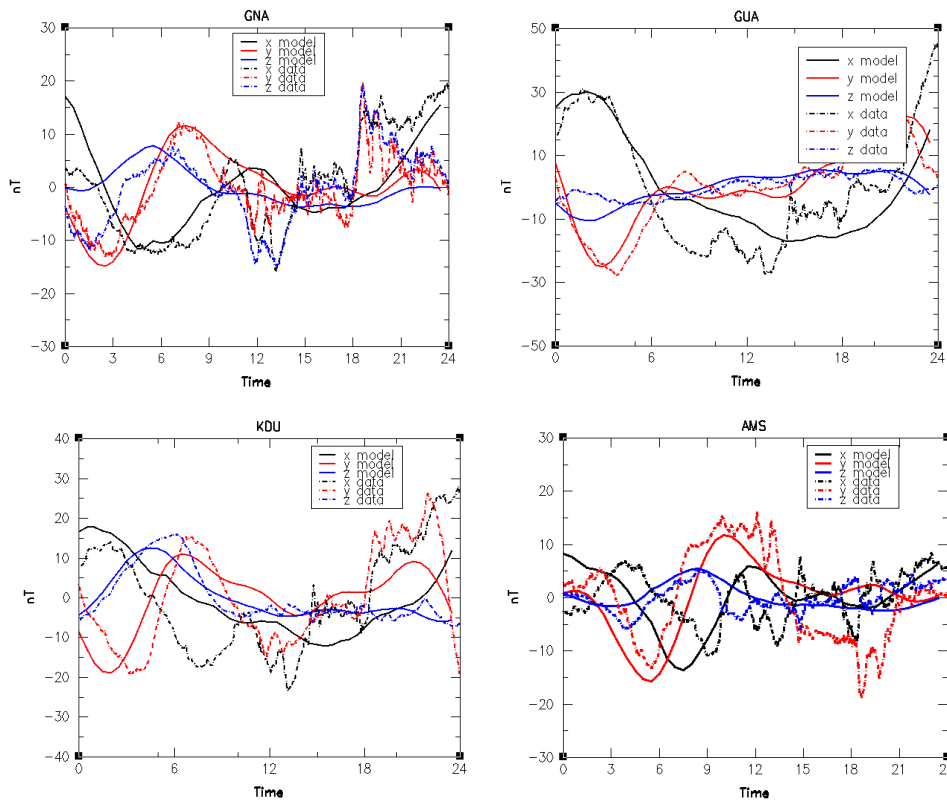


Figure 3.12: Moderately disturbed day comparison of X, Y, Z components for CM4 model predictions to the observatory station data for Oceanian stations (Gnangara, GNA; Guam, GUA; Kakadu, KDU; and Learmonth, LRM) on30/05/2006.

The CM4 model also performed reasonably well in predicting the horizontal X component features of the geomagnetic observatory data. This is seen in African observatories, where it did well predicting most of the daytime features (figure 3.7) and in South American, particularly in the electrojet observatory station of Huancayo (HUA), and Kourou (KOU). A noticeable fit between the CM4 model and the vertically downward Z component of the observatory data is also seen in African (BNG, MBO and TAM), Asian, European and North American stations.

The body of evidence showed in the signature plots of the figures shows that the CM4 model produces better predictions than expected, and shows the model predictions not doing so well during periods of rapid variations. As can be seen, the CM4 model is matching the regional type features of the observatory station data reasonably well for all three components (X, Y, and Z) of the geomagnetic field, but not the short time period features, which are often where we have the large misfit between the CM4 model and the observatory station data (not surprising due to limited time resolution of D_{st}). However, we can observe some coherence among the different plots, especially for the X component – showing global effect? But to compare will require global modelling. It should be recalled that the CM4 model was made to primarily analyse internal field variations of long wavelength timespan. Any predictions it can do with the external field beyond the effective range of D_{st} is an unexpected advantage. The fact that the CM4 model can produce an approximation to an active time field variation at all is an indication of its versatility.

3.3.3 Misfit Between the CM4 Model Predictions and Observatory Data

In order to study the consistency of the CM4 model in predicting the observatory station data within its timespan and outside of it, we calculated the relative RMS misfit between the CM4 model predictions and the observatory components (X, Y, Z) data for quiet periods (within and outside CM4 timespan) and for moderately disturbed period. In field modelling, one often looks at the RMS misfit between the model and the input data, in order to make the two kinds of data comparable.

For this study, we define the relative RMS misfit between the CM4 model and the observatory component data as:

$$\text{RMS (Data – Model)/RMS (Data)}$$

= 0 → Perfect fit (model predicts data perfectly),

= 1 → Non-correlation (Model uncorrelated with Data i.e. model explains precisely none of the data).

Increasing values away from zero (0) shows an increasingly poorer representation of the data by the model.

Table 3.1 lists the mean RMS misfit values between the observatory component data and the CM4 predictions. The misfit was calculated at each observatory location and the average for each region of the globe computed with the overall mean relative RMS value for each observatory component in each region shown in the table.

Direct comparison between CM4 and the observatory component data misfits is not straightforward. The observatory stations vary for each region for the different CM4 time period, but it is worth commenting on some patterns observed in the RMS misfits. The mean RMS misfits for all the

different regions have values less than 1 (< 1), showing that while the model does not predict the data perfectly, it shows some fair representation of the data. The mean RMS misfit values are lowest in the Y component, followed by X and then Z components for the observatory data. This may be due to most of the observatory station locations being at mid and low latitudes, where the data will be less contaminated by unmodelled sources of the field, particularly auroral current systems. The difference between the mean RMS misfit values for quiet period within the timespan of CM4 model and outside the timespan is very small (almost negligible), and even similar in some cases, justifying the extension of CM4 timespan outside the period the data covers. While the mean RMS misfit is slightly bigger for moderately disturbed period, it still shows the model fairly predicting or matching the data, albeit poorly, as most of the misfit values fall below 1, but very close to one in some components (here the model explaining precisely none of the data), which somewhat confirms the qualitative observations seen in the various plots of the comparison between CM4 and the observatory component data for X, Y and Z.

The mean RMS misfit values of the X component in all the periods are slightly higher than the Y component. This may, probably, be due to the impact of remaining unmodelled contributions from magnetospheric sources. At EEJ observatories (AAE, HUA, PHU), our observation shows that the RMS misfit values are smaller at AAE and PHU in all the field components than HUA for quiet time periods, but HUA show smaller misfit values in X and Y for moderately disturbed period. Generally, the mean RMS misfit values are smaller (better) for all components in all periods in Europe and North America, where observatory stations/data density is high.

| Regions | CM4 Quiet Period (Within timespan) | | | CM4 Quiet Period (Outside timespan) | | | CM4 Moderately Disturbed Period | | |
|---------------|------------------------------------|------|------|-------------------------------------|------|------|---------------------------------|------|------|
| | X | Y | Z | X | Y | Z | X | Y | Z |
| African | 0.51 | 0.44 | 0.77 | 0.55 | 0.51 | 0.78 | 0.90 | 0.83 | 0.93 |
| Asia | 0.65 | 0.50 | 0.75 | 0.66 | 0.51 | 0.78 | 0.94 | 0.87 | 0.91 |
| Europe | 0.38 | 0.32 | 0.51 | 0.40 | 0.38 | 0.55 | 0.69 | 0.61 | 0.72 |
| North America | 0.47 | 0.44 | 0.62 | 0.50 | 0.51 | 0.58 | 0.79 | 0.72 | 0.80 |
| South America | 0.61 | 0.54 | 0.74 | 0.66 | 0.60 | 0.76 | 0.86 | 0.84 | 0.93 |
| Oceania | 0.75 | 0.69 | 0.92 | 0.79 | 0.75 | 0.93 | 0.90 | 0.85 | 0.99 |

Table 3.1: Relative misfit between CM4 model and observatory data for quiet period (within and outside CM4 timespan) and for moderately disturbed day for each field components (X, Y, Z).

3.3.4 Trends in Failure Times of Model

Again, just as we observed for quiet time period plots, the fit between the CM4 model and the observatory station data shows latitudinal, geographical and regional behaviour and relationship. The geographical plots for moderately disturbed dataset in figures 3.7 to 3.12 show that the CM4 model models the Y and Z components across the globe better than the X component. The model sources the majority of its external field prediction from D_{st} , and D_{st} is based on the X component, which makes the X component to be more affected by external field sources. It should, however, be noted that the Z component direction also changes with activity in a way that relates specifically to D_{st} , but Z component is more susceptible to induction effects than the X component, making the

CM4 model better fit of Z component overall, but especially in coastal stations (oceanian), unexpected?

It is clear from the regional plots in the figures that the CM4 model does not produce such a good fit at all points on the globe. Y component performed reasonably well everywhere, except in South America (don't know why yet).

The ring current (RC) has been adduced as the main source of the magnetospheric field (Olsen et al. 2014; Olsen, 2002; Daglis et al. 1999; Stern, 1985; Sugiura, 1972). The RC's dipolar field is roughly aligned with the main magnetic field of the Earth; thus X and Z components will measure different magnitudes of signals from the RC with changing latitude. As X component is aligned to the direction of the RC field at the equator, it is expected here to have the greatest contribution from the RC field, while the Z component being perpendicular to the direction of the RC field; we see very little contribution from the RC field here. This may be the reason why the CM4 model fits the X component better than the Z component here (close to the equator).

This trend reverses as we go polewards; as a result X component will see little contributions from the RC field, while Z component gets the greatest contribution. This mechanism (maybe) causes predictable trends in the model failure identified in majority of the stations studied globally, with some shown in the plots above. Compounding this effect/trend is the fact that an unidentified model response may also be due to misrepresentation of the current system other than RC (ionospheric or magnetospheric tail current) by CM4. We really can't tell!

Since the plots are grouped geographically, there are no noticeable trends in the CM4 model failure times based on region. In all the figures shown in section 3.3.2, we see that there is a large misfit between the CM4 model and the observatory data in all the components during short time periods, indicating that the CM4 model response to these features is very poor. The CM4 model response to the regional type features in the various observatory stations is somewhat better, especially in the Y and Z components. Even though the equatorial regions are affected by signals from the EEJ current system, the CM4 model was still able to model the fine variations in these areas, most apparent in stations HUA and AAE in the X, Y and Z components. The fact that the model is performing better around America, Africa and Asia (region where the D_{st} index is calculated) underline the failings of the D_{st} to properly represent active times in a global sense. The CM4 model shows that D_{st} does not give equal descriptions of active data all over the Earth, reducing its usefulness despite the fact that it does fit some of the irregular trends globally.

What is clear from the plots however, is that the CM4 model gives better approximation to the physics of the external field for times away from quiet time than expected, though caution should be applied, as the physics of the external field in times away from quiet time are likely to vary depending on the scale of the magnetic activity. It may be useful, if possible, to attempt to clarify the relationship between the magnetic field activity and patterns of the ionospheric and magnetospheric current system dynamics.

Thus the conditions, level and extent for the CM4 model failure are really not globally uniform.

3.4 Global Maps of the Diurnal Field

In section 3.3.2, we observe some coherence among the different geographical plots, especially for the X component, suspecting global effect. To further investigate this we used the CM4 code to

model the diurnal field and create/generate global maps at different local times from CM4 and observatory station data.

In this section we present the global maps of the geomagnetic diurnal field generated at different local times and spherical harmonic degrees from CM4 and observatory station data at the Earth's surface. But first we briefly discussed the CM4 approach in modelling geomagnetic data.

3.4.1 Approach: How CM4 Models the Field

We have presented signature comparisons between CM4 model and the observatory station data showing some coherence among the plots. In an attempt to further investigate & model the field we generated global models of the diurnal field from observatory station data and CM4 model. CM4 code helps in generating these models by applying spherical harmonic inverse modelling of the full dataset from all observatory station data globally inputted. Since our interest is in geomagnetic daily variation models, CM4 is used to subtract well characterised internal and magnetospheric components from the data. Global maps of the diurnal field are then created at different local times and different spherical harmonic degrees.

In its simplest form, CM4 does the modelling through a three-route process (input, filter and output). The inputs are Time, Position and Magnetic Indices such as D_{st} and F10.7. The outputs are the model predictions to the observatory magnetic field data; and it does the filtering by solving a series of spherical harmonics as in equation 2.14, using over 16000 such parameters in describing the input data. Below is an itemised summation of the CM4 model approach:

- Inputs – Filter – Output



- Inputs: Time, Position, D_{st} , F10.7
- Output: Model Prediction to Magnetic Field Data
- Filter: A Series of Spherical Harmonics

$$\Phi = a \sum_{l=1}^{\infty} \left(\frac{a}{r} \right)^{l+1} \sum_{m=0}^l P_l^m(\cos\theta) \cdot [g_l^m \cos(m\phi) + h_l^m \sin(m\phi)] \quad] - \text{Internal Field}$$

$$+ a \sum_{l=1}^{\infty} \left(\frac{r}{a} \right)^l \sum_{m=0}^l P_l^m(\cos\theta) \cdot [q_l^m \cos(m\phi) + s_l^m \sin(m\phi)] \quad] - \text{External Field}$$

- CM4 Code Uses Over 16,000 Such Parameters to Describe the Input Data

3.4.2 Regularised Minimum-norm Approach

To investigate the coherence observed among the different plots, particularly for the X component, and see how global the effect is (section 3.3.2), we took the regularised minimum-norm approach to generate Sq diurnal variation models for both the CM4 model and the magnetic observatory measurements. This enables us to study and compare how well the CM4 model predicts the magnetic observatory measurements for days away from quiet time.

To achieve this we sought a continuously time-varying field model from an iterative least-squares fit to data, so return to the concept of inverse modelling (see section 3.1.1). Solving an inverse problem of this nature requires three things – a data set, the knowledge of errors on the data, and a way to represent the solution numerically.

Assuming a linear problem, equation 3.2 [$V = M^{-1} (V')$] may be written as,

$$\gamma = \mathbf{A}\mathbf{m} + \mathbf{e} \quad 3.3$$

Where \mathbf{A} is a matrix containing the equations of condition which link γ with \mathbf{m} . \mathbf{m} is the model vector containing the parameters to be determined, \mathbf{e} the error vector and γ is a vector containing the observational data.

Here, we attempt to find \mathbf{m} containing the Gauss coefficients that describes the Sq field away from quiet time. An issue of non-uniqueness arises as there are an infinite number of model solutions which fit the finite data.

Following the method of least-squares to obtain the model solution, \mathbf{m} , we construct the generalised inverse by multiplying both sides by \mathbf{A}^T

$$\mathbf{A}^T\gamma = \mathbf{A}^T\mathbf{A}\mathbf{m} + \mathbf{A}^T\mathbf{e} \quad 3.4$$

where $\mathbf{A}^T\gamma$ is the right hand side vector and $\mathbf{A}^T\mathbf{A}$ is referred to as the normal equation matrix.

Assuming the errors are distributed with zero mean (since our data are reduced to zero mean) and multiplying both sides by $(\mathbf{A}^T\mathbf{A})^{-1}$, we have

$$\mathbf{m} = (\mathbf{A}^T\mathbf{A})^{-1}\mathbf{A}^T\gamma \quad 3.5$$

this is comparable to seeking the objective function, R , which minimises the sum of the squares of the errors, \mathbf{e}^2 , between the model, \mathbf{m} , equations of condition $\mathbf{A}\mathbf{m}$, and the input data, γ ,

$$\mathbf{e} = \gamma - \mathbf{A}\mathbf{m} \quad 3.6$$

$$R = \mathbf{e}^2 = \mathbf{e}^T\mathbf{e} = (\gamma - \mathbf{A}\mathbf{m})^T (\gamma - \mathbf{A}\mathbf{m}) \quad 3.7$$

minimising the weighted least-squares, following Whaler and Gubbins (1981) and Gubbins (1983),

$$\mathbf{e}^T\mathbf{C}_e^{-1}\mathbf{e} \quad 3.8$$

where \mathbf{C}_e is the data error covariance matrix and \mathbf{e} is the vector of errors (residuals between the model and observatory measurements), we can write for the data error covariance matrix,

$$(\mathbf{C}_e)_{ij} = \text{cov}(e_i, e_j) \quad 3.9$$

with diagonal elements having information about the variance of the respective observatory measurements, assuming the errors are uncorrelated (covariance = 0 $i \neq j$).

3.4.3 Damping Parameter

We do not seek to minimise simply $\mathbf{e}^T \mathbf{e}$ but assume it to be normally distributed with zero mean, and thus seek to minimise the weighted least-squares as specify above (equation 3.8). Furthermore, as opposed to simply minimising the misfit, additionally, the model smoothness is considered in choosing the best solution, following the minimum norm approach. This smoothness is quantified through the use of a quadratic norm, N

$$\mathbf{N} = \mathbf{m} \Lambda \mathbf{m} \quad 3.10$$

where Λ is a positive definite matrix.

In the simplest case $\Lambda = \mathbf{I}$, where \mathbf{I} is the identity matrix. Λ (which is the norm used here), however, may also represent a more complex physical constraint. The objective function we therefore seek to minimise becomes

$$\mathbf{Q} = (\boldsymbol{\gamma} - \mathbf{A}\mathbf{m})^T \mathbf{C}_e^{-1} (\boldsymbol{\gamma} - \mathbf{A}\mathbf{m}) + \lambda \mathbf{m}^T \Lambda \mathbf{m} \quad 3.11$$

where λ is the damping parameter, a Lagrange multiplier.

Generally, in producing a geomagnetic field model, the damping parameter plays a significant role on the solution. The closeness of fit to the data is controlled by the damping parameter. The damping parameter is normally decided by plotting a trade-off curve. This is useful for examining and deciding the optimal level of the smoothing. Applying damping alongside the norm the null space of the normal equation is removed and very small eigenvalues are increased, considerably increasing the stability of the corresponding eigenvectors. As a result, models that are underdamped ($\lambda \rightarrow 0$) fit the data well, are less smooth and unrealistically complex and unstable, as the misfit is favourably minimised. Alternatively, models that are overdamped ($\lambda \rightarrow \infty$), are too smooth, producing large misfit to the data and the undetermined problem is stabilised.

Finally, to solve the model normal equations with the inclusion of damping, we find the maximum likelihood solution of the model parameters, $\hat{\mathbf{m}}$, which can be established through

$$(\mathbf{A}^T \mathbf{C}_e^{-1} \mathbf{A} + \lambda \mathbf{I}) \hat{\mathbf{m}} = \mathbf{A}^T \mathbf{C}_e^{-1} \boldsymbol{\gamma} \quad 3.12$$

$$\hat{\mathbf{m}} = (\mathbf{A}^T \mathbf{C}_e^{-1} \mathbf{A} + \lambda \mathbf{I})^{-1} \mathbf{A}^T \mathbf{C}_e^{-1} \boldsymbol{\gamma} \quad 3.13$$

This can be solved by employing various matrix decomposition methods. This study favours the Cholesky decomposition, with resolution analysis employing additional solving routine based on eigenvalue construction. This is carried out for a range of damping (λ).

Clearly there is a relationship between damping parameter and the smoothness/roughness of the models as well as the model-data-misfit. If we take the optimal solution (preferred damping parameter) and create a model, this model will fit the observations nicely. As a result the trade-off curve is a good tool used in choosing the preferred damping parameter.

Unfortunately, using the trade-off curve technique to determine our damping parameter was not possible, as there was no obvious ‘knee’. Returning to our model/data comparison plots presented in section 3.4.2, none of the plots differ very much when we varied the damping parameter. This may be explained by the lack of a ‘knee’ in our trade-off curve (not shown). As an alternative method, we used the residual of the model/data in terms of the error estimates on the measurements which value is as close to 1 as we can get. A residual of 1 means that we have fit the data to approximately one estimated standard deviation. The closer the residual is to 1, the better the model-fit-to-data. This gives a general guide as to when our models are in approximately the right parameter range – even though it’s only an approximation!

The use of regularisation to model the geomagnetic field have been in use in studies for decades (see Whaler and Gubbins, 1981; Shure et al. 1982; Gubbins and Bloxham, 1985). Regularised minimum norm inversions have continued to be used in analysis of geomagnetic field data, as it remains a unique approach in modelling the geomagnetic field. Table 3.1 shows the many models, from that of Bloxham (1987), that have employed the ‘regularization’ idea in modelling the time-varying magnetic field of the Earth.

| Model | N | Time Period | Expansion | References |
|--------------------|---------|--------------------------------------|-----------------------|--|
| MFSV/1900/1980/OBS | 8 10 | 1900-1980 1820-1900, 1900-1980 | Legendre Chebyshev | Bloxham (1987) Bloxham and Jackson (1989) |
| ufm1, ufm2 | 63 | 1690-1840, 1840-1990 | B-spline | Bloxham and Jackson (1992) |
| gufm1 | 163 | 1690-1990 | B-spline | Jackson et al. (2000) |
| CM3 | 14 | 1960-1985 | B-spline integrals | Sabaka et al. (2002) |
| CM4 | 24 | 1960-2002.5 | B-spline integrals | Sabaka et al. (2004) |
| CHAOS | 10 | 1999-2006 | B-spline and Taylor | Olsen et al. (2006) |
| POMME | 3 | 2000-2010 | Taylor | Maus et al. (2005) |
| GRIMM | 10 | 2001-2006.7 | B-spline | Lesur et al. (2008) |
| GRIMM-2 | 15 | 2001-2009.5 | B-spline | Lesur et al. (2010) |
| POMME-6 | 3 | 2000-2010 | Taylor | Maus et al. (2010) |
| Gufm-sat | 45 | 2000-2010 | B-spline | Finlay et al. (2012) |
| COV-OBS | 90 | 1840-2010 | B-Spline | Gillet et al. (2013) |
| CHAOS-4 | 38 | 1997-2013.5 | B-spline | Olsen et al. (2014) |

Table 3.2: List of models of the time-varying geomagnetic field which have used the regularised approach. N is the number of temporal basis functions used for each Gauss coefficient. Only the original and latest published sisters of models with sequence of models (e.g. GRIMM, POMME and CHAOS) are shown.

3.4.4 Model/Data Comparison

We use the CM4 modelling code to create models of the geomagnetic diurnal field at the Earth’s surface, based on selected datasets from moderately disturbed days ($K_p \leq 5_0$) 30/05/2006 and

04/07/2006. This allows the visualization and comparison of the CM4 model and the observatory station data. All the field plots presented in this study are plotted as equal area projection using Universal Time (UT) with the CM4 code.

Figures 3.13 to 3.16 shows exemplar plots showing surface diurnal field maps at different UT and spherical harmonic degrees. The diurnal variation surface field maps are of the Z component of the field truncated at spherical harmonic degrees, $n = 1, 3, 5,$ and 7 and $UT = 0, 6, 12,$ and 18 hours. The CM4 diurnal variation field maps (left panel in the figures) are regularised inversion of the CM4 model predictions. They are for a series of inversions for different maximum spherical harmonic degrees stated above. In deciding upon the damping parameter (λ), we explored the effect of changing it. To ensure fair comparative analysis between the CM4 model and the observatory station data, we explored a wide range of damping parameters, but only the one which produced models near optimal, in our view, is used and presented here. From the field plots shown in figures 3.13 to 3.16, it is clear that there is a relationship between the spherical harmonic degree and the model to data misfit.

At low spherical harmonic degree, $n = 1$, in figure 3.13, the map show basically a dipolar structure which is divided into areas of strong intensity and weaker intensity lobes separated by areas of null/zero intensity. The surface field can only be described by a limited number of large scale Gauss coefficients, resulting in a high residual (table 3.1 shows the residuals of the CM4 model and observatory station data at different UT for different spherical harmonic degrees). The most prominent/striking feature is that while the lobes in the data plots have remained almost unchanged (approximately stationary), with the weaker intensity lobe (blue lobe) dominating the northern hemisphere and the strong intensity lobe (red lobe) the southern hemisphere, with respect to their vicinity, and bounded by the null intensity area separation, that in the model plots have drifted. This feature of the lobe drifting in the model plots and staying steady in the data plots (model showing short term variability compared to data) is seen in all the different spherical harmonic truncations studied. We don't know the reason for this. It is obvious from the diurnal field maps that there are differences between the CM4 model and the observatory data. This difference is seen in the 0000hr, 1200hrs and 1800hrs UT maps. Only at 0600hrs that we can see some similarity between the CM4 model and the observatory data plots, as the weaker intensity lobe, occupying a central position in the model plot at 0000hr drifted upwards and sideways. Here the CM4 model nearly matches the observatory data in large-scale features, such as in areas of low and high magnetic field intensities (depicted by the red and blue patches respectively).

As we increase the spherical harmonic degree truncation to degree 3 ($n = 3$), more details of the diurnal field are revealed in terms of weak and strong magnetic intensities as shown in figure 3.14. Again we see the drifting of the lobes in the CM4 model, while the lobes in the data plot remaining approximately steady. Some similarities can be observed between both plots at 0600hrs with the positions of the weak and strong intensity lobes, with some minor improvement in predicting the certain parts of the globe at 1800hrs UT map. As the spherical harmonic degree truncation increases to higher values ($n = 5$ and 7), we can see the maps increasingly complex field structure and the CM4 model to observatory station data misfit is increasingly reduced. Comparing the global maps of the S_q diurnal field at the Earth's surface between the CM4 model and the observatory data for spherical harmonic degree 5 in figure 3.15, what is strikingly obvious is that the large areas of zero intensity appears in most of the central part of the globe, with the model largely agreeing well with the observatory data concerning much of the very strong intensity areas, particularly at the south

western and eastern parts of the globe, at 0000hrs. The CM4 model also matches the observatory data in some parts for the low magnetic intensity features at 0600hrs, 1200hrs, and 1800hrs UT.

For the higher spherical harmonic degree 7 ($n = 7$) in figure 3.16, details of most of the magnetic features are homogeneously distributed in the southern part of the globe, for both the strong and weak intensity features. The northern part of the map is mostly dominated by zero magnetic intensity.

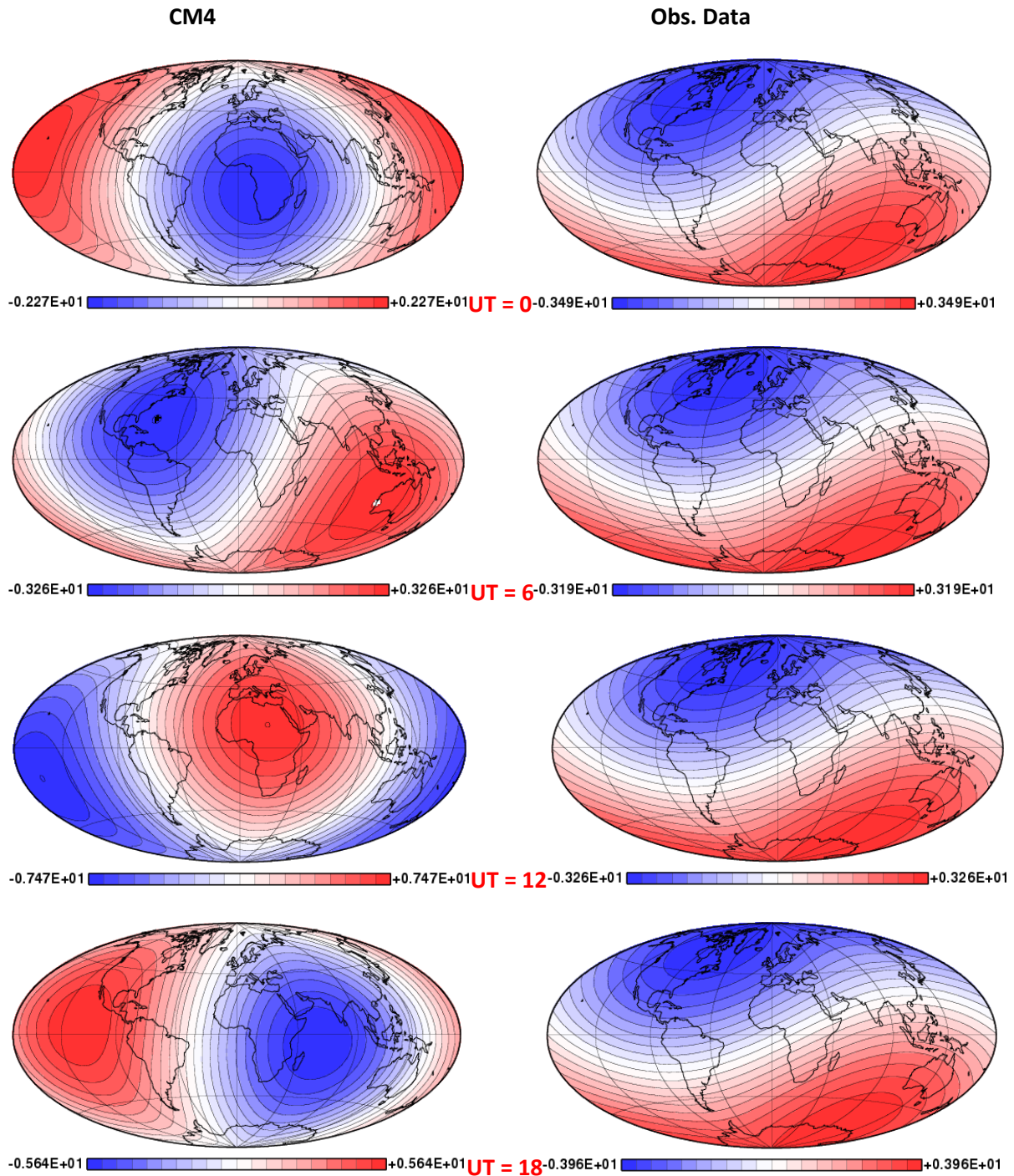


Figure 3.13: Plots of the Z component of the diurnal variation field at the surface from spherical harmonic models of data synthesised from the CM4 model and observatory data, for spherical harmonic degree up to 1. Left hand panels are of models of data synthesised from CM4. Large scale features, not much can be deduced.

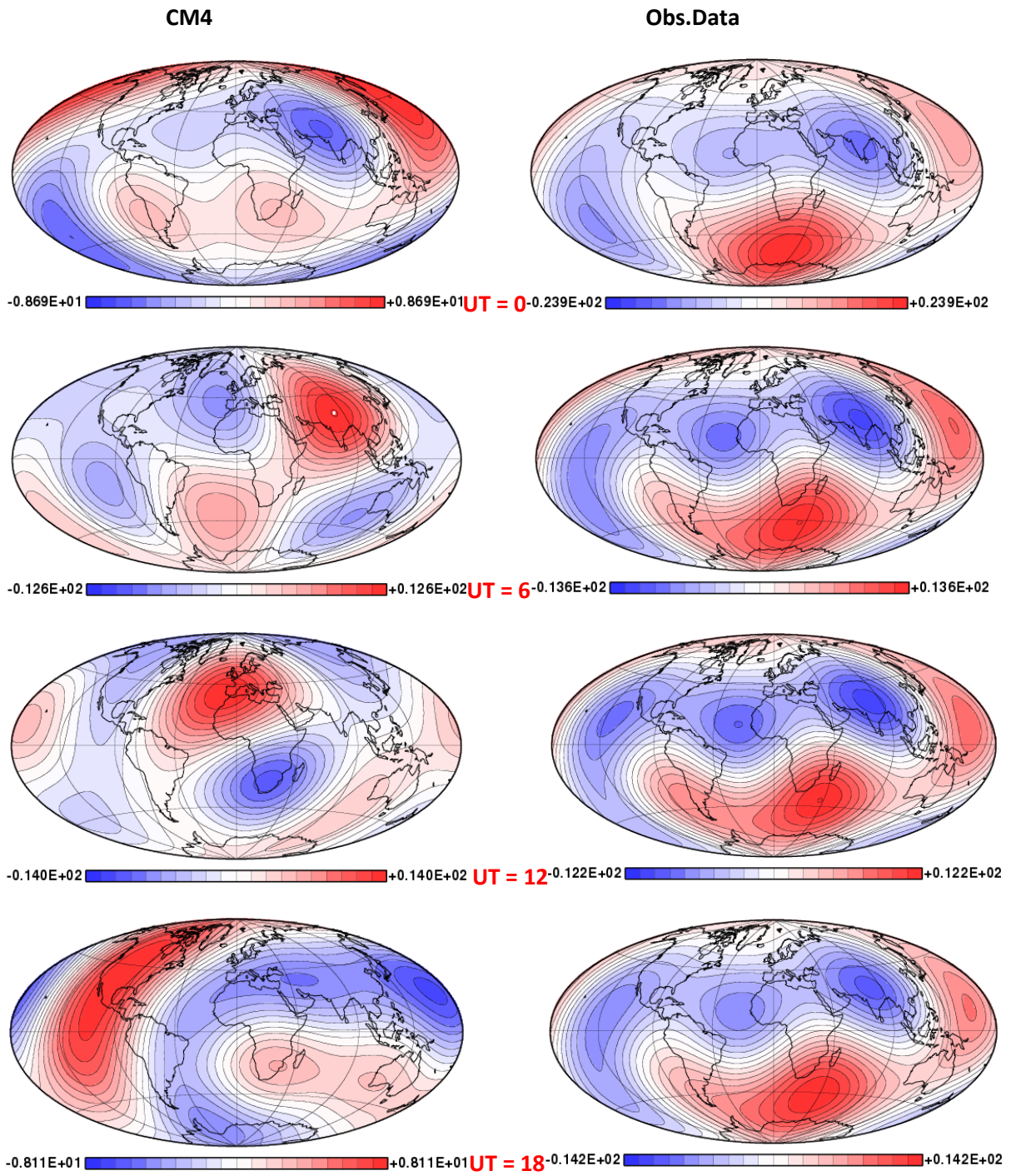


Figure 3.14: Similar to figure 3.13, for spherical harmonic degree up to 3. More features starts to be revealed.

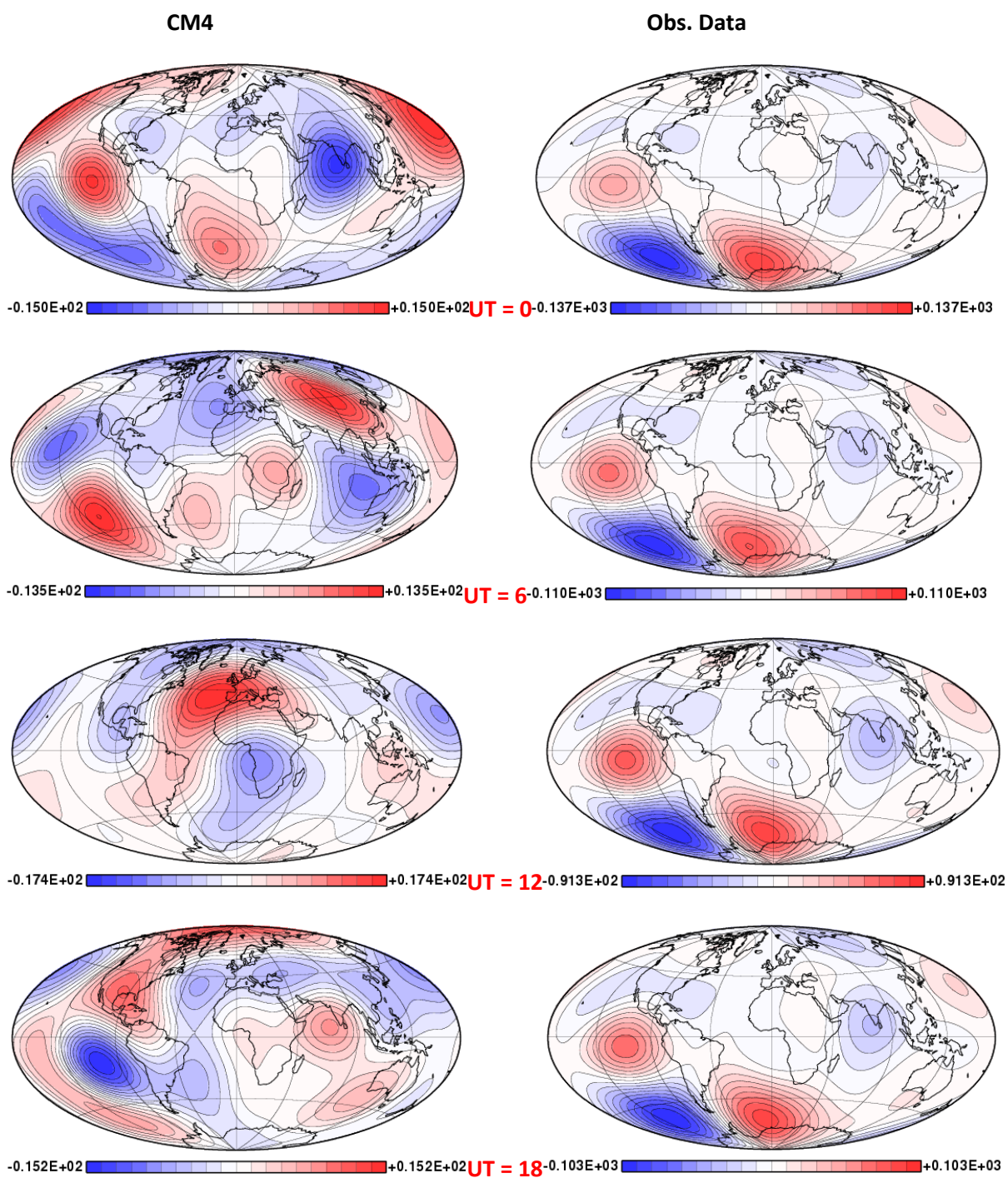


Figure 3.15: Similar to figure 3.13, for spherical harmonic degree up to 5. More small scales features and more coherence between CM4 and Observatory station data.

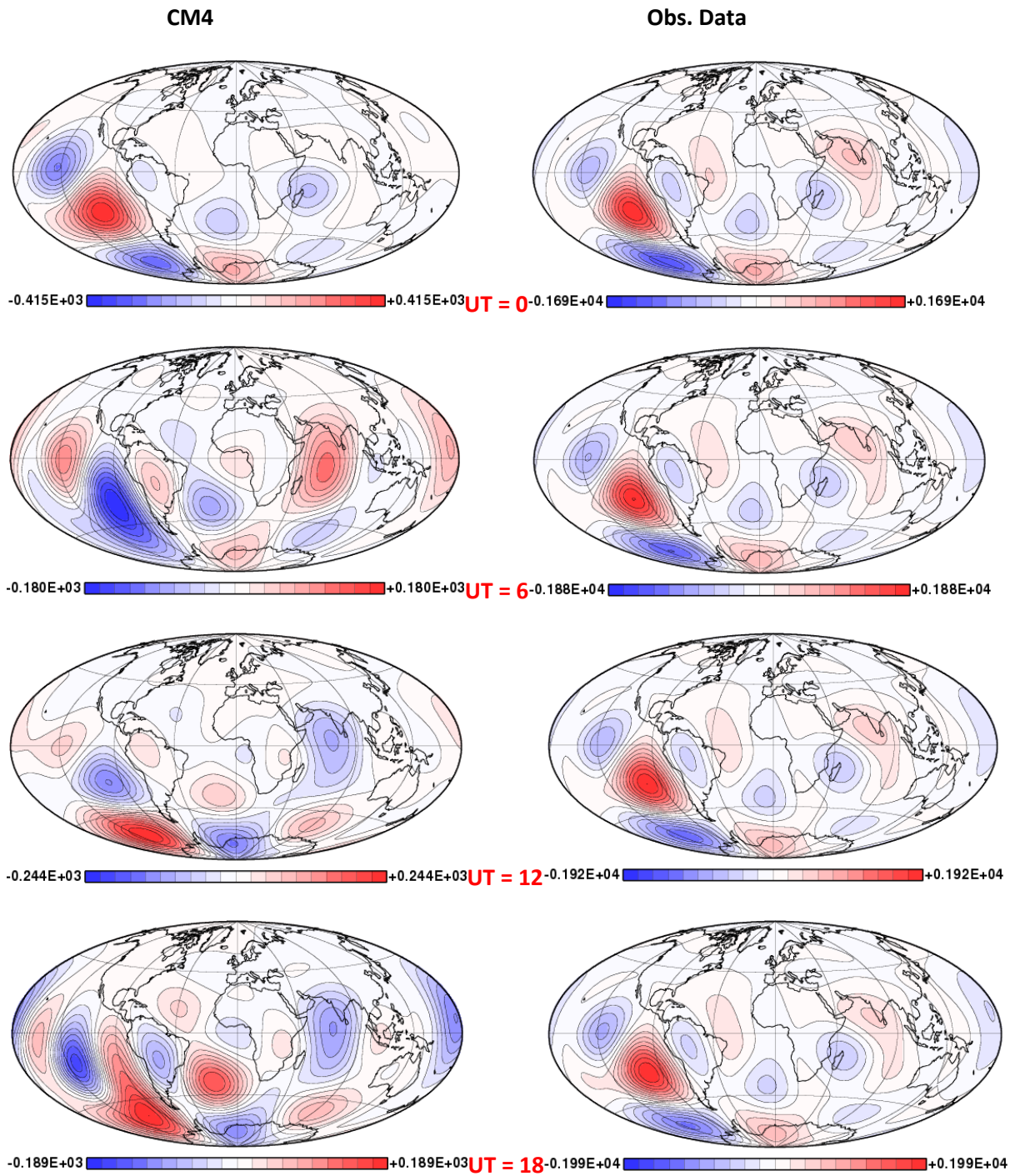


Figure 3.16: Similar to figure 3.13, for spherical harmonic degree up to 7. Improved coherence between CM4 and observatory data.

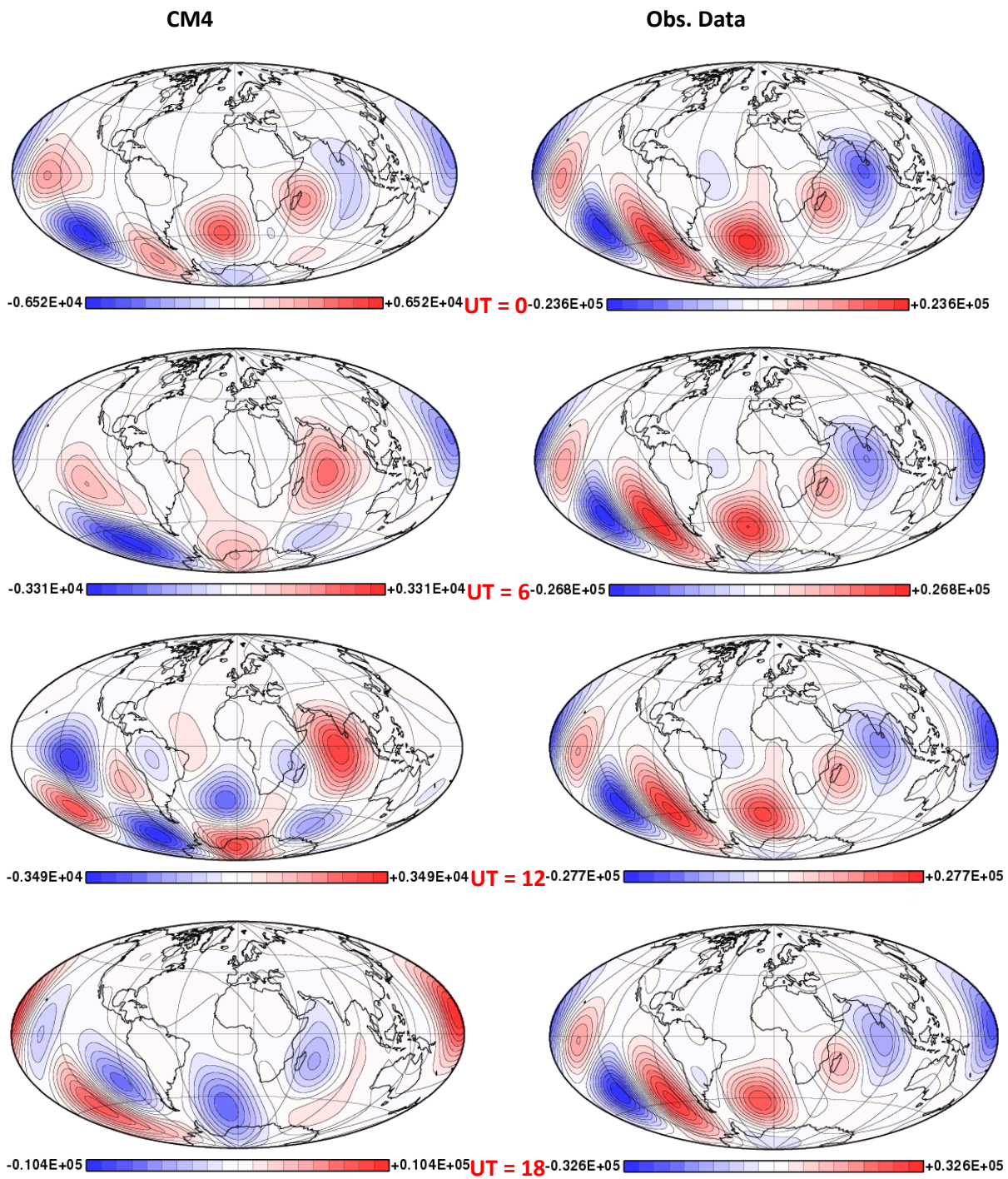


Figure 3.17: Similar to figure 3.13, for spherical harmonic degree up to 8. Not much difference in complexity and configuration between maps in degree 7 and these in figure 8.

| Time (UT) | CM4 Model Residuals | Station Data Residuals |
|-----------------|---------------------|------------------------|
| <i>Degree 1</i> | | |
| 0 | 1.41 | 3.31 |
| 6 | 1.76 | 3.24 |
| 12 | 1.92 | 3.21 |
| 18 | 1.40 | 3.24 |
| <i>Degree 3</i> | | |
| 0 | 0.82 | 2.95 |
| 6 | 0.73 | 2.96 |
| 12 | 0.97 | 2.93 |
| 18 | 0.82 | 2.94 |
| <i>Degree 5</i> | | |
| 0 | 0.69 | 2.57 |
| 6 | 0.56 | 2.66 |
| 12 | 0.70 | 2.61 |
| 18 | 0.67 | 2.60 |
| <i>Degree 7</i> | | |
| 0 | 0.54 | 1.96 |
| 6 | 0.41 | 2.10 |
| 12 | 0.56 | 2.02 |
| 18 | 0.56 | 2.00 |

Table 3.3: Residuals of the CM4 model and Observatory station data for different Universal Times (in hours) and spherical harmonic degrees. Residuals decreases as the spherical harmonic degree increases to higher values.

The model reproduces the features of the magnetic diurnal field map of the observatory data such as the weak and strong intensity fields in much parts of the globe. Owing to the higher spherical harmonic degree truncation and regularization, the Sq diurnal maps show a comparatively high level of detail while simultaneously suppressing small-scale noise. The differences here between the CM4 model and observatory data at spherical harmonic degree 7 are small. These differences may be due to short term variations in regional or local conductivity anomalies where they exist. To a large extent the CM4 model provides a good description of the features of the diurnal variation field over the globe at spherical harmonic degree 7. In other words, as we move onto higher spherical harmonic degree truncation, we can see some similarities between the CM4 model and observatory station data. As we increase the spherical harmonic degree truncation, the model to data misfit reduces. But this relationship between increasing the spherical harmonic degree and reducing the misfit can be restricted by the data quality, quantity and coverage. Also, the model roughness increases with increase in spherical harmonic degree truncation, as smaller scale features are capable of being incorporated, which does little to improve the complexity of the field or change the configuration. This we can see in figure 3.17, when increasing the spherical harmonic degree from 7 to 8. This increase in spherical harmonic degree truncation, misfit reduction and increase roughness has a toll on the model viability, as seen in the excessively high intensity values at higher truncation spherical harmonic degrees. Our observation shows that at higher spherical harmonic degree truncation level ($n > 5$), it starts going horribly wrong, because by including terms up to degree 5 and above, there are too many free parameters that are unaccounted for. This accounts for why the values indicated in the scales at higher degree truncation are excessively high. Here, even though

the misfit between the model and data is considerably reduced, the roughness increases dramatically as seen in the plots, scales and figure 3.18 below.

At higher altitude, our observation showed that the structure of the field maps for both the model and data is more complicated than at the surface. More details of the field are revealed at higher spherical harmonic than when plotted at the Earth's surface in terms of small scale features. This may be due to the fact that degree spherical harmonics amplified more as we get closer to the source of the external field contributions. Also, as observed for the plots plotted at the Earth's surface (figures 3.13 – 3.17), the lobes indicative of areas of strong and weak intensities are seen to behave in a similar way, with those in the data remaining almost steady in their approximate positions all through the day and those in the model drifting, slowly in this case.

While the results are qualitatively better when plotted at higher altitude, as the model prediction of the data is better than when plotted at the Earth's surface, the values in the scales (intensity) are way higher (excessively particularly for the data), but the residual values remain the same as in table 3.3 above.

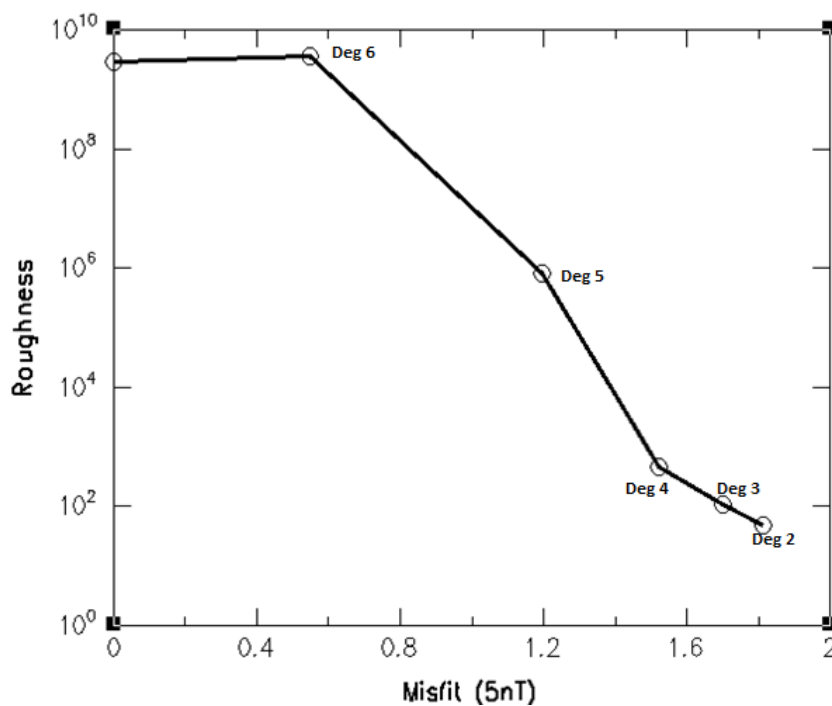


Figure 3.18: Plot of roughness against misfit for spherical harmonic degree truncation ($n = 2, 3, 4, 5$ and 6). The roughness gives you a measure of when the data/model-misfit starts going wrong, which is at $n > 5$.

3.4.5 Spatial Power Spectrum

One way to study variations in the geomagnetic field is by analysing how these changes are distributed as a function of spatial frequency. A way of doing this is by estimating the spectrum of the geomagnetic variations. Geomagnetic power spectrum density, which is a measure of the power in geomagnetic field variations, is an important tool in field modelling. It allows comparison of field models estimated from different datasets. It can be used to identify noise level and systemic errors

(Maus, 2008). Power spectra allow the geomagnetic field models to be examined in terms of contribution from different degree, n , components.

Loves (1974) is one of the most widely used spectra, and is defined as,

$$R_n = (n + 1) \sum_{m=0}^{\infty} [(g_n^m)^2 + (h_n^m)^2] \quad 3.1$$

This produces a measure of the mean square field from different n , as a proportion of the total modelled field.

In main geomagnetic field studies, where power spectrum has found wide applications, when the spectrum of the field is plotted at the core mantle boundary (CMB), the dipole dominates, as it does at the surface. Also, higher n components approach an equivalent level of contribution, making the spectra to flatten and become 'white' for uncorrelated field, such as the Earth's crustal magnetic field at long wavelengths (Maus, 2008). For daily variation and harmonics, the energy comes from diurnal heating of the ionosphere. This creates high frequency energy in the Earth-Ionosphere cavity. At high frequencies there is assumed to be continued fall off on the national spectrum. Our attempt at plotting the spectrum of the diurnal field in this study produced a continuous straight line (not shown). This trend was repeated at various λ and n .

3.4.6 Spatial Differences

For a more direct comparison between the CM4 models and the magnetic observatory data models, we have taken differences between the CM4 models and the magnetic observatory data models at higher spherical harmonic degrees (5 and 7), where we can see some close similarity and coherence between the CM4 model and the observatory data (figures 3.15 and 3.16). This is because a straight forward measure of the quality of the CM4 model fit to the observatory data is given by the difference between the model predictions and the respective observations.

Figures 3.19 and 3.20 show exemplar maps of the differences between the CM4 models and the magnetic observatory data models for spherical harmonic degrees 5 and 7 at 6-hourly intervals.

The difference reflects pretty much what is seen in the main models. With most of the areas where the magnetism is strong (red lobes) in the main models showing weak magnetism (blue lobes) in the difference map, and vice versa. Generally, the difference is small and no obvious pattern can be gleaned from it.

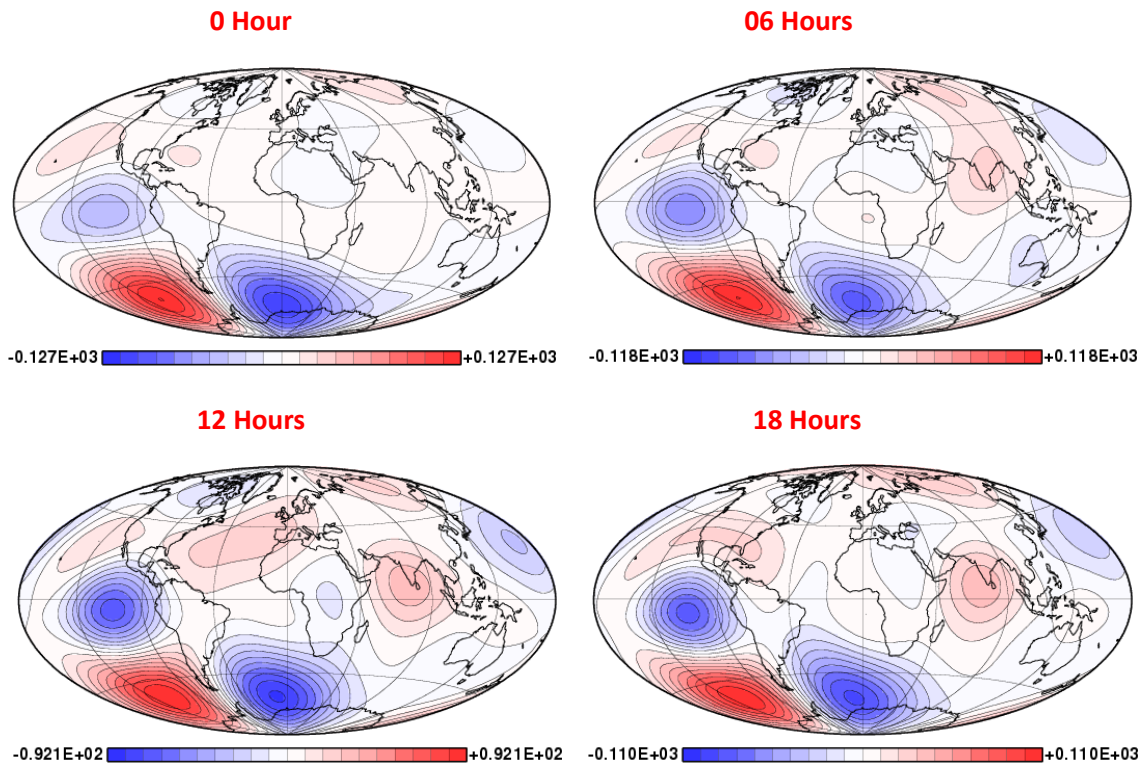


Figure 3.19: Similar to figure 3.15 for differences between the CM4 model predictions and magnetic observatory data models at spherical harmonic degree up to 5 at 0, 6, 12 and 18 hours.

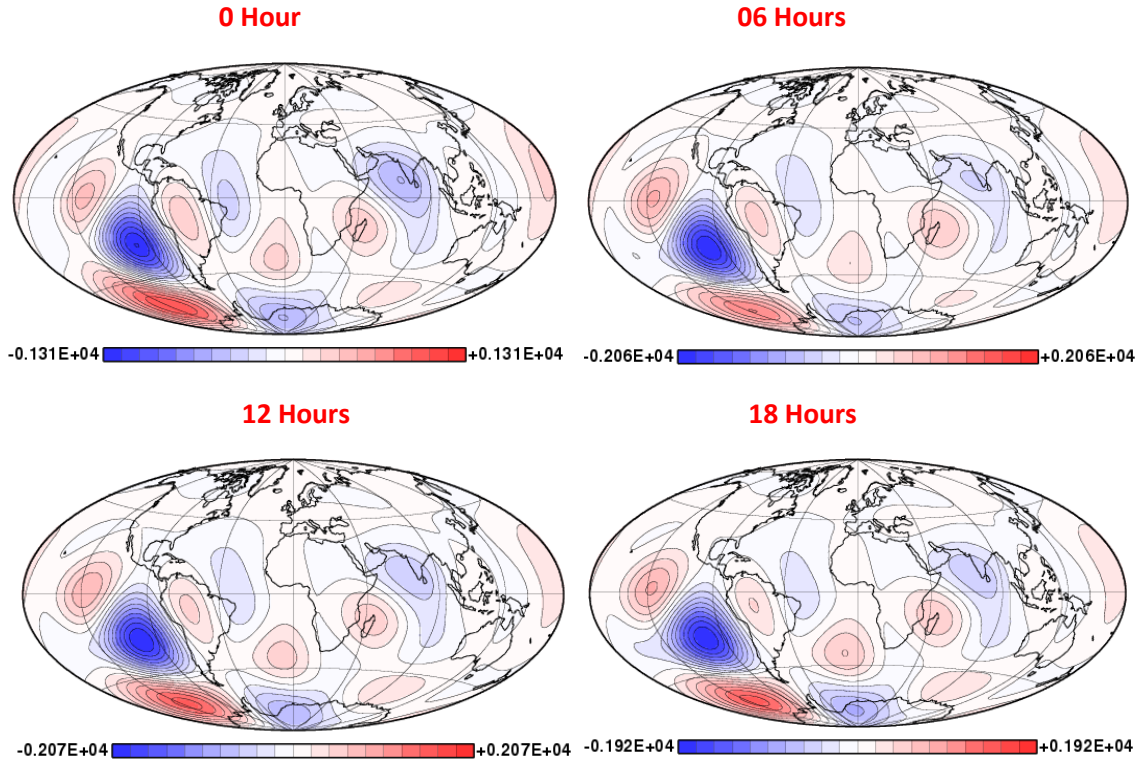


Figure 3.20: Similar to figure 3.16 for differences between the CM4 model predictions and magnetic observatory data models at spherical harmonic degree up to 7 at 0, 6, 12 and 12 hours.

3.5 Modelling Summary

The focus of this chapter has been on testing the CM4 model code to see how well it performs predicting the magnetic observatory data, in view of the updating (extending the timespan) of the CM4 code to recent period. We could see clearly that the CM4 model is predicting the daily variation of the parameterized fields during quiet period outside the timespan of the model. Most of the signature profiles of the CM4 and the magnetic observatory data reflect well the diurnal variations expected for the different geographical regions and latitudes.

Away from quiet time period, the CM4 model is producing more reasonable predictions than expected, despite the lack of active data in the original model dataset. The model is fitting the regional type features of the geomagnetic components of the observatory data in most of the geographic regions. However, the model is not doing well predicting short term features during period of rapid variations (seen as wiggles in the signature profiles), especially for the X component. This is where we have the greatest misfit between the CM4 model and magnetic observatory data. The CM4 predicts the Y and Z components better than the X component. This may be due to the fact that the X component is affected more by external sources and since the model sources majority of its external field predictions from D_{st} which is based on the X component.

When comparing the different modelled maps of the CM4 model and the magnetic observatory data, we find that increasing the spherical harmonic degree decreases the residuals and reduces the misfit of the model to data. This produces better coherence and close match between the CM4 model and magnetic observatory data. Our attempt at plotting a power spectrum produced a continuous straight line; furthermore, our trade-off curve produced no 'knee', making it difficult choosing our preferred damping parameter through the trade-off curve technique.

The above scenario provides the motivation to investigate more the nature of the variations further in the following chapters. For more rapid variations, particularly the noisier data, we investigate the relationship with the RC index, by detrending the data sequences with spline fits, and try to really compare these data with the RC values – to see if they match.

Chapter 4

Correlated Errors, Residuals and Covariant Modelling

As shown in the previous chapter, we have observatory data that are showing Sq variation. On the average, this is well fit by the comprehensive model (CM4). Individual days when compared against the comprehensive model show deviations. These deviations are of two kinds – one, long period (a day or so) variations that show variations between days of slowly varying feature – difference in Sq signal from the average or long time unmodelled magnetosphere/induction? Two, more rapid variations, particularly seen on the noisier data (these are days away from quiet period). These have fluctuations/‘wiggles’ unmatched and unexplained by the comprehensive model. We look at these against the RC index, to see if these variations are reasonably well matched with RC index.

In order to do this and explain this part of the observed field unmatched and not explained by the comprehensive model, we took an approach to determine the error correlation of the field model residuals. This we did by estimating the data covariance matrix posterior to the field modelling procedure directly from the field model residuals.

In taking this approach, we looked for this at detrending the observatory data sequences with spline fits, compare these observatory data with the RC index values, and see if we can establish the nature of the variations. It was possible to compare with individual trends against RC. Possibly more interesting is to compare an eigenvector decomposition of the residuals from the detrending. Expectation might be that the noisiest of the three eigenvectors (i.e. associated with the largest eigenvalue) would correlate particularly well with RC variations. For the RC variations, we also decided it will be particularly interesting to look at the decomposition for two observatories combined. If these two observatories showed large variations that were coherent, then they would show up in combination in the eigenvector for the largest eigenvalue, and this eigenvector could then be compared against RC. This is particularly a question to see whether RC was doing well for all observatories or only European ones.

In this chapter, we present results obtained for the data covariance modelling of the observatory field model when error correlation is taken into account, and all that is discussed above. With the data covariance matrix known, it is possible to estimate the uncertainty of a field model and quantities infer from the field model. Also, understanding of how the errors correlate can be used to enhance the field model. But first, we begin with a summary of comparison between RC and D_{st} , showing the coherence between them, summary of earlier studies of error correlation and field model uncertainty estimates in order to inspire and show the motivation behind the significance of determining the covariance of the field model errors/residuals.

4.1 RC versus D_{st}

The comprehensive model (CM4) used in this study produced from satellite and observatory data sets include parameterization of the field generated by the magnetospheric ring current, based on the D_{st} index. We suspect that the more rapid variations we see on our noisier data (away from quiet time) are due to the effect of ring current. Thomson and Lesur (2007), reported that the assumption behind both the D_{st} and RC modelling approaches is that rapid variations of the inner magnetospheric field are mainly due to a symmetric ring current, where the perturbations are aligned with the internal dipole axis. These rapid variations seen in our observatory data could not

be explained by D_{st} , and so we decided to try to compare these to RC values. D_{st} is derived from four low-latitude observatory data time-series, at one hour time resolution. There are other more rapid indices related to it. This and other uses of long time series data (especially satellite data) have revealed the weaknesses of D_{st} index. A couple of these weaknesses include the uncertainties in its baseline, and in the relative contribution from internal (induced) fields. (Olsen et al. 2005; Maus and Weidelt, 2004).

In an attempt to improve the parameterization of the ring current Olsen et al (2000) derived and constructed the RC index using data from 21 INTERMAGNET observatories (See section 2.3.3). RC index is derived from the horizontal (X) components only and consist of the sum of the magnetospheric and induced part, similar to D_{st} , but describes the strength of the magnetospheric ring better than D_{st} . RC describes the magnetospheric and induced fields even during quiet conditions, when the baseline instabilities of D_{st} normally lead to less than optimal results. Unlike D_{st} , which is constructed from just four observatories, RC index is constructed from 21, showing a wider global coverage, and it also has higher temporal resolution. Figure 4.1 shows the comparison between D_{st} and RC index for some selected days used as part of this study. There is clearly reasonable agreement between the D_{st} and RC index. Is the variation enough to account for the rapid fluctuations we see, even though the fluctuations do appear to be coherent between observatories?

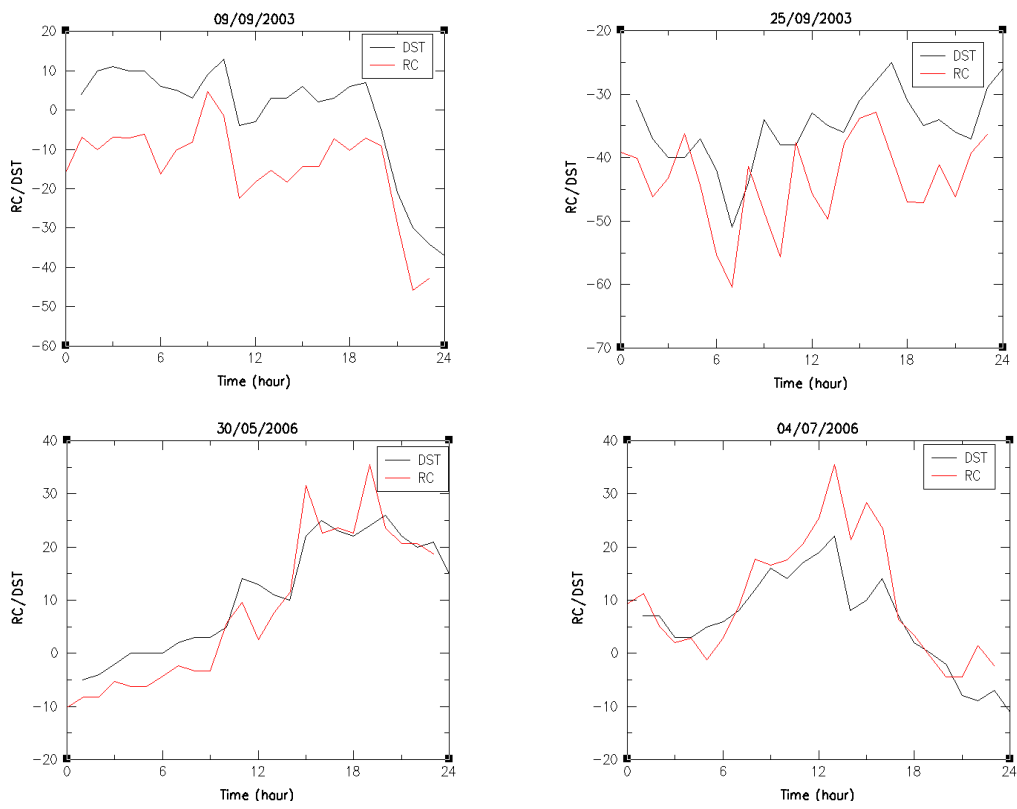


Figure 4.1: Comparison of the RC and D_{st} for some selected days, 9 September 2003, 25 September 2003, 30 May 2006 and 4 July 2006. These are days of moderately high magnetic activity (away from quiet time), with $K_p \leq 5-$, 4+, 4- and 4- respectively.

4.2 Uncertainty Estimates of Geomagnetic Field Models

Any numerical model of the geomagnetic field can only be an approximation to the true field, and we would like to have a reasonable estimate of the errors involved (Lowes and Olsen, 2004). Uncertainty estimates are important prior information for global geomagnetic field modelling. This is because they ensure proper weighting of different data sources. Geomagnetic field models usually consist of coefficients of a truncated spherical harmonic analysis derived by weighted least squares analysis (Langel et al. 1989). Geomagnetic data are typically assumed to be uncorrelated, and an estimated, diagonal, data covariance matrix is incorporated as an inverse weighting function. To make uncertainty estimates of geomagnetic field models, observations are repeated several times at different locations giving several independent but similar data sets, from which geomagnetic field models are created from the distributions of the resulting Gauss coefficients. Accuracy estimates on the derived coefficients are taken to be the usual output covariance matrix. Evaluating all the Gauss coefficients of a geomagnetic field model or error correlations in space and time, particularly for the ones including secular variation, crustal field, the external field, etc., would require the inversion of a dense matrix whose dimension is the number of data, using extensive computations. This is a formidable task! To overcome this, the correlations of the Gauss coefficients or data errors are considered within each observatory site. The covariance matrix is block diagonal with 3x3 blocks (or 6x6 blocks for 2 combined observatory sites), which could be easily inverted.

Geomagnetic field models do not take all the fields into account, and there may likely be systematic errors from unmodelled fields – correlated errors are frequently observed in geomagnetic field modelling due to unmodelled fields. Holme et al. (2003) showed that the errors on the data used for the CO2 (CHAMP and the two Ørsted satellites) field model were highly correlated both within and between orbits, and the primary cause was believed to be unmodelled magnetospheric field. Lowes and Olsen (2004), on their part showed that by assuming that errors are uncorrelated in estimating variances of the Gauss coefficients, the estimated level of uncertainty may be wrong – as a result we will have no reliable uncertainty estimates of the geomagnetic field models. Deficiencies in uncertainty error estimates in geomagnetic field models have long been known. Langel (1989) and (1991), Jackson (1990), Rygaard-Hjalsted et al (1997) and Lowes and Olsen (2004), using different approaches and concentrating on different aspects, have done studies on how to make more realistic uncertainty estimates.

Langel et al (1989) studied uncertainty error estimates in core field models. They found that the uncertainty is underestimated, since the modelling procedure does not take into account the fields from truncated terms, the presence of crustal fields or the presence of external fields, such as Sq. Using statistical representations of the unknown fields from the truncated terms, the crust and the ionosphere, they concluded that not accounting for error correlation in field modelling does not significantly influence the results of the Gauss coefficients, only their uncertainty estimates.

Jackson (1990), looked at the effect of crustal field on core field models. He introduced a stochastic representation of the crust and described the theory necessary for calculating the correlation functions from which relevant elements of data covariance matrix are calculated for typical satellite magnetic data. He suggested that assuming the magnetization of the crust is completely uncorrelated in space, nevertheless correlations appears to be significant over angular separations of up to 15° at satellite altitude. Taking geologic evidence into consideration, which suggests

correlated crustal magnetization, we may have even larger correlation length of crustal field at satellite altitude – underlining the importance of taking error correlation when making field models.

Rygaard-Hjalsted et al (1997), also studied the effect of the crustal field on core field models, looking at two plausible statistical models for the crustal magnetization described by Jackson (1994). They investigated the effect of making erroneous assumptions, in terms of the validity of the previously widely used assumption that the contribution to the data error from the crustal field in core field models is white noise. Using statistical representation of the crustal field, in which the crustal magnetization is given as a realization of a stationary, isotropic, random process, they suggested a number of things:

- That at satellite altitude the associated fields exhibited significant correlation over ranges as great as 15° or more, which introduces off-diagonal elements into the covariance matrix.
- That the Gauss coefficients for models where correlation were accounted for compared to where they are neglected differed by as much as 27% with the maximum discrepancies near degree 11.

They concluded that off-diagonal elements should be included in the covariance matrix due to correlation of crustal field in core field modelling. Failure to include this, they said, leads to bias and inconsistent core field models. They suggest that one way to reduce this problem of error correlation and avoid a non-diagonal covariance matrix is using a data set with large data spacing.

Lowes and Olsen (2004), looking at the variances of the Gauss coefficients of the OSVM (Ørsted Main and Secular Variation Models), developed a method to mimic the uncertainty estimates based on comparison of the geomagnetic field models with data not included in the field modelling – they called this the subset approach. They suggest that this method is advantageous as the whole data set can be used to make the field model, thereby obtaining more realistic variances than by using a simple diagonal covariance matrix, reducing computational costs. In the study, they found that systematic errors were present due to inadequately modelled ionospheric and magnetospheric currents, which enhanced the variation of the degree and order of the variances given in the data distribution. Also, serial correlation tends to increase the variance of the sectoral and near-sectoral coefficients, decreasing it for other harmonics. They also showed that in the CM3 model (precursor to CM4) there are still fields of a few nanotesla at satellite level at night times, produced by currents induced inside the Earth by the time-varying ionospheric field. Finally, they suggested that whichever method is used to determine the variances of Gauss coefficients, it would be advisable to compare the obtained variances with estimates based on their subset approach – and that it would be realistic to use a simple overall uncertainty of 25% of the Gauss coefficients.

All the studies summarised above dealt with the uncertainty error estimates in core field models, where most of the data errors are due to effects from ionospheric, magnetospheric and other external field sources. Here we are looking at the error correlation of the geomagnetic observatory data showing S_q diurnal variation. Our aim is to try to ascertain the correlation of the field model residuals in order to construct the data covariance matrix. We take a direct statistical study approach of the field model residuals to investigate and try to explain the behaviour of the observatory magnetic data plots left unexplained by the comprehensive model developed from our observatory data. With this approach we make no assumptions about the error or variance of our individual measurements, and we do not consider whether the field model is sufficiently good at resolving all non-random parts. The analysis of the results of our error correlation work is presented

later in this chapter, but first we briefly discuss geomagnetic field model residuals in the next section.

4.3 Geomagnetic Field Model Residuals

Geomagnetic field models are only approximations of the observed field, although they can be very extensive. There are always parts of the field that a given model does not account for – these are the unmodelled fields. This unmodelled field may express itself as a correlation of the field model residuals. Analysing the part of the observed field that is not explained by a given model (in our case the rapid variations/fluctuations seen in our noisier data), the residuals can provide more understanding into the inadequacy of the geomagnetic field model. The unmodelled field, in addition to the instrument error, constitute the errors in the data used to develop the model. Being only an approximation to the observed, the geomagnetic field model will have some degree of uncertainty. It is therefore important to have a feeling for the level of uncertainty as it can provide a measure of the validity of a given geomagnetic field model.

The field model residuals consist of unmodelled signals and instrument errors found by subtracting values predicted by the model (comprehensive model in our case) from the observatory data. They are often considered an estimate of the data error and are typically assumed to be uncorrelated and have a Gaussian distribution (assumptions not totally justified). Walker and Jackson (2000) showed that unmodelled fields do, to a large extent, cause serial correlation of the errors, and that the field model residuals, in general, do not have a Gaussian distribution.

Field model residuals can provide understanding into the imperfection or weakness of a field model, give a feeling of the level of uncertainty of the field model, and clues on how to improve the model. The residuals not only reveal the behaviour of the unmodelled field but also characterise the important sources of the unmodelled fields.

4.4 Data Covariance Matrices and EigenAnalysis

4.4.1 Methodology: Penalised least-squares Spline

Spline functions are a class of piecewise polynomials which satisfy continuity properties depending on the degree of polynomials. They have desirable properties which have made them a powerful numerical tool for mathematical approximations. A popular type of spline, B-spline, has been used for decades as temporal basis functions in representation of time-dependent geomagnetic field models. Early models used fourth-order (cubic) B-splines, with the order gradually increased to sixth-order (Lesur et al. 2010) for satellite models seeking to determine secular acceleration adequately. Among the reasons for the popularity of B-spline technique is that it provides a flexible basis for smoothing varying descriptions of the data. It is one of the most famous properties of B-spline functions that they have minimal support to a given degree of freedom, smoothness and domain partition. B-spline models are best because they provide similar results even when using low-degree splines to the models produced using higher degree polynomials while avoiding instability at the edges of an interval (Runge's phenomenon) (DeBoor, 1978). B-splines have been employed in many of the geomagnetic field models from that of Bloxham and Jackson (1992). Table 3.2 (section 3.4.3) show a list of widely used models of the time-varying magnetic field that have employed the use of B-spline.

In this study, we employed a penalised least-squares technique with space-time cubic B-spline based on DeBoor (1978) algorithm. Penalised least-squares technique is used in solving practical problems that frequently arises in the analysis of geomagnetic data i.e. fitting a smooth curve of unknown parametric form to a time series of observations. It is a means of studying long term trends or to remove a trend and look at the remaining part of the signal. It is of particular importance when one is dealing with irregularly spaced noisy data, especially for the purpose of obtaining smooth curves from noisy data records.

Let $B_j(x; q)$ denote the value at x of the j th B-spline of degree q .

A fitted curve \bar{y} to data (x_i, y_i) is the linear combination $\bar{y}(x) = \sum_{j=1}^n \hat{a}_j B_j(x; q)$, when the degree of the B-splines is clear from the context, or use $B_j(x)$ instead of $B_j(x; q)$ if immaterial.

Indexing of B-splines requires care. The indexing connects a B-spline to a knot i.e. it gives the index of the knot that characterizes the position of the B-spline. Choice of knots has been subject of much research. However, by adopting a penalised least-squares fit to a model, we can over-parameterise our model (i.e. give it too many knots) and use damping to ensure the result is not sensitive to the choice of knot spacing. Our choice here is not to specify the knot spacing, but to follow automatic schemes for optimizing the number and positions of the knots. This is because we just want to fit a smooth curve to a set of noisy observations using the spline function.

So we employed this least-squares spline technique to analyse the ionospheric and magnetospheric signals in our geomagnetic diurnal variation observatory data, for which we found it necessary to remove some trends that are associated with these signals and look at what is left (residuals). To do this, we detrended the data sequences with spline fits. We use spline to fit a spline curve through the comprehensive model predictions, we then want the predictions of this fit for the higher density times given by the observatory data.

The comprehensive model, CM4, gives us predictions for both the ionospheric and magnetospheric fields for particular observatory (day and period). We want to obtain data that remove these predictions so that we can look at the eigenvalues and eigenvectors of what is left over, in order to discover to what extent CM4 is able to make useful predictions, and study the field that is left over. In other words, we want to subtract the prediction of the comprehensive model from the data, and get the residuals to look at the "wiggles" seen in our observatory data. In particular, we are interested in looking at the minute data after the ionosphere or the magnetosphere or both are subtracted, so that we can look at the correlation of what remains.

We have used the comprehensive model (CM4), as model for generating all the synthetic data. We modified certain parts of the comprehensive model to subtract specific field contributions in order to generate the different data of interest:

- Data uncorrected with CM4 (i.e. removing the contributions from ionosphere and magnetosphere)
- Data corrected for ionosphere and magnetosphere (i.e. contributions from ionosphere and magnetosphere contributed)
- Data corrected for ionosphere only (i.e. only contributions from ionosphere computed)
- Data corrected for magnetosphere only (i.e. only contributions from magnetosphere contributed)

Here, we present the results/analysis of the treatment of the covariance by considering the covariance between the different diurnal variation residuals in the X, Y, Z directions for each observatory location. The treatment of covariance between the different components allows for higher temporal sensitivity of the model. For secular variation (SV) studies, it is expected that the error would be dominated by unmodelled signals from external variations, in particular, the ring current, especially in midlatitude, leading to a particularly strong error correlation between the X and Z components (Wardinski and Holme, 2006 and 2011).

The correlation of data errors was considered within each observation location, and the covariance matrix is block diagonal with 3 x 3 blocks. The eigenvectors and eigenvalues were computed iteratively from the covariance matrix of the residuals to the model at each observatory location for each data scenario mentioned above. This is in order to look at the eigenvectors and eigenvalues of what is left over, to see to what extent the comprehensive model is able to make useful predictions. Also, it allows us to look at the field that is left over and see what the difference between removing and not removing different components of the comprehensive model comes down to. Can we see any strong correlations shown by Sq between components with or without the comprehensive model?

The application of correlation between the three vector components at a particular location was first considered in the modelling of attitude errors in vector magnetic satellite data (Holme and Bloxham, 1996). To give an impression of the structure of the data covariance matrices, some examples are shown below for each data scenario for different observatory location globally.

4.4.2 Results of Covariance/EigenAnalysis

We computed iteratively the eigenvalues and eigenvectors from the covariance matrix of the residuals for each observatory location (geographically). This was done using a full daily residual data, with applied corrections to the input data, using external fields (ionospheric and magnetospheric) calculated by comprehensive model 4 (CM4). We test the effect of the data selection and correction criteria for different selected observatory locations. The use of CM4 to correct the input data before calculating the eigenvalues and eigenvectors removes a strong bias from internal field sources.

A covariance matrix quantifies the uncertainties in the model estimates due to inaccuracies in the measurements. Given two signals, X and Y, it is interesting to know how well they correlate. The covariance of X and Y can be defined generally as

$$M(X,Y) = E[(X-E(X))(Y-E(Y))] \quad 4.1$$

Given N number of signals, the covariance is NxN matrix whose ij^{th} entry is

$$M_{ij} = C(X,Y) \quad 4.2$$

The correlation between the two signals is defined in terms of the elements of the covariance matrix as

$$M(X,Y) = C(X,Y)/\sigma(X)\sigma(Y) \quad 4.3$$

The correlation has a value of 1 for signals highly correlated, and a value of 0 for signals not correlated. (Here we assume our standard deviation to be 1, as in equation 5.1 in section 5.4)

If the values are uncorrelated, then the covariance matrix will be diagonal with the variances on the diagonal. But if some of the variables depend on each other or simply correlate, the covariance matrix will have non-zero off-diagonal elements. Thus the number of non-zero elements in the covariance matrix is related to the correlation of the different variables. In other words, if X is positively correlated with Y, Y is also positively correlated with X. Therefore, the covariance matrix is always a symmetric matrix with the variances on the diagonal and the covariance off-diagonal.

Eigenvalues and eigenvectors represent the basic characteristics of the physical properties of the covariance matrix, in turn, of the model. The covariance matrix is completely defined by its eigenvalues and eigenvectors. This means that

$$Mv = \lambda v \tag{4.4}$$

where $M = [m_{ij}]$ is a square matrix and λ is a number corresponding to the eigenvalue. Each λ obtained has corresponding to it a solution of v called an eigenvector.

In other words, $v = 0$ is a solution for any value of λ not normally useful; but for non-trivial solution, where $v \neq 0$, the values of λ are the eigenvalues of M and the corresponding solutions of equation 4.4 are the eigenvectors of M .

Expressed as a set of separate equations,

$$Mv = \lambda v \equiv Mv - \lambda v = 0 \tag{4.5}$$

and $(M - \lambda I)v = 0 \tag{4.6}$

Introducing a unit matrix, I , since we can only subtract a matrix from another matrix.

Note that for a set of homogenous linear equations, such as the right hand constants all zero in equation 4.6, to have a non-trivial solution, $|M - \lambda I|$ must be zero.

Equation 4.4 holds for each eigenvector-eigenvalue pair of matrix M . In the 3x3 case, we obtain 3 eigenvectors and 3 eigenvalues. Following Holme and Bloxham (1996), if the eigenvalues (λ) and the eigenvectors (v) are known, then the subblock of the data error covariance matrix can be stated as a sum of vector dyadic

$$C_e = \sum_{i=1}^3 \lambda_i v_i v_i^T, \quad C_e^{-1} = \sum_{i=1}^3 \frac{1}{\lambda_i} v_i v_i^T \tag{4.5}$$

(Wardinski and Holme, 1996)

Keeping in mind that the eigenvalues of a real symmetric matrix are real and its eigenvectors orthogonal.

As an example, the eigenvalues (λ) and eigenvectors (v) for one selected observatories in different geographical region of the Earth in local geomagnetic elements, the X, Y and Z directions, for the different input data corrected for the specified field contributions are displayed in table 4.1 below. The day is 30th May, 2006, and the $K_p \leq 4-$.

| λ | V_1 | V_2 | V_3 |
|---|--------|--------|--------|
| Mbour (MBO) in Africa | | | |
| 1 = 468.46 | 0.801 | -0.386 | -0.457 |
| 2 = 94.68 | 0.277 | 0.920 | -0.257 |
| 3 = 12.44 | 0.519 | 0.070 | 0.852 |
| Beijing Ming Tombs (BMT) in Asia | | | |
| 1 = 370.18 | -0.223 | 0.972 | 0.052 |
| 2 = 253.46 | 0.952 | 0.206 | 0.225 |
| 3 = 12.36 | -0.208 | -0.100 | 0.973 |
| Niemegk (NGK) in Europe | | | |
| 1 = 388.73 | -0.056 | 0.985 | 0.162 |
| 2 = 246.36 | 0.958 | 0.007 | 0.268 |
| 3 = 21.55 | -0.281 | -0.171 | 0.944 |
| Boulder (BOU) in North America | | | |
| 1 = 439.47 | -0.186 | 0.964 | 0.188 |
| 2 = 60.05 | 0.340 | -0.116 | 0.933 |
| 3 = 39.21 | 0.922 | 0.238 | -0.306 |
| Trelew (TRW) in South America | | | |
| 1 = 83.38 | 0.715 | 0.486 | 0.502 |
| 2 = 40.05 | -0.531 | 0.845 | -0.061 |
| 3 = 15.73 | -0.454 | -0.223 | 0.863 |
| Gnangara (GNA) in Oceania | | | |
| 1 = 110.94 | 0.783 | 0.315 | 0.536 |
| 2 = 46.92 | -0.612 | 0.542 | 0.576 |
| 3 = 8.99 | 0.109 | 0.779 | -0.617 |

(a)

| λ | V_1 | V_2 | V_3 |
|---|--------|--------|--------|
| Mbour (MBO) in Africa | | | |
| 1 = 90.26 | 0.801 | -0.449 | -0.401 |
| 2 = 50.22 | -0.065 | -0.730 | 0.680 |
| 3 = 9.95 | 0.596 | 0.519 | 0.613 |
| Beijing Ming Tombs (BMT) in Asia | | | |
| 1 = 200.52 | 0.936 | -0.345 | -0.073 |
| 2 = 46.19 | 0.341 | 0.938 | -0.067 |
| 3 = 2.51 | 0.092 | 0.038 | 0.995 |
| Niemegk (NGK) in Europe | | | |
| 1 = 124.49 | 0.987 | -0.156 | 0.038 |
| 2 = 61.20 | 0.155 | 0.988 | 0.007 |
| 3 = 5.246 | -0.039 | -0.001 | 0.999 |
| Boulder (BOU) in North America | | | |
| 1 = 101.55 | -0.509 | 0.852 | 0.125 |
| 2 = 42.46 | 0.838 | 0.523 | -0.157 |
| 3 = 12.72 | 0.199 | -0.025 | 0.980 |
| Trelew (TRW) in South America | | | |
| 1 = 101.46 | 0.805 | 0.516 | 0.291 |
| 2 = 24.42 | -0.593 | 0.704 | 0.392 |
| 3 = 6.72 | -0.002 | -0.488 | 0.873 |
| Gnangara (GNA) in Oceania | | | |
| 1 = 103.36 | 0.678 | 0.225 | 0.700 |
| 2 = 17.06 | -0.134 | 0.974 | -0.183 |
| 3 = 5.76 | -0.723 | 0.030 | 0.691 |

(b)

(c)

| λ | V_1 | V_2 | V_3 |
|---|--------|--------|--------|
| Mbour (MBO) in Africa | | | |
| 1 = 137.20 | -0.563 | 0.776 | 0.283 |
| 2 = 69.63 | -0.463 | -0.581 | 0.670 |
| 3 = 25.08 | 0.684 | 0.246 | 0.687 |
| Beijing Ming Tombs (BMT) in Asia | | | |
| 1 = 226.80 | 0.979 | -0.203 | -0.001 |
| 2 = 120.98 | 0.203 | 0.978 | -0.491 |
| 3 = 3.14 | 0.011 | 0.048 | 0.999 |
| Niemegk (NGK) in Europe | | | |
| 1 = 172.52 | 0.961 | -0.264 | 0.085 |
| 2 = 139.41 | 0.261 | 0.965 | 0.040 |
| 3 = 7.81 | -0.092 | -0.016 | 0.996 |
| Boulder (BOU) in North America | | | |
| 1 = 176.57 | -0.307 | 0.944 | 0.121 |
| 2 = 37.84 | 0.947 | 0.290 | 0.140 |
| 3 = 24.25 | -0.097 | -0.158 | 0.983 |
| Trelew (TRW) in South America | | | |
| 1 = 155.55 | 0.901 | 0.351 | 0.255 |
| 2 = 42.96 | -0.412 | 0.876 | 0.252 |
| 3 = 4.48 | -0.135 | -0.332 | 0.934 |
| Gnangara (GNA) in Oceania | | | |
| 1 = 114.69 | 0.611 | 0.455 | 0.648 |
| 2 = 32.06 | -0.268 | 0.889 | -0.371 |
| 3 = 8.53 | -0.745 | 0.053 | 0.665 |

(d)

| λ | V_1 | V_2 | V_3 |
|---|--------|--------|--------|
| Mbour (MBO) in Africa | | | |
| 1 = 415.95 | 0.848 | -0.291 | -0.442 |
| 2 = 45.21 | 0.190 | 0.947 | -0.259 |
| 3 = 14.98 | 0.494 | 0.136 | 0.859 |
| Beijing Ming Tombs (BMT) in Asia | | | |
| 1 = 302.34 | -0.645 | 0.764 | 0.014 |
| 2 = 159.92 | 0.744 | 0.623 | 0.241 |
| 3 = 10.26 | -0.176 | -0.166 | 0.970 |
| Niemegk (NGK) in Europe | | | |
| 1 = 234.62 | -0.258 | 0.949 | 0.179 |
| 2 = 168.55 | 0.937 | 0.202 | 0.284 |
| 3 = 16.90 | -0.234 | -0.241 | 0.942 |
| Boulder (BOU) in North America | | | |
| 1 = 277.38 | -0.241 | 0.946 | 0.214 |
| 2 = 49.24 | -0.687 | -0.323 | 0.651 |
| 3 = 32.47 | 0.686 | 0.010 | 0.728 |
| Trelew (TRW) in South America | | | |
| 1 = 91.41 | 0.241 | 0.887 | 0.394 |
| 2 = 40.34 | 0.606 | -0.455 | 0.653 |
| 3 = 18.30 | 0.758 | 0.081 | -0.647 |
| Gnangara (GNA) in Oceania | | | |
| 1 = 104.36 | 0.908 | 0.061 | 0.415 |
| 2 = 62.68 | -0.335 | 0.701 | 0.630 |
| 3 = 19.80 | 0.252 | 0.711 | -0.657 |

Table 4.1: Eigenvalues (λ) and eigenvectors (v) for selected observatories in different geographical region of the globe in X, Y and Z directions for: (a) Data uncorrected with CM4 (b) Data corrected for CM4 (ionosphere and magnetosphere) (c) Data corrected for Ionosphere only, and (d) Data corrected for Magnetosphere only.

4.4.3 Discussion/Analysis

Examination of the global eigenvalue/eigenvector results of the residuals in the X, Y, and Z components of the different components of the field read a random pattern of positive and negative errors. It revealed some biases, patterns, covariance and correlations between the components X, Y, and Z. Also, the distribution of residuals of each component reveals some complex spatial patterns, with strong temporal variation. The results of the eigenvalues and eigenvectors in each component of the variation obtained from the residuals of the observatory data shown in figure 4.1 above show that X direction is consistently the noisiest (most disturbed), with the Z direction the least disturbed (quiet), and Y direction more disturbed (medium). The eigenvalue is an indication of the noise level in the variation, and the eigenvector directions are controlled by the noise in the data (Wardinski and Holme, 2011). The covariance matrices here describe the coherency of signals between the X, Y, and Z components. The associated eigenvectors and eigenvalues describe respectively the direction and magnitude of these signals. Information regarding external field signals is contained in the residuals between the observatory data and the magnetic field approximated by the model. Wardinski and Holme (2011) showed that coherent signals between the residuals of the X, Y and Z components can be described by a 3x3 covariance matrix, assumed to be constant through time at each given magnetic observatory location. The eigenvalues and eigenvectors of the residual covariance matrix can then be used to study the observed modelled field components in terms of their directions from least disturbed (quiet), more disturbed (intermediate) to most disturb (noisy), corresponding to the eigenvectors with the smallest to the largest magnitude eigenvalue. Smaller eigenvalues imply less coherent signals' and looking at the eigenvalue results in table 4.1 for all the field components in all the regions, it can be seen that the eigenvalues for X and Y are of greater magnitude, and therefore the covariance of the signals between X and Y is greater for most of the field components. This observation is true for most of the observatory locations studied both European and non-European. This is not overly surprising as the X component of the field is more easily influenced by variation from the external fields' sources of ionospheric and magnetospheric contributions.

In the eigenvalues and eigenvectors result in table 4.1 for observatories in the different geographical regions, we see a degree of dominance of the largest eigenvalues and eigenvectors in all the different components of the field. The largest eigenvalues for the two horizontal components (X and Y) are more dominant than that for the vertical component (Z). Induction effects might be an issue present in Z component, and for daily/rapid variations, which our data is showing, the conductivity of the surface is effectively infinite. As a result, there is low penetration of Z, and more or less doubling of the strength of the horizontal field as seen in X, and in some locations of Y components, especially for residual data corrected for CM4 (ionosphere and magnetosphere). Therefore, we can see in figure 4.1(b), for data corrected for CM4, that the strong covariance comes between X and Y, in most observatory locations, depending on the direction of the horizontal plane. Our focus is on the first eigenvalue (λ_1) with its associated eigenvectors (where $v_1 = X$, $v_2 = Y$ and $v_3 = Z$) as it is the most disturbed (noisiest) and gives the source of our greatest error and misfit between the model and data. Hence, there is little covariance with Z, which is not very well explained. An exception is Mbour (MBO) in Africa, and Gngara (GNA) in Oceania, where we observe some covariance between X and Z with correlations between X and Z.

Eigenvalue/eigenvector results in table 4.1(a), (c) and (d) for data uncorrected with CM4, data corrected for ionosphere only and data corrected for magnetosphere only respectively, show this

trend in GNA where the covariance is between X and Z (the eigenvectors, v_1 and v_3 , having the largest values) and MBO (except in 4.1(c), where it shows covariance between X and Y). It is clear from the eigenvalues and eigenvectors values in table 4.1 that the European, Asian, North American and South American observatories tend to show significant, consistent covariance between the X and Y components in this study, as the eigenvectors corresponding to X (v_1) and Y (v_2) components give the largest values among the 3 components. Although, TRW (South America) differ from this trend, showing covariance between X and Z (for data uncorrected with CM4) and covariance between Y and Z (for data corrected for magnetosphere only).

Figures 4.2 – 4.5 shows the residuals plots between the modelled variations in all 3 components (X, Y, Z) for selected observatory locations. These were the same residuals used for calculating the covariance matrix, eigenvalues and eigenvectors above. The essence is to show graphically the covariance and correlation between the residuals of the 3 components for the selected observatory locations, to support the results and analysis of the eigenvalues and eigenvectors results in terms of the covariance between them. In most of the plots, we observe that there is anti-correlation between the X and Y components, which is well pronounced, except in TRW and GNA, where this anti-correlation is not seen or pronounced. The CM4 corrections applied to the data residuals in the plots of figure 4.2 and ionospheric corrections applied in figure 4.3 clearly does a good job of removal, as the amplitudes of the components, especially in X and Y, are somewhat reduced, compared to that in figures 4.4 and 4.5, for data where no corrections was applied and for data where magnetospheric corrections only was applied respectively. Shows the magnetosphere obviously doesn't get rid of the fluctuations.

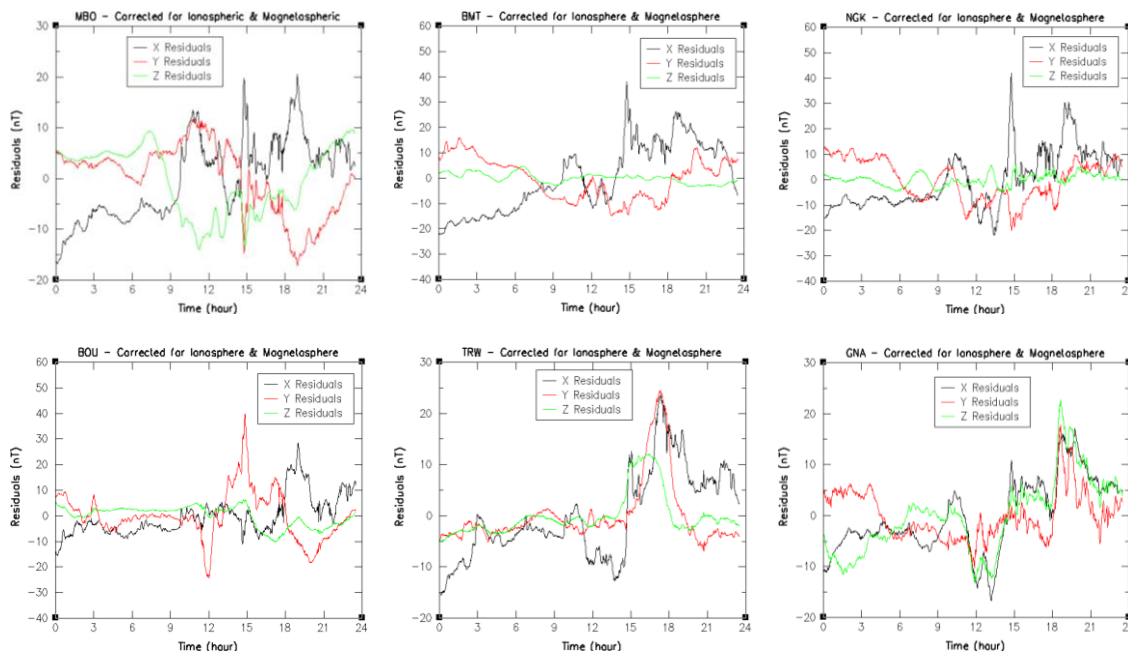


Figure 4.2: Plots of the residuals of the 3 components (X,Y,Z) used for calculating the covariance matrix, eigenvalues and eigenvectors at six observatory locations MBO, BMT, NGK, BOU, TRW and GNA. This is for the case where we apply corrections to the input residual data for ionosphere and magnetosphere (i.e. data corrected for ionosphere and magnetosphere).

Much of what we observed here is unlike what obtains in slow and longer variations, where the effective infinite conductivity sphere is well beneath the surface and hence strong correlation is seen between X and Z residuals (Wardinski and Holme, 2006; Manda and Olsen, 2006; Began et al.,2009). The pattern observed in this study can be seen in much of the observatory locations studied globally, indicating a kind of global phenomenon – showing that this is well explained by CM4 model. Another pattern observed in the residuals corrected for ionosphere and magnetosphere is that the eigenvectors in the X direction tends to be strongly biased positively compared to the eigenvectors in the Y direction (inversely correlated) which display negative signs. This is seen in most of the European, Asian and African observatory locations. The North America stations display features opposite this (negative X direction and positive Y direction), while the South American and Oceania stations show positive signs in both X and Y directions.

A clear similarity can be seen in the field behaviour of the observatory locations for all three components for residual data corrected for CM4 (ionosphere and magnetosphere) and for residual data corrected for ionosphere only. The residual plots in X, Y, and Z directions for data corrected for ionosphere only is shown in figure 4.3. We can still see much of the stronger covariance coming between the X and Y directions, with little covariance between X and Z. Gnanagara (GNA) in Oceania is the only exception, as we can see some correlations between X and Z. Here the behaviour of the different components mirror what we see in figure 4.2, with anti-correlation between X and Y for most of the plots and much of the day, except in GNA and TRW.

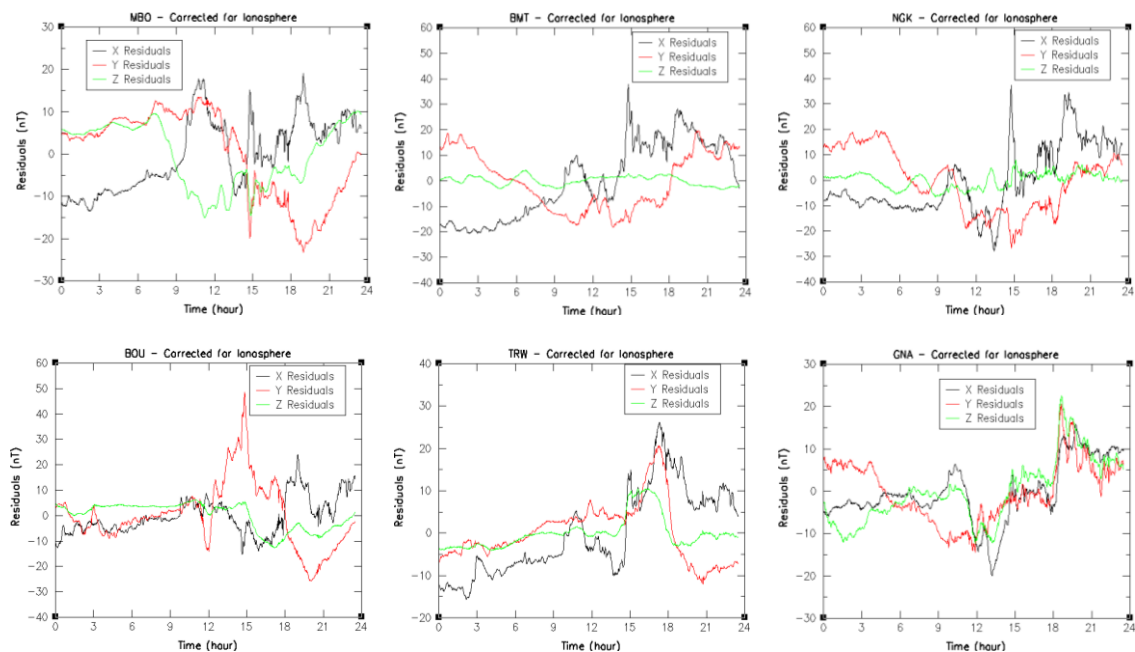


Figure 4.3: Plots of the residuals of the 3 components (X,Y,Z) used for calculating the covariance matrix, eigenvalues and eigenvectors (X,Y,Z) at six observatory locations MBO, BMT, NGK, BOU, TRW and GNA. This is for the case where we apply corrections to the input residual data for ionosphere only.

Clear similarities can also be observed in the field behaviour of the three components for the residual data where no correction was applied (raw residual data) and that corrected for magnetosphere only. See figures 4.4 and 4.5 for raw residual data plots and that for which magnetospheric corrections was applied respectively.

Some covariance between X and Y directions can still be seen in most of the observatory locations, showing inverse correlations, except the South American (Trelew,TRW) and Oceania

(Gnangara,GNA) locations. Here we can also see some Z correlations, which gets stronger for the case where no corrections was applied (i.e. raw residual data uncorrected with CM4). In general, while we can see anti-correlation in the residuals for the X and Y directions in most of the observatory locations globally, they show no correlation of both with Z, except in Gnangara (GNA), where we can see some anti-correlation with X. The lack of strong or clear cut patterns or X, Y, and Z component biases and the cross covariance of the residuals in the three components in some cases in most of the observatory locations, provides support for the consideration of performing error covariance analysis between different field elements at a single location.

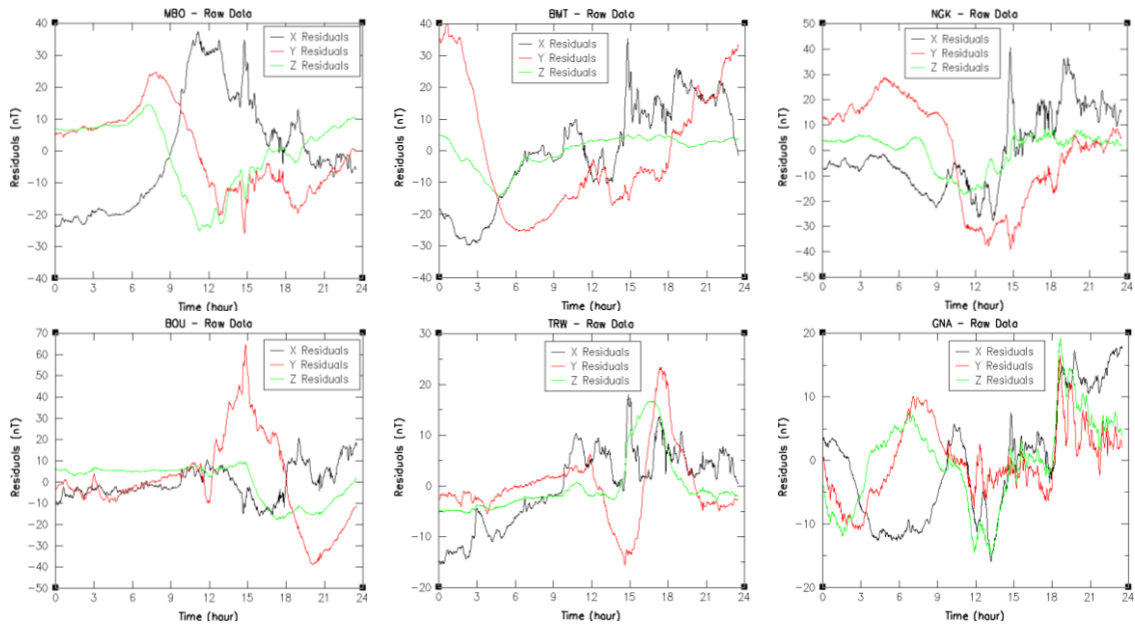


Figure 4.4: Plots of the residuals of the 3 components (X,Y,Z) used for calculating the covariance matrix, eigenvalues and eigenvectors (X,Y,Z) at six observatory locations MBO, BMT, NGK, BOU, TRW and GNA, for raw residual data (data uncorrected for CM4).

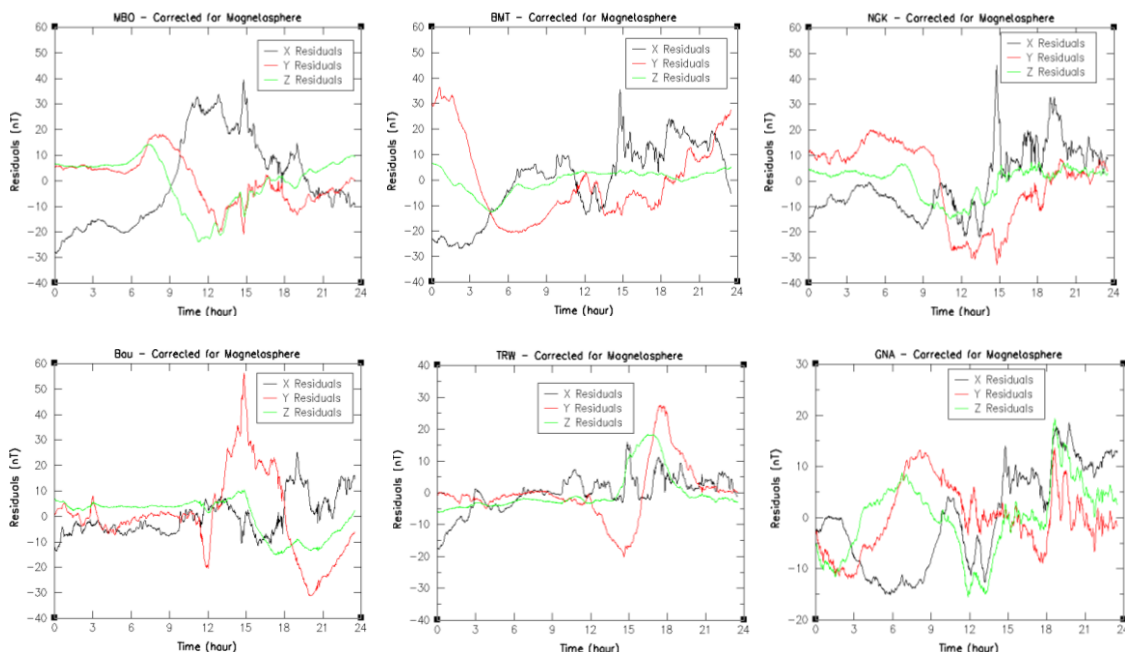


Figure 4.5: Plots of the residuals of the 3 components (X,Y,Z) used for calculating the covariance matrix, eigenvalues and eigenvectors (X,Y,Z) at six observatory locations MBO, BMT, NGK, BOU, TRW and GNA, for residual data with magnetospheric corrections applied.

4.4.4 Combined Observatory Locations

In addition to the case of single observatory location above, we look at the case of combined observatories, as it might be particularly interesting to do and look at the decomposition for two observatory locations at a time; to look at the covariance in the behaviour of the three components, X, Y, and Z, for the residual data when uncorrected and also when corrected for different field contributions with CM4 (ionospheric and magnetospheric) or corrected for only ionospheric and only magnetospheric respectively. We calculated the eigenvalues and eigenvectors from a 6x6 covariance matrix. In the 6x6 case, we obtain 6 eigenvalues and 6 eigenvectors, with the first 3 eigenvectors (V_1, V_2 and V_3) representing that of the first observatory and the next 3 eigenvectors (V_4, V_5 , and V_6) representing that of the second observatory, corresponding to each eigenvalue (λ) (with the eigenvalue with the largest value being the one of interest, as it is the one with the noisiest signal). It is expected that if these two combined observatory locations showed large variations that are coherent, then the expectation is that they would show up in combination in the eigenvector for the largest eigenvalue. The final eigenvalues and eigenvectors for two combined European observatories (NGK and AQU) and a combined European and non-European observatories (NGK and MBO) are shown in table 4.2 and 4.3 below. This is also for the same day and Kp as for the single observatory location analysed above.

| λ | V_1 | V_2 | V_3 | V_4 | V_5 | V_6 |
|------------|--------|--------|--------|--------|--------|--------|
| 1 = 217.22 | 0.730 | -0.161 | 0.029 | 0.635 | -0.193 | 0.027 |
| 2 = 94.57 | 0.222 | 0.773 | 0.014 | 0.120 | 0.579 | -0.060 |
| 3 = 6.265 | -0.616 | 0.773 | 0.259 | 0.710 | -0.058 | -0.195 |
| 4 = 5.28 | 0.118 | -0.119 | 0.946 | -0.172 | 0.144 | 0.162 |
| 5 = 2.12 | -0.144 | -0.346 | -0.187 | 0.222 | 0.567 | 0.690 |
| 6 = 0.99 | 0.069 | -0.484 | -0.039 | -0.004 | 0.552 | -0.674 |

(a)

| λ | V_1 | V_2 | V_3 | V_4 | V_5 | V_6 |
|------------|--------|--------|--------|--------|--------|-------|
| 1 = 785.54 | -0.103 | 0.697 | 0.103 | -0.259 | 0.635 | 0.148 |
| 2 = 323.52 | 0.825 | 0.133 | 0.254 | 0.428 | 0.069 | 0.223 |
| 3 = 37.45 | -0.019 | -0.250 | 0.722 | -0.494 | -0.138 | 0.391 |
| 4 = 3.71 | -0.031 | -0.545 | -0.335 | 0.060 | 0.546 | 0.537 |
| 5 = 3.51 | -0.523 | -0.016 | 0.468 | 0.698 | 0.136 | 0.029 |
| 6 = 1.41 | -0.185 | 0.369 | -0.269 | 0.120 | -0.506 | 0.698 |

(b)

Table 4.2: Eigenvalues and eigenvectors for two combined European observatories (NGK and AQU) where: (a) Residual data corrected for CM4 (i.e. ionosphere and magnetosphere), and (b) Residuals uncorrected for CM4 (i.e. raw data).

| λ | V_1 | V_2 | V_3 | V_4 | V_5 | V_6 |
|------------|--------|--------|--------|--------|--------|--------|
| 1 = 202.14 | 0.743 | -0.193 | 0.034 | 0.509 | -0.344 | -0.179 |
| 2 = 92.55 | 0.280 | 0.703 | 0.036 | -0.193 | -0.343 | 0.520 |
| 3 = 23.04 | 0.200 | 0.598 | -0.149 | 0.178 | 0.583 | -0.456 |
| 4 = 11.57 | 0.370 | -0.292 | -0.106 | -0.005 | 0.626 | 0.613 |
| 5 = 7.86 | -0.403 | 0.158 | 0.317 | 0.781 | 0.064 | 0.313 |
| 6 = 4.21 | 0.173 | -0.011 | 0.929 | -0.249 | 0.169 | -0.124 |

(a)

| λ | V_1 | V_2 | V_3 | V_4 | V_5 | V_6 |
|------------|--------|--------|--------|--------|--------|--------|
| 1 = 832.58 | -0.029 | 0.657 | 0.137 | -0.586 | 0.308 | 0.332 |
| 2 = 314.42 | 0.830 | -0.053 | 0.268 | -0.148 | -0.420 | 0.197 |
| 3 = 56.86 | 0.444 | 0.503 | -0.337 | 0.550 | 0.332 | -0.155 |
| 4 = 19.41 | -0.122 | 0.412 | -0.331 | -0.224 | -0.650 | -0.482 |
| 5 = 4.95 | -0.187 | 0.090 | -0.400 | 0.262 | -0.366 | 0.771 |
| 6 = 4.01 | -0.253 | 0.367 | 0.726 | 0.462 | -0.247 | -0.002 |

(b)

Figure 4.3: Eigenvalues and eigenvectors for combined European and non-European observatories (NGK and MBO) where: (a) Residual data corrected for CM4 (i.e. ionosphere and magnetosphere), and (b) Residuals uncorrected for CM4 (i.e. raw data).

Here, we can see that for the combined European locations (NGK and AQU), and the combined European and non-European locations (NGK and MBO), the noisy signal gets combined in the two eigenvectors with the two largest eigenvalues. The largest correlates very well with the largest eigenvalues/eigenvectors from the single observatory location analysis outlined above (figures 4.2 and 4.4) i.e. the X, Y and Z components from both observatories showed good correlation. This can be seen from just looking at the residual plots (see figure 4.6 and 4.7) for both cases when the residuals were corrected for CM4 and not corrected (raw data) – these correlate very well. We also see that the covariance comes between X and Y in the combined European observatories (table 4.2) as the eigenvectors V_1 and V_2 , and V_4 and V_5 show for both cases (where residuals are corrected for CM4 and uncorrected respectively). In table 4.3, we also observe this covariance between X and Y when residuals are corrected for CM4, but notice some Z covariance when residuals are uncorrected (raw data).

Next, we take the RC and try to compare the RC index values with the residuals data i.e. comparing the individual trends of the residual data, both corrected and uncorrected, against RC. In other words we seek to compare the eigenvector decomposition of the residual data from our detrending. Expectation might be that the noisiest of the three eigenvectors (i.e. largest eigenvalue) would correlate particularly well with RC variations, both for single observatory location and the combined observatory locations.

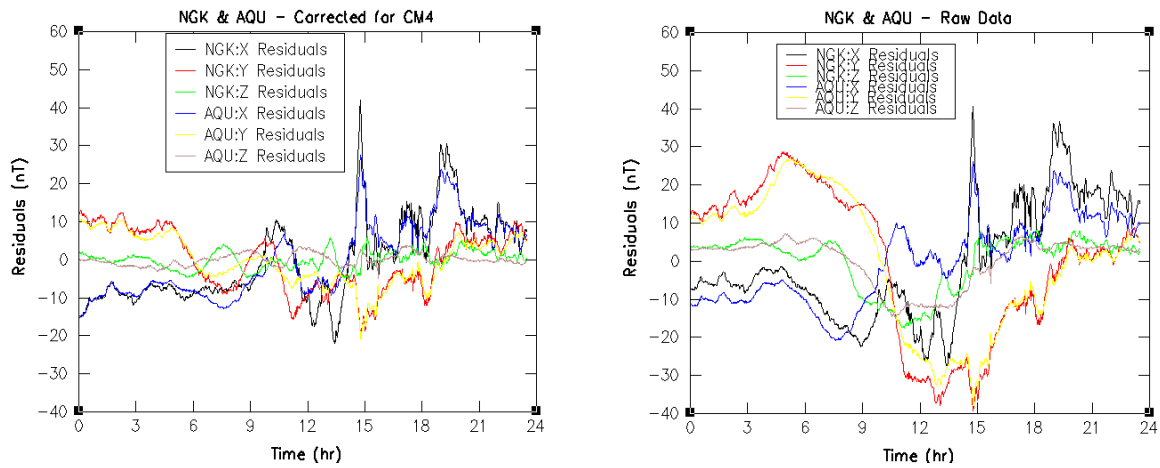


Figure 4.6: Residual plots of the X, Y and Z components used for calculating the eigenvalues and eigenvectors for two combined European observatory locations (NGK and AQU), when data is corrected for CM4 and uncorrected respectively. NGK residuals for X, Y and Z are black, red and green lines respectively, while AQU residuals for X, Y and Z are blue, yellow and brown lines respectively.

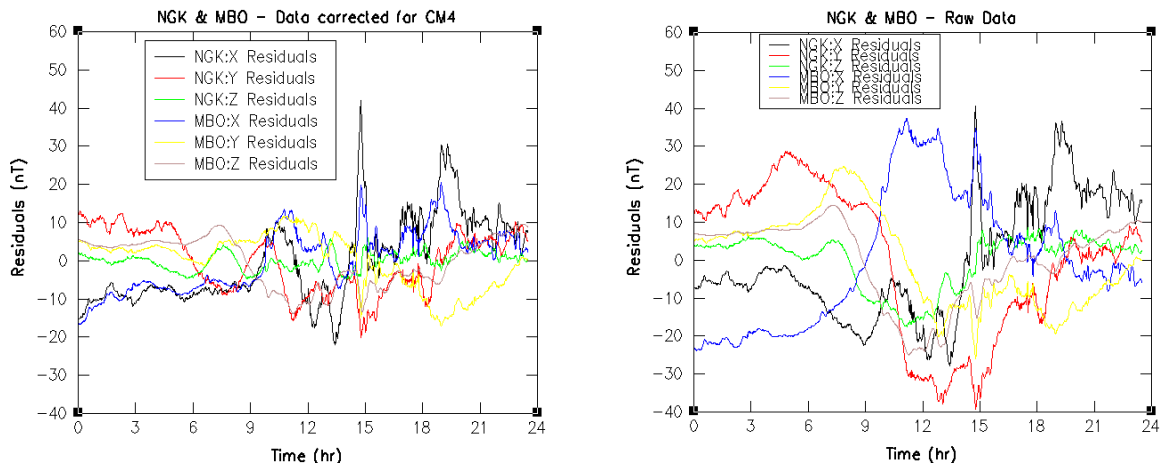


Figure 4.7: Residual plots of the X, Y and Z components used for calculating the eigenvalues and eigenvectors for combined European and non-European stations (NGK and MBO), when data is corrected for CM4 and uncorrected respectively. NGK residuals for X, Y and Z are black, red and green lines respectively, while MBO residuals for X, Y and Z are blue, yellow and brown lines respectively.

4.4.5. Comparing with RC

The daily records for each of the observatory locations presented in chapter 3 and in this chapter show coherent structures that are essentially S_q , daily variation. The signature plots of different observatory located at different geographical regions (and latitudes) exhibit the same common pattern in the wiggles/fluctuations seen, especially in the residuals of X component. This suggests that the observed phenomenon might be due to global effect, not caused by observatory or measurement error. It also shows that the external field descriptions included in the comprehensive model, CM4 could not sufficiently explain the field contributions for days away from quiet time, which impedes our ability to establish the nature of the variations for days away from quiet time, in order to see how well we can understand them. Hence we decide to compare with individual trends against RC. In this comparison, we are focusing on the northward, X component, for a couple of reasons:

1. It is the component that is the most influenced by the external field sources from ionospheric and magnetospheric origins.
2. If our assumptions about RC are correct, our expectation is that the noisiest of the three eigenvectors i.e. largest eigenvalue (which consistently happen to be residuals from the X component) produced from our error covariance matrix analysis using the available data residuals, would correlate particularly well with the RC variations.

Therefore, we searched for the ring current signature in the residuals, by comparing the residuals of the X component against the RC index values. Again, we want to look at the residuals after the different field contributions (ionosphere and magnetosphere) are removed, so that we can look at the correlation of the remaining signals with RC index. To do this, we made use of the RC index residuals which we obtained by subtracting Dst index values from that of the RC values (in other words, we remove a Dst trend to look at the small temporal scale ring current variation after the subtraction of Dst). This was analogous to what we did to obtain the observatory data residuals (subtracting the model predictions from the observatory station data). According to Verbanac et al. (2006, 2007), since the ring current generates an almost homogeneous field aligned with the dipole axis, and as mentioned above, the X component of the geomagnetic field is the most influenced by the external field of ionospheric and magnetospheric contributions, we expect good agreement between the X component residuals and the RC variations (i.e. X component residuals should correlate particularly well with RC variations).

Figures 4.8, 4.9, 4.10, 4.11 show the comparison between the obtained residual signal for the X component and the RC index values. These are for the residual data uncorrected (raw residuals data) and that corrected for CM4 (ionospheric and magnetospheric fields), ionospheric field only and magnetospheric field only, for different observatory locations in different geographical regions. The residual signature of the X component as shown in almost all the figures contain a series of similar prominent peaks, and there are more obvious correlation with the RC variation. The European and Asian observatories show very strong coherence between the X components at different observatory locations. This may be statistically disrupted by short period variations when something odd happens. This strong coherence between the same components is also observed in the Y and Z components, especially in European observatories at different locations. This reflection in the observed similarity of the short term period signal in the European observatory locations maybe due to the relative homogeneity of the external field influences in a small region such as Europe.

We can see some peculiarities in the residual plots. The observations in South American and Africa, especially at Huancayo (HUA) and Addis Ababa (AAE) observatories, for cases when the residual data is uncorrected (raw data) and when corrected for magnetospheric sources, conform fairly well with Chapman's results concerning equatorial electrojet stations, where he found the variations of horizontal component to be abnormally large in comparison to those at other latitudes (Chapman, 1948). Rastogi (2006) showed that increased magnetic activity variations in the X component is shown to be enhanced over observatory stations close to the dip equator, and that the equatorial electrojet is shown to be closely affected by ionospheric as well as magnetospheric currents induced by these sub-surfacing conducting regions. This was more pronounced for case when the residual data is uncorrected and when corrected for magnetospheric sources only, compared to cases when the residual data was corrected for CM4 (ionospheric and magnetospheric sources) and only ionospheric sources. Even at that, we could still observe some little coherence between the X residuals and the RC, exception at AAE observatory, where a pronounced morning depression in the

X component can be observed. This morning depression in the X residual signature is a common occurrence in some of the plots in African, Asian and European stations.

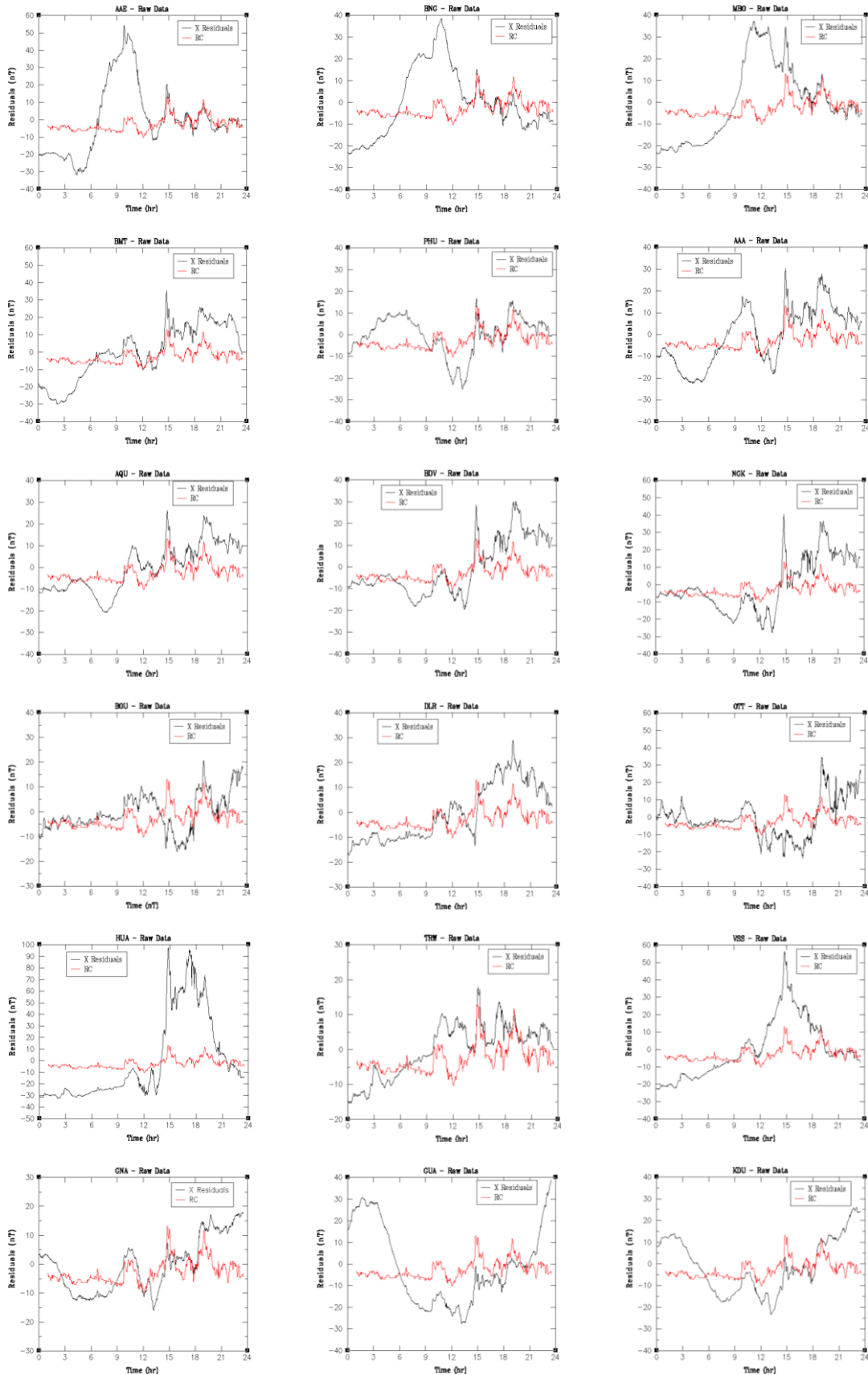


Figure 4.8: Comparison between the X residuals and RC for raw data (uncorrected) at different global observatory sites.

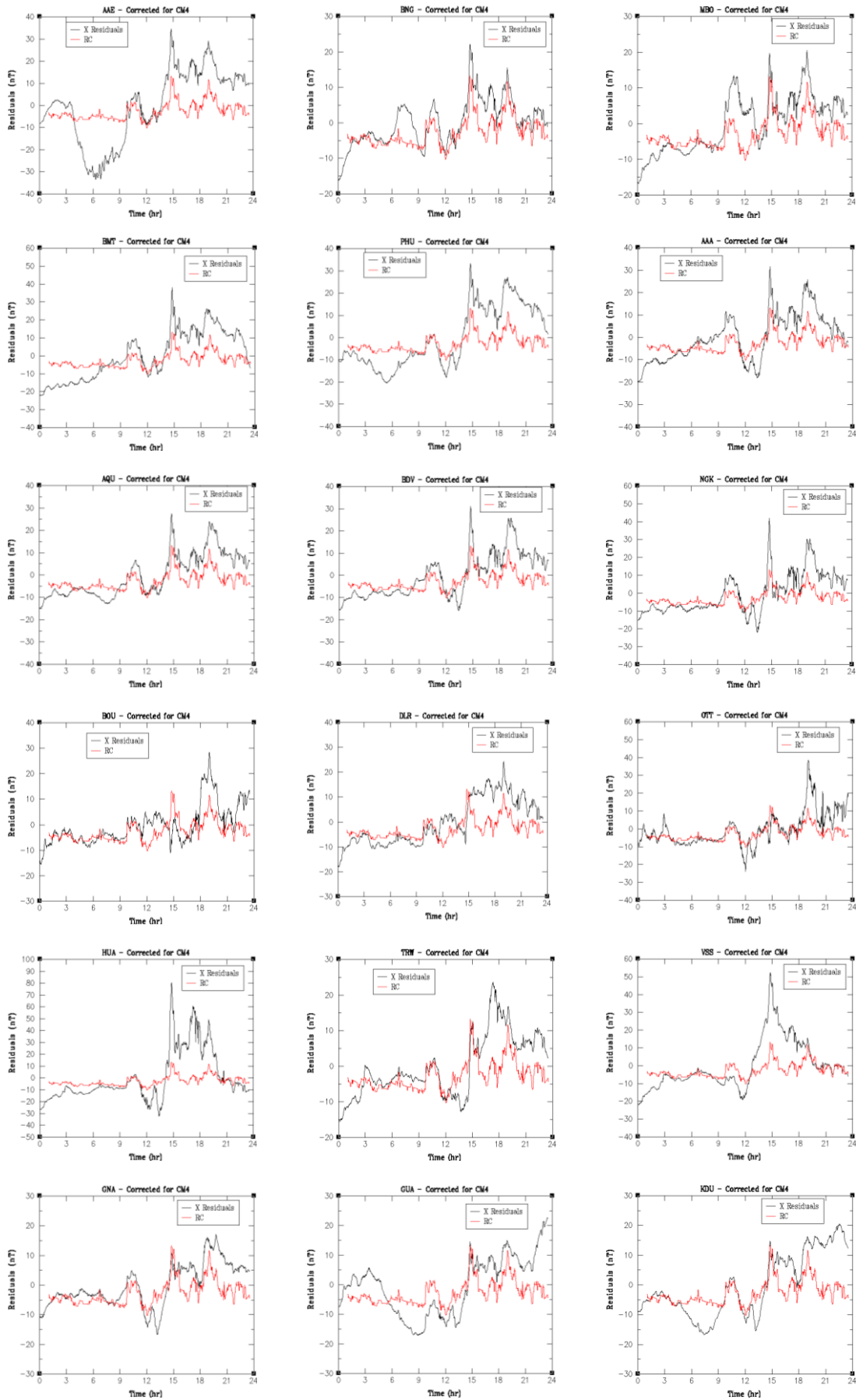


Figure 4.9: Comparison between the X residuals corrected for CM4 and RC at different global observatory sites.

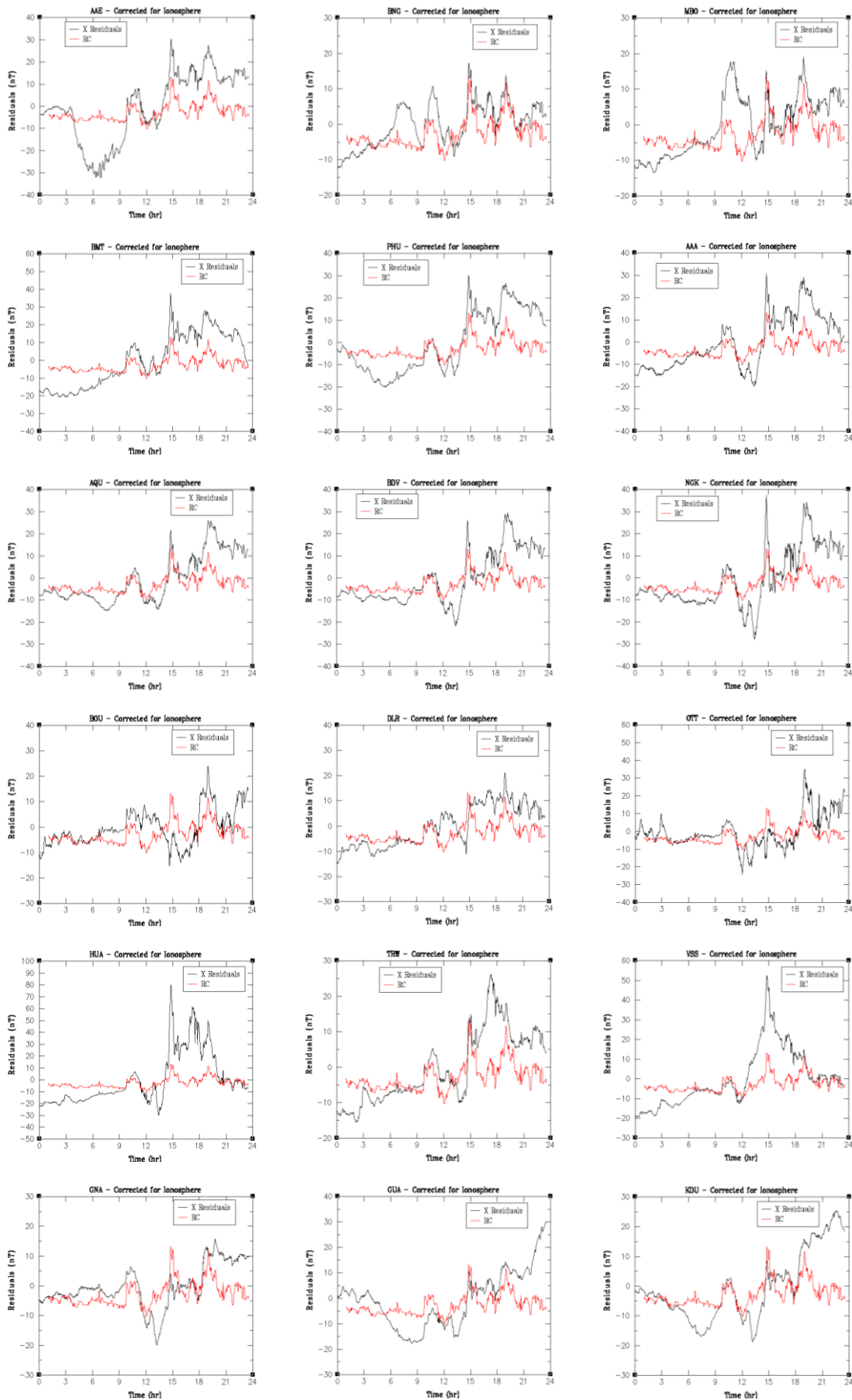


Figure 4.10: Comparison between the X residuals corrected for ionosphere and RC at different global observatory sites.

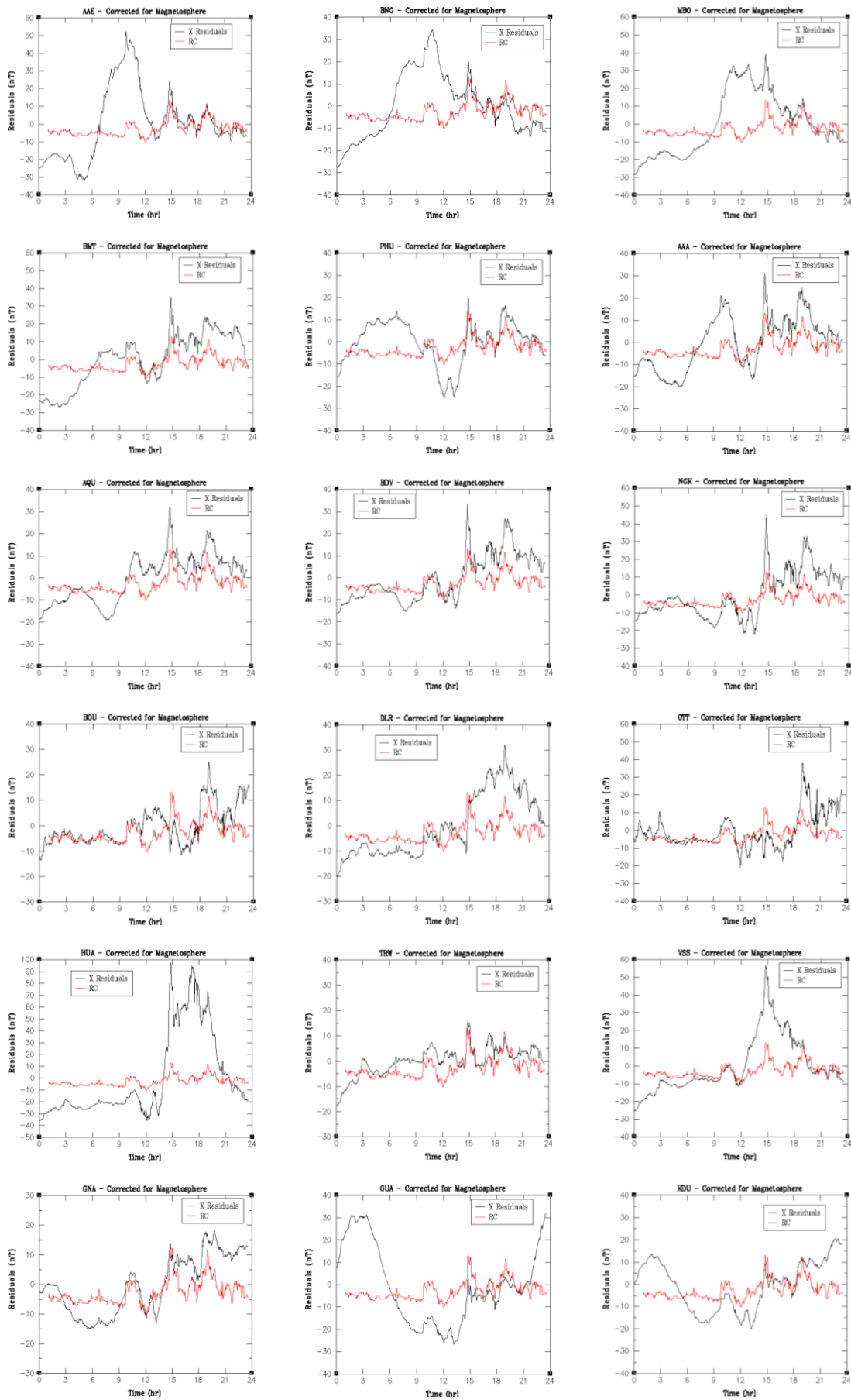


Fig 4.11: Comparison between the X residuals corrected for magnetosphere and RC at different global observatory sites.

Even though the plots in figures 4.8 to 4.11 reveal quite similar patterns for most of the short term variations in the X residuals at almost all the observatory locations (with this pattern most prominent in the African, Asian, European and South American stations), and we can see some coherence between the signature pattern and RC, there are still some misfits. This misfit is shown more in the case when the residual data is uncorrected or corrected for magnetospheric sources only, and the biggest misfit or difference between the X residual data signature and the RC variation is observed in the morning hours. This is clearly seen in African, especially AAE, Asian, European and Oceanian observatory locations (figures 4.8 and 4.11).

Figure 4.8 shows the results obtained for the residuals comparison between the X component and the RC index for raw data (uncorrected with CM4 model) at different representative observatory locations globally. We see reasonable agreement between the residuals of the X component and the RC index. The pattern is similar in most regions and reveals the short term variations of the X component residuals at all the observatories in the afternoon period. This variation trend is most prominent with vertical stripes of maxima and minima correlated with the RC index from 1500hrs. This short term variations (maximum and minimum amplitudes) agreement between the X component residuals and the RC index is most strongly observed in all the observatories globally. The only exception is Ottawa (OTT) in North America, where instead of correlation between the X component residuals and the RC index from 1500hrs, we see some anti-correlations. This may be due to possible local effects and not regional, as other observatories in the region (Boulder, BOU and Del Rio, DLR) show reasonably good agreement between the X component residuals and the RC index. Where significant differences are seen between the X component residuals and the RC index in most of the observatories is in the morning period. Most of the observatories are characterized by a pronounced morning minimum or depression at various times (between 0000hr and 0900hrs), except PhuThuy (PHU) in Asia, which features an enhancement at this time period. Here there is clear lack of agreement and correlation between the X component residuals and the RC index in all the observatories. But we can see some agreement and correlation in some of the observatories without pronounced morning depression, like BOU in North America.

The plots shown in figure 4.9 reveal quite a similar pattern for most of the short term variations of the X component residuals as that in figure 4.8. These are for X component residuals corrected with CM4 model (for ionospheric and magnetospheric sources). It reveals a clear agreement between the X component and the RC index, having good correlation in the areas of maximum and minimum amplitudes in all the observatories globally. Even at OTT in North America where we saw some anti-correlation between the X component and RC index in the afternoon period short term variations for raw data (figure 4.8), here we see very clear correlation between the X component and RC index. Also, except for Addis Ababa (AAE) in Africa, where the pronounced morning depression seen in the X component (figure 4.8) persists, most of the observatories are without this pronounced depression, and we see a better correlation between the X component residuals and the RC index. The correction applied by CM4 model (for both ionosphere and magnetosphere) brought a noticeable improvement in the X component residuals around the morning depressions in most of the observatories.

Figures 4.10 and 4.11 show some representative cases for the comparison between the X component residuals and the RC index corrected for ionosphere only and magnetosphere only respectively. Close inspection shows that the results for the case of X component residuals corrected for ionosphere only (figure 4.10) are in typical agreement with the case when the X component

residuals are corrected for CM4 model (ionosphere and magnetosphere) (figure 4.9). No large differences can be observed. The short term variations (maximum and minimum amplitudes) agreement and correlation between the X component residuals and the RC index in the afternoon period reflects what we see in the case above shown in figure 4.9. Similar morning trend is repeated here, showing the ionospheric correction applied did a good job of removing the wiggles/fluctuation. The trends, both for period of good correlation and otherwise, seen in figure 4.11 for case when the X component residuals are corrected for magnetosphere only are similar to those seen in figure 4.8 when the X component residuals are uncorrected with the CM4 model (raw data). The pronounced morning depression seen in most of the observatories and the lack of agreement between the X component residuals and the RC index shows that the magnetospheric corrections obviously did remove the wiggles/fluctuations like the ionosphere.

In general, the corrections applied to the X residual data for CM4 (ionospheric and magnetospheric sources) and ionospheric sources only seem to produced better agreement/coherence between the X residual signatures and the RC signature. Again, the exception is in AAE, where the morning depression in X residual signature is still well pronounced, even after the applied corrections (figures 4.9 and 4.10). Several inferences can be invoked to explain the observed differences between the X residual signatures and the RC. These may include other external field influences in the observatory diurnal variation data, induction effects, insufficient representation of the external field descriptions in the CM4 model and finally instrument drift and data errors. To identify common features and explain possible regional or global effects, we may have to look at small-scale features in each of the residuals (X, Y, and Z) of the observatory data.

4.4.6 Combined Observatories

Just as we did in section 4.4.5 looking at the correlation of the eigenvalues and eigenvectors for combined observatory locations, we also looked at the comparison of the X residuals for combined observatory locations against the RC index values. Since our combined observatories showed large variations that are coherent, especially when the comprehensive model corrections were applied (both for combined European observatories, and combined European and non-European observatories), which showed up in the combination of eigenvector for the largest eigenvalue, we saw the need in comparing these against the RC index values. This was particularly a question to see whether RC was doing well for all observatories or only European ones.

So using the same RC index residual values (same as the ones used in plotting figures 4.8 – 4.11), we compare these against our combined observatory data residuals. The results show a clear correlation between RC and the X components of our combined observatory residual data. Figures 4.12, 4.13 and 4.14 shows the comparison between RC residuals and X residuals for combined observatories. Figures 4.12 and 4.13 involve observatories which were used in calculating the RC index values. In figure 4.14 we used observatories that were not used in calculating the RC index values, to be sure we are not comparing the same thing. All the figures clearly shows RC is doing a reasonably good job fitting the fine variations, particularly when corrected for CM4. The correlation is better for the combined European observatories, Niemegek, NGK and L'Aquila, AQU (figure 4.12), than that combined European and non-European observatories, Niemegek, NGK and Mbour, MBO (figure 4.13). As it is calculated from the fine variations, this perhaps, should not be a complete shock. The second eigenvector (Y residual – not shown) doesn't show much obvious correlation with the RC – the RC is being effectively separated.

When we look at the combined observatories in figure 4.14 which are not used for calculating the RC index, we see clearly that the RC index correlating well with the X component residuals for the combined observatories of Budkov (BDV) in Europe and Bangui (BNG) in Africa. It reveals similar pattern as obtained in figures 4.12 and 4.13, with a better correlation seen in the case when the X component residuals are corrected with CM4 model (ionosphere and magnetosphere) and when corrected for ionosphere only than for the other cases (raw data and when corrected for magnetosphere only respectively).

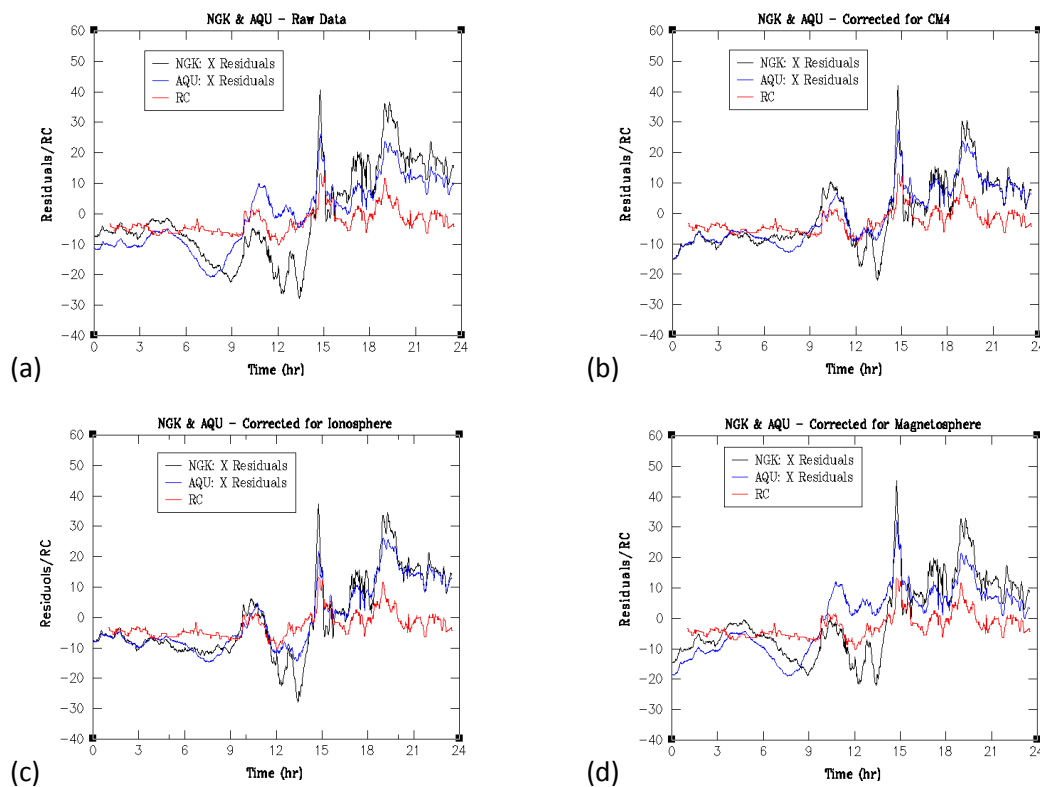


Figure 4.12: Comparison between RC and combined Niemegek (NGK) and L'Aquila (AQU) observatories in Europe for 30/05/2006. (a) For raw residual data with no corrections applied (b) For residual data with CM4 (ionospheric and magnetospheric) corrections (c) Residual data with only ionospheric corrections (d) Residual data with only magnetospheric corrections.

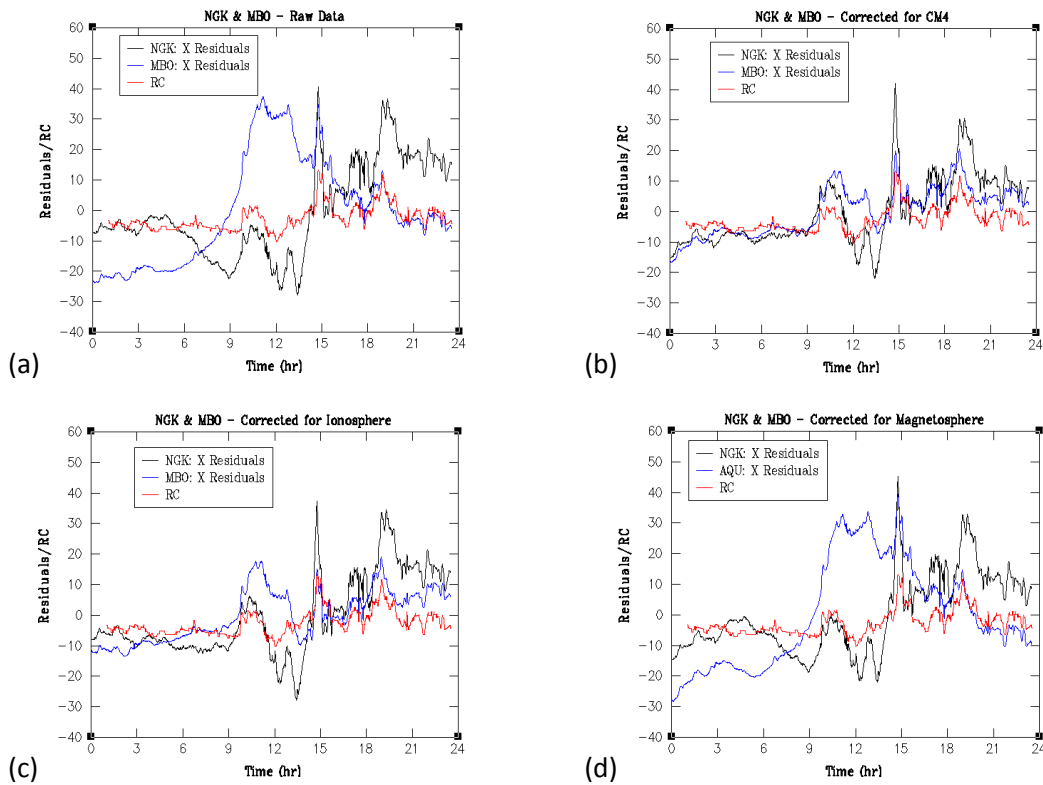


Figure 4.13: Comparison between RC and combined Niemegek (NGK) and Mbour (MBO) observatories for 30/05/2006. (a) For raw residual data with no corrections applied (b) For residual data with CM4 (ionospheric and magnetospheric) corrections (c) Residual data with only ionospheric corrections (d) Residual data with only magnetospheric corrections.

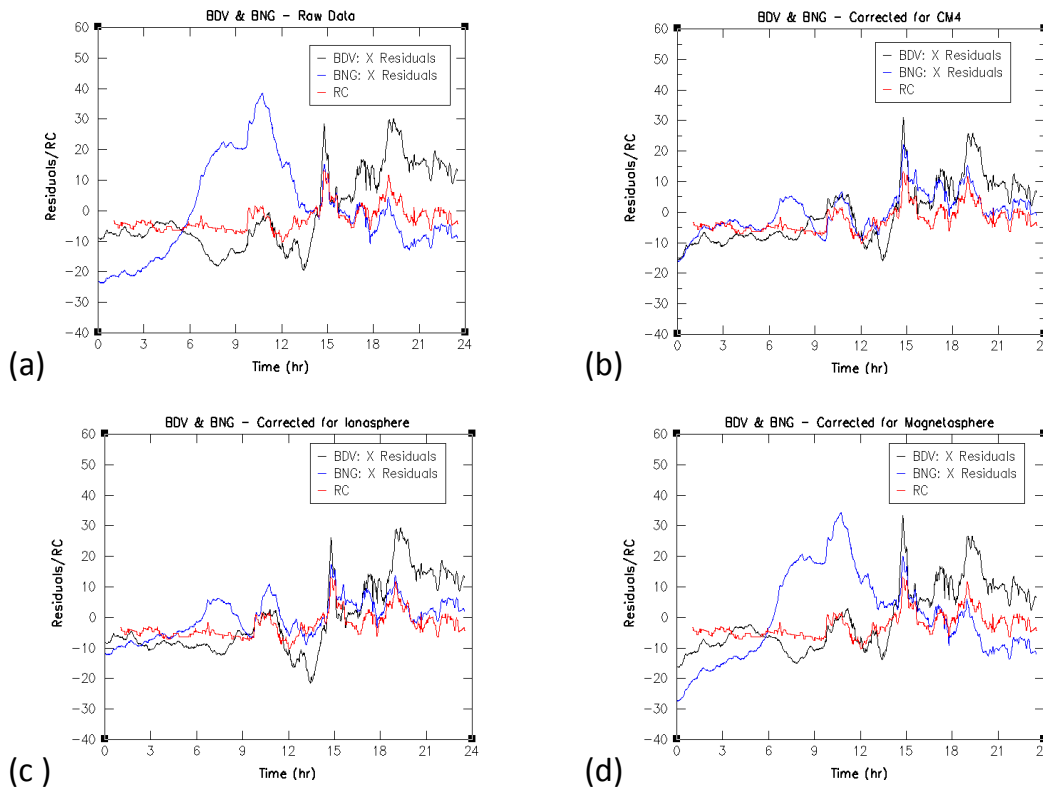


Figure 4.14: Similar to figures 4.12 and 4.13 for Budkov (BDV) and Bangui (BNG). Observatories not used in calculating RC index values.

4.5 Removing Error Source

In furtherance of our aim to establish the nature of the variations for days away from quiet time, we attempted to do more detrending of our observatory data sequences and analyse the resulting output in an attempt to remove an error source. Removal of error sources in terms of time-varying effects may lead to more refinements in our field analysis, and minimise the differences or misfits seen in our plots. The identification and refinement of these time-varying field sources may provide us with a physical realization of these differences and lead to better predictions and fitting for the rapid variations seen in our observatory data for days away from quiet time.

We attempted this by trying to subtract the largest eigenvalue eigenvector from our observatory residual data. In some previous work, especially Holme and de Viron (2013), this was looking only at residuals for a well-fitting model (averaged over time), and this made sense, because it removed an error source in that study. But when applied here, the largest eigenvalue eigenvector corresponded to a component of the field. We therefore ended up removing this component of the field, which was not particularly informative – so clearly that method didn't work here!

Figure 4.15 shows the results obtained from this operation for selected observatories before and after the subtraction routine. We have only shown that for the three components (X, Y, Z) observatory residuals where corrections for CM4 is applied for one observatory location in different geographical region of the globe, as an example.

4.6 Covariant Modelling Summary

In this chapter we have discussed data residuals, correlated errors and covariance matrices used in this study, in terms of their temporal and spatial behaviour in observatory locations globally. We have determined the error correlation of our field model residuals by taking the approach of estimating the covariance directly from the residuals. Our analysis shows that much of the covariance comes between the residuals of the X and Y components (rapid Z variations removed by induction? X and Y gives forcing direction?). This is unlike what is generally observed in slow and longer variations, where strong correlation is seen between the X and Z residuals.

Our observations and results show that the external field descriptions included in the comprehensive model could not sufficiently explain the field contributions for days away from quiet time. This has made it inadequate for establishing up till now the magnetospheric ring current as the cause, as we assumed may have given rise to the wiggles seen in our observatory data plots. The observatory data residuals have shown coherent structure that is essentially Sq daily variation. Some observatories, especially the European ones, show very strong coherence between the same components of the field at different observatory locations.

Simple eigenanalysis of single days is not particularly proving as useful as we would have liked, but still shows the comparison with the RC index doing a reasonable good job fitting the fine variations. Therefore, fine variations are global. When we take ionosphere/magnetosphere field stated from CM4 away from the data, the ionosphere clearly does a good job of removal. The magnetosphere obviously doesn't get rid of the wiggles because D_{st} is not high enough time resolution. Hence the suggestion for RC...

There are definitely coherent features showing up in rapid variation (i.e. between Niemegk and Mbour combined and also Budkov and Bangui combined). The spline operation have proved not very satisfactory in isolating them.

So far we have only considered the residuals of the X component in the comparison against RC, because it is the most affected by external field sources. For more analysis of external field influences on other components (Y and Z residuals), we look to more small scale features – taking a simple running average. We tried subtracting the largest eigenvalue eigenvector from the data. This was in a bid to look at the residuals in order to remove an error source. But the largest eigenvalue eigenvector corresponded to a component of the field, and so we ended up removing a component, which was not helpful.

Our results so far have shown that clearly some external influences may be dominating the observatory residual variations. This may be regarded as evidence for the magnetospheric ring current present or causing the wiggles seen in the signatures of our observatory data plots. Whilst in our discussion here we tried to extensively establish the link between RC and rapid variations seen in our noisy data, there may be room for further solution and other parameter investigations. In the next chapter (chapter 5) we try to look at and analyse further the coherence between small scale features, to establish to what extent the link between the variations seen and RC is a global phenomenon.

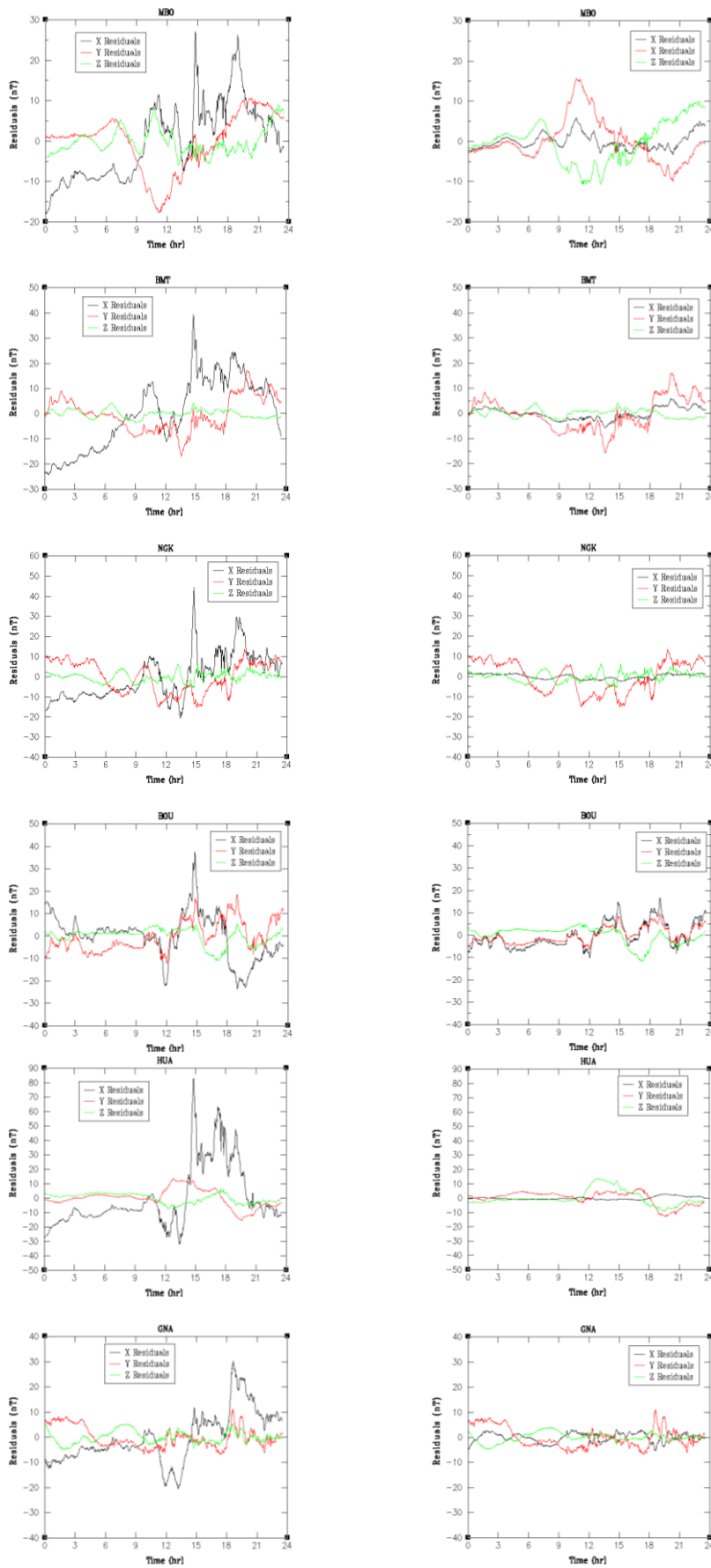


Figure 4.15: Observatory residual plots showing amplitude of field components (X, Y, Z) before and after the attempted error removal routine (which didn't work) was applied for one observatory location in different geographical region of the globe.

Chapter 5

Modelling Small Scale Features

As seen in the previous chapter, there are definitely coherent features showing up in the rapid variation between the residuals of the X component of the observatory geomagnetic diurnal field and the residuals of the RC index. This is observed both in the single observatory locations and the combined observatory locations (for example, X between Niemegek, NGK, and Mbour, MBO). How to isolate them? The spline method has proved not very satisfactory.

We have been encouraged by the good agreement between the X component residuals and the RC index residuals. However, despite this encouragement there are still clearly coherent signals remaining in the data residuals as observed in the various plots. This may possibly due to the inadequacies in modelling the geomagnetic diurnal variation data for days away from quiet time using the CM4 model. So our attempt to do the clever thing with the penalised least-squares spline detrending and fitting, and the removal of an error source didn't produce exactly what we had in mind.

In this chapter, we look at the coherence and agreement between small scale features, to establish to what extent the coherence and agreement seen in our various plots is a global phenomenon. Section 5.1 begins with the taking of a simple running average, and then the difference between the running average and what we started with. The simple running average was taken for one hour, and this was taken for all the three components (X, Y, Z) of the observatory data residuals and the RC index residuals. The idea is to compare the different variations on different time scales. In section 5.2, we present the results of comparing what is left of the difference between the residuals of the different observatory components and the RC index. This is in a bid to explore in depth the coherence and agreement in the rapid variations seen between the residuals of the observatory components and the RC index, to establish to what extent the RC matches the fluctuations seen in our diurnal variation data for days away from quiet time. A comparison with observatory locations which show strong equatorial electrojet influence is explored and presented in section 5.3. Finally, in section 5.4 we investigate further the coherence in the small scale features by looking at the correlation between the different quantities looked at in section 5.2. This is by analysing the correlation coefficients between the rapid oscillations in the different components and RC. The aim is to start getting some numbers and physical conclusions out about the nature of the rapid variations in our observatory data. In section 5.5, we summarise our primary conclusion.

5.1 Running Average Approach

Our attempt at using the penalised least-squares spline detrending and fitting didn't exactly produce what we had in mind, so we decided to do the simple thing by taking a simple running average of about one hour, and then the difference between the running average and what we started with, in order to look at the small scale features and see if we can sufficiently establish the nature of the rapid variation seen in our data.

Running averages are generally known to be bad e.g. in seismology due to large side-lobes in frequency space, and they are essentially a top hat/boxcar filter. But they are useful for eliminating well-defined periods of oscillation, and it is reasonably easy to understand what they have done.

In figure 5.1 we show some representative plots of taking a simple one hour running averages of the residuals of the different components of the data and the RC index, and then the difference between the running averages and what we started with. These are for the RC index and selected observatory locations from different geographical regions of the globe – Addis Ababa, AAE (X component), L' Aquila, AQU (Y component) and Beijing Ming Tomb, BMT (Z component).

From this, undeniably, simple operation, the signal accounting for the difference between the running averages and what we started with should be clear enough for us to analyse the small scale features in our data. We then compare these signals from the RC index residuals against those of the different components (X, Y, Z) of the data of observatory locations. The results and analysis are presented in the next section.

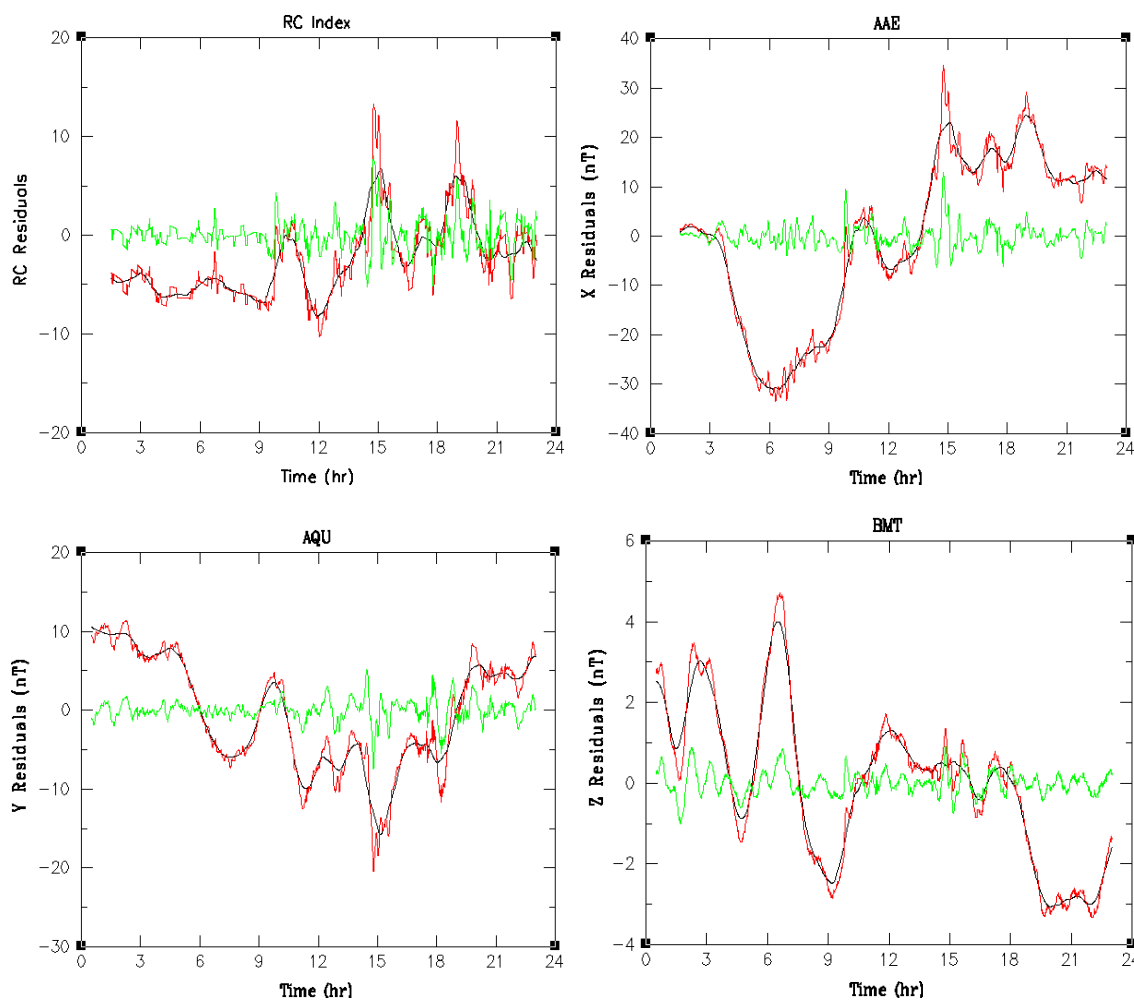


Figure 5.1: Detrended data sequences (with one-hour running average) for a) RC index residuals, b) X component residuals at AAE, c) Y component residuals at AQU, and d) Z component residuals at BMT. Red lines show the residuals of the different components and RC, black lines the running average and the green lines the difference between the running average and what we started with. These are for 30/05/2006.

5.2 Coherence between Small Scale Features Analysis

Following the simple running average approach in section 5.1, here we seek to analyse comparability of the difference between removing a one-hour running average and what we started with of the signals of the RC index residuals and that of the different components of the observatory data. As usual our focus is global, looking at the performance of selected observatory locations in different geographical regions of the Earth, as we want to establish the global extent of the phenomenon. We also stayed with our approach of comparing the observatory data residuals against the RC index for different field contributions using the CM4 to take away contributions from fields stated from the data.

Unlike the previous chapter where we only considered the residuals of data from the X component (since this component is the most influenced by external field sources), our analysis here is performed on residual values of the X (northward), Y (eastward) and Z (vertically downward) components for about 120 worldwide located geomagnetic observatories, and the RC index. The overall objective is to systematically study and explain the short-term/more rapid variations observed in the our observatory data residuals for days away from quiet time, influenced by the external fields, linked to solar activity and the ring current. The analysis is based on our usual comparison of real observatory residual data against the RC index residuals, all obtained from observatory locations and the published RC index values. The different field contributions were corrected/subtracted with the help of the CM4 model. All the different field contributions for the residuals of the different values of the X, Y and Z components were individually compared against the residuals of the RC index values. (Note that it is the signals of the difference between the running average and the original data time-varying residuals for both the different components of the observatory data and the RC index that we are comparing).

The results and analysis for the different field contributions is presented next. For space constraint only selected observatory locations in each geographical region are shown in our figures as representative of that region.

5.2.1 Results for Data Corrected for CM4 (Ionospheric and Magnetospheric Fields)

We compared the signals of the observatory residuals after removing a one-hour running average and what we started with of the time-varying residuals at all available observatory locations data to that of the RC index residuals. For this series the observatory data residuals for each of the three geomagnetic components were corrected for ionospheric and magnetospheric field contributions using the CM4 model. The results of the comparison for some representative cases are displayed in figures 5.2a and 5.2b.

In the X component, we can clearly observe that there is generally good coherence and agreement between the residuals of the observatory data and the RC index globally. This strong coherence/good agreement is very high even outside the European region, like in Africa (BNG, MBO) and Asia (BMT, AAA) in figure 5.2a, North America (BOU, DLR), South America (VSS, TRW) and Oceania (GUA, GNA) in figure 5.2b, suggesting a global phenomenon. In the Y component, most of the observatory locations show anti-correlation, some strongly, between the observatory residual data and the RC index. This is seen particularly in BNG, MBO (Africa), AQU (Europe), BMT, AAA (Asia), GNA, GUA (Oceania).

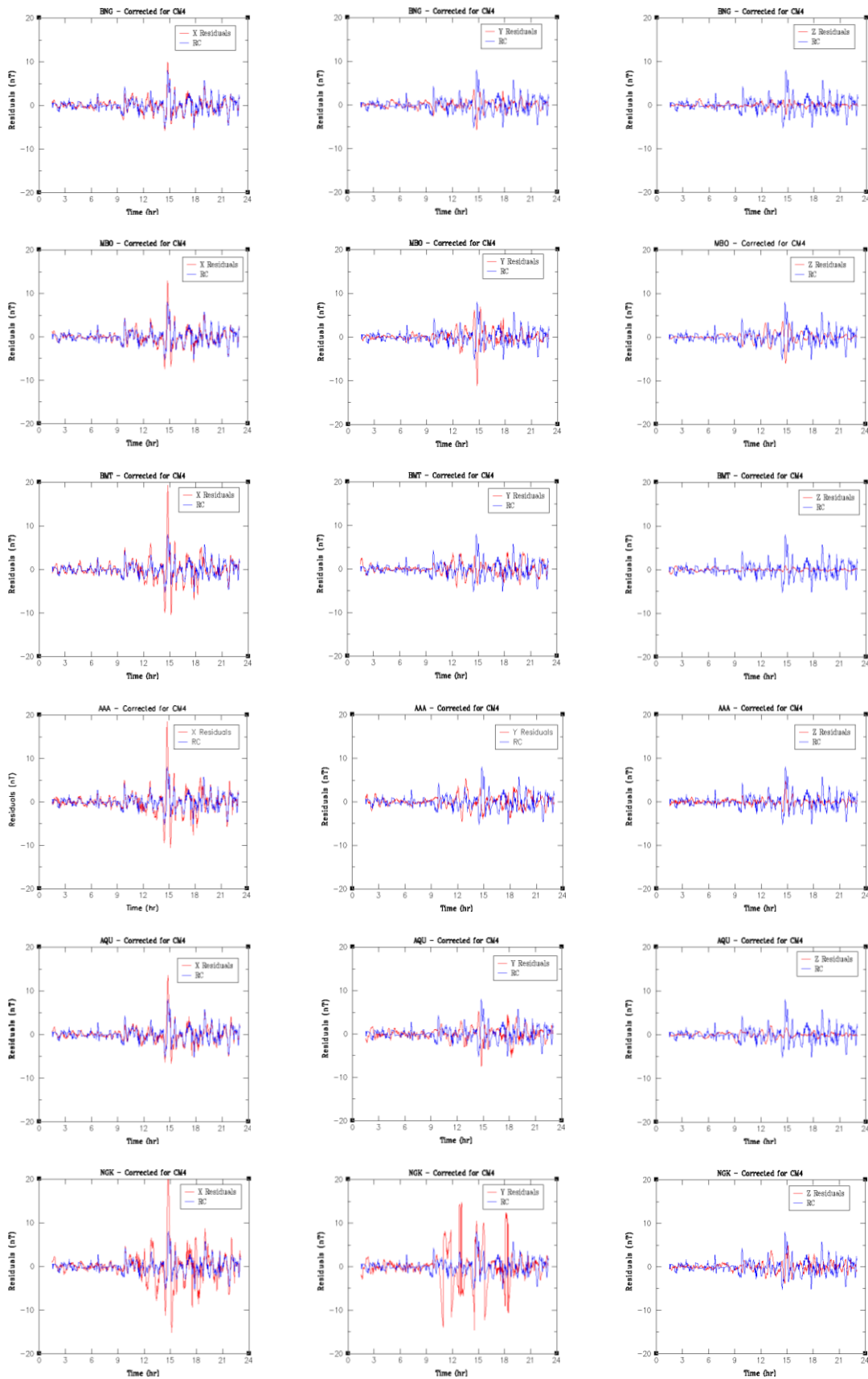


Figure 5.2a: Comparison between X, Y and Z residuals (red lines) corrected for CM4 model (ionospheric and magnetospheric) and RC index residual (blue line) for Africa (BNG, MBO), Asia (BMT, AAA) and European (AQU, NGK) observatory locations. X show good agreement. Notice the large amplitude variation in Y at NGK between 12 noon and 18hours. These are for 30/05/2006 with $K_p \leq 4$.

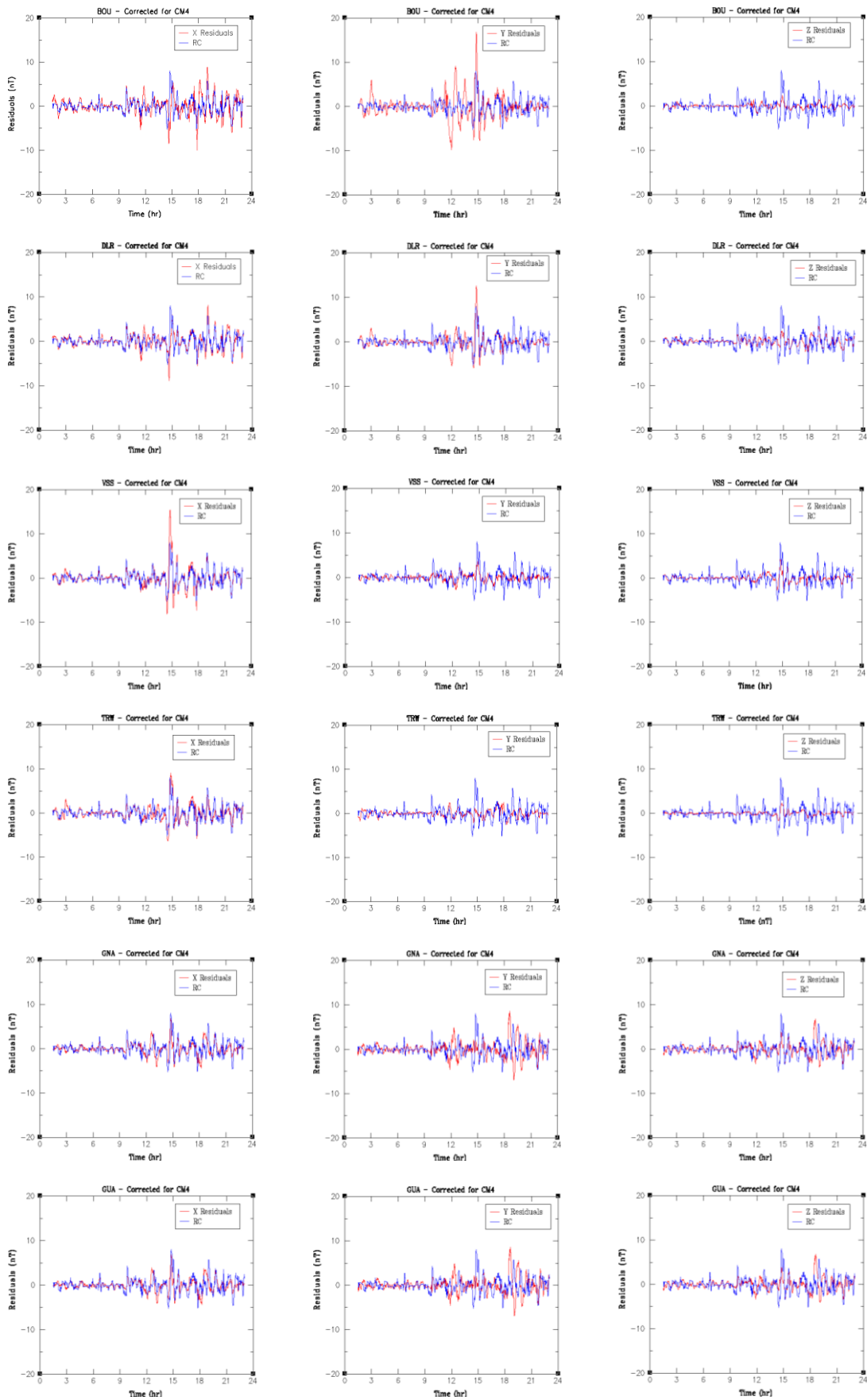


Figure 5.2b: Similar to figure 5.2 for North America (BOU, DLR), South America (VSS, TRW) and Oceania (GNA, GUA). Similar good agreement between X and RC index. A mixture of small coherence and anti-correlation in Y and Z with RC index.

European observatories have shown better and strong coherence, when compared to other regions in previous plots, between the same components of the field at different locations, but here we see Niemegek, NGK behaving rather differently to other European observatory locations for the Y component. This may be due to statistical disruption by short period variations when something odd happens. This can be seen from the large amplitude variation in the Y component at Niemegek (NGK) observatory (between 1200hours and 1800hours, figure 5.2a) compared to other European locations. As a result we can see some coherence between the Y component residuals and that of the RC index at certain periods of the day, with others showing anti-correlation. We can also observe a mixture of small coherence and anti-correlation between the Y component observatory data residuals and the RC index in locations like BOU and DLR in North America, and coherence at most hours of the day with few odd anti-correlations at VSS and TRW in South America.

The Z component follows no obvious discernible trend globally, like the Y component. Here we can see anti-correlations at the African observatories of Bangui, BNG and Mbour, MBO, small coherence in Asian observatories of Beijing Ming Tomb, BMT and Alma Ata, AAA, and a mixture of small coherence and anti-correlations in European observatories of L' Aquila, AQU and Niemegek, NGK. BOU and DLR in North America show a mixture of coherence with small anti-correlations at few times. We can also see strong coherence (similar and almost identical trends) in the comparison between the same components of the field and RC index at both observatory locations. South America observatories, Vassouras, VSS and Trelew, TRW, show some coherence/correlations in both components, while the Oceania observatories, Gngara, GNA and Guam, GUA, record a mixture of small coherence and anti-correlations. Where these anti-correlations are strong are where there are particularly strong oscillations, as in NGK and BOU in the Y component.

Amongst the representative observatories shown in figures 5.2a and 5.2b, Mbour, MBO (Africa), Niemegek, NGK (Europe), Gngara, GNA and Guam, GUA (Oceania) are RC observatories (i.e. Observatories used in calculating the RC index).

In general, the results obtained for all three components are in reasonable agreement with what we expected, particularly for the X component comparison (that the noisiest of our signals, the X component, would correlate particularly well with the RC residuals). Unlike the X component, no obvious trend can be seen from the Y and Z components comparisons with the RC index. This may be due to various reasons unknown to us, or due to the fact that the observatory data are influenced differently by external field sources, and measurement errors at different observatory locations, and changes due to induction effects affecting some of the components (particularly the Z component) more than others. Taking this into account, we expect good agreement/strong coherence between the X component residuals and that of the RC index, based on the fact that the X component of the field is largely more influenced by external field sources (magnetospheric ring current being one) compared to the Y and Z components of the field.

5.2.2 Results for Raw Data, Data Corrected for Ionosphere only, and Data Corrected for Magnetosphere only

Here we look at the comparison between the signals of the difference between removing a one-hour simple running average and what is left of the time-varying residuals at all available observatory locations data to that of the RC index residuals, for different field contributions. These include when the observatory data residual is uncorrected with the CM4 model (raw data), when the observatory data residual is corrected for ionosphere only, and when the observatory data residual is corrected

for magnetosphere only. The CM4 model, as we know, gives us predictions for both the ionosphere and magnetosphere. We want to look at the observatory data residuals when these predictions are removed or when anyone of them is present, to look at what is left over and to discover to what extent the CM4 model is able to make useful predictions, and to study and understand the field that is left over.

Figures 5.3a and b, 5.4a and b, 5.5a and b respectively shows some representative cases for the comparison between the X, Y and Z components between the variations of the difference between removing a one-hour running average and what is left of the data residuals of the RC index and the observatory data in different geographical regions of the globe for the raw data, data corrected for ionosphere only and data corrected for magnetosphere only respectively. The plots shown in all the figures for the respective field contributions reveal quite similar patterns in all the comparison for all the residuals between the components of the observatory data and the RC index in all the observatory locations, as seen in section 5.2.1 (where the data were corrected for CM4 i.e. both ionosphere and magnetosphere) – except the Y component in NGK in Europe. Here the Y component in NGK follows the same trend as the other European observatory locations.

The X component follow the same trend in having good agreement/strong coherence between the observatory data residuals and that of the RC index in all the observatory locations in the different geographical regions of the world, clearly suggesting global effect or phenomenon. The Y and Z components also follow similar trends as in the previous case where correction is made for CM4 (ionosphere and magnetosphere), in all the different field contributions – raw data, corrected for ionosphere only and corrected for magnetosphere only – in all observatories. The Y component shows some anti-correlation between the observatory residual data and the RC index residual in most of the observatory locations, and the Z component shows anti-correlation in the African observatories, some coherence in the Asian observatories (figures 5.3a, 5.4a and 5.5a) and a mixture of both small coherence and anti-correlation in the North American, South American and Oceania observatory locations (figures 5.3b, 5.4b and 5.5b). The coherence and anti-correlation is particularly very strong in the Y and Z components in observatory locations where there are particularly large oscillations in those components, as can be seen in MBO, BOU, GNA and GUA.

So, while we can observe clear preference in agreement between the observatory data residuals and the RC index residuals in the X component in all the observatory locations for all the different field contributions, in the Y and Z components there are no clear preferences in the coherence, correlation and anti-correlation trends seen in the comparison of the observatory data residuals against the RC index residuals.

The Z component appears to have a higher coherence/agreement and correlation in the comparison between the observatory data residuals and the RC index residuals than the Y component. But this is lower and weaker when compared with the comparison between the X component observatory data residuals and the RC index data residuals. In all the three components, the dependence of the variations on geomagnetic and geographical latitude is played out, as there is largely strong coherence between the same components of the field at different observatory locations, with largely similar changes in the amplitudes variations.

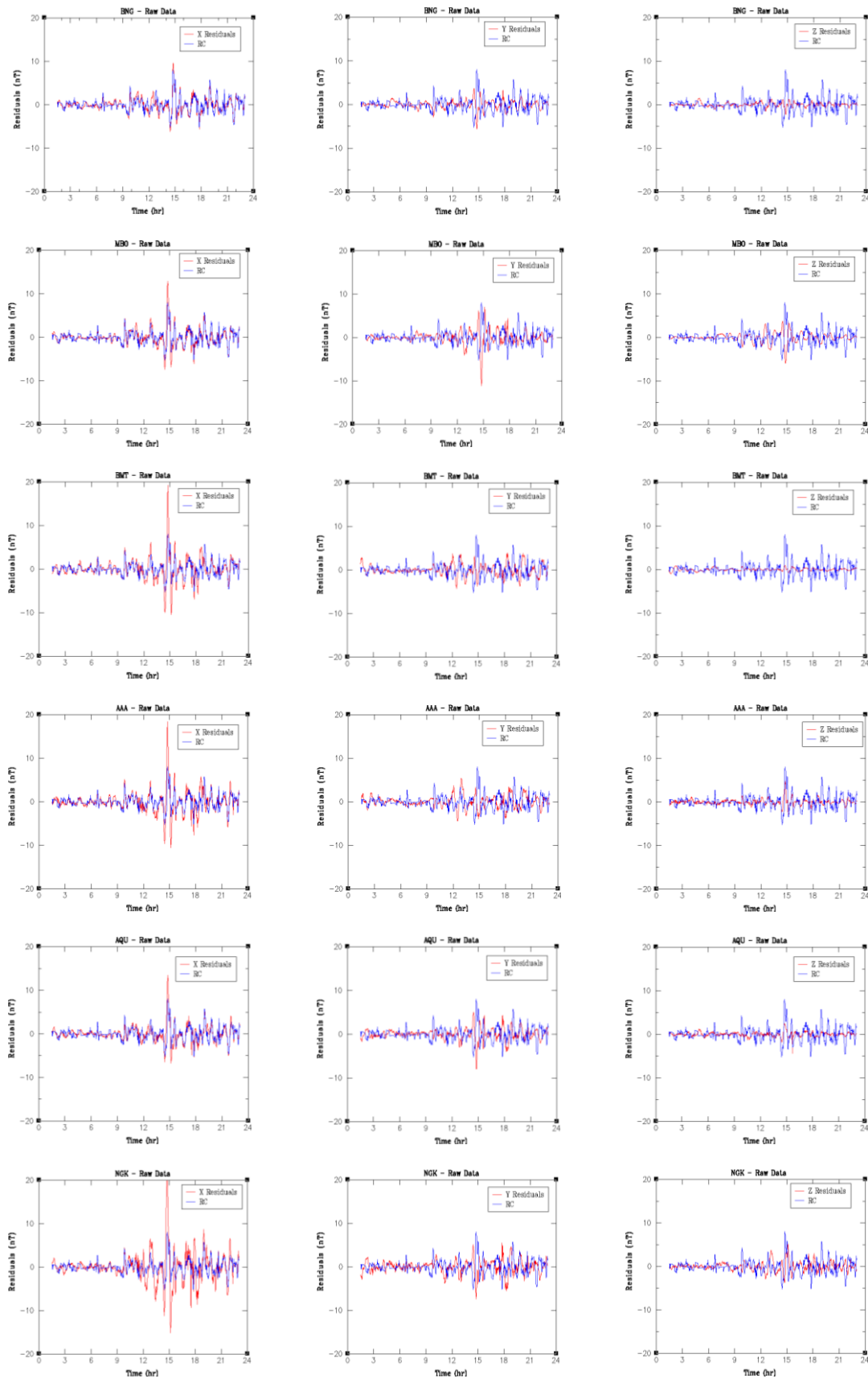


Figure 5.3a: Comparison between X, Y and Z residuals (red lines) uncorrected with CM4 model (raw data) and RC index residual (blue line) for Africa (BNG, MBO), Asia (BMT, AAA) and European (AQU, NGK) observatory locations. Good agreement between X and RC index in all observatories. Anti-correlation observed in Y, and a mixture of good agreement and anti-correlation between Z and RC index.

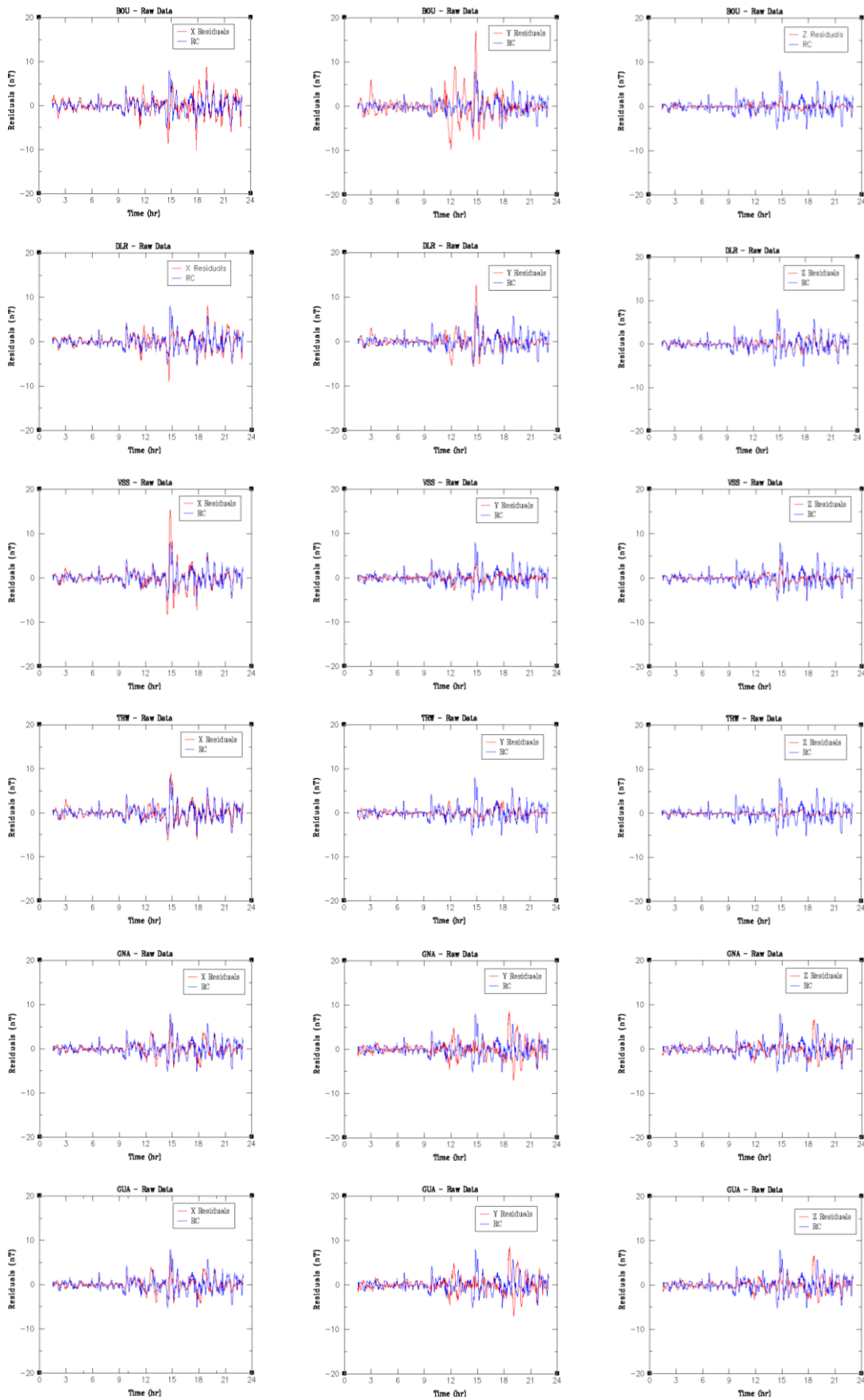


Figure 5.3b: Similar to figure 5.4 for North America (BOU, DLR), South America (VSS, TRW) and Oceania (GNA, GUA). Good correlation between X and RC, anti-correlation in much of Y with RC, correlation between Z and RC but not as strong as that of X.

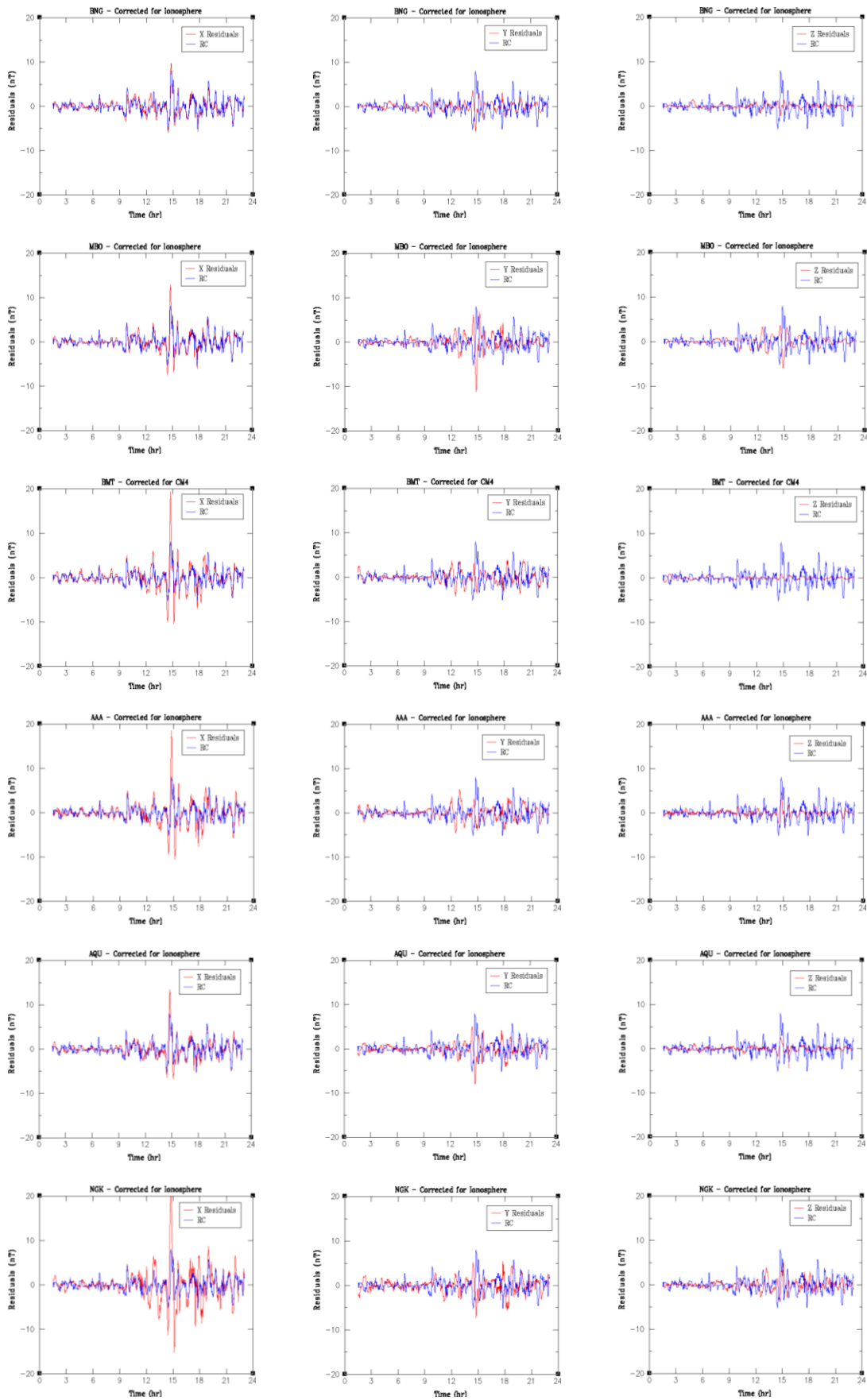


Figure 5.4a: Comparison between X, Y and Z residuals (red lines) corrected for ionosphere and RC index residual (blue line) for Africa (BNG, MBO), Asia (BMT, AAA) and European (AQU, NGK) observatory locations. Follows similar pattern as seen in figure 5.4a.

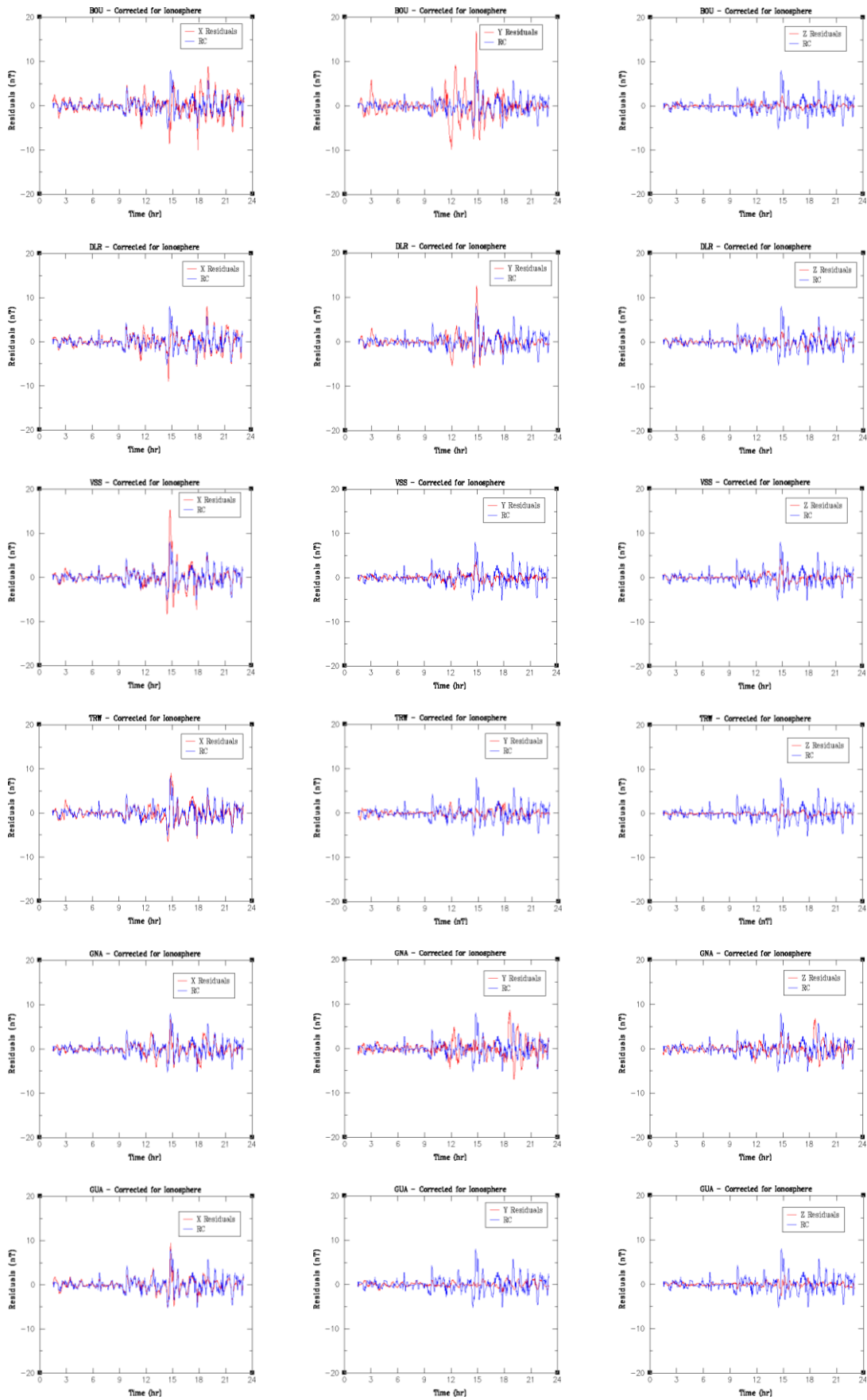


Figure 5.4b: Similar to figure 5.6 for North America (BOU, DLR), South America (VSS, TRW) and Oceania (GNA, GUA). Follows similar pattern as seen in 5.4b.

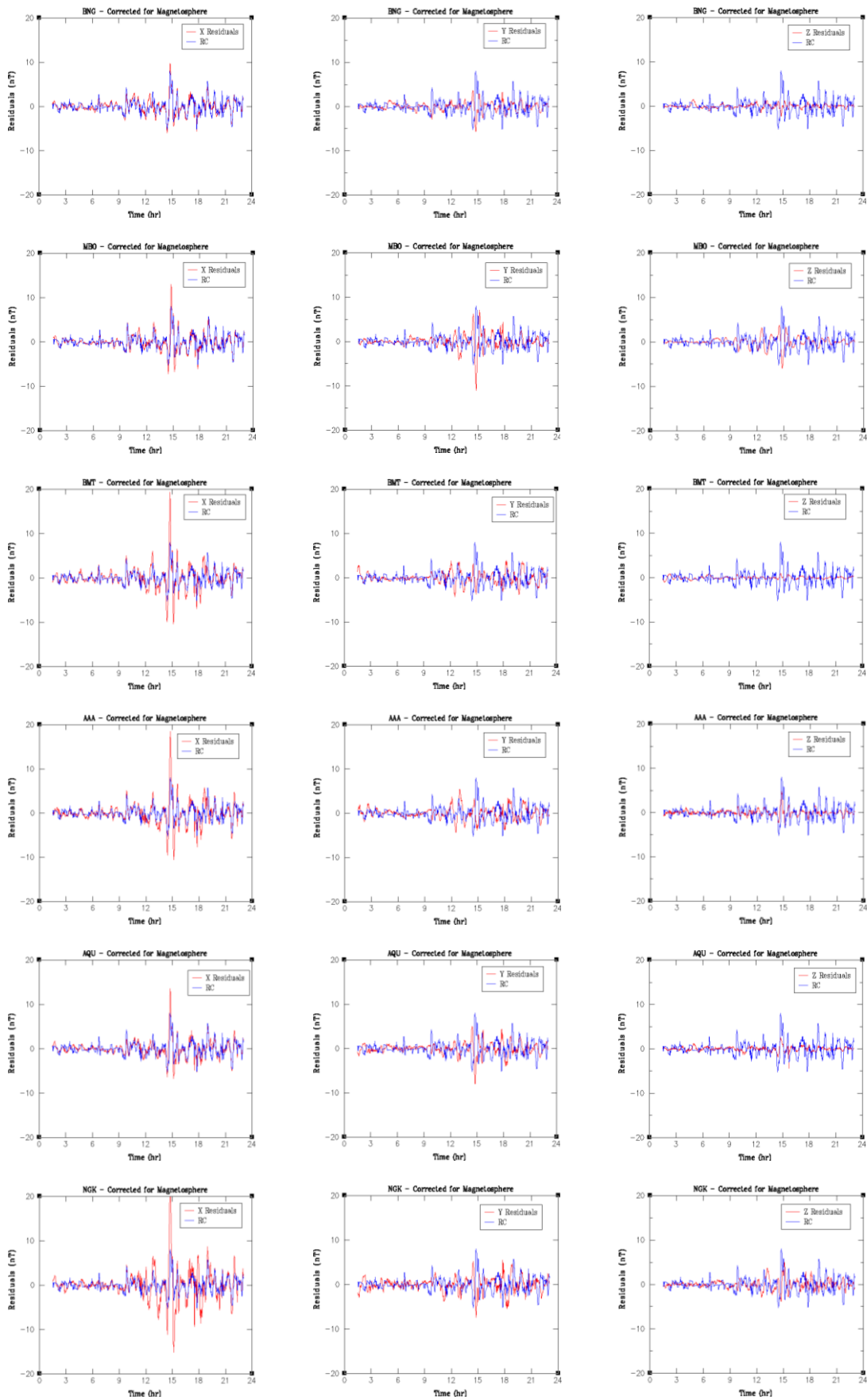


Figure 5.5a: Comparison between X, Y and Z residuals (red lines) corrected for magnetosphere and RC index residual (blue line) for Africa (BNG, MBO), Asia (BMT, AAA) and European (AQU, NGK) observatory locations. Follows similar pattern as seen in 5.4a.

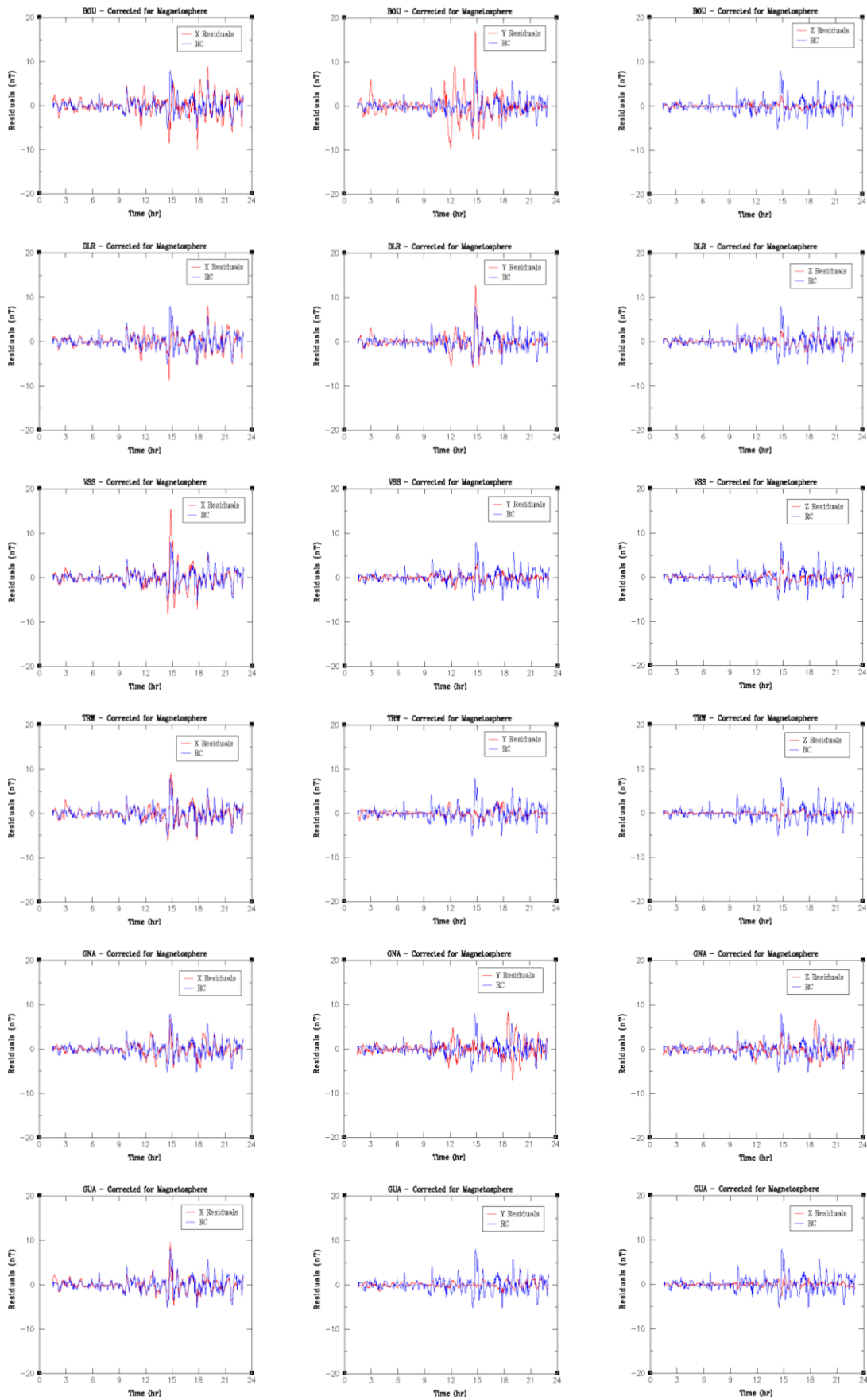


Figure 5.5b: Similar to figure 5.8 for North America (BOU, DLR), South America (VSS, TRW) and Oceania (GNA, GUA). Follows similar pattern as seen in 5.4b.

In general, in Y and Z components, we observe the clear reduction in the influence of the external fields based on the lack of substantial agreement between the observatory data residuals and the RC index, but in the X component, a significant level of external field influence can be seen notwithstanding the notable level of variability at different observatory locations. The limited performance of the CM4 model in the Y and Z components could be attributed to the very simple conductivity model which does not take into account regional or local induction effects, and also the external field variation is strongest and more influenced in the X component. The model (which is a least-squares fit) fits the large signal and ignores anything smaller. So for the Y and Z components it makes no difference whether the external field contributions described by the CM4 model is well described or not.

Before discussing further whether the variation seen can be linked to the observed external field influences of magnetospheric ring current, we further our investigation by looking at the comparison of the RC index residuals with observatory data residuals for observatory locations which show strong equatorial electrojet influences. This is to see if there are any differences with those observatory locations that don't show equatorial electrojet influences.

5.3 Comparison with Observatory Showing Equatorial Electrojet Influences

In figure 5.10, the variations of the X, Y and Z residuals of the observatory locations which show strong electrojet influences are shown in comparison with the corresponding variation of the residuals of the RC index for the Huancayo, HUA observatory. As it is to be expected with variations at observatories showing electrojet influences, we can see the abnormally large range of amplitude in the X component, associated with the eastward band of electric currents in the ionosphere which is the equatorial electrojet current. Despite this abnormal large range of amplitude, the X component follows similar trends in all the different field contributions as obtained in all the other observatory locations globally. It shows strong coherence and good agreement with the RC index residuals despite this abnormal enhancement of the solar daily variation and the effects of the magnetic disturbances on the X component caused by the equatorial electrojet. We can still observe very clear correlation between the X component residuals and that of the RC index.

Unlike what we observe in the other observatory locations worldwide in the Y and Z components, where we see a mixture of both some correlations and anti-correlations in the comparison, here we see clear correlation in both the Y and Z components with RC index residuals. At HUA observatory as seen in figure 5.6, the Z component has a much higher correlation and better agreement with the RC index than the Y component. The correlation is almost as good as that of the X component's correlation with the RC index residuals. A couple of reasons may be responsible or invoked to explain this observed reasonably good agreement/correlation between the Z component at HUA electrojet observatory with the RC index. According to Rastogi (2004 and 2006), the daily variation of the Z field at electrojet stations is found to represent very closely the temporal gradient of the X field. This abnormality is attributed to the effect of eddy currents induced in subsurface conductivity anomalies. Also, induction effects on the equatorial electrojet seem to be absent in central and eastern parts of South America and in the African region (Rastogi, 2004).

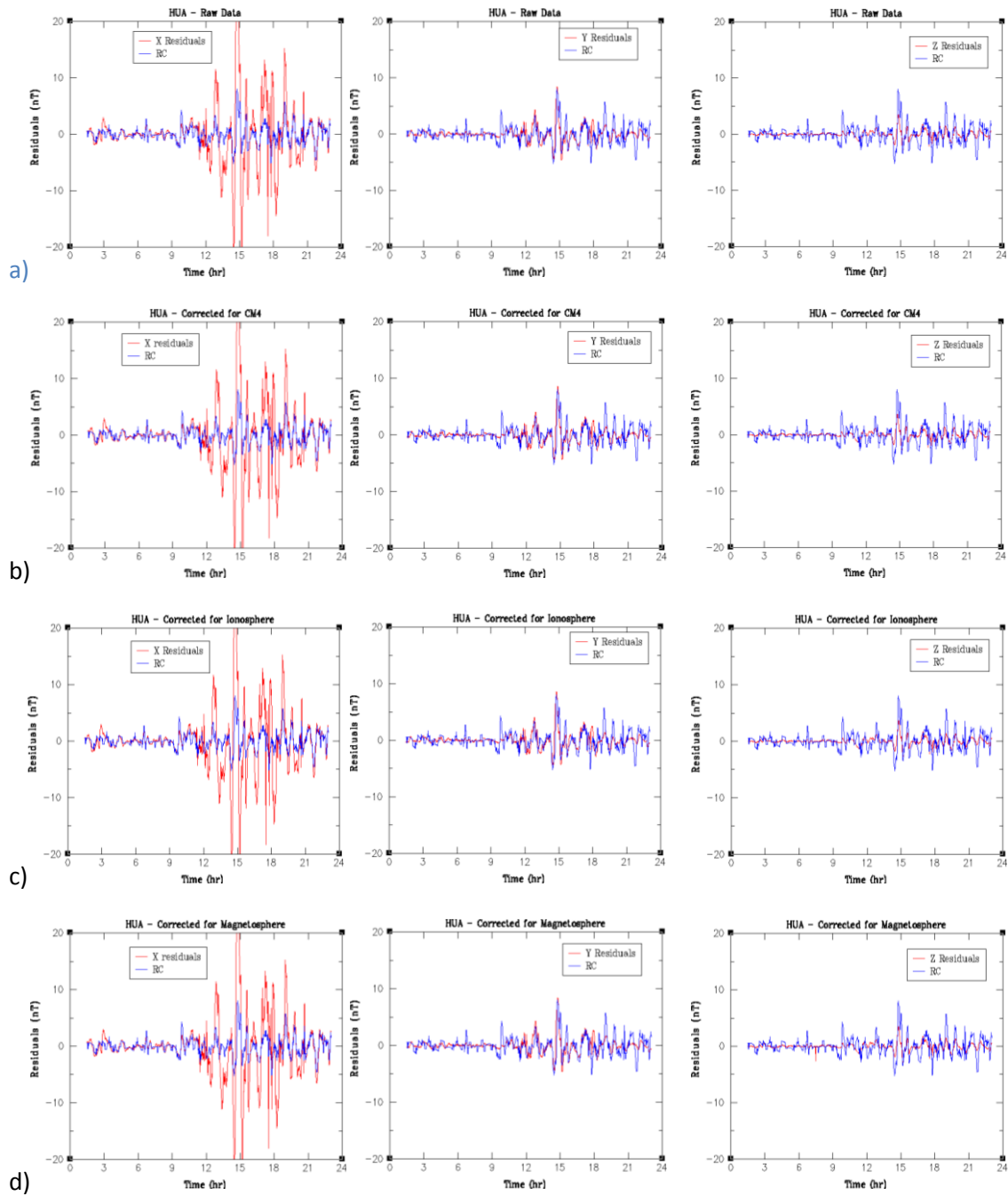


Figure 5.6: Comparison between X, Y and Z residuals (red lines) and RC index residual (blue line) for Huancayo (HUA) electrojet observatory for a) Raw Data uncorrected with CM4 model, b) Data corrected with CM4 model (for both ionosphere and magnetosphere), c) Data corrected for ionosphere and d) Data corrected for magnetosphere. Observe X component showing electrojet influences with abnormal large range of amplitude, but still follows similar trend as seen in other observatories, showing good agreement with RC index. Unlike other observatories, Y and Z here shows good correlation with RC index, with Z showing a higher correlation and better agreement with RC index than Y.

5.4 Cross-Correlation Function

To further interpret and explain the results of the small scale features modelling, our residuals from all available observatory locations for the field components and the RC index are further analysed by means of cross-correlation functions.

The cross-correlation function between the residuals of the different observatory components and that of the RC index is estimated by the cross-correlation function defined according to Wardinski and Holme (2011)

$$R(l) = \frac{\frac{1}{(N-l)} \sum_{k=l}^{N-l} \{[x(k)] \cdot [y(k+l) - \bar{y}]\}}{\sigma_x \cdot \sigma_y} \quad (5.1)$$

This means the mutual correlations between two independent series x , y (set as the geomagnetic field components and the RC index in this) having sample length N at sample lag l . σ_x and σ_y represents the standard deviations (we assume our standard deviations to be 1).

In geomagnetic studies of this nature, a cross-correlation function analysis provides linear measurements of the correlation between two or more observed quantities. For this study we adopt a maximum lag, $l = 120$ in order to avoid so-called large-lag standard error (Box and Jenkins, 1976), which is $1/11^{\text{th}}$ of the total series length. We plotted the cross-correlation function as a function of geographical location and different field contributions with the RC index residuals. As usual, our aim is to establish the global and widespread nature of the correlation and coherence between the observatory residuals and the RC index, and to see the effect in each field contribution of the correlation.

5.4.1 Correlation Between Observatory Data Residuals and the RC index

The plots for the cross-correlation functions are presented in figures 5.7 and 5.8. These are for the raw (original) data and the case where the observatory data residuals are corrected with CM4 (ionosphere and magnetosphere). The maxima at zero lag indicate that the variation of the residual components and RC are correlated or anti-correlated, respectively. To obtain the cross-correlation function, we cross-correlated each of the components with RC, and RC with each of the components (i.e. swapping x and y in equation 5.1), and from their meeting point at zero lag we estimated the cross-correlation coefficient. The cross-correlation coefficient is an estimate that determines the degree of similarity between two independent series (x and y) that are compared. If the series are identical, then the cross-correlation coefficient is 1. The resulting plots are very similar for each of the components at most of the observatories, and it is quite evident from the different plots that for all the different field contributions there exists a similar pattern between the residuals of the different observatory components and the RC index irrespective of geographical region.

The cross-correlation coefficients between the RC index and the X components of the observatory residuals are seen to be largely higher at $l = 0$. A very strong correlation with cross-correlation coefficients between 0.7 – 0.85 exists between the RC index and the X components of the observatory residuals. The only exceptions are NGK (0.65), BOU (0.45), OTT (0.4) (see table 5.1) and GNA (0.58) where there are lower correlations and cross-correlation coefficient between the RC index and the X components of the observatory residuals. Numerical support for this is given by the results for some selected observatory locations from different geographical region of the Earth displayed in table 5.1. Perhaps the only surprise is the low cross-correlation coefficients, even for observatory locations like NGK and GNA which are part of the observatories from which the RC index is constructed. But their cross-correlation coefficients of 0.65 and 0.58 respectively is still reasonably good (> 0.5). This low cross-correlation coefficient recorded for BOU, OTT and GNA, between the X component residuals and the RC index may be due to additional non-coherent, non-RC index related signals present in the X component residuals.

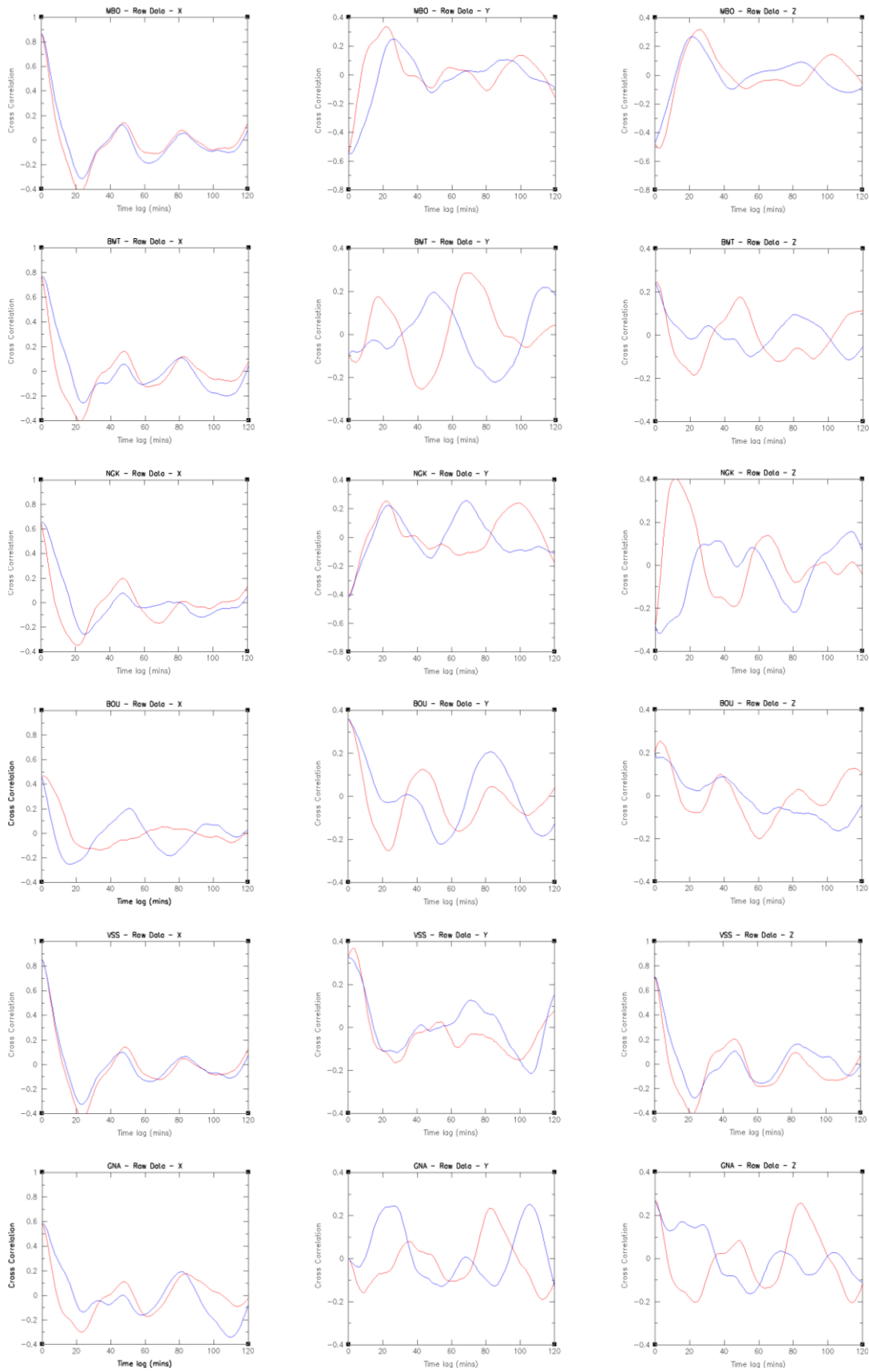


Figure 5.7: Cross-correlation between X, Y and Z residuals and RC index residual for raw data in selected observatory locations in different geographical region of the Earth. X shows good cross-correlation. Profiles show somewhat periodic oscillation of 20 minutes interval. X shows consistent negative feature at 20 minutes, Y mostly positive exception of BOU and VSS, while Z shows negative except MBO and NGK.

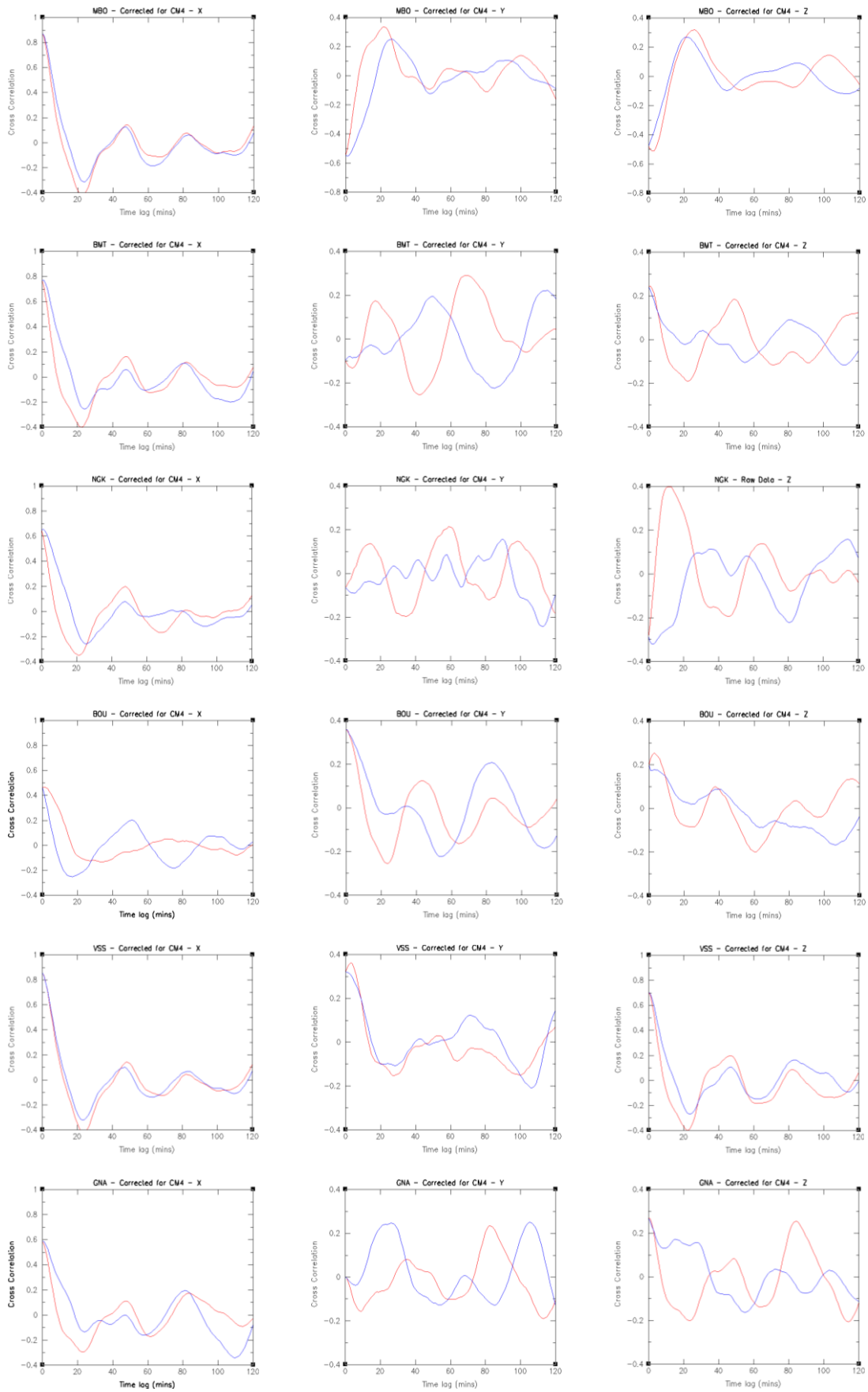


Figure 5.8: Cross-correlation between X, Y and Z residuals and RC index residual for data corrected with CM4 (for both ionosphere and magnetosphere in selected observatory locations in different geographical region of the Earth. Display similar pattern as seen in figure 5.7.

The resulting plots show that the correlation between the X component residuals and the RC index does not have strong geographical dependence or field contributions dependence, as the cross-correlation coefficient results follow similar trends in all geographical regions and in the different field contributions. Even in North America where BOU, OTT and FRN recorded poor and low cross-correlation coefficients, we still see DLR in the same region showing very good cross-correlation of 0.70, depicting good agreement/correlation between the X component residuals and the RC index.

Thus, we can generally say that a high cross-correlation exists between the X component residuals of the observatory data and the RC index, and this is seen irrespective of the different field contributions, as good cross-correlation exists between the X component residuals and the RC index in almost all the observatory locations in all the field contributions [raw data (figure 5.7), data corrected with CM4 model (figure 5.8), data corrected for ionosphere (not shown) and data corrected for magnetosphere (not shown)]. The cross-correlation coefficients estimated between the X component residuals of the observatories and the RC index range between 0.80 – 0.85 for Africa, 0.75 for Asia, 0.65-0.75 for Europe, 0.40-0.70 for North America, 0.70-0.85 for South America and 0.58-0.80 for Oceania regions. The magnitude of the cross-correlation coefficient show that it is independent of geographical region, as we see very strong cross-correlation coefficients of up to 0.70 in the regions, and low cross-correlation coefficients in North America and Oceania. The cross-correlation coefficients between the X component residuals and the RC index suggests that the rapid variations are coming from a large scale source – ring current magnetosphere – of external origin to the Earth.

On the other hand, the RC index residual variations are not well correlated with the residuals of the Y and Z components of the observatory data. The cross-correlation coefficient range from a reasonably strong anti-correlation (-0.55) to reasonably good cross-correlation (0.50) in the Y component and reasonably strong anti-correlation (-0.55) to poor anti-correlation (0.45) in the Z components. However, there were some exceptional cases where some good cross-correlations are seen in the Y and Z components, like in HUA with cross-correlation coefficient of 0.60 in the Y component and 0.70 in the Z component. VSS and TRW recorded cross-correlation coefficients of 0.70 and 0.55 respectively in the Z components. DLR in North American sector recorded cross-correlation coefficients of 0.50 and 0.70 in the Y and Z components respectively also. The improved cross-correlation coefficients in HUA in the Y and Z components could be due to the fact that it is an equatorial electrojet (EEJ)observatory station, but similar trend could not be seen in AAE, another EEJ observatory station, although PhuThuy (PHU) recorded a cross-correlation coefficient of 0.60 in the Z component.

Careful observation of the signals in the cross-correlation between the residuals of the observatory components and the RC index reveals characteristic of certain periodic oscillations. Although the amplitudes of the oscillations are variable, they seem to be present continuously. The oscillation appears to be expressed primarily by the increase and decrease of the amplitude of the cross-correlation signals at 20 minutes interval (i.e. the alternation from positive to negative amplitude appears to occur at 20 minutes interval). There is a common negative feature in the amplitude at 20 minutes. Figures 5.7 and 5.8 show this negative feature at 20 minutes continuously exists in each profile of the cross-correlation, though the amplitude is modulated. This feature is clearly demonstrated in all the cross-correlation profiles of the X component with RC index, and we see the same in the cross-correlation profiles between the X components of the different observatories. It also shows up in autocorrelation function (i.e. when the same series is compared to phase shifted

copies of itself – frequently used for the extraction of fundamental frequency) profiles (not shown), in which case, we assume it may just be a feature of a common signal.

The cross-correlation profiles of Y and Z components with RC index also show this periodic characteristic oscillation at 20 minutes interval, but not as clear as that of the X component profiles. Unlike the X component, the Y component show positive amplitude at 20 minutes, except at BOU and VSS which show negative like X component. Z component profiles record negative feature at 20 minutes like X component in most observatories, except MBO and NGK, though the feature is not as clear as that of X component.

In general, in all the available observatory locations studied (both the ones shown and not shown here), irrespective of field contributions and geographical location, the cross-correlation coefficients between the X component and the RC index are good and well correlated. But the cross-correlation coefficients between the Y and Z components and the RC index are not that significant in almost all the cases. This is consistent with the ring current not having any significant effects on the Y and Z components, but influencing the rapid variations seen in the X components in our diurnal variation data for days away from quiet time.

| Observatory Location | Code | Correlation Coefficient X with RC index | Correlation Coefficient Y with RC index | Correlation Coefficient Z with RC index |
|----------------------|------|---|---|---|
| Addis Ababa | AAE | 0.80 | -0.45 | 0.10 |
| Bangui | BNG | 0.85 | -0.50 | -0.35 |
| Mbour | MBO | 0.85 | -0.55 | -0.50 |
| Tamanrasset | TAM | 0.85 | -0.55 | -0.35 |
| Beijing M T | BMT | 0.75 | -0.10 | 0.25 |
| PhuThuy | PHU | 0.75 | 0.00 | 0.60 |
| Alma Ata | AAA | 0.75 | -0.35 | 0.55 |
| Kakioka | KAK | 0.75 | 0.15 | 0.70 |
| L'Aquila | AQU | 0.75 | -0.55 | 0.45 |
| Budkov | BDV | 0.75 | -0.45 | 0.08 |
| Niemegk | NGK | 0.65 | -0.40 | -0.30 |
| Belsk | BEL | 0.70 | -0.35 | 0.20 |
| Boulder | BOU | 0.45 | 0.35 | 0.20 |
| Del Rio | DLR | 0.70 | 0.50 | 0.70 |
| Ottawa | OTT | 0.40 | 0.35 | 0.15 |
| Fresno | FRN | 0.55 | 0.35 | 0.50 |
| Huancayo | HUA | 0.70 | 0.60 | 0.70 |
| Vassouras | VSS | 0.85 | 0.35 | 0.70 |
| Trelew | TRW | 0.70 | 0.15 | 0.55 |
| Kourou | KOU | 0.85 | -0.30 | -0.70 |
| Gnangara | GNA | 0.58 | 0.00 | 0.25 |
| Guam | GUA | 0.80 | 0.10 | -0.50 |
| Kakadu | KDU | 0.70 | -0.10 | -0.55 |
| Learmonth | LRM | 0.65 | -0.40 | -0.60 |

Table 5.1: Cross-correlation coefficients of X, Y and Z components of the geomagnetic diurnal field with the RC index for selected observatory locations in the different geographical regions of the Earth. Red are African observatories, Black are Asian observatories, Green are European observatories, Purple are North American observatories, Blue are South American observatories and Orange are Oceania observatories.

5.4.2 Correlation between Observatory Locations

Motivated by the encouraging agreement and coherence, particularly in the X component, in the correlation of the residuals between the observatory location data and the RC index (figures 5.7-5.8 and table 5.1), we decided to compare the correlation and cross correlation between the X component residuals of the different observatories in different locations, both within the same geographical region and without. (Again, the residuals compared are the differences between removing running average of one-hour and what is left.)

Figures 5.9 and 5.10 illustrate the correlation profiles between selected observatories. We can see that the two signals matches each other very well, showing very strong coherence and correlation between the X components of the field at the different observatory locations. In terms of geographical extent, we compared correlations between observatories in different countries located in the same region i.e. Bangui (Central African Republic) and Mbour (Senegal) in Africa, and observatories located in different regions i.e. Niemegek (Germany) in Europe and Mbour (Senegal) in Africa. Here, we can even observe that a smoother correlation profile is obtained from comparing the signals between the X component residuals from different observatory sites than the comparison between the X component residuals of the observatory sites and that of the RC index. The only exception is the low correlation between the observatories at VSS and DLR (figure 5.10). This low/poor cross-correlation is seen in most of the comparison between the X components of observatories of the North American sector and the South American sector and the Oceania sector. We are tempted to assume that these low/poor cross-correlation observed between the North American and the South American/Oceania observatories may be due to the observatory stations located at different hemispheres on the Earth surface. It is already well established that the different hemispheres (North and South) are subjected to dynamo currents (Sq current system) flowing in the E-region ionosphere due to atmospheric tidal motion, composed of two cells, one for each hemisphere (Vichare et al. 2012; Pedatella et al. 2011; Matsushita and Campbell, 1987). These are essentially responsible for the Sq diurnal variations measured on the Earth's surface. The currents flow clockwise in the Southern hemisphere and anti-clockwise in the Northern hemisphere. Also, in the Northern hemisphere, the X component is negative (southward) above the focus of the Sq, and positive (northward) below the Sq focus.

There is no clear anti-correlation at any time in all the profiles studied, not even for the low cross-correlation between VSS and DLR. What, however, is strikingly clear is that all the resulting profiles are very similar with broad amplitude peaks at 15hours UT in the comparison/correlation profiles. This trend is similar and visible in all the observatory locations (figures 5.9 and 5.10).

The plots for the cross-correlation coefficients also confirm that the observatories show very strong coherence between the X components of the field, particularly for observatory locations within the same geographical region i.e. they correlate clearly with each other. The cross-correlation coefficients between the X component of the observatories at different locations within the same geographical regions are very high – AQU and NGK in Europe (0.90), BNG and MBO in Africa (0.90), PHU and BMT in Asia (0.95), BOU and DLR in North America (0.85), VSS and TRW in South America (0.80) and GNA and KDU in Oceania (0.90) (table 5.2). Also, the cross-correlation coefficients of the X component between the observatory locations at different geographical regions are good in most of the combined observatory locations. Examples include NGK and MBO (0.80), NGK and BMT (0.80), AAA and MBO (0.85) and even at the EEJ observatories at HUA and AAE (0.70) (perhaps a good

correlation between EEJ observatories is not surprising) (table 5.3). This demonstrates that the effect is large scale, but not necessarily global.

Only at KDU and BDV (0.65), VSS and DLR (0.45) and GNA and DLR (0.15) are the cross-correlation coefficients recorded are below 0.70 and poor respectively, confirming the low/poor correlation observed between observatories located in different part of the hemispheres, especially between North America and South America and Oceania.

The strong coherence and high cross-correlation exhibited by the signals of the compared X component of the observatories lead us to assume that the differences in regional or local features may not have, or are only marginally, affected the signals. These features, particularly the crustal and local conductivity structure may not have adversely affected the signals, at least as far as their time variation is concerned. If not, we would have expected the cross-correlation between the residuals of the X component of the different observatories to vary with location more characteristically, and sometimes to become smaller in amplitude and correlation coefficients than the cross-correlation between the X component residuals of the observatory location data and that of the RC index residuals.

| Observatory Location | Code | Correlation Coefficient X between observatories |
|------------------------------|-------------|--|
| Bangui & Mbour | BNG & MBO | 0.90 |
| L'Aquila & Niemegek | AQU & NGK | 0.90 |
| PhuThuy & Beijing Ming Tombs | PHU & BMT | 0.95 |
| Boulder & Del Rio | BOU & DLR | 0.85 |
| Vassouras & Trelew | VSS & TRW | 0.80 |
| Gnangara & kakadu | GNA & KDU | 0.90 |

Table 5.2: Cross-correlation coefficients of X component between observatory sites located within the same geographical locations. Notice the very strong correlation between the X component of the field at different sites irrespective of geographical region.

| Observatory Location | Code | Correlation Coefficient X between observatories |
|-------------------------------|-------------|--|
| Niemegek & Mbour | NGK & MBO | 0.80 |
| Niemegek & Beijing Ming Tombs | NGK & BMT | 0.80 |
| Alma Ata & Mbour | AAA & MBO | 0.85 |
| Huancayo & Addis Ababa | HUA & AAE | 0.70 |
| Kakadu & Budkov | KDU & BDV | 0.65 |
| Vassouras & Del Rio | VSS & DLR | 0.45 |
| Niemegek & Trelew | NGK & TRW | 0.40 |
| Gnangara & Del Rio | GNA & DLR | 0.15 |

Table 5.3: Similar for table 5.2 above for observatory sites located at different geographical regions. Observe the low/poor correlation coefficient between observatory sites located at different hemispheres on the Earth surface.

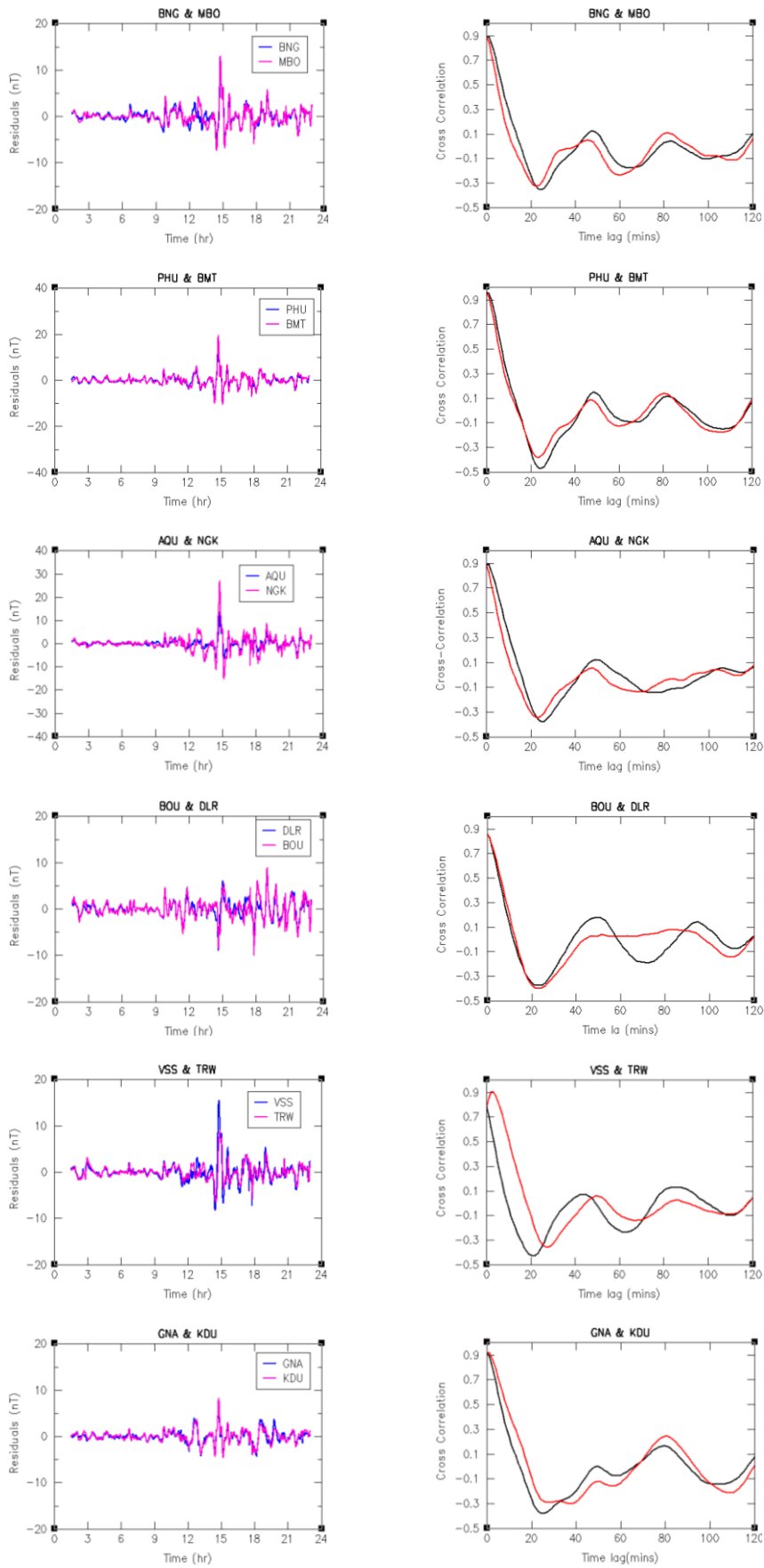


Figure 5.9: Comparison (left) and cross-correlation (right) profiles between observatories in same geographical regions. Notice the very high cross-correlation coefficient of approximately 0.90 between the X components.

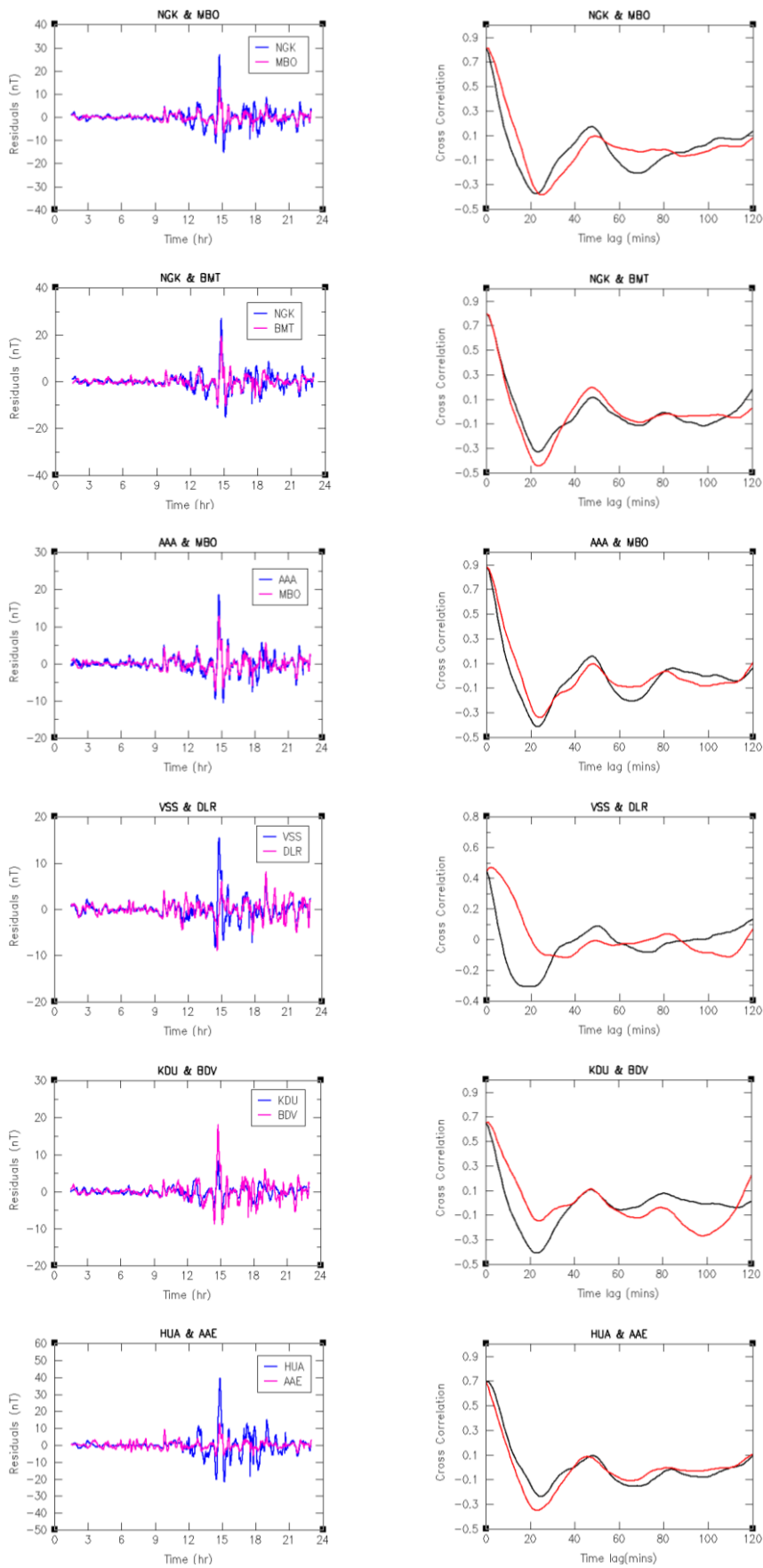


Figure 5.10: Similar to figure 5.9 between observatories in different geographical regions. Notice the low cross-correlation coefficient of about 0.45 between VSS and DLR located in Brazil and America respectively.

5.5 Small Scale Features Summary

Based on the various results obtained, shown and the analysis provided in this chapter, we can argue that the residuals of our observatory location data for days away from quiet time, particularly the X component residuals, include a strong component in the rapid variations that is related to global external field variation, most likely arising from magnetospheric ring current.

A very strong coherence and correlation is seen to exist between the X component of the observatory data residuals and the RC index. This strong correlation/coherence is also seen between the X component residuals of the observatories at different observatory locations within the same geographical regions, and in some observatories at different geographical regions. This feature leads us to characterise the RC index as being a good representation of most of the observatories for rapid variations globally.

This was, however, not the case in the other geomagnetic components (Y and Z). We observed strong anti-correlation and low correlation in the Y and Z components, and a few good correlation in the Z components, especially in DLR, PHU, HUA and VSS. In general, some of the signals can be said to be global (as in the X component – results show global correlation and coherence) and some not (as in the Y and Z components).

Chapter 6

Synthesis, Additional Analysis and Future Work

The geomagnetic diurnal variation occurs everywhere on the Earth's surface. It is the most consistent component of the time-varying part of the Earth's magnetic field. Its susceptibility to harmonic analysis makes it possible for it to be expressed in terms of elements of 24, 12, 8 and 6 hours (Chapman and Bartels, 1940; Matsushita, 1967) (It could be argue that this is really the other way around – the strong period signals suggest harmonic analysis).

Present-day published Earth's magnetic field models perform well over much of the globe. However, this has not been the case when it comes to Sq diurnal variation models, particularly Sq away from quiet time, where the magnetic activity is highly irregular and unpredictable. Presently, most of the Sq diurnal variation models and studies have dwelt on the behaviour of the diurnal variation during quiet times, periods of very low or negligible magnetic activity. This is geared towards studying the diurnal variation during when the effects posed by the highly time-varying external magnetic field sources are highly reduced, especially those associated with ionospheric and magnetospheric sources.

Over the course of this thesis, we have presented an examination of the geomagnetic Sq diurnal variation field for days away from quiet time (but of only moderate activity). We have demonstrated the potential for using the RC index specific to the rapid variations external sources of magnetospheric ring currents to better analyse and study the rapid variations of the Sq diurnal field for days away from quiet time. Here in this final chapter, we present an overview of the whole study. We begin in 6.1 by doing a synthesis and discussion of the study. In 6.2, we briefly look at the implications for magnetic surveys of our study, and in 6.3 we look at the effects of equatorial electrojet on magnetic surveys in the light of our study. We conclude the thesis in section 6.4 with a brief discussion of avenues for further work which might improve on the work, and provide us with a better understanding of the behaviour of the diurnal variation field for days away from quiet time (which we have shown that much of the signal is not Sq as commonly understood).

6.1 Synthesis and Discussion

In our study of the comprehensive model (CM4) as a model for predicting the magnetic observatory data (chapter 3), we find that the CM4 model is predicting the daily variation of the parameterized fields during quiet periods, outside the timespan of the CM4 model. The profile plots obtained using the CM4 model (section 3.3.1) comparing the model and the observatory data reflects the Sq diurnal variations expected for the different geographical regions and latitudes. Away from quiet time, despite the lack of active data in the original CM4 model dataset, we find the CM4 model predicting the regional type features of the observatory data. It is in predicting the short term features of the rapid variations that the model is not doing well in its prediction (figures 3.7-3.12). This is particularly more evident in the X component where we see the greatest misfit between the CM4 model and the observatory data. This is in part because Dst is not parameterized for short-time variation.

The comparison of the modelled diurnal maps of the CM4 model and the observatory data shows that increasing the spherical harmonic degree decreases the residuals and reduces the misfit of the CM4 model to the observatory data i.e. the CM4 model appears to do reasonably well in predicting the diurnal field (away from quiet time) as we move to higher degree of harmonics. This produces a

better coherence and close match between the CM4 model and observatory data (figures 3.13-3.17). This is instructive as it shows that as we move from lower to higher harmonic degree, more small scale features are revealed and the similarity between the CM4 model and the observatory data is seen in the comparison.

This motivates delving into the nature of the signals that we are seeing, particularly in the X component, since this may be the reason for the misfit between the CM4 model and the observatory data comparison. In order to identify the nature of the rapid variation, we investigated its relationship with the external fields using the RC index. This becomes necessary as our results show that the external field descriptions included in the CM4 model (F10.7 and D_{st}) could not sufficiently explain the field contributions for days away from quiet time. D_{st} as a global index measuring the disturbances in the magnetic field, and describing the time-space structure of the magnetospheric ring current, does not provide a high enough time resolution. As a result the CM4 model is hampered in its bid to fully describe the external field variations for days away from quiet time. So we deemed it advantageous to make use of the new RC index which provides a higher time resolution and may not suffer from baseline instabilities like the D_{st} index, in order to investigate the rapid variation nature of the property seen in the X component of our data.

Our observatory data show coherent structure that is essentially Sq diurnal variation, with most of the observatory locations, particularly the European ones, showing very strong coherence between the same components of the field at different observatory locations. When comparing individual days against the comprehensive model, they show deviations of two kinds: long period variations that show variations between days of slowly varying feature, and more rapid variations, particularly for the data for days away from quiet time.

Using eigenanalysis and detrending the data sequences with spline fits, we compared these against the RC index. When comparing the observatory data residuals with the RC index we find that the RC index residual is doing a reasonably good job fitting the time variations. Taking the ionosphere/magnetosphere stated from CM4 away from the observatory data, the ionosphere clearly does a good job of removal (section 4.5.5). There are definitely coherent features showing up in the rapid variation, not only for the single observatory locations, but also seen in the combined observatory locations (i.e. between Niemegek and Mbour, and Budkov and Bangui in figure 4.13 and 4.14 respectively). In this comparison, we only considered the X component residuals against the RC index, because it is the component that is most easily influenced by the external field sources of ionospheric and magnetospheric origin. The different results show clearly that external influences dominate the observatory data residual variations for days away from quiet time.

In trying to establish the nature of these rapid variations for days away from quiet time seen in our noisier data, and to see how well we can understand them, we tried to establish the link between the RC index and the rapid variations observed. Are they related to the ring current effect (in which case such variations would be fully explainable by the RC index)? Or are they related to changes in the pattern of Sq – slightly different structure for S_{not_sq} ?

Looking at the coherence and correlation between small scale features, and trying to establish whether these coherence and correlation between the components of the observatory data residuals and the RC index have a global spread, we took the path of a simple running average of one hour, then the difference between the running average and what is left (chapter 5). We clearly observe that there is a general coherence and agreement between the RC index and the residuals of

the X component of the observatory data. This coherence and agreement is seen in observatory locations in all the geographical regions of the globe. This suggests a global phenomenon. This trend is replicated in all the different field contributions, for both raw data and when the ionospheric/magnetospheric fields are corrected with CM4 model. However, this was not the case for the Y and Z components of the field. Here there are no clear trends, as they show a mixture of low correlation/coherence and anti-correlation against the RC index. But the Z component shows more correlation and coherence with the RC index than the Y component. This lack of substantial agreement/coherence between the Y and Z components and the RC index show the clear lack of influence of the external field variations of ionospheric and magnetospheric origins compared to the X component.

Looking at observatory locations which show strong equatorial electrojet (EEJ) influences e.g. Huancayo observatory, we observe some coherence in the Y and Z components unlike what obtains in other observatory locations. Here the coherence/agreement between the Z component and the RC index is almost as good as that of the X component against the RC index.

To substantiate the level of coherence and correlation or lack of it observed in the profile plots comparison between the observatory data residuals and RC index, we looked at the cross-correlation coefficients for the different observatory components with RC index. The cross-correlation coefficient between the X component residuals of the observatory locations and the RC index is generally higher in almost all the observatory locations in all geographical regions of the globe, ranging from 0.70-0.85 (section 5.4.1), confirming the strong coherence between the X component and the RC index seen in our correlation comparison profile plots. For the Y and Z components, the cross-correlation coefficients show that these components are not generally well correlated with the RC index, having cross-correlation coefficients ranging from -0.55-0.50 in most observatory locations. However, some exceptional cases are seen in the cross-correlation coefficients in the Z component, which confirms the earlier suggestion that the Z component has a better coherence with RC index than the Y component. Here we recorded cross-correlation coefficient as high as 0.70 in the Z component with RC index for some observatory locations (HUA, VSS, and KAK) (table 5.1).

In addition, we also investigated the correlation between the X component residuals between the different observatory locations, both within the same geographical locations, and situated at different geographical locations. The profile plots show strong coherence and correlation between the X components of the field at different observatory stations within the same geographical location. This is confirmed in the cross-correlation coefficients with values ranging from 0.80-0.95. This is also seen in some of the cross-correlation coefficients across different geographical regions, except those between North America and those of South America and Oceania observatory stations, i.e. VSS and DLR, GNA and DLR, etc. (section 5.4.2).

The comparison of the RC index and the observatory residual components for both single and combined observatory locations characterise the RC index as a good representation of most of the observatory stations for rapid variations, particularly for the X component. This tells us that the rapid variations we see in our observatory data, showing Sq diurnal variation, for days away from quiet time are coming from a large scale source (magnetospheric ring current). Therefore, corrections for exploration activities conducted during disturbed times maybe considered to be global, particularly

for X component. Also, looking at rapid variation observatory data results for combined locations (more than one base station) might be a good remote referencing technique.

6.2 Implications for Magnetic Surveys

One of the major problems associated with magnetic surveys during days away from quiet time is the increase in magnetic disturbances. These disturbances reflect increase activities in the Earth's ionosphere and magnetosphere, related to solar activity. Major diurnal disturbances, fluctuations or variations of certain nature and intensity maybe observed on certain days which are clearly undesirable during magnetic surveys. In order to operate accurately and effectively, it may be necessary to allow for diurnal variations using observatory or remote base-station information. In certain part of the globe where logistics play significant factor, it may not be possible to use ideal base-station network and a compromise has to be made with survey accuracy.

Rapid variations/fluctuations are a crucial factor in magnetic surveying. This is because they form a 'noise background' against which survey data are recorded. As a result, an important part of magnetic survey practice has always been the correction of survey data for effects of fluctuations/variations. As a modern practice, it is conventional to subtract a fixed base-station record from the record of the mobile survey instrument. The exactness or accuracy of this procedure will clearly depend upon the spatial uniformity of the magnetic variations/fluctuations themselves.

Natural geomagnetic variations occur with a wide range of timescales (although its diurnal variations, both its long period and more rapid variation parts, operates on time-scales that are short in comparison with the time taken to carry out a magnetic survey), and the knowledge of these magnetic variation patterns, especially the rapid variations seen on disturbed days is very relevant to magnetic exploration i.e. aeromagnetic surveys.

The Sq (derived from solar quiet) is traditionally used to describe the quietest part of the geomagnetic diurnal variation (Bello et al.2014; Turner et al.2007; Lilley et al.1999), which is common from day to day, with a number of analyses based on data derived from global network of geomagnetic observatory stations. These could also be extended for analyses of Sq diurnal variation for days away from quiet time. Just as for Sq diurnal variation, these analyses typically present profile plots for the geomagnetic daily variation away from quiet time, as seen in this study, in traditional geomagnetic observatory coordinates of X, Y and Z. These also work in local solar time and magnetic latitude (Merrill et al. 1996).

For magnetic survey purposes, particularly aeromagnetic surveys, it is the total component, F of Sq which is important for much magnetic surveying. Aeromagnetic surveys aim to record the variations in F with x and y over a survey area while eliminating all time-based variations (Reeves, 2005). The F component contains a decent contribution from the X component, a negligible contribution from the Y component, and a major contribution from the Z component. The profile plots presented in this study for magnetic diurnal variation from different geographical regions of the globe does not include the total field component, F, but as outlined in section 2.5 (equation 2.5) this can be derived easily.

Our observatory data shows Sq diurnal variation, with more rapid variations seen, particularly on data for days away from quiet time. The variations on these data, for the X component, reasonably well matched the RC index, both for single and combined observatory stations. This suggests the RC

index is a good representation for most observatories globally (for X component) for rapid variations, not just for European observatory stations only. Thus, this tells us that the rapid variations are coming from a large scale source (magnetospheric ring current), and therefore, corrections for days away from quiet time (during magnetic surveys) may be considered global or regional.

6.2.1 Applications:

Improved Remote Referencing Application in Aeromagnetic Survey: In modern aeromagnetic mapping, an aircraft flies around a grid of lines overlaying the area to be mapped carrying a magnetometer. Time variations of the magnetic field which may occur during the mapping are typically controlled by two strategies (Luyendyk, 1997). One of the strategies is the setting of a base station to record simultaneously with the survey aircraft, as it is relatively easy to run a magnetometer at a fixed location on the ground while the aircraft is flying, and subtract the time-synchronised variations at the base from the profiles recorded from the aircraft. This is on the assumption that the time-varying field is spatially uniform from base station to survey aircraft. The problem with this is the assumption, when applying corrections, that the base station variations are fully representative of variations over the whole survey area. This may not be so for large scale aeromagnetic surveys (e.g. aircraft which is hundreds of kilometres from its base station) in a region where anomalies in the Earth's electrical conductivity structure cause the time-varying magnetic fields to change signature over distances of about 20km. Several studies have shown that error in this assumption tends to increase over distances beyond about 50km, and may be significant over much shorter distances in terrains with highly variable electrical conductivity (Lilley, 1982, 1984; Chamalaun and Cuneen, 1990; Kusi et al. 1998). The process of correcting for this rapidly time-varying magnetic field (of external sources) is called remote referencing.

For large scale aeromagnetic surveys (particularly for days away from quiet time) we suggest the use of more than a single base station as a good remote referencing technique, instead of just the usual readings from a fixed base station being subtracted from the survey measurements. This will ensure better reduction in the contamination from rapidly time-varying field sources. In addition, the use of one or more remote magnetic observatories in the region will also aid in better correction of survey data, since our results show particularly high and similar cross-correlations between the X components of the observatory data and the RC index, and between the X components of the field at different observatories in the same region. Turbitt and Clark (1994) has also showed that, on disturbed days, the cross-correlations between two sites peaked at zero lag, showing that the disturbance fields affected both sides simultaneously and caused similar field perturbations. Testing the use of more than one base station (or the use of a base station and magnetic observatory), we hope, will improve remote referencing, which relies on the assumption that any rapid field variations are large scale (the X component of our noisier data shows this to be so), and so the same at point of reference and the measurement location. Even when the base station may be some distance away from the survey area i.e. hundreds of kilometres, which often lead to substantial differences in the field between the two locations, our study shows that corrections may still be applied regionally (for days away from quiet time), consistent with the high cross-correlations seen in our results (section 5.4.1 and 5.4.2).

Improving Well Position Accuracy: External field variations, such as those that can be observed in geomagnetic observatory data, are sources of error for magnetic down-hole survey tools used in directional drilling. These tools, which include magnetic probes, are used in measurement while

drilling (MWD) methods to monitor the well-bore position and navigate to the planned oil and gas targets (Russell et al. 1995; Williamson et al. 1998; Reay et al. 2005). Significant deviations from the well plan can be avoided by using data from magnetic observatories to correct survey measurements.

While the north-seeking gyroscopic (NSG) survey remains the most accurate means of determining wellbore position, it is also the most expensive (Poedjono et al. 2011). To place wellbores accurately when using magnetic guidance, surveyors must account for or eliminate two important sources of survey errors – local variations in the magnetic field (particularly between magnetic north and true, or geographic, north), and interference caused by magnetized elements in the drillstring (Buchanan et al. 2013). To address these issues, surveying engineers use Geomagnetic Referencing, which accounts for the influence of crustal field and the time-varying disturbance field as well as secular variations in the main magnetic field.

Geomagnetic Referencing, as a technique for improving wellbore position accuracy, provides the mapping between magnetic north and true north that is necessary to convert magnetically determined orientations to geographic ones on a local scale (Poedjono et al. 2010, 2011, 2013; Buchanan et al. 2013). It uses the Earth's magnetic field to determine accurate wellbore positioning essential for success in today's complex drilling programs, either as alternative or a complement to NSG survey. The mapping accounts for secular variations and include an accurate crustal model. For days of higher magnetic activity (away from quiet time) or areas of rapid time-varying disturbance field, correction for this must be incorporated. Since the magnetic field of external sources varies rapidly with time, and as data are available from magnetic observatories, surveyors are able to incorporate disturbances caused by diurnal variation activity into the data processing. Standard practice is making use of data from local magnetic surveys near a wellsite to characterize the crustal field, a technique referred to as in-field referencing (IFR) (Russell et al. 1995; Williamson et al. 1998). A position extension to this technique, we suggest, is incorporating data from one or more remote observatory stations (multistation analysis) to account for the time variations and accurate data corrections. This may be a viable possibility as our results show the variation, for days away from quiet time, to be large scale. This will provide the best estimate of the local magnetic field which is critical for geomagnetic referencing and multistation drillstring compensation.. The key innovation will be development of improved techniques for incorporating data from nearby magnetic observatories to improve the positioning model. This will enable the achievement of the desired accuracy even at mid to high latitudes, where the local magnetic field variations are somewhat extreme, and would otherwise induce unacceptable positional errors. This will result in a degree of accuracy in data correction that approaches that of NSG while costing significantly less.

However, the suggested applications of improved remote referencing application and improving well position accuracy, should not in any way mean we lose sight of other traditional data corrections procedures that should be made. For example, differences arise more seriously from fields induced on the ground other than the external sources themselves. Variations in subsurface electrical

conductivity produce considerable variations in the time-variation of the field with location. A critical question to address is whether the induction is local or regional. A particularly significant effect is due to the contrast between highly conducting ocean and more poorly conducting land – what is called the ‘coast effect’ (Parkinson, 1979; Heison et al. 1993; Kuvshinov, 2008).

6.3 Effects of Equatorial Electrojet

The objective of magnetic survey, particularly aeromagnetic surveys, is to map the static, time invariant magnetic responses of structures and lithologies, as most aeromagnetic surveys are designed for looking at the crustal field. As a result, any other rapidly varying temporal or spatially varying magnetic field represents unwanted noise (Rigoti et al. 2000).

It has been a regular practice to remove diurnal variation by using tie-line/flight line levelling schemes (simple assumption of certain spatial uniformity of the magnetic variations), and even when a direct subtraction of a base-station is made, a line levelling scheme is used to correct for remaining errors (Reeves, 1993; Minty, 1991; Yarger et al.1978). However, in the equatorial region (where a local enhancement of the ionospheric conductivity in the direction parallel to the geomagnetic dip equator causes equatorial electrojet, EEJ), there are concerns by some that standard line levelling procedures do not adequately correct for the strong nonuniformity of the equatorial electrojet magnetic field (Rigoti et al. 2000). Validity of any interpretation made on aeromagnetic data depends on the accuracy with which the variation of the external field sources are removed or corrected in measurements of total magnetic intensity. Since a large area of the globe comes under the influence of EEJ, the evaluation of the impact of such concentration of ionospheric currents on aeromagnetic data is of particular interest.

Studies carried out by Rigoti et al. (2000), show that most of the residual magnetic variations come from the X and Z components contribution to the total magnetic field intensity, F. However, their observation in the study suggests that the effect of the inhomogeneity of the EEJ on the total field measured in the aeromagnetic surveys will not be critical as might be assumed if one considered only the variation of the single X or Z component. The study therefore concludes that the effect of the EEJ is not detrimental to standard aeromagnetic surveying.

6.4 Suggestion for Further Work

Clearer idea of the nature of the rapid variations observed on our data for days away from quiet time should be possible and enhanced as the potential for using more models as an independent means improves. The potential to look beyond the CM4 model could become a viable option as the need to look at specific field contributions become highly desirable - example is using CHAOS 4 for studying the active magnetospheric fields.

For the CM4 model, there is need to incorporate the RC index as part of the data for parameterising the external field contributions, as D_{st} is not of high enough resolution.

An obvious extension to our study is the use of satellite data. The integration of satellite and observatory station data would go a long way in establishing more informatively the nature of the rapid variations. With the abundant satellite data available from CHAMP, Orsted and now Swarm, this will allow the investigation and possibly high improvements to the Sq diurnal variation models, and more insight into the nature of the variations on magnetically active days, and its global spread.

Appendix

Additional Information

Names and Coordinates of Observatory Stations

African Stations

| NAME | IAGA CODE | COUNTRY | LATITUDE | LONGITUDE |
|----------------|-----------|--------------------------|----------|-----------|
| Addis Ababa | AAE | Ethiopia | 09.04 | 38.77 |
| Bangui | BNG | Central African Republic | 04.33 | 18.57 |
| Hartebeesthoek | HBK | South Africa | -25.88 | 27.71 |
| Hermanus | HER | South Africa | -34.43 | 19.23 |
| Mbour | MBO | Senegal | 14.38 | 343.03 |
| Tamanrasset | TAM | Algeria | 22.79 | 05.53 |
| Antananarivo | TAN | Madagascar | -18.92 | 47.55 |
| Tsumeb | TSU | Namibia | -19.20 | 17.58 |

Asian Stations

| NAME | IAGA CODE | COUNTRY | LATITUDE | LONGITUDE |
|--------------------|-----------|------------|----------|-----------|
| Alma Ata | AAA | Kazakhstan | 43.18 | 76.92 |
| Alibag | ABG | India | 18.64 | 72.87 |
| Beijing Ming Tombs | BMT | China | 40.30 | 116.20 |
| Guangzhou | GZH | China | 23.09 | 113.34 |
| Kakioka | KAK | Japan | 36.23 | 140.19 |
| Kanoya | KNY | Japan | 31.42 | 130.88 |
| Lanzhou | LZH | China | 36.09 | 103.85 |
| Memambetsu | MMB | Japan | 43.91 | 144.19 |
| Phuthuy | PHU | Vietnam | 21.03 | 105.95 |
| Qsaybeh | QSB | Lebanon | 33.87 | 35.64 |

South American Stations

| NAME | IAGA CODE | COUNTRY | LATITUDE | LONGITUDE |
|--------------|-----------|------------------|----------|-----------|
| Huancayo | HUA | Peru | -12.05 | 284.67 |
| Kourou | KOU | French Guiana | 05.21 | 307.27 |
| Port Stanley | PST | Falkland Islands | -51.70 | 302.11 |
| Trelew | TRW | Argentina | -43.27 | 294.62 |
| Vassouras | VSS | Brazil | -22.40 | 316.35 |

European Stations

| NAME | IAGA CODE | COUNTRY | LATITUDE | LONGITUDE |
|------------------------|-----------|----------------|----------|-----------|
| Abisko | ABK | Sweden | 68.36 | 18.82 |
| L'Aquila | AQU | Italy | 42.38 | 13.32 |
| Budkov | BDV | Czech Republic | 49.08 | 14.02 |
| Belsk | BEL | Poland | 51.84 | 20.79 |
| Brorfelde | BFE | Denmark | 55.63 | 11.67 |
| Black Forest | BFO | Germany | 48.33 | 08.32 |
| Borox | BOX | Russia | 58.07 | 38.23 |
| Chambon-la-Foret | CLF | France | 48.03 | 02.26 |
| Dourbes | DOU | Belgium | 50.10 | 04.60 |
| Ebro | EBR | Spain | 40.96 | 00.33 |
| Eskdalemuir | ESK | United Kingdom | 55.31 | 356.79 |
| Furstenfeldbruck | FUR | Germany | 48.17 | 11.28 |
| Grocka | GCK | Serbia | 44.63 | 20.77 |
| Qeqertarsuaq (Godhavn) | GDH | Greenland | 69.25 | 306.47 |
| Guimar-Tenerife | GUI | Spain | 28.32 | 343.56 |
| Hartland | HAD | United Kingdom | 50.99 | 355.52 |
| Hel | HLP | Poland | 54.61 | 18.816 |
| Hurbanovo | HRB | Slovakia | 47.87 | 18.19 |
| Hornsund | HRN | Poland | 77.00 | 15.56 |
| Irkutsk | IRT | Russia | 52.17 | 104.45 |
| Kandilli | ISK | Turkey | 41.06 | 29.06 |
| Lerwick | LER | United Kingdom | 60.14 | 358.82 |
| Lovoe | LOV | Sweden | 59.34 | 17.82 |
| Lviv | LVV | Ukraine | 49.90 | 23.75 |
| Manhay | MAB | Belgium | 50.30 | 05.68 |
| Narsarsuaq | NAQ | Greenland | 61.17 | 314.57 |
| Nagycenk | NCK | Hungary | 47.63 | 16.72 |
| Niemegk | NGK | Germany | 52.07 | 12.68 |
| Nurmijarvi | NUR | Finland | 60.51 | 24.66 |
| Novosibirsk | NVS | Russia | 54.85 | 83.23 |
| Panagjurishte | PAG | Bulgaria | 42.52 | 24.18 |
| San Fernando | SFS | Spain | 36.67 | 354.06 |
| Sodankyla | SOD | Finland | 67.37 | 26.63 |
| San Pablo-Toledo | SPT | Spain | 39.55 | 355.65 |
| Surlari | SUA | Romania | 44.68 | 26.25 |
| Qaanaaq (Thule) | THL | Greenland | 77.48 | 290.83 |
| Tihany | THY | Hungary | 46.90 | 17.90 |
| Uppsala | UPS | Sweden | 59.90 | 17.35 |
| Valentia | VAL | Ireland | 51.93 | 349.75 |
| Wingst | WNG | Germany | 53.74 | 09.07 |

North American Stations

| NAME | IAGA CODE | COUNTRY | LATITUDE | LONGITUDE |
|--------------------------------------|--------------|--------------------------|----------|-----------|
| Baker Lake | BLC | Canada | 64.32 | 263.99 |
| Boulder | BOU | United States of America | 40.14 | 254.77 |
| Barrow | BRW | United States of America | 71.30 | 203.38 |
| Stennis Space Centre (Bay St. Louis) | BSL | United States of America | 30.35 | 270.36 |
| Cambridge Bay | CBB | Canada | 69.12 | 254.97 |
| College | CMO | United States of America | 64.87 | 212.14 |
| Del Rio | DLR | United States of America | 29.49 | 259.08 |
| Fort Churchill | FCC | Canada | 58.76 | 265.91 |
| Fredericksburg | FRD | United States of America | 38.21 | 282.63 |
| Fresno | FRN | United States of America | 37.09 | 240.28 |
| Iqaluit | IQA | Canada | 63.75 | 291.48 |
| Meanook | MEA | Canada | 54.62 | 246.65 |
| Newport | NEW | United States of America | 48.27 | 242.88 |
| Ottawa | OTT | Canada | 45.40 | 284.45 |
| Poste-de-la-Baleine | PBQ | Canada | 55.28 | 282.26 |
| Resolute Bay | RES | Canada | 74.69 | 265.11 |
| Shumagin | SHU | United States of America | 55.35 | 199.54 |
| Sitka | SIT | United States of America | 57.07 | 224.67 |
| San Juan | SJG | Puerto Rico | 18.112 | 293.85 |
| St. Johns | STJ | Canada | 47.60 | 307.32 |
| Teoloyucan | TEO | Mexico | 19.75 | 260.82 |
| Tucson | TUC | United States of America | 32.17 | 249.27 |
| Victoria | VIC | Canada | 48.52 | 236.58 |
| Yellowknife | YKC | Canada | 62.48 | 245.52 |

Australian/Oceania Islands

| NAME | IAGA CODE | COUNTRY | LATITUDE | LONGITUDE |
|-------------------|-----------|-----------------------------------|----------|-----------|
| Argentine Islands | AIA | Antarctica | -65.25 | 295.75 |
| Martin de Vivies | AMS | French Southern & Antarctic Lands | -37.80 | 77.57 |
| Apia | API | Western Samoa | -13.82 | 188.22 |
| Ascension Island | ASC | United Kingdom | -07.95 | 345.62 |
| Alice Springs | ASP | Australia | -23.76 | 133.88 |
| Canberra | CNB | Australia | -35.32 | 149.36 |
| Charters Towers | CTA | Australia | -20.09 | 146.26 |
| Port Alfred | CZT | French Southern & Antarctic Lands | -46.43 | 51.87 |
| Dumont d'Urville | DRV | French Southern & Antarctic Lands | -66.67 | 140.01 |
| Eyrewell | EYR | New Zealand | -43.42 | 172.36 |
| Gnangara | GNA | Australia | -31.78 | 115.95 |
| Guam | GUA | Guam | 13.59 | 144.87 |
| Honolulu | HON | United States of America | 21.32 | 202.00 |
| Kakadu | KDU | Australia | -12.69 | 132.47 |
| Learmonth | LRM | Australia | -22.22 | 114.10 |
| Mawson | MAW | Australia | -67.60 | 62.88 |
| Macquarie Island | MCQ | Australia | -54.50 | 158.95 |
| Port-aux-Francais | PAF | French Southern & Antarctic Lands | -49.35 | 70.26 |
| Pamatai | PPT | French Polynesia (Tahiti) | -17.57 | 210.43 |
| Scott Base | SBA | New Zealand | -77.85 | 166.76 |

Bibliography

- Alexandrescu, M., D. Gilbert, G. Hulot, J-L. Le Mouel, G. Saracco (1995), Detection of geomagnetic jerks using wavelet analysis, *Journal of Geophysical Research*, 100, 12,557-12,572.
- Backus, G., R. Parker, and C. Constable (1996), Foundations of geomagnetism, *Cambridge University Press*, Cambridge.
- Backus, G., and F. Gilbert (1968), The resolving power of gross Earth data, *Geophysical Journal of Royal Astronomical Society*, 16 (2), 169-205.
- Backus, G., and F. Gilbert (1967), Numerical applications of formalism for geophysical inverse problems, *Geophysical Journal of Royal Astronomical Society*, 13 (1-3), 247-276.
- Barkhatov, N. A., L. I. Gromova, A. E. Levittin, and S. E. Revunov (2008), The relation between solar activity and orientation of the solar wind electric field relative to the Earth's magnetic moment, *Geomag. Aeron.*, 48, 713-718.
- Bartels, J. ((1949), The standardized index, K_s , and the planetary index, K_p , *IATME Bull*, 12B, 109.
- Bartels, J., and H.F. Johnson. (1940a), Geomagnetic tides in the horizontal intensity at Huancayo, 1: *Terrestrial Magnetism & Atmospheric Electricity (Journal of Geophysical Research)*, 45, 269-308.
- Bartels, J., and H.F. Johnson. (1940b), Geomagnetic tides in the horizontal intensity at Huancayo, 2: *Terrestrial Magnetism Atmospheric Electricity (Journal Geophysical Research)*, 45, 485-592.
- Bartels, J., N. H. Heck, and H. F. Johnson (1939), The three-hour-range index measuring geomagnetic activity, *Journal of Geophysical Research*, 44, 411.
- Beggan, C.D., K. A. Whaler, & S. Macmillan (2009), biased residuals of core flow models from satellite-derived 'virtual observatories', *Geophysical Journal International*, 177 (2), 463-475.
- Bello, O.R., A.B. Rabiou, K. Yumoto, and E. Yizengaw (2014), Mean solar quiet daily variations in the Earth's magnetic field along East African longitudes, *Advances in Space Research*, 54, 283-289.
- Berthelier, A. (1993), The geomagnetic indices: derivation, meaning and uses in solar terrestrial physics, in *STPW-IV proceedings*, J. Hruska, M. A. Shea, D. F. Smart, and G. Heckman, editors. US Gov. Publications Office, Boulder, 3-20.
- Bloxham, J., and A. Jackson (1992), Time-dependent mapping of the magnetic field at the core-mantle boundary, *Journal of Geophysical Research*, 97, 19537-19563.
- Bloxham, J., D. Gubbins and A. Jackson (1989), Geomagnetic secular variation, *Philosophical Transactions of the Royal Society of London*, Vol. 329, 415-502.
- Box, G.E.P. and G.M. Jenkins (1976), Time series analysis, forecasting and control, *Holden Day*, San Francisco, CA.
- Buchanan et al. (2013), Geomagnetic referencing – Real-time compass for directional drillers, *Oilfield Review Autumn*, 25, 3, 32-47.

- Cain, J. C., and R. Sweeney (1973), The POGO data, *Journal of Atmospheric and Terrestrial Physics*, 35, 1231.
- Campbell, W.H. (1997). Introduction to geomagnetic fields. Vol.1. *Cambridge University Press*. 290.
- Campbell, W. H. (1996), Geomagnetic storms, the D_{st} ring current myth and lognormal distributions, *Journal of Atmospheric and Terrestrial Physics*, vol. 58, 10, 1171-1187.
- Campbell, W.H., (1989). An Introduction to Quiet Daily Geomagnetic Fields, *Pure and Applied Geophysics*, 131, 3, 315-331.
- Campbell, W.H. and E.R. Schiffmacher. (1985). Quiet ionospheric currents of the Northern Hemisphere derived from geomagnetic field records, *Journal of Geophysical Research*, 90, 6475-6486.
- Campbell, W.H. and E.R. Schiffmacher. (1988). Quiet ionospheric currents of the Southern Hemisphere derived from geomagnetic records, *Journal of Geophysical Research*, 93, 933-944.
- Carbary, J. F. (2005), A K_p -based model of auroral boundaries, *Space weather*, 3, S10, 001.
- Chamalaun, F.H., and P. Cuneen (1990), The Canning basin geomagnetic induction anomaly, *Australian Journal of Earth Science*, 37, 401-408.
- Chapman, S. (1951). The equatorial electrojet as detected from the abnormal current distribution above Huancayo, Peru and elsewhere, *Meteorology and Atmospheric Physics*, Vol. 4, 1, 368-390.
- Chapman, S. (1948), The abnormal daily variation of horizontal force at Huancayo and in Uganda, *Terrestrial Magnetism and Atmospheric Electricity*, vol. 53, 3, 247-250.
- Chapman, S. (1919), An outline of a theory of magnetic storms, *Proceedings of Royal Society of London*, A-95, 61-83.
- Chapman, S. and K.S.Raja Rao. (1965). The H and Z variations along and near the equatorial electrojet in India, Africa and the Pacific, *Journal of Atmospheric and Terrestrial Physics*, vol. 27, 559-581.
- Chapman, S., and J. Bartels (1940), *Geomagnetism: Oxford University Press*.
- Constable, S. (2007), Geomagnetic induction studies. In: Kono M (ed) *Treatise on geophysics*, vol. 5, Elsevier, Amsterdam, pp 237-276.
- Courtillot, V., and J-L. Le Mouel (1984), Geomagnetic secular variation impulses, *Nature*, 311, 709-717.
- Courtillot, V., and J-L. Le Mouel (1988), Time variations of the earth's magnetic field: from daily to secular, *Annual Review of Earth & Planetary Sciences*, 16, 389-476.
- Daglis, A. I., R. M. Thorne, W. Baumjohann, and S. Orsini (1999), The terrestrial ring current: Origin, formation, and decay, *Review of Geophysics*, 37, 4, 407-438.
- de Boor, C. (1978), *A Practical Guide to Splines*, Springer-Verlag, New York.

- Dessler, A. J., and E. N. Parker (1959), Hydromagnetic theory of magnetic storms, *Journal of Geophysical Research*, vol. 64, 2239-2259.
- Dormy, E., and J-L. Le Mouel (2008), Geomagnetism and the dynamo: where do we stand? *C. R. Physique*, 9, 711-720.
- Dungey, J. W. (1961), Interplanetary magnetic field and the auroral zones, *Physical Review Letters*, 6, 47-48.
- Dunlop, D. J., O. Özdemir (2007), Magnetisations in rocks and minerals, in *Treatise on Geophysics*, ed. by M. Kono, vol. 5 (Elsevier, Amsterdam), pp. 278–331. Chap. 8.
- Egedal, J. (1947). The magnetic diurnal variation of the horizontal force near the magnetic equator, *Terrestrial Magnetism and Atmospheric Electricity, (Journal of Geophysical Research)*, vol. 52, 4, 449-451.
- Egedal, J. (1948), Daily variation of the horizontal force at the magnetic equator, *Nature*, 161, 443-444.
- Feldstein, Y. I., and G. V. Starkov (1967), Dynamics of the auroral belt and polar geomagnetic disturbances, *Planet Space Science*, 15, 209.
- Finlay et al. (2009), International Geomagnetic Reference Field: 11th Generation, *Report at Fall AGU Meeting*, 2009, San Francisco, CA.
- Friis-Christensen, E., H. Lühr, G. Hulot, R. Haagmans and M. Purucker (2009), Geomagnetic Research from Space, *Eos*, 90, 213-214.
- Friis-Christensen, E., H. Lühr, D. Knudsen, and R. Haagmans (2008), Swarm – an Earth observation mission investigating Geospace, *Advance Space Research*, 41, 210-216
- Friis-Christensen, E., H. Lühr, and G. Hulot (2006), Swarm: A constellation to study the Earth's magnetic field, *Earth Planets Space*, 58, 351-358.
- Finlay, C. C., et al. (2010), International Geomagnetic Reference Field: the eleventh generation, *Geophysical Journal International*, 183, 1216-1230.
- Gilbert, W. (1600), *De Magnete*. Original 1600 book translated by P. Fleury Mottelay in 1893, republished by Dover publications, New York, 1958.
- Gonzalez, W. D., A. Joselyn, Y. Kamide, H. W. Kroehl, G. Rostoker, B. T. Tsurutani, and V. M. Vasylunas (1994), What is a geomagnetic storm? *Journal of Geophysical Research*, 99, A4, 5771-5792.
- Gubbins, D. (1983), Geomagnetic field analysis-i. stochastic inversion, *Geophysical Journal of the Royal Astronomical Society*, 73 (3), 641-652.
- Gubbins, D., and J. Bloxham (1985), Geomagnetic field analysis - 111. Magnetic fields on the core-mantle boundary, *Geophysics Journal of Royal Astronomical Society*, 80, 695-713.
- Gubbins, D., A. L. Jones, and C. C. Finlay (2006), Fall in earth's magnetic field is erratic, *Science*, 312, 900.

- Hadamard, J. (1923), Lectures on the Cauchy problem in linear partial differential equations, New York: *Yale University Press*.
- Hasagawa, M. (1936a). On the type of diurnal variations of terrestrial magnetism on quiet days, *Proceedings of Imperial Academy*, Tokyo, 12, 88-90.
- Hasagawa, M. (1936b). Representation of the field of diurnal variations of terrestrial magnetism by the method of graphic integration, *Proceedings of Imperial Academy*, Tokyo, 12, 225-228.
- Hasagawa, M. (1936c). On the progressive change of the field of diurnal variations of terrestrial magnetism, *Proceedings of Imperial Academy*, Tokyo, 12, 277-280.
- Heison, G, S. Constable, and A. White (1993), The electrical conductivity of the lithosphere and asthenosphere beneath the coastline of southern California, *Exploration Geophysics*, 24, 195-200.
- Hirono, M. (1952), A theory of diurnal magnetic variation in equatorial regions and conductivity of the ionosphere e-region, *Journal of Geomagnetism and Geoelectricity*, 4, 5-11.
- Holme, R., and O. de Viron (2013), Characterization and implications of intradecadal variations in length of day, *Nature*, 499, 202-204.
- Holme, R., and O. de Viron (2005), Geomagnetic jerks and a high-resolution length-of-day profile for core studies, *Geophysics Journal International*, 160, 435-439.
- Holme, R., and N. Olsen (2006), Core surface flow modelling from high-resolution secular variation, *Geophysics Journal International*, 166, 518-528.
- Holme, R., and J. Bloxham (1996), The treatment of attitude errors in satellite geomagnetic data, *Physics of the Earth and Planetary Interiors*, 98, 221-233.
- Holme, R., N. Olsen, M. Rother, and H. Lühr (2003), CO2 - a CHAMP magnetic field model. In C. Reigber, H. Lühr, and P. Schwintzer, editors, *First CHAMP Mission Results for Gravity, Magnetic and Atmospheric Studies*, pages 220–225. Springer, Berlin.
- Hulot, G., C. Eymin, B. Langlais, M. Mandaia, and N. Olsen (2002) Small-scale structure of the geodynamo inferred from orsted and magsat satellite data, *Nature*, 416, 620-623.
- Jackson, A (1994), Statistical treatment of crustal magnetization, *Geophysics Journal International*, 119, 991-998.
- Jackson, A. (1990), Accounting for crustal magnetization in models of the core magnetic field, *Geophysical Journal International*, 103:657–673.
- Jackson, A. A., R. T. Jonkers, and M. R. Walker (2000), Four centuries of geomagnetic secular variation from historical records, *Philosophical Transactions of the Royal Society*, London, A, 358, 957-990.
- Jonkers, A.R.T. (2007), Discrete scale invariance connects geodynamo timescales, *Geophysical Journal International*, 171, 581-593.

- Joselyn, J.A. (1989). Geomagnetic quiet day selection, *Pure and Applied Geophysics*, 131, 3, 333-341.
- Kamide, Y., W. Baumjohann, I.A. Daglis, W. D. Gonzalez, M. Grande, J. A. Joselyn, R.L. McPherron, J. L. Phillips, E.G. D. Reeves, G. Rostoker, A. S. Shanna, H. J. Singer, B.T. Tsurutani, and V. M. Vasyliunas (1998), Current understanding of magnetic storms: Storm-substorm relationships, *Journal of Geophysical Research*, 103, A8, 17, 705-17,728.
- Karinen, A., and K. Mursula (2005), A new reconstruction of D_{st} index for 1932-2002, *Annales Geophysicae*, 23, 478-485.
- Kane, R.P. (1976), Geomagnetic Field Variations, *Space Science Reviews*, 18, 413-540.
- Kappenman, J. G., L. J. Zanetti, and W. A. Radasky (1997), Geomagnetic storm forecasts and the power industry, *Eos Trans. AGU*, 78, 37-45.
- Kato, S. (1956). Horizontal wind systems in the ionospheric E region deduced from the dynamo theory of geomagnetic Sq variation, Part II – Rotating Earth, *Journal of Geomagnetism and Geoelectricity*, 8, 24-37.
- Kerridge, D. (2001), INTERMAGNET: Worldwide near-real-time geomagnetic observatory data, in *Proceedings of Space Weather Workshop*, ESTEC.
- Kivelson, M.G and C.T. Russel (1995). Introduction to space physics, *Cambridge University Press*.
- Klausner, V., A.R.R. Papa, O. Mendes, M.O. Domingues, and P. Frick (2013), Characteristics of solar diurnal variations: A case study based on records from the ground magnetic station at Vassouras, Brazil, *Journal of Atmospheric and Solar-Terrestrial Physics*, 92, 124–136.
- Kono, M. (2007), Geomagnetism in perspective, in Geomagnetism, *Treatise on Geophysics*, vol. 5, edited by M. Kono, chap. 3, pp. 1-31, Elsevier.
- Kreil, K. (1839), Herschel Letters, Vol. 11, 70, *Royal Society*.
- Kullen, A., S. Ohtani, and T. Karlsson (2009), Geomagnetic signatures of auroral substorms preceded by pseudobreakups, *Journal of Geophysical Research*, 114, A04, 201.
- Kusi, R., A. White, G. Heison and P. Milligan (1998), Electromagnetic induction studies in the Eyre peninsula, South Australia, *Geophysics Journal International*, 132, 687-700.
- Kuvshinov, A.V. (2008), 3-D Global Induction in the Oceans and Solid Earth: Recent Progress in Modeling Magnetic and Electric Fields from Sources of Magnetospheric, Ionospheric and Oceanic Origin, *Survey in Geophysics*, 29, 139–186.
- Kuvshinov, A. V., and N. Olsen (2005), 3D modelling of the magnetic field due to ocean flow. In: Reigber C, Luhr H, Schwintzer P, Wickert J (eds) *Earth observation with CHAMP*, results from three years in orbit, Springer, Berlin.
- Lalanne, X., A. Peltier, A. Chulliat, A. Telali, and B. Heumez (2012), A new measurement method for magnetic repeat stations, *Proceedings of the XVth IAGA Workshop on Geomagnetic Observatory Instruments, Data Acquisition and Processing*, San Fernando, Cadiz, Spain.

- Langel, R. A. (1991), Recent progress in estimating uncertainty in geomagnetic field modeling, *Geophysical and Astronomical fluid dynamics*, Vol. 60 (1-4), pp. 37-88.
- Langel, R. A. (1987), The main field. In J. A. Jacobs, editor, *Geomagnetism*, vol. 1, chap. 4, pp. 249-512, Academic Press, London.
- Langel, R.A., and R.H. Estes (1982), A geomagnetic field spectrum, *Geophysical Research Letters*, Vol. 9, 4, 250-253.
- Langel, R. A., and R. H. Estes (1985), The near-Earth magnetic field of 1980 determined from MAGSAT data, *Journal Geophysical Research*, 90, 2495-2509.
- Langel, R.A., and R.H. Estes (1985a), Large-scale, near-Earth magnetic fields from external sources and the corresponding induced internal fields, *Journal of Geophysical Research*, 90, 2487-2494.
- Langel, R. A., T. J. Sabaka, R. T. Baldwin, and J. A. Conrad (1996), The near-Earth magnetic field from magnetospheric and quiet-day ionospheric sources and how it is modelled, *Physics of the Earth & Planetary Interior*, 98, 235-267.
- Langel, R.A., R. H. Estes, and T. J. Sabaka (1989), Uncertainty estimates in geomagnetic field modeling, *Journal of Geophysical Research*, 94:12,281–12,299,
- Langlais, B., V. Lesur, M. E. Purucker, J. Connerney, and M. Mandaia ((2010), Crustal magnetic fields of terrestrial planets, *Space Science Review*, 152, 223-249.
- Lanza, R., and A. Meloni (2006), The Earth's magnetism – An introduction for geologists. *Würzburg; Springer*.
- Lanzerotti, L. J. (1994), Impacts of solar-terrestrial processes on technological systems, in solar-terrestrial energy program, *COSPAR colloq, ser., vol. 5*, ed. By D. N. Baker, V. O. Papitashvili, and M. J. Teague, pp 547-555, Pergamon, Tanytown, NY.
- Larsen, J and C, Cox (1966), Lunar and Solar Daily Variation in the Magnetotelluric Field beneath the Ocean, *Journal of Geophysical Research*, 71, 18, 4441-4445.
- Lester, M., S. E. Milan, G. Provan, and J. A. Wild (2006), Review of ionospheric effects of solar wind magnetosphere coupling in the context of the expanding contracting polar cap boundary model, *Space Science Review*, 124, 117-130.
- Lesur, V., S. Macmillan, and A. Thomson (2005), A geomagnetic field model with daily variations of the magnetospheric field and its induced counterpart in 2001, *Geophysical Journal International*, 160, 79-88.
- Lesur, V., I. Wardinski, M. Rother, and M. Mandaia (2008), GRIMM: The GFZ reference internal magnetic model based on vector satellite and observatory data, *Geophysics Journal International.*, 173, 382-394.
- Lesur, V., I. Wardinski, M. Hamoudi, and M. Rother (2010), The second generation of the GFZ Reference Internal Magnetic Model: GRIMM-2, *Earth Planets Space*, 62, 765-773.

- Lilley, F.E.M. (1982), Geomagnetic field fluctuations over Australia in relation to magnetic surveys, *Bulletin of Australian Society of Exploration Geophysics*, 13, 68-76.
- Lilley, F.E.M. (1984), On the spatial pattern of magnetic fluctuations in the Cobar area, NSW, *Exploration Geophysics*, 15, 79-83.
- Lilley, F.E.M., A.P. Hitchman, and L.J. Wang (1999), Time-varying effects in magnetic mapping: amphidrones, doldrums and induction hazard, *Geophysics*, vol. 64, 6, 1720-1729.
- Love, J. J. (2008), Magnetic monitoring of the Earth and space, *Physics Today*, 61, 31-37.
- Love, J. J., and K. J. Remick (2007), Magnetic indices, in *Encyclopedia of Geomagnetism and Paleomagnetism*, edited by D. Gubbins and E. Herrero-Bervera, pp. 509-512, Springer, Dordrecht, Neth.
- Lowes, F. (1974), Spatial power spectrum of the main geomagnetic field, and extrapolation to the core, *Geophysical Journal of the Royal Astronomical Society*, 36 (3), 717-730.
- Lowes, F. J. and N. Olsen (2004), A more realistic estimate of the variances and systematic errors in spherical harmonic geomagnetic field models, *Geophysical Journal International*, 157:1027–1044.
- Luhmann, J. G. (1995), Ionospheres, In M. G. Kivelson and C. T. Russell, editors, *Introduction to Space Physics*, Cambridge University Press, Cambridge, 183-202.
- Luhr, H., and S. Maus (2010), Solar cycle dependence of quiet-time magnetospheric currents and a model of their near-earth magnetic field, *Earth Planets Space*, Vol. 62 (10), pp. 843-848.
- Luyendyk, A.P.J. (1997), Processing of airborne magnetic data, *Journal of Australian Geology and Geophysics*, 17, 31-38.
- Macmillan, S. (2007a), Observatories, Overview, in *Encyclopedia of Geomagnetism and Paleomagnetism*, edited by D. Gubbins and E. Herrero-Bervera, pp. 708-711, Springer.
- Macmillan, S., and S. Maus (2005), International Geomagnetic Reference Field – the tenth generation, *Earth Planets Space*, 57, 1135-1140.
- Macmillan, S., and C. Finlay (2011), Geomagnetic observations and models, Chapter 10, the International Geomagnetic Reference Field, *AGA Special Book Series*, Springer.
- Macmillan, S., and N. Olsen (2013), Observatory data and the swarm mission, *Earth Planets Space*, 65, 1355-1362.
- Maeda, H. (1955), Horizontal wind systems in the ionosphere E region deduced from the dynamo theory of geomagnetic Sq variation, Part I. *Journal of Geomagnetism and Geoelectricity*. 7, 121-132.
- Maeda, K. (1952). Dynamo-theoretical conductivity and current in the ionosphere, *Journal of Geomagnetism and Geoelectricity*. 4, 63-82.
- Malin, S.R.C. (1973). Worldwide distribution of geomagnetic tides, *Philosophical Transactions of the Royal Society*, London, A274, 551-594.

- Malin, S.R.C and J.C. Gupta. (1977). The Sq current system during the International Geophysical Year. *Geophysical Journal of Royal Astronomical Society*, 49, 515-529.
- Mandea, M. (2007), Main field modelling. In D. Gubbins and E. Herrero-Bervera, editor, *Encyclopedia of Geomagnetism and Paleomagnetism*, pp. 679-683, Springer.
- Mandea, M. (2006), Magnetic satellite missions: where have we been and where are we going? *Comptes Rendus Geoscience*, 338, 1002-1011.
- Mandea, M., and N. Olsen (2006), A new approach to directly determine the secular variation from magnetic satellite observations, *Geophysical Research Letters*, Vol. 33, L15306.
- Mandea, M., and M. Purucker (2005), Observing, modelling and interpreting magnetic fields of the solid Earth, *Surveys in Geophysics*, 26, 415-459.
- Mandea, M., R. Holme, A. Pais, K. Pinheiro, A. Jackson and G. Verbanac (2010), Geomagnetic jerks: Rapid core field variations and core dynamics, *Space Science Review*, 155, 147-175.
- Mandea, M., H. Luhr, M. Korte, G. Balasis, H. –J. Linthe, K. Hemant, E. Pulz, P. Ritter, M. Rother, C. Stolle, E. Thebault, I. Wardinski (2006), A comprehensive view of the Earth's magnetic field from ground and space observations, *Zweijahresbericht GeoForschungsZentrum Potsdam 2004/2005*, 63-76.
- Matsushita, S. (1967), Solar quiet and lunar daily variation fields, in Matsushita, S and Campbell, W. H., Eds., *Physics of Geomagnetic Phenomena*: Academic Press, 302-424.
- Matsushita, S. and W.H. Campbell (1967), Solar quiet and lunar variation fields, *Physics of Geomagnetic Phenomena*, Vol. 1, Academic Press.
- Matsushita, S., and H. Maeda (1965), On the geomagnetic solar quiet daily variations during International Geophysical Year, *Journal of Geophysical Research*, Vol. 70, 11, 2535-2558.
- Matzka, J., A. Chulliat, M. Mandea, C. C. Finlay, and E. Qamili (2010), Geomagnetic observations for main field studies: From ground to space, *Space Science Review*, 155, 29-64.
- Maule, C. F., M. E. Purucker, and N. Olsen (2009), Inferring magnetic crustal thickness and geothermal heat flux from crustal magnetic field models, *Danish Centre Climate Report 09-09*, Danish Meteorological Institute.
- Maus, S. (2008), The geomagnetic power spectrum, *Geophysical Journal International*, 174, 135-142.
- Maus, S. (2007b), Electromagnetic ocean effects. In: Gubbins D, Herrero-Bervera E (eds) *Encyclopedia of geomagnetism*, Springer, Heidelberg.
- Maus, S and H. Luhr (2005), Signature of the quiet-time magnetospheric magnetic field and its electromagnetic induction in the rotating Earth, *Geophysical Journal International*, 162, 755–763.
- Maus, S., and P. Weidelt (2004), Separating the magnetospheric disturbance magnetic field into external and transient internal contributions using a 1D conductivity model of the Earth, *Geophysical Research Letters*, 31, L12, 614.

- Maus, S., H. Lühr, G. Balasis, M. Rother, and M. Manda (2005b), Introducing POMME, Potsdam Magnetic Model of the Earth, *Earth Observation with CHAMP: Results from three years in Orbit*, pp. 293-298.
- Maus, S., T. Sazonova, K. Hemant, J. D. Fairhead, and D. Ravat, (2007), National Geophysical Data Center candidate for the World Digital Magnetic Anomaly Map, *Geochemistry Geophysics Geosystem*, 8, ISSN: 1525-2027.
- Maus, S., H. Lühr, M. Rother, G. Balasis, P. Ritter, and C. Stolle (2007a), Fifth-generation lithospheric magnetic field model from CHAMP satellite measurements, *Geochemistry Geophysics Geosystem*, 8(5).
- Maus, S., M. Rother, K. Hemant, C. Stolle, H. Lühr, A. Kuvshinov, and N. Olsen (2006b), Earth's lithospheric magnetic field determined to spherical harmonic degree 90 from CHAMP satellite measurements, *Geophysical Journal International*, 164, 319-330.
- Maus, S., M. Rother, C. Stolle, W. Mai, S. Choi, H. Lühr, D. Cooke, and C. Roth (2006c), Third generation of the Potsdam Magnetic Model of the Earth (POMME), *Geochemistry Geophysics Geosystem*, 7, Q07, 008.
- Maus, S., M. Rother, R. Holme, H. Luhr, N. Olsen, and V. Haak (2002), First scalar magnetic anomaly map from CHAMP satellite data indicates weak lithospheric field, *Geophysical Research Letters*, 29, 47.
- Maus, S., S. Macmillan, Frank Lowes, and T. Bondar (2005), Evaluation of candidate geomagnetic field models for the 10th generation of IGRF, *Earth Planets Space*, 57, 1173-1181.
- Maus, S., F. Yin, H. Lühr, C. Manoj, M. Rother, J. Rauberg, I. Michaelis, C. Stolle, and R. D. Muller (2008), Resolution of direction of oceanic magnetic lineations by the sixth-generation lithospheric magnetic field model from CHAMP satellite magnetic measurements, *Geochemistry Geophysics Geosystem*, 9, Q07, 021.
- Maus, S., C. Manoj, J. Rauberg, I. Michaelis, and H. Lühr (2010), NOAA/NGDC candidate models for the 11th Generation International Geomagnetic Reference Field and the concurrent release of the 6th generation POMME Magnetic Model, *Earth Planets Space*, 62, 729-735.
- Maus et al. (2005), The 10th generation international geomagnetic reference field, *Physics of the Earth & Planetary Interior*, 151, 320-322.
- Mayaud, P. N. (1980), Derivation, meaning and use of geomagnetic indices, *Geophysical Monogram Series*, AGU, Washington, D.C.
- McPherron, R. L. (1995), Magnetospheric dynamics. In M. G. Kivelson and C. T. Russell, editors, Introduction to Space Physics, pp. 1-26, *Cambridge University Press*, Cambridge.
- Mendes Jr, O., A. M. da Costa, and F. C. P. Bertoni (2006), Effects of the number of stations and time resolution on D_{st} derivation, *Journal of Atmospheric & Solar-Terrestrial Physics*, 68, 2127-2137.
- Menvielle, M. (2001), Recent and future evolution in geomagnetic indices derivation and dissemination, *contributions to geophysics and geodesy*, Vol. 3, 1.
- Menvielle, M. (1998), Derivation and dissemination of geomagnetic indices, *Revista Geofisica*, 48, 51-66.

- Menvielle, M., and A. Marchaudon (2007), Geomagnetic indices in solar-terrestrial physics and space weather, in *Space weather: Research towards applications in Europe, Astrophysics and space science library*, vol. 344, pp. 277-288, Springer, Dordrecht, Neth.
- Merrill, R., P. McFadden and M. McElhinny (1998). The magnetic field of the earth: paleomagnetism, the core, and the deep mantle, *Academic*, san Diego.
- Merrill, R.T., M.W. McElhinny and P.L. McFadden (1996), The magnetic field of the Earth: Paleomagnetism, the core, and the deep Mantle, *Academic Press*.
- Milan, S. E., T. A. Evans, and B. Hubert (2010), Average auroral configuration parameterized by geomagnetic activity and solar wind conditions, *Annales Geophysicae*, 28, 1003-1012.
- Minty, B.R.S. (1991), Simple micro-levelling for aeromagnetics data, *Exploration Geophysics*, 22, 591-592.
- Moss, N. A. F. (1910), Colaba magnetic data, 1846 to 1905. 2. The phenomenon and its discussion, Bombay, India: Central Government Press.
- Mozzoni, D.T. (2008), The changing geomagnetic field from the ionosphere to the core-mantle boundary, *Scientific Technical Report STR08/02*, GeoForschungsZentrum Potsdam.
- Murayama, T. (1982), Coupling function between solar wind parameters and geomagnetic indices, *Review of Geophysics & Space Physics*, 20, 623-629.
- Nagao, H., T. Iyemori, T. Higuchi, and T. Araki (2003), Lower mantle conductivity anomalies estimated from geomagnetic jerks, *Journal of Geophysical Research*, 108, 2254.
- Neubert, T., M. Mandea, G. Hulot, R. von Frese, F. Primdahl, J. L. Jorgensen, E. Friis-Christensen, P. Stauning, N. Olsen, and T. Risbo (2001), Ørsted satellite captures high-precision geomagnetic field data, *Eos Trans. AGU*, 82 (7), 81.
- Newitt, L. R., C. E. Barton, and J. Bitterly (1996), Guide for magnetic repeat station surveys, *International Association of Geomagnetism and Aeronomy*, Boulder.
- Nikolaeva, N. S., Y. I. Yermolaev, and I. G. Lodkina (2011), Dependence of geomagnetic activity during magnetic storms on the solar wind parameters for different types of streams, *Geomagnetism and Aeronomy*, 51, 49-65.
- O'Brien, T. P., and R. L. McPherron (2000), Forecasting the ring current index D_{st} in real time, *Journal of Atmospheric & Solar-Terrestrial Physics*, 62, 14, 1295-1299.
- Olsen, N. (1993), The solar cycle variability of lunar and solar daily geomagnetic variations, *Annales Geophysicae*, 11, 254-262
- Olsen, N. (2002), A model of the geomagnetic field and its secular variation for epoch 2000 estimated from Ørsted data, *Geophysical Journal International*, **149**, 454-462.
- Olsen, N., and S. Kotsiaros (2011), Magnetic satellite missions and data, in *IAGA Special Sopron Book Series*, vol. 5, chap. 2, pp. 27-44, Springer.

- Olsen, N., and M. Manda (2008), Rapidly changing flows in the Earth's core, *Nature Geoscience*, 1, 390-394.
- Olsen, N., G. Hulot, and T. J. Sabaka (2007), The present field, in *Geomagnetism, Treatise on Geophysics*, vol. 5, edited by M. Kono, chap. 2., pp. 33-75, Elsevier.
- Olsen, N., T. J. Sabaka, and F. Lowes (2005), New parameterization of external and induced fields in geomagnetic field modelling, and a candidate model for IGRF 2005, *Earth Planets Space*, 57, 1141–1149.
- Olsen, N., M. Manda, T. J. Sabaka, and L. T. Clausen (2009), CHAOS-2 a geomagnetic field model derived from one decade of continuous satellite data, *Geophysical Journal International*, 179.
- Olsen, N., M. Manda, T. J. Sabaka, and L. Toffner-Clausen (2010), The CHAOS-3 geomagnetic field model and candidates for the 11th generation IGRF, *Earth Planets Space*, 62, 719-727.
- Olsen, N., H. Lühr, C. C. Finlay, T. J. Sabaka, I. Michaelis, J. Rauberg, and L. Tøffner-Clausen (2014), The CHAOS-4 geomagnetic field model, *Geophysical Journal International*, 197 (2): 815-827.
- Olsen, N., H. Lühr, T. J. Sabaka, M. Manda, M. Rother, L. Toffner-Clausen, and S. Choi (2006), CHAOS - A model of Earth's magnetic field derived from CHAMP, Ørsted, and SAC-C magnetic satellite data, *Geophysical Journal International*, 166, 67-75.
- Olsen, N., G. Hulot, and T. J. Sabaka (2010). Sources of the geomagnetic field and the modern data that enable their investigation, in *Handbook of Geomathematics*, edited by W. Freedman, M. Z. Nashed, and T. Sonar, chapter 5, pp. 106–124.
- Olsen et al., (2013), The Swarm Satellite Constellation Application and Research Facility (SCARF) and swarm data products, *Earth Planets Space*, 65, 1189-1200.
- Olson, W.P. (1989). The Contribution of Magnetospheric Currents to Sq, *Pure and Applied Geophysics*, Vol. 131, 3, 447-462.
- Østgaard, N., R. R. Vondrak, J. W. Gjerloev, and G. Germany (2002), A relation between the energy deposition by electron precipitation and geomagnetic indices during substorms, *Journal of Geophysical Research*, 107.
- Ouabego et al. (2013), Rock magnetic investigation of possible sources of the Bangui magnetic anomaly, *Physics of the Earth and Planetary Interiors*, 224, 11-20.
- Parkinson, W.D. (1979), The geomagnetic coast effect, *Reviews of Geophysics and Space Physics*, Vol. 17, 8.
- Parkinson, W. D., and V. R. S. Hutton (1989), The electrical conductivity of the Earth. In: J. A. Jacobs (ed) *Geomagnetism*, vol. 3. Academic, London, pp 261-321.
- Pedatella, M.N., J.M. Forbes, and A.D. Richmond (2011), Seasonal and longitudinal variations of the solar quiet (Sq) current system during solar minimum determined by CHAMP satellite magnetic field observations, *Journal of Geophysical Research*, Vol. 116, A04317.

- Poedjono, B., E. Adly, M. Terpening, and X. Li (2010), Geomagnetic referencing service – A viable alternative for accurate wellbore surveying, Paper Presented at IADC/SPE Drilling Conference and Exhibition, Louisiana, USA.
- Poedjono, B., E. Adly, M. Terpening, and X. Li (2011), Using geomagnetic referencing technology for precise wellbore placement, Paper AADE-11-NTCE-13, presented at AADE Technical Conference and Exhibition, Houston, Texas, USA.
- Poedjono, B., N. Beck, A. Buchanan, L. Borri, S. Maus, C.A. Finn, E.W. Worthington, and T. White (2013), Improved geomagnetic referencing in the arctic environment, SPE Arctic and Extreme Environment Technical Conference and Exhibition, Moscow, Russia.
- Potgieter, M.S. (2013), Solar modulation of cosmic rays, *Living Review of Solar Physics*, 10, 3.
- Pudovkin, M.I. (1974). Electric fields and currents in the ionosphere, *Space Science Review*, 16, 727-770.
- Pulkkinen, T. (2007), Space weather: Terrestrial perspective, *Living Review of Solar Physics*, 4.
- Pumfrey, S. (1989), A sociological analysis of the discovery of secular magnetic variation in 1634, *The British Journal for the History of Science*, Vol. 22, 2, pp. 181-214.
- Purucker, M. E. (2007), MAGSAT, in *Encyclopedia of Geomagnetism and Paleomagnetism*, edited by D. Gubbins and E. Herrero-Bervera, pp. 673-674, Springer.
- Rajaram, M. (1993), MAGSAT's contribution to geophysical surveys, *Advances in Space Research*, 13, 33-42.
- Rastogi, R. G. (2006), Effects of ionospheric, magnetospheric and induced current on equatorial electrojet over India, *India Journal of Radio and Space Physics*, vol. 35, pp. 149-166.
- Rastogi, R.G. (2004), Electromagnetic induction by the equatorial electrojet, *Geophysics Journal International*, 158, 16-31.
- Ravat, D., K. A. Whaler, M. Pilkington, T. J. Sabaka, M. E. Purucker (2002), Compatibility of high-altitude aeromagnetic and satellite altitude magnetic anomalies over Canada, *Geophysics*, **67**, 546–554.
- Ravat, D., R. A. Langel, M. Purucker, J. Arkani-Hamed, and D. E. Alsdorf (1995), Global vector and scalar Magsat magnetic anomaly data, *Journal of Geophysical Research*, 100, 20,111 – 20,136.
- Reay, S.J., W. Allen, O. Baillie, J. Bowe, E. Clark, V. Lesur, and S. Macmillan (2005), Space weather effects on drilling accuracy in the North sea, *Annales Geophysicae*, 23, 3081-3088.
- Reeves, C. (2005), Aeromagnetic surveys – principles, practices and interpretation, e-published by GEOSOFT (<http://www.geosoft.com/knowledge>).
- Reeves, C.V. (1993), Limitations imposed by geomagnetic variations on high quality aeromagnetic surveys, *Exploration Geophysics*, 24, 115-116.
- Regan, R. D. (1979), The reduction and analysis of satellite magnetometer data, *Journal of Geophysical Research*, 3 (4), 331-349.

- Regan, R. D., and P. Rodriguez (1981), An overview of the external magnetic field with regard to magnetic surveys, *Geophysical surveys*, 4, 255-296.
- Reigber, C., H. Lühr, and P. Schwintzer (2002), CHAMP mission status, *Advances in Space Research*, 30 (2), 129-134.
- Richmond, A.D. (1979). Ionospheric wind dynamo theory: a review. *Journal of Geomagnetism & Geoelectricity*, 31, 287-310.
- Richmond, A.D., S. Matsushita and J.D. Tarpley. (1976). On the production mechanism of electric currents and fields in ionosphere. *Journal of Geophysical Research*, 81, 547-555.
- Rigoti, A., A.L. Padilha, F.H. Chamalaun and N.B. Trivedi (2000), Effects of the equatorial electrojet on aeromagnetic data acquisition, Short Note, *Geophysics*, vol. 65, 2, 553-558.
- Ritter, P., H. Lühr, S. Maus, and A. Viljanen (2004b), High-latitude ionospheric currents during very quiet times: their characteristics and predictability, *Annales Geophysicae*, 22, 2001-2014.
- Russell, C. T. (2001), Dynamics of planetary magnetosphere, *Planetary and Space Science*, 49, 1005-1030.
- Russell, C. T. (2000), The solar wind interaction with the Earth's magnetosphere: A tutorial, *IEEE Transactions on Plasma Science*, Vol. 28, 6.
- Russell, J.P., G. Shiells, and D.J. Kerridge (1995), Reduction of wellbore positioning uncertainty through application of a new geomagnetic in-field referencing technique, Paper SPE30452, presented at SPE Annual Technical Conference and Exhibition, Dallas, USA.
- Rygaard-Hjalsted, C., C. G. Constable, and R. L. Parker. (1997), The influence of correlated crustal signals in modelling the main geomagnetic field, *Geophysical Journal International*, 130:717-726.
- Sabaka, T. J., and R. T. Baldwin (1993), Modeling the Sq magnetic field from POGO and MAGSAT satellite and cotemporaneous hourly observatory data: Phase 1, *Technical Report Contract Report HSTX/G&G9302*, Hughes STX Corp., for NASA/GSFC Contract NAS5-31 760, NASA.
- Sabaka, T. J., N. Olsen, and R. A. Langel (2002), A comprehensive model of the quiet-time near-Earth magnetic field: phase 3. *Geophysical Journal International*, 151, 32-68.
- Sabaka, T.J, N. Olsen and M.E. Purucker (2004). Extending Comprehensive models of the Earth's magnetic field with Oersted and CHAMP data. *Geophysical Journal International*, 159, 521-547.
- Schildreg, J.P., S.V. Vankateswaran and A.D. Richmond. (1973). The ionospheric dynamo and equatorial magnetic variations, *Journal of Atmospheric & Solar-Terrestrial Physics*, 35, 1045-1061.
- Schmucker, U. (1985), Magnetic and electric fields due to electromagnetic induction by external sources. *In Landolt-Bornstein, new-series*, 5/2b, Springer, Berlin-Heidelberg, pp 100-125.
- Schuster, A. (1889). The diurnal variation of terrestrial magnetism. *Philosophical Transactions of the Royal Society*, London, A180, 467-518.

- Schuster, A. (1902). On some definite integrals and a new method of reducing a function of spherical coordinates to a series of spherical harmonics, *Philosophical Transactions of the Royal Society*, London, A200, 181-223.
- Schuster, A. (1908), The diurnal variation of terrestrial magnetism, *Philosophical Transactions of the Royal Society*, London, A208, 163-204.
- Sckopke, N. (1966), A general relation between the energy of trapped particles and the disturbance field near Earth, *Journal of Geophysical Research*, 71, 3125.
- Shure, L., R.L. Parker, and G.E. Backus (1982), Harmonic splines for geomagnetic modelling, *Phys. Earth Planet. Int.*, 28, 215-229.
- Siscoe, G., and D. Odstrcil (2008), Ways in which ICME sheaths differ from magnetosheaths, *Journal of Geophysical Research*, 113, A9.
- Snyder, C. W., and M. Neugebauer (1963), Solar wind velocity and its correlation with cosmic-ray variations and with solar and geomagnetic activity, *Journal of Geophysical Research*, 68.
- Stening, R. J. (2003), Space weather in the equatorial ionosphere, *Space Science Review*, 107, 263-271.
- Stern, D. P. (2006), A millennium of geomagnetism, *Review of Geophysics*, 40, 3, 1-30.
- Stern, D. P. (1985), Parabolic harmonics in magnetospheric modelling: the main dipole and the ring current, *Journal of Geophysical Research*, Vol. 90, A11, 10,851-10,863.
- Stewart, B. (1882). Hypothetical Views Regarding the Connection between the State of the Sun and Terrestrial Magnetism, *Encyclopedia Britannica*, 9th ed., vol.16, 181 – 184.
- Sugura, M. (1972), Equatorial current sheet in the magnetosphere, *Journal of Geophysical Research*, Vol. 77 (31), 6,093-6,103.
- Sugiura, M. (1964), Hourly values of equatorial D_{st} for the IGY, *Annals of the International Geophysical Year*, 35, 945-948.
- Suttie, N., R. Holme, M.J. Hill and J. Shaw (2011), Consistent treatment of errors in archaeointensity implies rapid decay of the dipole prior to 1840, *Earth and Planetary Science Letters*, 304, 13-21.
- Takeda, M. (2002a), Features of global geomagnetic Sq field from 1980 to 1990, *Journal of Geophysical Research*, 107(A9), 1252, doi:10.1029/2001JA009210.
- Takeda, M., Yamada, Y. and Araki, T., Simulation of ionospheric currents and geomagnetic field variations of Sq for different solar activity (1986), *Journal of Atmospheric and Terrestrial Physics*, 48, 277-287.
- Tarantola, A. (2005), Inverse problem theory and methods for model parameter estimation, Philadelphia: *Society for Industrial and Applied Mathematics* (SIAM).
- Thebault, E., M. Purucker, K. A. Whaler, B. Langlais, and T. J. Sabaka (2010), The magnetic field of the Earth's lithosphere, *Space Science Review*, 155, 95-127.

- Thomsen, M. F. (2004), Why K_p is such a good measure of magnetospheric convection, *Space weather*, vol. 2, S11004.
- Thomson, A. W. P., and V. Lesur (2007), An improved geomagnetic data selection algorithm for global geomagnetic field modelling, *Geophysics Journal International*, 169, 951-963.
- Torta, J.M., J.J. Curto, and P. Bencze (1997), Behaviour of the quiet day ionospheric current system in the European region, *Journal of Geophysical Research*, vol. 102, A2, 2483-2494.
- Troshichev, O. A., V. G. Andrezen, S. Vennerstrom, and E. Friis-Christensen (1988), Magnetic activity in the polar cap – a new index, *Planet Space Science*, 36, 1095-1102.
- Tsyganenko, N. A. (1989), A magnetospheric magnetic field model with a warped tail current sheet, *Planet Space Science*, 37, 5-20.
- Tsyganenko, N. A. (1995), Modelling the Earth's magnetospheric magnetic field confined within a realistic magnetopause, *Journal of Geophysical Research*, 100, 5599-5612.
- Tsyganenko, N. A. (1996), Effects of the solar wind conditions on the global magnetospheric configuration as deduced from data-based field models, *European Space Agency Special Publication*, ESA SP-389, 181.
- Tsyganenko, N. A. (2002a), A model of the near magnetosphere with a dawn-dusk asymmetry – 1. Mathematical structure, *Journal of Geophysical Research*, 107.
- Turbitt, C.W., and T.D.G. Clark (1994), The use of Lerwick variometer measurements to estimate magnetic disturbances over the North sea, British Geological Technical Report WM/94/21C.
- Turner, G. M., J. L. Rasson, and C. V. Reeves (2007), Observation and measurement techniques. In: M. Kono (ed) *Treatise on Geophysics*, vol. 5. Elsevier, Amsterdam.
- Turner, J.P.R., D.E. Winch, D.J. Ivers, and R.J. Stening (2007), Regular daily variations in satellite magnetic total intensity data, *Annales Geophysicae*, 25, 2167-2174.
- Verbanac, G., H. Lühr, and M. Rother (2006b), Evidence of ring current effect in geomagnetic observatories annual means, short communication, *GEOFIZIKA*, vol. 23, 1, 13-20.
- Verbanac, G., B. Vrsnak, M. Temmer, M. Manda, and M. Korte (2010), Four decades of geomagnetic and solar activity: 1960-2001, *Journal of Atmospheric & Solar-Terrestrial Physics*, 72, 607-616.
- Verbanac, G., H. Lühr, M. Rother, M. Korte, and M. Manda (2007), Contributions of the external field to the observatory annual means and a proposal for their corrections, *Earth Planets Space*, 59, 251-257.
- Vichare, G., R. Rawat, A. Hanchinal, A.K. Sinha, A. Dhar, and B.M. Pathan (2012), Seasonal evolution of Sq current system of sub-auroral latitude, *Earth Planets Space*, 64, 1023-1031.
- Walker, E. (1866). *Terrestrial and Cosmical Magnetism*, Deighton, Bell & Co., Cambridge, 336 pp
- Walker, M. R., and A. Jackson (2000), Robust modelling of the Earth's magnetic field, *Geophysical Journal International*, 143, 799-808.

- Wardinski, I., and R. Holme (2011), Signal from noise in geomagnetic field modelling: denoising data for secular variation studies, *Geophysical Journal International*, 185, 653-662.
- Wardinski, I., and R. Holme (2006), A time-dependent model of the earth's magnetic field and its secular variation for the period 1980-2000, *Journal of Geophysical Research*, 111, B12101
- Waler, K. A. (2007), Geomagnetism in the satellite era, *Astronomy & Geophysics.*, 48
- Waler, K. A., and R. A. Langel (1996), Minimal crustal magnetizations from satellite data, *Phys. Earth Planet Int.*, 98, 303-319.
- Waler, K., and D. Gubbins (1981), Spherical harmonic analysis of the geomagnetic field: An example of a linear inverse problem, *Geophys. J. R. Astr. Soc*, 65, 645-693.
- Williamson, H.S., P.A. Gurden, D.J. Kerridge, and G. Shiells (1998), Application of interpolation in-field referencing to remote offshore locations, Paper SPE49061, presented at SPE Annual Technical Conference and Exhibition, New Orleans, Louisiana, USA.
- Yamazaki, Y., and M. J. Kosch (2014), Geomagnetic lunar and solar daily variations during the last 100 years, *Journal of Geophysical Research, Space Physics*, 119, 6732-6744.
- Yarger, H.L., R.R. Robertson, and R.L. Wentland (1978), Diurnal drift removal from aeromagnetic data using least-squares, *Geophysics*, 43, 1148-1156.
- Zhao, L., and C. Y. Tu (2005), A relation between the auroral X-ray total intensity and the substorms index-AE, *Journal of Geophysics.*, 48, 739-743.